UNIVERSITÉ DU QUÉBEC À CHICOUTIMI

THÈSE

PRÉSENTÉ À

L'UNIVERSITÉ DU QUÉBEC À CHICOUTIMI

COMME EXIGENCE PARTIELLE

DU DOCTORAT EN INGÉNIERIE

PAR

Serageldin Salem Mohamed

EFFETS DES PARAMÈTRES MÉTALLURGIQUES SUR LE DÉVELOPPEMENT DES CONTRAINTES RÉSIDUELLES DANS LES ALLIAGES DE TYPE AL-SI UTILISÉS DANS LA FABRICATION DE BLOC MOTEUR

Juin 2018

UNIVERSITY OF QUEBEC AT CHICOUTIMI

THESIS PRESENTED TO THE

UNIVERSITY OF QUEBEC AT CHICOUTIMI

IN PARTIAL FULFILLMENT OF

THE REQUIREMENTS FOR THE DEGREE OF

DOCTOR OF PHILOSOPHY IN ENGINEERING

BY

Serageldin Salem Mohamed

EFFECTS OF METALLURGICAL PARAMETERS ON THE DEVELOPMENT OF RESIDUAL STRESSES IN AL-SI ALLOYS USED IN ENGINE BLOCK MANUFACTURING

June 2018

Dedicated to my parents, my wife Asmaa,

and to my children Talia and Mohamed.

RÉSUMÉ

L’utilisation de matériaux léger est devenue un important facteur dans l’industrie de l’automobile du aux restrictions imposées par les gouvernement en matières de consomation de carburant fossile. Les alliages d’aluminium sont 65% plus léger que la fonte, ce qui permet une reduction de poids significative. Cependant, il existe encore plusieurs défis à relever concernant l’utilisation d’alliage Al-Si hypoeutectic dans la fabrication de bloc moteur. Cette these enquête sur les facteurs infulençant le développement de contraintes résiduelles dans les bloc moteur I-4 et V-6 dus à différents traitements thermiques et introduisant un traitement sous zéro comme moyen de réduction des contraintes résiduelles.

La première partie de cette thèse, explore le développement de contraintes résiduelles avec différents paramètres de coulée dans des pièces de géométries simples en alliage A356.1 et B319.1. Cette analyse comprend la mesure des propriétés de traction, l'analyse microstructurale et la mesure de la contrainte résiduelle à l'aide de la technique de coupe. Les paramètres de coulée comprennent la vitesse de refroidissement, les milieux de trempe, le temps de vieillissement et la température de vieillissement. La deuxième phase de cette étude examinera le développement des contraintes résiduelles dans les pièces coulées, avec une forme plus complexe comme dans les blocs moteurs I-4 et V-6 avec chemises en fonte grise coulée, avec différents paramètres de traitement thermique et traitement sous zéro.

Une analyse des résultats montre que les matériaux de résistance plus élevée, comme dans l'alliage B319.1, produisent des contraintes résiduelles plus élevées que les matériaux de moindre résistance comme dans le cas du A356.1. Les résultats montrent également qu'il existe une proportionnalité directe entre les contraintes de traction ultimes (UTS) et les contraintes résiduelles (RS) avec la vitesse de trempe. Les contraintes résiduelles diminuent graduellement avec des vitesses de refroidissement / trempe décroissantes du milieu de trempe. Le processus de la trempe dans l'eau froide développe les contraintes résiduelles les plus élevées et le refroidissement à l'air développe les contraintes résiduelles les plus basses. La relaxation des contraintes résiduelles dépend de manière significative de la température de vieillissement et se déroule en douceur avec l'augmentation du temps de vieillissement. Enfin, une augmentation significative des contraintes résiduelles est observée dans les échantillons à faible SDAS, comme dans la coulée en L (taux de solidification élevé), tandis que les contraintes résiduelles plus faibles sont mesurées dans les échantillons à fort SDAS, comme dans la coulée en bloc (taux de solidification bas).

Pour les blocs-cylindres I4 et V-6, les résultats suggèrent qu'il y a un raffinement de la microstructure en raison de l'augmentation de la vitesse de refroidissement le long du cylindre. Les contraintes résiduelles développées se sont révélées être en traction pour les blocs moteurs I-4 et V-6. De plus, la variation des contraintes résiduelles développées s'est avérée insignifiante. Les résultats indiquent également que le refroidissement par air a produit les contraintes résiduelles les plus élevées par rapport à la trempe à l'eau chaude et à l'eau froide. Le traitement thermique et la congélation en solution ont conduit à une relaxation maximale de la contrainte résiduelle, lorsque 50% des contraintes résiduelles ont été réduites après l'étape de traitement thermique en solution. Le temps de vieillissement et la température de vieillissement sont directement proportionnels à la relaxation des contraintes résiduelles.

ABSTRACT

Using light-weight materials have become an important factor in the automotive industry due to stringent government regulations on fuel consumption. Aluminum alloys are 65% lighter than cast iron enabling significant weight reduction. However, there are several significant challenges associated to the use of hypoeutectic Al-Si alloys in engine block applications. This dissertation investigated the factors influencing the development of residual stresses in I-4 and V-6 engine blocks due to different heat treatments and introducing sub-zero treatment as a mean for reducing residual stresses.

The initial section of this thesis explores the development of residual stresses with different casting parameters in A356.1 and B319.1 castings with simple geometries. This analysis involved measurement of tensile properties, microstructural analysis, and residual stress measurement using sectioning technique. The casting parameters include cooling rate, quenching media, aging time and aging temperature. The second phase of this study will investigate the development of residual stress in castings, with more complex shape such as in I-4 and V-6 engine blocks with cast-in gray iron liners, with different heat treatment parameters and sub-zero treatment.

An analysis of result shows that higher strength materials, as in B319.1 alloy, produce higher residual stresses compared to material with lower strength, as in the case of A356.1. The results also show that there is direct proportionality between ultimate tensile stresses (UTS) and residual stresses (RS) with quenching rate. The residual stresses were found to gradually decrease with decreasing cooling/quenching rates of the quenching medium. The quenching process develops the highest residual stresses, where quenching in cold water develops the highest, and air cooling the lowest, residual stresses. The relaxation of residual stresses is significantly dependent on aging temperature and proceeds smoothly with the increase in aging time. Finally, significant increase in the residual stresses is observed in specimens with low SDAS, as in the L-shaped casting (high solidification rate), while lower residual stresses are measured in specimens with high SDAS, as in the block casting (low solidification rate).

For I4 and V-6 engine blocks, the results suggest that there is refinement in microstructure due to increases cooling rate along the cylinder. The developed residual stresses were found to be tensile for both I-4 and V-6 engine blocks. Furthermore, the variation in the developed residual stresses was found to be insignificant. The results also indicate that air cooling produced the highest residual stresses compared to warm water and cold-water quenching. Solution heat treatment and freezing led to maximum amount of residual stress relaxation where 50% of the residual stresses were reduced after SHT step.

Aging time and aging temperature is directly proportional to the residual stresses relaxation.

ACKNOWLEDGEMENTS

First and foremost I would like to thank my advisor Professor F.H. Samuel. It has been an honor to be his student. I appreciate all his contributions of time, ideas, and funding to present my PhD. the way it is today. I would also like to thank Professor A.M Samuel for her continuous guidance and support and for providing me helpful suggestions in improving the quality of my thesis. Without their continuous guidance and support it would have been impossible to complete my PhD degree.

It is a pleasure to thank all those who have contributed in any way to the completion of this study: Mr. Sameul Dessureault from TAMLA Group for carrying out the foundry work; Dr. Emad El-gallad and Dr. Mohamed Ibrahim of TAMLA Group for helping and guiding me in experimental work;

Financial support in the form of scholarships received from the Natural Sciences and Engineering Research Council of Canada (NSERC), General Motors Powertrain Group (U.S.A), and Corporativo Nemak (Mexico) is gratefully acknowledged.

Lastly, I would like to thank my family: my parents, my brother and my sister for all their love and encouragement. And most of all for my loving, supportive, encouraging, and patient wife Asmaa whose faithful support during the whole stages of my PhD. is so appreciated. I would like to take this opportunity to express my profound gratitude to her for her patience and her continuous support. Thank you!

Table of Contents

List of Figures

List of Tables

CHAPTER 1
DEFINITION OF THE PROBLEM

Chapter 1
Definition of the PROBLEM

1.1 Introduction

Residual stress is generally referred as an internal stress, which exists in equilibrium inside a component in the absence of any external forces or constraints, temperature gradients, or any other external influences [1]. Any existing residual stresses are considered as elastic stresses that are kept under static equilibrium. Elastic limit is the maximum value that can be reached by any residual stresses. Any stresses higher than the value of elastic limit with no opposing forces will be relieved by plastic deformation until it reaches the value of the yield stress [2].

Residual stresses are an accidental result or by-product of processing conditions such as welding, forging, extrusion, casting (especially after heat treatment). Plastic deformation, thermal stresses, phase transformation, multi-phase materials, and welding are the main sources for residual stresses in any component [1] [3]. Residual stresses can lead to warping or distortion during machining in addition to reducing fatigue strength, crack resistance and encouraging surface crack growth which can affect the structural integrity of the casting.

The evolution of residual stresses is mandatory as it is a product of all the manufacturing processes of the structure. The magnitude and sign of the residual stresses determine whether its effect on the structure will be beneficial or detrimental. Currently,

engine blocks are made of Al-Si alloys with grey cast iron inserted in the cylinder bores to compensate for the wear resistance deficiency of this alloy system.

During engine block casting, several factors determine the magnitude and sign of casting residual stresses naming namely, quenchant severity, temperature difference, thickness of the part, the implementation method of the cast iron liners, and material thermal properties such as heat expansion coefficient, thermal conductivity, specific heat and density of the material [4]. In order to ensure that production of parts meet the required specifications, minimizing distortion and cracking problems generated from the presence of residual stresses while improving mechanical properties, process optimization is required by optimizing both part geometry and quenching process design.

1.2 Definition of the Problem

With a view to improving fuel efficiency, most diesel engine blocks are made from Al-Si-Cu alloys followed by proper machining for enhancing surface quality. This alloy type provides several characteristics that are satisfactory for engine block application such as good castability, good machinability, and high thermal conductivity, and high mechanical properties at both room and elevated temperatures. Due to their low wear resistance, however, the use of protective cylinder liners in the combustion chamber of the engine block is required to compensate for the insufficient wear resistance of Al-Si-Cu-type alloys.

Excessive residual stresses may be generated due to the large difference in thermal expansion coefficient between the aluminum alloy (2.4×10^{-5} K^{-1}) and cast iron (1.5×10^{-5} K-1) [5]. The presence of these residual stresses renders engine blocks prone to either

distortion or failure. Distortion of the cylinder bores results in a loss in compression of the air-fuel mixture due to improper sealing between the cylinder wall and the piston. This loss of sealing causes a portion of the compressed air-fuel mixture to leak out of the combustion chamber by a process known as “blow-by” [6] [7]which reduces the engine efficiency. Figure 1-1 illustrates the blow-by phenomena for the engine’s compression and power strokes.

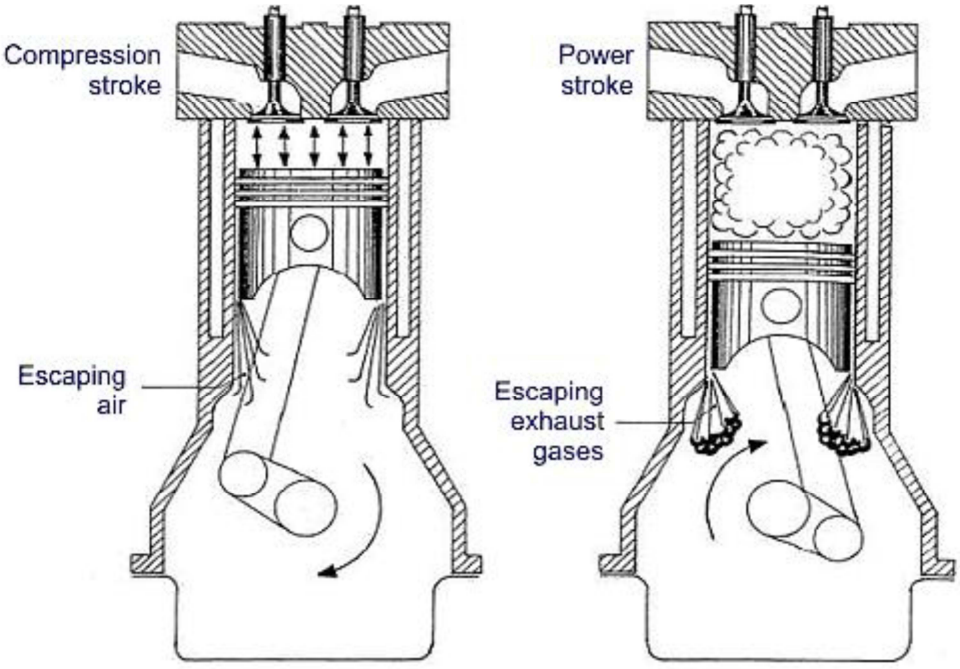

Figure 1-1 Cross-section of engine cylinder illustrating the blow-by phenomenon during operation [7]

In addition to distortion, tensile residual stresses have a devastating impact on engine block performance due to their influence on the mechanical behaviour resulting from reduced fatigue strength and crack resistance which encourages surface crack growth which

leads to engine failure and expensive maintenance costs ranging between 6000 to 10000$. Figure 1-2 shows a crack developed in an engine block bridge due to residual stresses.

In conclusion, aluminum engine blocks with gray iron cylinder liners are prone to tensile residual stresses along the cylinder bores, which results in distortion, cracks, and a reduction in engine efficiency. Several ideas have been introduced in order to change the cast iron liners with another suitable replacement but due to technical and economic problems cast in liners are considered the most effective option in engine block manufacturing [8].

This research study will investigate residual stress generation in 319 aluminum alloy cylinder blocks with cast iron inserts under different casting conditions in order to reach the appropriate heat treatment schedule, in addition to determining how residual stresses are relieved with time during solution heat treatment. Microstructural and mechanical characterization will be carried out by using samples sectioned from the engine block, employing optical and scanning and transmission electron microscopy techniques for microstructural characterisation, and hardness and tensile testing for mechanical characterization.

The main objectives of this research study are therefore summarized as follows:

- Study the factors that directly influence the residual stresses in different Al-alloys to understand their evolution and relaxation.
- Provide reliable data on the magnitude of residual stresses generated inside an engine block through a series of measurements carried out to evaluate the residual stresses in critical regions of cast engine blocks made from heat treatable B319.1, with cast iron inserts.

- Compare the results obtained from above points to extend our understanding of the development and relaxation of residual stresses.
- Optimize the heat treatment parameters required to improve casting integrity of engine blocks and enhance their efficiency.

By gaining an insight into the above aspects, the best manufacturing parameters conditions for producing engine blocks with optimum mechanical performance and lowest locked-in stresses may be determined. In order to achieve these objectives, the study will involve optical, scanning and transmission electron microscopy for microstructural characterization, tensile and hardness testing for mechanical properties characterization, and analysis of selected regions with high amounts of residual stresses inside the engine cylinder blocks using the sectioning technique.

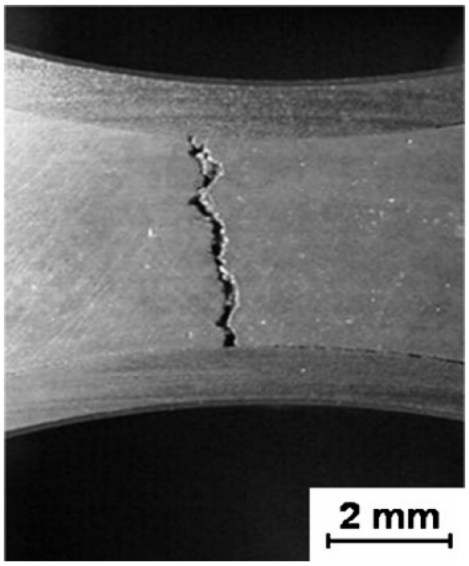

Figure 1-2 Crack within Engine Block Bridge [8]

CHAPTER 2
SURVEY OF LITERATURE

Chapter 2
Survey of Literature

2.1 Introduction

Aluminum and its alloys occupy the third place among commercially used engineering materials. In commercial aluminum casting alloys, Al–Si base alloys are perhaps the most commonly used alloys due to their attractive characteristics such as high strength-to-weight ratio, good workability, excellent castability, good thermal conductivity, good corrosion resistance and high-temperature performance. The use of aluminum alloys has increased significantly over the past several years in numerous applications, successfully replacing iron and steel due to its high specific strength when compared to steel.

The 19^{th} century is considered the starting point of an evolutionary era in the development of aluminum casting which played an integral role in the growth of the aluminum industry [9]. Consumption of aluminum castings has increased from 85,000 tonnes in 1995 to 43.989 million tonnes in the year 2011 [10]. Production of aluminum castings using Al–Si alloys has received acceptable agreement in recent decades due to their attractive properties. This class of alloys is emerging as one of the most dominant materials in a number of sectors like transport, military, aviation and general engineering. Al-Si alloys usage in the transport sector has increased from just 6% in 1950 to 23% in the year 2000 due to their good mechanical properties at room and high temperature. Due to increase in market demand, research and development efforts have played an important role in the dramatic growth in consumption of aluminum alloys.

Aluminum–silicon alloys are classified into three different categories: hypo-eutectic (5-10%Si), eutectic (11-13%Si) and hyper eutectic (more than 13%Si), depending on the Si content, the eutectic point occurring at ~12 wt.% Si. Change in the composition is made by the addition of alloying elements such as copper, magnesium, manganese, and iron. These are the most used alloying elements in Al-Si alloys where they form a solid solution and form intermetallic phases during solidification. Their addition makes Al-Si alloys heat treatable, where the mechanical properties of the alloy are enhanced through precipitation hardening treatment. The size, shape and volume fraction of the precipitated intermetallic phases and the eutectic structure determines the final mechanical properties [11]. The change in microstructure is strongly dependent on the alloy chemistry, solidification conditions and heat treatment.

Automotive and aerospace industries are the main areas where aluminum processing is crucial. Aluminum processing involves smelting of the metal, casting, and then carrying out suitable heat treatments to reach the desired properties in the cast part; through such processing, the manufacturing of many applications such as cylinder heads, engine blocks, pistons, and other parts is made possible. In recent years, the development of diesel and direct fuel injection gasoline engines with high generated powers has resulted in a marked performance impact on piston materials due to increased combustion pressure and piston temperatures.

Aluminum castings often are subjected to a T6/T7 heat treatment to increase their mechanical properties. These treatments generally include a solution treatment at a relatively high temperature to form a super saturated solid solution (SSSS), followed by

rapid quenching in a cold medium, such as water, where the aluminum becomes super saturated due to quench. the treatment is then age hardened at an intermediate temperature [12] . During heat treatment of aluminum alloys, residual stresses and distortion may be observed especially in castings with complex geometry due to non-uniform temperature distribution during the quenching process [12] [13].

Many automobile parts are made of aluminum alloys such as engine blocks, cylinder heads, and suspension parts, and to perform efficiently and eliminate premature failure, residual stresses must be minimized. During service, these parts undergo heating and cooling cycles which promote residual stresses. Presence of residual stresses in the casting deteriorates fatigue life and dimensional stability of the part [12]. Tensile residual stresses can result in distortion and cracking of the component during quenching or machining and if this occurs during service, it can cause a reduction in efficiency or failure of the part [13]. The presence of residual stresses and/or distortion in a structural component, such as an aluminum casting, has a negative influence on the component's dimensional tolerance, performance and fatigue life [12].

There are multiple factors that hinder the prediction of residual stresses because they are the product of all the manufacturing process stages and they can evolve during the life time of the product [1] [14]. Their influence depends on their magnitude, sign, and extent relative to the controlling length, area or volume of material associated with any particular mode of failure [1] [14]. According to the sign of the residual stresses, they can increase or decrease the levels of the applied stresses which can lead to unexpected failure [1] [15]. Since, characterizing and anticipating the residual stress induced in every location

in a component under industrial production conditions is difficult, in addition to concerns that the residual stress state might change during the long service life of the part, it is important to study the origin of the residual stresses, develop methods to measure them, study their role on failure processes and develop techniques to reduce them.

2.2 Aluminum alloys

2.2.1 Aluminum alloys designation systems

Aluminum alloys are commonly grouped into various alloy series, depending upon the alloying elements they contain. These alloys are divided into two major groups, wrought alloys and cast alloys, depending on their method of fabrication. Cast alloys are those where the melt is directly cast into the final form by one of various methods such as sand-, permanent mold-, or pressure die casting, while wrought alloys are those where casting is followed by hot or cold working to the final desired shape such as sheets, plates, tubes, forgings, etc.

Generally, in both systems, similar alloying elements are added, but in different quantities. Based on the principal alloying elements, wrought alloys are divided into seven groups starting with 1XXX and ending with the 7XXX group. 1XXX, 3XXX, 4XXX and 5XXX series are not heat-treatable, while 2XXX, 6XXX and 7XXX series are the heat-treatable groups which can be strengthened through precipitation hardening treatment [16].

The most common designation system for cast aluminum alloys is that proposed by the Aluminum Association (AA). The system uses a three digit number (i.e., lxx.x, 2xx.x, etc.) followed by a decimal point to identify the composition limits for casting [16] [17].

The first digit indicates alloying group while the second and third digits identify the specific aluminum alloy according to its alloying elements, or indicate aluminum purity for the aluminum (lxx.x) series. The decimal values (.0, .2 or .3) indicate the chemical composition limits for casting (.0) or ingots [16] [18]. A prefix letter is always included in the AA designation system to distinguish alloys of a general composition (with the same alloy number), and differing only in the percentage of impurities or minor alloying elements, e.g., 319, A319 and B319. Table 2-1 lists the AA designations of aluminum casting alloy series.

Table 2-1 Aluminum Association designation system for aluminum casting alloys [19]

Series	**Major alloying**
1xx.x	pure aluminum (unalloyed series)
2xx.x	AI-Cu
3xx.x	AI-Si-Mg, AI-Si-Cu, AI-Si-Cu-Mg
4xx.x	AI-Si
5xx.x	AI-Mg
6xx.x	Un used
7xx.x	AI-Zn
8xx.x	Al-Sn
9xx.x	Unused

2.2.2 Aluminum-Silicon alloys

Aluminum-silicon (Al-Si) alloys are an important class of materials that constitute the majority of aluminum cast parts produced, due to their superior properties and excellent casting characteristics. More than 90% of aluminum castings are made from Al–Si base alloys due to their attractive characteristics such as high strength-to-weight ratio, good workability, excellent castability, good thermal conductivity, good corrosion resistance, reduction in thermal expansion and high-temperature performance. The use of aluminum alloys has increased significantly over the past several years in numerous applications, successfully replacing iron and steel due to their high specific strength when compared to steel [20].

The automotive industry is the largest consumer of Al-Si cast alloys, where these alloys have replaced steel for the sake of greater fuel efficiency and higher performance, attributed to their much lighter weight and high thermal conductivity. Thus, Al-Si castings have gradually replaced automobile parts such as transmission cases, intake manifolds, engine blocks and cylinder heads that were formerly manufactured using steel and cast iron.

For improving the mechanical properties of Al-Si alloys, several studies have been carried out to evaluate the role of elements constituting alloys. These elements are present either as impurities or intentionally added as alloying elements, see Table 2-2.

The most common aluminum casting alloys that are used in the automotive industry are 319.0 (Al-6Si-3.5Cu), 332.0 (Al-9.5Si-3Cu-l.0Mg), 355.0 (Al-5Si-l.3Cu-0.5Mg), A356.0 (Al-7Si-0.3Mg), A357.0 (Al-7Si-0.5Mg), 380.0 (Al-8.5Si-3.5Cu), 390.0 (Al-

17.0Si-4.5Cu-0.6Mg), 413.0 (Al-12Si) and 443.0 (Al-5.2Si) alloys. Amounts of alloying elements differ between different series, leading to changes in the final properties.

Within the family of 3xx.x aluminum alloys, the Al-Si-Cu 319-type and Al-Si-Mg 356-type cast alloys are of commercial importance because of their applications in the automotive industry. These alloys have excellent castability and fluidity due to the high concentration of Si. In addition, they offer a high degree of strength, light weight and good machinability in both permanent mold and sand castings. Table 2-3 illustrates different casting properties of B319.1 and A356.1 alloys.

In the present work, the Al-Si-Cu family, represented by B319.1, was chosen for this study, due to its high demand in the automobile industry. B319.1 contains silicon, copper, and magnesium as the hardening elements. This alloy is widely used in automotive cylinder heads, internal combustion engine blocks and piano plates, as well as in other applications where good casting characteristics, weldability, pressure tightness and moderate strength are required. Alloy 319.0 refers to the composition of 319 castings, whereas 319.1 and 319.2 refer to those of the ingots. The prefixes A, B, etc. indicate the differences in impurities or minor alloying elements such as Mg. It has been reported that mechanical properties are relatively insensitive to impurities when the impurity limits are exceeded. B319.1 has a composition of 85.8-91.5 wt.% Al, 5.5-6.5 wt.% Si, 3-4 wt.% Cu, maximum 0.35 wt.% Ni, maximum 0.25 wt.% Ti, maximum 0.5 wt.% Mn, maximum 1% Fe, maximum 0.1 wt.% Mg, and maximum 1 wt.% Zn [21].

Table 2-2 Summarized effect of alloying elements in A-Si systems

Element	|Type	Effect
Antimony	alloying elements	Eutectic silicon modification by transformation from its acicular plate like form into a lamellar or fibrous form
Strontium		
Calcium		
Sodium		
Phosphorus	impurity	Reduces the effectiveness of elements such Na and Sr
Titanium	alloying elements	grain refiners
Boron		
Copper	alloying elements	enhances castability, increases strength and hardness in heat-treatable alloys at the expense of a reduction in corrosion and hot tearing resistance
Magnesium	alloying elements	enhances strengthening response of the material, improves the response of the material to heat treatment by enhancing the precipitation response during aging.
Manganese	alloying elements	neutralizes the effect of the brittle Al_5FeSi intermetallic phase by converting it to a compact Chinese script form
Iron	impurity	forms insoluble brittle intermetallics such as (Al_5FeSi) that have a direct impact on the ductility of the alloy
Silver	alloying elements	increase the age-hardening response of the alloy
Zinc		

Table 2-3 Characteristics of various aluminum-silicon casting alloys [13]

Alloy	Casting Method	Resistance To Tearing	Pressure Tightness	Fluidity	Shrinkage Tendency	Machinability
319.0	S,P	2	2	2	2	3
A356.0	S,P	1	1	1	1	3
Rating: 1- best, 5- worst; S = sand casting, P = permanent mold casting						

This alloy is rarely used in its as-cast state since it yields relatively average mechanical properties. This can be attributed to the presence of a coarse acicular silicon eutectic phase which, because of its morphology of sharp ends and edges, acts as a stress raiser for the material under an applied load. In order to enhance the mechanical properties, chemical and thermal treatments are applied to the alloy. Chemical and thermal treatments will be discussed in detail in a further section.

The melting temperature range is 675°-815°C and the casting temperature is about 675°-790°C; depending on the amount of Mg, solution heat treatment is usually carried out at a temperature of 500°C to 505°C, for 12 h (sand casting) or 8 h (permanent mold casting) at this temperature in order to (i) dissolve the solutes, mainly Cu, present in the alloy which are responsible for the hardening response; (ii) homogenize the casting, and (iii) spheroidize the eutectic silicon. Quenching is accomplished in warm water at ~65 °C. Aging using T6 temper is carried out at 150° to 155°C, for times ranging from 2 to 5 h to obtain highest mechanical properties as shown in Table 2-4 while T7 aging (> 200^0C for at least 3 h) is employed for stabilizing the properties at a higher temperature. The strength

obtained for Al–Si–Cu–Mg alloys after heat treatment is much higher than that for Al-Si-Cu alloys, where the addition of Mg provides an increase in yield strength from 337 to 415MPa for peak ageing at 150 °C, but the elongation decreases to less than 1% [1] .

In addition to good corrosion resistance and good mechanical properties, this alloy has good casting characteristics such as excellent resistance to hot cracking and solidification shrinkage, as well as excellent pressure tightness and fluidity. These characteristics make B319.1 alloy is suitable for engine block manufacturing.

Table 2-4 Typical mechanical properties of cast test bars of alloy 319.0.[16]

Property	**Sand cast**		**Permanent mold cast**	
	As Cast	**T6**	**As cast**	**T6**
Tensile strength, MPa[a]	185	250	235	280
Yield Strength, MPa[a]	125	165	130	185
Elongation, %	2	2	2.5	3
Hardness, HB[b]	70	80	85	95
Shear strength. MPa	150	200	165	185
Fatigue Strength, MPa[c]	70	75	70	-----
Compact Yield Strength, MPa	130	170	130	-----
(a) In 50 mm or 2 in. (b) 500kg load; 10mm ball, (c) at 5* 10^8 cycles; R. R. Moore type test.				

2.2.3 Microstructure of Al-Si-Cu alloys (B319.1)

Al-Si-Cu alloys such as B319.1 contain Si and Cu as the main alloying elements and maybe small additions of Mg, and to some extent, impurity elements such as Fe, Mn, Ni, and Cr. During solidification of B319.1 alloy, the main sequence of phase precipitation occurs as follows: the primary α-Al dendrite network forms first at ~608°C, followed by the main Al-Si eutectic reaction at ~563°C, and the formation of $CuAl_2$ at about 550°C; with Mg_2Si and other complex phases precipitating from the remaining liquid towards the end of

solidification. An example of these phases is shown in Figure 2-1. The development sequence that occurs during solidification is listed in Table 2-5, while describes the characteristics of the phases formed. Depending on the alloying content of the alloy and solidification rate, formation of brittle intermetallic phases such as α AI_{15} $(Mn, Fe)_3Si_2$ and /β-A_{l5}FeSi takes place. Finally, solidification ends with the Al-Si eutectic reaction accompanied by the formation of eutectic Si particles and precipitation of eutectic phase and eutectic $CuAI_2$ phase [22].

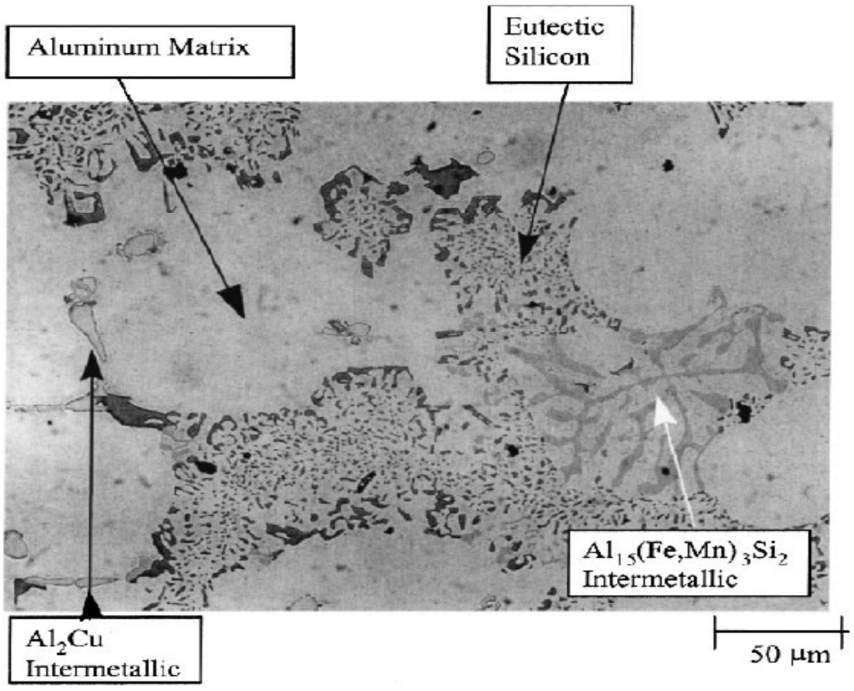

Figure 2-1Typical microstructural features observed in a 319-type aluminum alloy [23]

Commercial Al-Si foundry alloys normally contain about 50 to 90% vol. Al-Si eutectic and the remaining phases are α-Al dendrites, Fe bearing intermetallics such as β-Al5FeSi and α-$Al_{15}(Fe,Mn)_3Si_2$, eutectic and blocky Al_2Cu and some Mg bearing phases such as $Al_5Mg_8Cu_2Si_6$ and Mg_2Si [23]. During solidification of the Al-Si alloy, silicon

phase form in the shape of acicular shape which has a devastating effect on the mechanical properties of the alloy.

In 1920, Pacz [24] discovered that Al-Si alloys containing 5 to 15% Si could be treated with an alkali fluoride (sodium fluoride) to ‘modify’ the morphology of the silicon phase from its harmful acicular lamellar shape to smaller rod shaped particle clusters (partially modified) or a fine fibrous structure (fully modified) that improved the ductility and machinability of the alloy. Thereafter, the study of modification was investigated by several researchers, earlier studies dealing mainly with the use of Na as the modifying agent [24] [25]. The use of strontium as a better alternative was reported by Hess and Blackmun [26] in the 1970’s, following which numerous investigations were carried out to examine the effect of Sr as a modifier of Al-Si alloys with respect to improving the alloy properties as well as the increase in porosity associated with its addition. While several elements are known to cause eutectic Si modification, Sr is the modifier of choice in current foundry operations. In addition to such chemical modification, modification may also be obtained through heat treatment, where the eutectic Si particles undergo fragmentation, dissolution and spheroidization during the solution treatment stage. The morphology of unmodified, partially modified and fully modified Al-Si eutectic is shown in Figure 2-2.

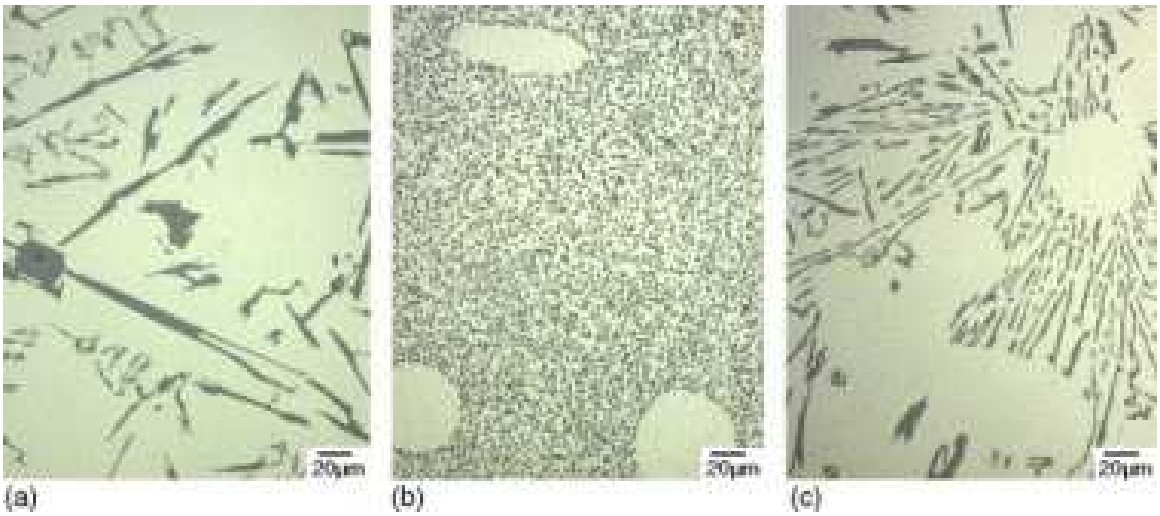

Figure 2-2Optical micrograph showing Al-Si eutectic morphology: (a) unmodified, (b) fully modified, (c) partially modified [25]

A significant decrease in melting point and eutectic temperature of Al-Si-Cu alloys due to the addition of copper which cause noticeable enhancement on the heat treatability of aluminium alloys. Copper phases can solidify in two different forms: blockyAl_2Cu and eutectic Al_2Cu. The eutectic Al_2Cu morphology is characterized as an alternating lamellar structure consisting of Al_2Cu and α-Al, while the blocky Al_2Cu form appears as large particles (20-40μm) embedded in the α-Al matrix. Depending on the alloying element and cooling rate, the evolution of one form may be favored over the other. High solidification rates promote the formation of the eutectic Al_2Cu phase, while Sr modification increases the fraction of the blocky Al_2Cu phase [27] [28] [29], see Figure 2-3.

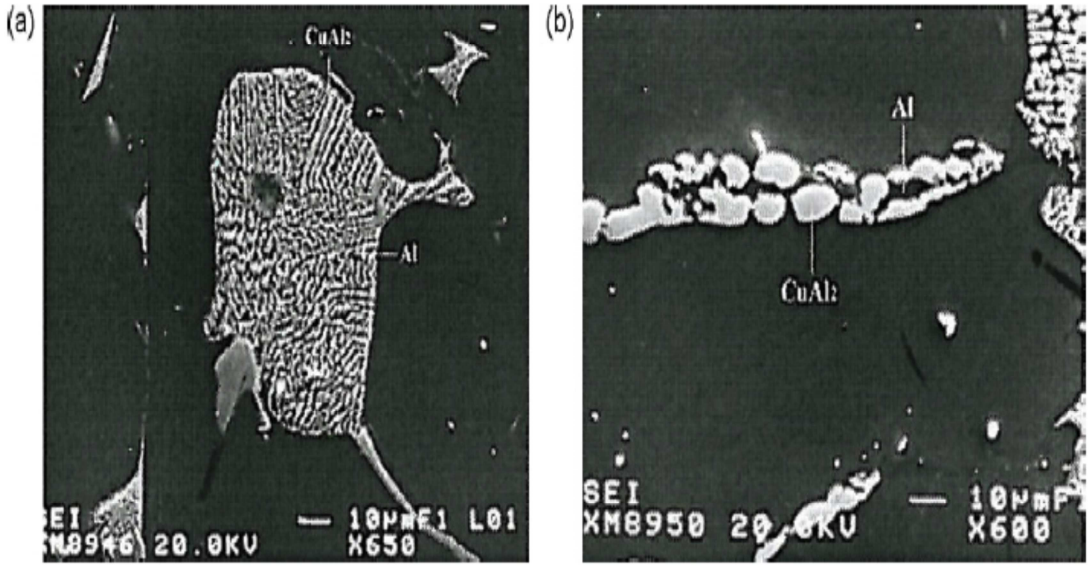

Figure 2-3 Eutectic Al_2Cu and (b) blocky Al_2Cu[29]

Table 2-5 Reactions observed during solidification of alloy 319 [30]

Reaction No.	Reactions	Suggested Temperature (°C)
1	Development of dendritic network	609
2a	Liq. --->Al + $Al_{15}Mn_3Si_2$	590
2b	Liq.---> Al +Al_5FeSi+ $Ali_5Mn_3Si_2$	590
3	Liq.---> Al + Si+ Al_5FeSi	575
4	Liq.---> Al +$CuAl_2$+ Si+ Al_5FeSi	525
5	Liq.---> Al + $CuAl_2$ + Si + $Al_5Mg_8Cu_2Si_6$	507

Table 2-6 Phases observed by optical microscopy/SEM/EDX in alloy A319

phase	**α -Al***	**Si***	**$CuAl_2$***	**Al_5FeSi***	**$Al_{i5}Mn_3Si_2$**	**$Al_5Mg_8Cu_2Si_6$**
Char.	Dendrite	Gray	Pink particle	Needle	Brown Chinese script	Brown bulk
* Confirmed by X-Ray Diffraction (XRD)						

The mechanism of Al_2Cu precipitation in modified 319 alloys is represented schematically by the model depicted in Figure 2-4, which illustrates the different stages of solidification where the formation of the α-aluminum dendrite network is associated with segregation of Si and Cu in the liquid. As the temperature approaches the Al-Si eutectic temperature, rounded/fibrous Si particles precipitate, leading to a local concentration of Cu in the remaining areas.

Magnesium (Mg) is commonly added in the B319.1 alloy, which has an impact on both the mechanical properties and the final micro structure. Accelerating the dissolution and precipitation kinetics during heat treatment, accompanied by increasing strength are the main effects of Mg addition on mechanical properties level. As for the microstructure, low Mg additions lead to the formation of the quaternary $Al_5Mg_8Cu_2Si_6$ intermetallic phase, which forms in the interdendritic regions together with small globular Mg_2Si particles clustered with the eutectic Si phase [31]. According to Sameul et al. [30], the $Al_5Mg_8Cu_2Si_6$ intermetallic phase forms at the end of solidification where it grows out from Al_2Cu. Finally, Mg addition also promotes the formation of Al_2Cu [31] [32] .

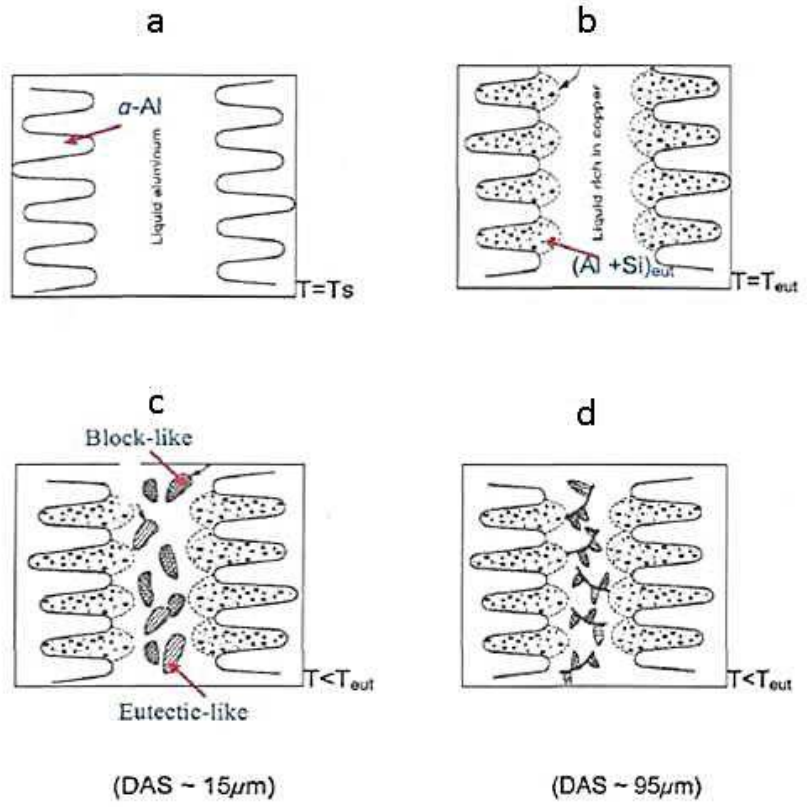

Figure 2-4 Schematic diagram demonstrating different solidification stages of modified 319 alloy (a) formation of α -Al dendritic network, (b) formation of eutectic Si, (c) precipitation of both blocky and eutectic Al_2Cu, SDAS-15 μm and (d) dominance of blocky Al_2Cu [28] .

2.2.3.1 Iron intermetallics in Al-Si-Cu alloys

Control of iron content is mandatory in most aluminum production as iron forms brittle and hard insoluble intermetallics detrimental to the mechanical properties. The presence of Iron as an impurity stems from the bauxite and steel equipment used during production and from remelted scrap castings. The most common iron intermetallics phases observed in casting alloys are monoclinic/orthorhombic β-AlFeSi and hexagonal α-AlFeSi, and [33]. Iron intermetallics have a negative effect on the ductility and tensile strength of aluminum alloys [2], particularly at low cooling rate normally observed in sand mold

casting. At low cooling rate, the platelet-shaped β-AlFeSi phase is formed which has a relatively low bond strength with the matrix. The platelets, which appear as needles in a cross-section, act as stress raisers and facilitate cracking [23] [33] [34]. They also increase porosity by blocking feeding of liquid metal in interdendritic regions during solidification. Compositions such as Al_5FeSi and $Al_9Fe_2Si_2$ have been reported for this phase [35]. Higher cooling rates tend to reduce the average size of these.

The α-iron phase, with its Chinese script morphology, exhibits an irregular, curved growth, conforming to the shape of the spaces between the α-Al dendrites. It has several forms such as α-$Al_{12}Fe_3Si_2$, α-$Al_{15}Fe_3Si_2$, α-Al_8Fe_2Si and α-$Al_{15}(Fe,Mn)_3Si_2$, where the latter phase is another form of the α-iron phase, known as sludge that is observed in the form of star-like or polygonal particles [35]. The α-phase is considered less detrimental to the mechanical properties than the β-phase because of its more compact morphology that reduces the stress concentration at the particle-matrix interface, which improves the mechanical properties of the 319.

Iron may also be added deliberately as an alloying element for enhancement of specific properties such as improving the high-temperature strength of Al-Cu-Ni alloys and improving corrosion resistance at elevated temperature in Al-Fe-Ni alloys, despite its negative effect on the strength and ductility of aluminum alloys. A higher amount of iron may be permitted (above 0.8%) in permanent mold and pressure die-cast alloys because of the higher cooling rates obtained with these casting processes compared to sand molds leading to the formation of finer iron intermetallic particles. Another reason for increasing

the iron content in permanent mold and pressure die-cast alloys is to prevent sticking between the metal and the mold [35].

Several studies have introduced techniques in an attempt to neutralize the deleterious effect of the β-AlFeSi iron Intermetallics using suitable neutralizers such as Mn, Cr, Be, Co, Mo, Ni, V, W, Cu, Sr, or the rare earth elements [35] [36] [37]. The addition of these elements suppresses the formation of the β-AlFeSi, and promotes that of the α-AlFeSi phase instead, in Chinese script, polyhedral or star like shape [38]. Figure 2-5 illustrates the change in morphology of the iron phase using Mn as a neutralizer. Other factors which influence the extent of morphology modification using neutralizers are the cooling rate, heat treatment, initial Si and Fe content, and other elements.

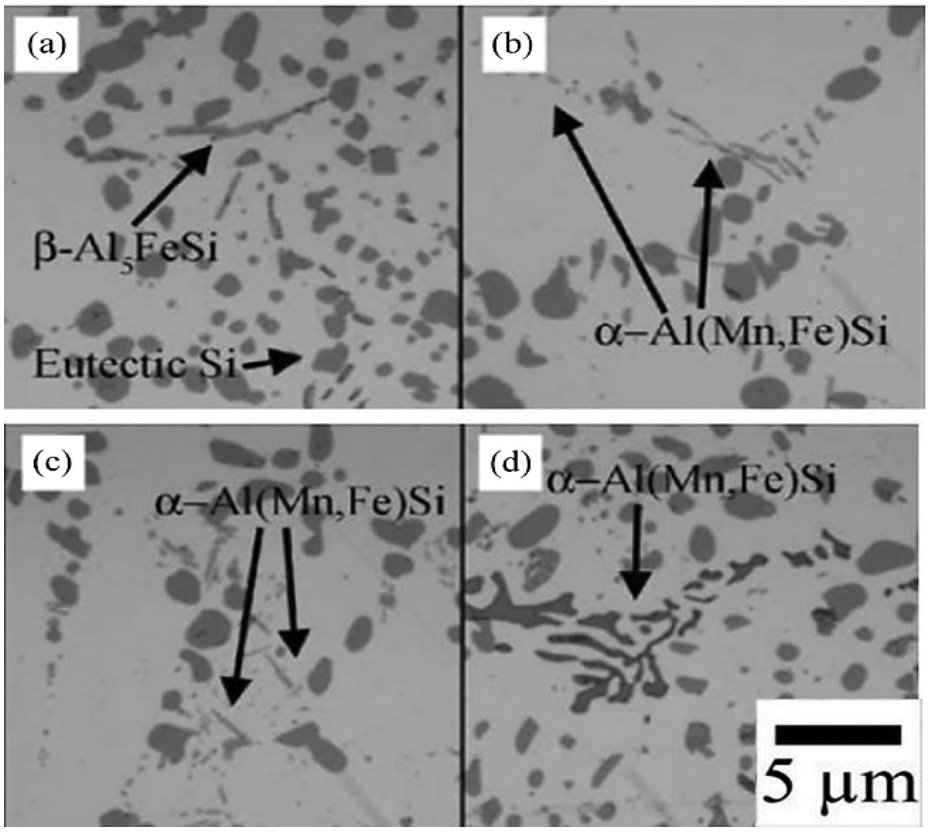

Figure 2-5 Morphology of a-$Al_{15}(Fe, Mn)_3Si_2$ particles (a) 0.2% Fe, (b) 0.2% Fe-0.07% Mn, (c) 0.2% Fe-0.13% Mn, and (d) 0.2%Fe-0.2% Mn [35].

2.2.4 Heat Treatment

A heat treatment process comprises a set of heating and cooling operations that are performed for the purposes of changing the mechanical properties, the metallurgical structure, or the residual stress state of a metal product. Strengthening of aluminum is achieved during heat treatment through precipitation hardening [39]. Precipitation hardening is one of the major methods used to enhance the mechanical properties of heat-treatable Al-Si alloys. The main objectives of precipitation hardening heat treatment can be summarized as follows [24]:

- Increase strength and produce the particular mechanical properties that are associated with specific final tempers,
- Stabilize mechanical or physical properties or resistance to corrosion, and avoid changes that would otherwise occur with time at normal or elevated temperatures,
- Ensure dimensional stability during service, particularly for parts that operate at elevated temperatures and require close dimensional control.
- Relieve residual stresses induced by differential deformation or non-uniform cooling resulting from casting, quenching, welding or forging operations

The basic requirement for an alloy to be amenable to age-hardening is a decrease in the solid solubility of one or more of the alloying elements present with decreasing temperature. Three basic operations are carried out when heat treating aluminum castings: solution heat treatment, quenching, and aging.

B319.1 alloys are heat treated using either T6 or T7 treatments. When full strength is required, the T6 treatment is desired. This treatment involves solution heat treatment, quenching, and precipitation hardening through artificial aging (150-180^{0}C). When the aim of the treatment is to improve corrosion resistance and/or to increase the stability and performance at elevated temperatures, the T7 stabilization treatment is applied. The T7 treatment involves the same steps as the T6 treatment, except that the artificial aging is carried out at higher temperatures (200-240°C) [19].

2.2.4.1 Solution Treatment

The first stage in a heat treatment process is solution treatment, where the alloy is heated to a suitable temperature and held at that temperature long enough to allow the constituents, mainly hardening solutes such as Cu and Mg, to become supersaturated in solid solution in the aluminum matrix, followed by quenching (cooling) the alloy rapidly enough to avoid precipitation of the excess solute.

Figure 2-6 illustrates the required solubility-temperature relationship needed in precipitation strengthening accompanied with the temperature ranges required for solution treatment and subsequent precipitate hardening in the aluminum-copper system. To start the solution treatment process, the alloy - which is composed of α and small amounts of second phase θ-Al_2Cu is heated at a temperature higher than the solvus temperature to produce a single homogeneous solid solution α, allowing dissolution of the second phase θ and eliminating the segregation in the alloy [1]. The solution treatment temperature is considered an important factor that determines the final properties of the alloy, where higher solution treatment temperatures lead to greater dissolution of chemical heterogeneities and result in a more homogenized structure.

In the case of Al-Si-Cu-Mg alloys, the purpose of the solution heat treatment process is to [29] dissolve soluble phases containing Cu and Mg formed during solidification, homogenize the alloy, and spheroidize the eutectic Si particles [29]. The main objective for an effective solution treatment process for Al-Si-Cu alloys is to modify the Al-Si eutectic morphology and dissolve the Al_2Cu particles which appear either in blocky or eutectic form as mentioned previously. The modification of the eutectic Si

morphology has been observed to occur in the following sequence during solution heat treatment (SHT): (1) necking of acicular Si particles, (2) fragmentation of Si particles, (3) spheroidization of fragments, and (4) coarsening of spherical Si particles. This process is highly dependent on the solution temperature and the amount of modification that occurs during casting. At high solution temperatures, the diffusion rates are high which aid in morphological modification rates.

It has been found that the dissolution mechanism for eutectic Al_2Cu takes place by fragmentation into smaller segments that spheroidize and finally dissolve by radial diffusion of Cu into the surrounding matrix, as illustrated in Figure 2-7. On the other hand, the Al_2Cu blocky form dissolves only by spherodization with no fragmentation of the particles which is considered a harder process for dissolution [1] [40]. The dissolution of Al_2Cu is a time-consuming process as the operation is directly dependant on solution heat treatment temperature and the shape of the Al_2Cu [41]. In addition to the morphology of the secondary phases, alloy chemistry, specifically the Cu and Mg concentrations, secondary dendrite arm spacing (SDAS) are the other factors that influence the final amount of dissolution.

To reach the full extent of SHT process and in order to achieve the full aging potential of the alloy, it is important that Mg-and Cu-containing phases dissolve through solution treatment. Copper and magnesium compounds (θ –Al_2Cu and β-Mg_2Si) are easy to dissolve while Q-$Al_5Cu_2Mg_8Si_6$ is harder to dissolve. on the other hand, iron intermetallics particles are hard to dissolve where phases such as β-Al_5FeSi platelets undergo gradual dissolution at very high solution temperature for time, while phases such as α-

$Al_{15}(Fe,Mn)_3Si_2$ (Chinese script) phase is not affected through the solution treatment process [41].

In order to achieve best dissolution of Al_2Cu for SHT, it is highly recommended that the process is carried out at a temperature, in the range of 480-500°C on the process temperature while avoiding incipient melting of copper intermetallics phases for alloys with low amounts of Mg (Mg <0.5%). On the other hand, dissolution of Al_2Cu phase was found to be effective when carried out at 520°C for B319.1 with higher amounts of Mg [1] [42]. Increasing solution temperature can raise the risk of incipient melting of Al_2Cu phases which results in shrinkage cavities, thereby causing distortion of the casting and substantially reduced mechanical properties [40] [41] [43].

After completion of the solution treatment stage and in order to limit the diffusion process of the atoms toward potential sites of nucleation, quenching is applied rapidly. This process leads to the formation of super saturated solid solution (SSSS) which is a non-equilibrium phase. Finally, to stabilize this unstable structure, aging starts where the atoms of Cu diffuse to several sites of nucleation and fine precipitates are formed [1].

The standard T6 treatment specifies that the solution heat treatment should be carried out at approximately 500°C and maintained for 4-12 hours depending on the casting method. Shorter periods of time are recommended for permanent mold castings and longer times for sand castings. Several studies have been carried out with the intent of optimizing solution treatment process during precipitation strengthening of B319.1 alloy. Samuel et al. [41] [44] stated that the best solution treatment for B319.1 was at 495°C for 8 hours where optimum dissolution of $CuAl_2$ is observed. They also reported that the Al_2Cu phase is

observed in two forms, the blocky form and finer eutectic form where the latter is more likely pronounced in the alloy structure. This phase was found to start fragmentation and dissolution at 480°C, the process being accelerated at higher temperatures [41] [43].

Figure 2-8 shows a schematic diagram by Samuel et al. [44], which illustrates the change in strength (yield or ultimate tensile strength) for the 319 Al alloy (Mg content < 0.3wt%) as a function of solutionizing temperature. Region I corresponds to the change in tensile properties due to the onset of dissolution of Al_2Cu. Region II represents the recommended solution treatment temperature range. Region III represents a continuation of region II until peak properties are attained, which indicates the start of incipient melting, while Region IV corresponds directly to the advance of incipient melting with the increase in solution temperature [44].

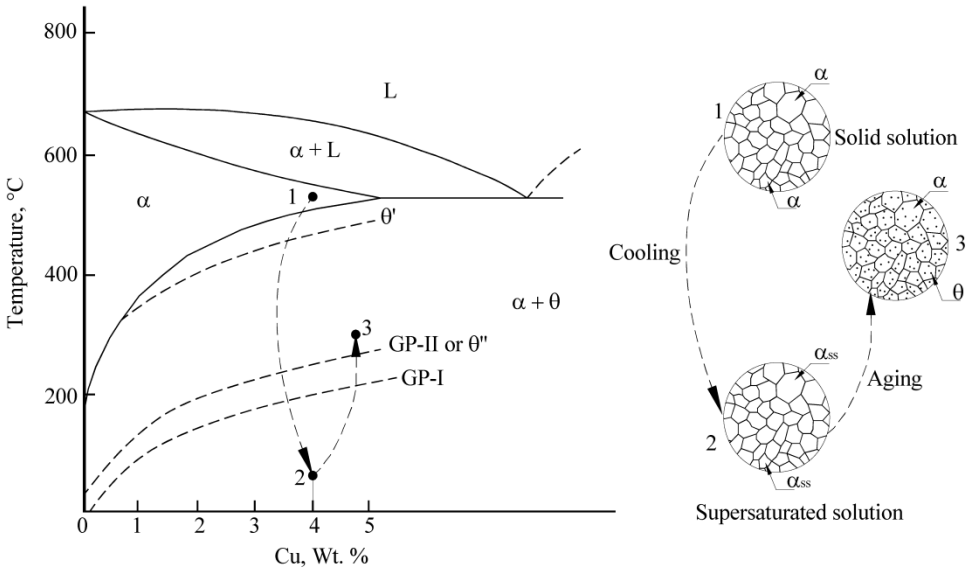

Figure 2-6 Aluminum-cooper phase diagram rich in aluminum showing the solutionization and precipitation process [1].

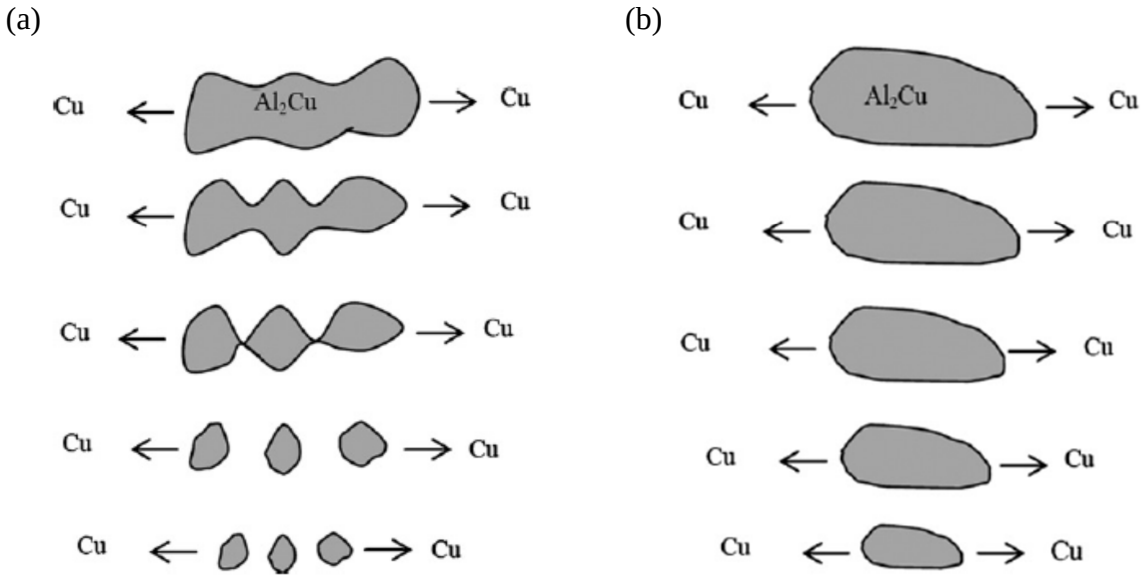

Figure 2-7 Dissolution process of (a) eutectic Al_2Cu and (b) blocky Al_2Cu particles [29]

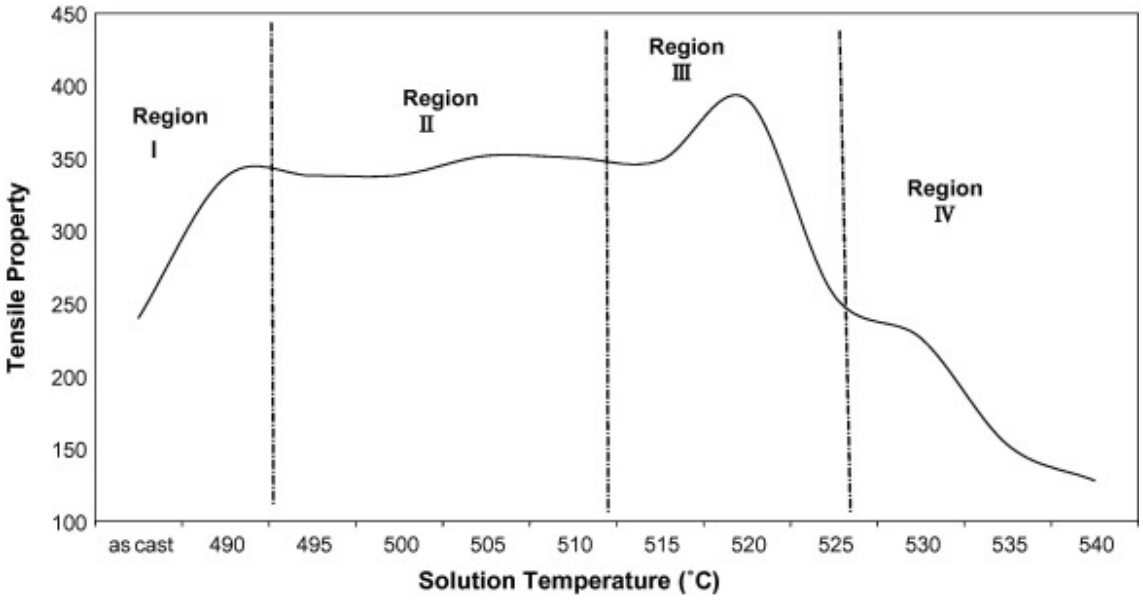

Figure 2-8 Schematic showing tensile strength of 319 alloy as a function of solution treatment temperature [44]

2.2.4.2 Quenching

This stage is largely dependent on the degree of supersaturation and on the diffusion rate of the constituents. Quenching must be performed as soon as solution treatment is completed in order to suppress precipitation and maintain the super saturated solid solution developed from the solution treatment and produce a high number of vacancies. If not, precipitation will occur at grain boundaries which will reduce the yield stress after aging. Quenching should be carried out as fast as possible to avoid nucleation and growth of precipitates. For most Al-Si casting alloys precipitates form rapidly due to a high level of supersaturation and a high diffusion rate of copper and magnesium in α-matrix [45].

In the quenching, the balance between fast quenching and the minimization of residual stresses and distortion which occur with fast quenching is required. The quenching must be initiated within the 45 seconds after finishing the solution treatment stage [46]. Any delay in the quenching will result in a temperature drop and rapid formation of coarse precipitates in a critical temperature range at which the effects of precipitation are ineffective for hardening purposes which are highly dependent on the quench sensitivity of the alloy.

Generally, wrought alloys are quenched in cold water while cast alloys are quenched in hot water between 65^0C and 80^0C or poly alkaline glycol or forced air [46]. After the quenching stage of the T6 treatment, the next stage is aging during which precipitation hardening of the alloy takes place.

2.2.4.3 Aging

The aging step is the final stage of precipitation hardening strengthening where diffusion of solute atoms takes place at several nucleation sites to stabilize the developed super saturated solid solution (SSSS) phase. Strengthening of the structure starts at this stage when dispersed second phase particles are generated where they act as obstacles to dislocations. The degree of hardening depends on the volume fraction and size of the particles and the interaction of these particles with dislocations [1]. Depending on the temperature used there are two types of aging one is at room temperature (natural aging) and one at an elevated temperature in the range of 150–240°C (artificial aging).

Al–Si–Cu alloys harden slowly at room temperature. Higher temperatures are used to accelerate the aging process so artificial aging is preferred for such alloys. In aging treatment of Al-Cu, the sequence of precipitation of the second phase θ is illustrated in Table 2-7. First, Guinier-Preston or GP zones form as two-dimensional discs, about 3 to 5 nm in diameter. As aging progresses, these zones increase in number and are ultimately replaced by the θ' phase. Subsequently, a transition phase θ' forms and coexists with θ" where they are coherent to semi coherent phases with the aluminum matrix and resulting in hardening of Al-Cu alloys. Finally transformation of semi coherent θ" phase to the non-coherent equilibrium phase θ (AI_2Cu) [19].

The same sequence occurs when aging Al-Si-Cu-Mg but several hardening phases formed such as θ' (AI2Cu), namely β" (Mg2Si), S' (Al_2CuMg), and the quaternary phase Q-AlMgSiCu [47]. These phases are formed by the additions of both Cu and Mg as alloying elements with Al-Si alloy. Precipitation of theses phase depends on the Mg:Si ratio, copper

concentration, and aging temperature [46]. These additions allow for a good combination of mechanical properties through precipitation of θ', β" and S'[48]. Alloy 319 belongs to the family of Al-Si-Cu, with minor additions of Mg to increase the response to heat treatment through the precipitation of the abovementioned phases.

Table 2-7 Precipitation-hardening system of Al-Cu alloys [19]

SSSS (α)	⟶	G.P zones	⟶	θ″	⟶	θ′	⟶ θ
				Disk-Like Coherent		Disk-Like Semi-Coherent	Al_2Cu Equilibrium Incoherent

Many investigations have been made to study the effect of alloying elements and their role in enhancing the mechanical properties of B319.1 alloy. It was found that the mechanical properties of cast components are largely dependent on the shape and distribution of Si particles in the matrix. Optimum tensile, impact and fatigue properties are obtained with small, spherical and evenly distributed Si particles which can be achieved through the addition of strontium [49]. The Sr addition converts or 'modifies' the large brittle eutectic silicon flakes in the as-cast non-modified alloy to a fibrous form. The fibrous morphology is much easier to fragment and spheroidize during solution treatment, so that the mechanical properties may be enhanced using shorter solution treatment times [1]. Silicon also imparts heat treating ability to the casting through the formation of compounds with Mg [50].

Increasing the level of Cu improves the strength of the aluminum alloy through the formation of Cu based precipitate such as Al_2Cu during heat treatment. Mg as an alloying element leads to the precipitation of Mg_2Si which results in a pronounced improvement in strength properties of Al-Si alloys. Thus, additions of Mg, Si, and Cu increase the

mechanical strength sacrificing some of the B319.1 alloy ductility. Usually, small amounts of Mn and Cr have been used in order to modify the microstructure and thus improve the ductility of the alloys [51].

2.2.4.4 Strengthening mechanism of precipitation hardening treatment

Hindrance of dislocation movement is the main cause for strengthening aluminum alloys using heat treatment. The strength is determined by the size and distribution of the precipitates and by the coherency of the precipitates with the matrix and their interaction with dislocation movement. Some mechanisms have been introduced, involving interactions of the precipitated particles with dislocations such as Orowan looping and particle shearing. If the particle is big and hard, Orowan mechanism suggests that dislocations will bypass the particle either by looping or cross-slip and the particle will remain unchanged as illustrated in Figure 2-9. These mechanisms are greatly dependent on the coherency of the particle with the matrix and the inter-particle spacing. If, however, the strength and size of the particles are such that the maximum resistance force is attained, then the shearing mechanism will prevail, as shown in Figure 2-10 [1] [2].

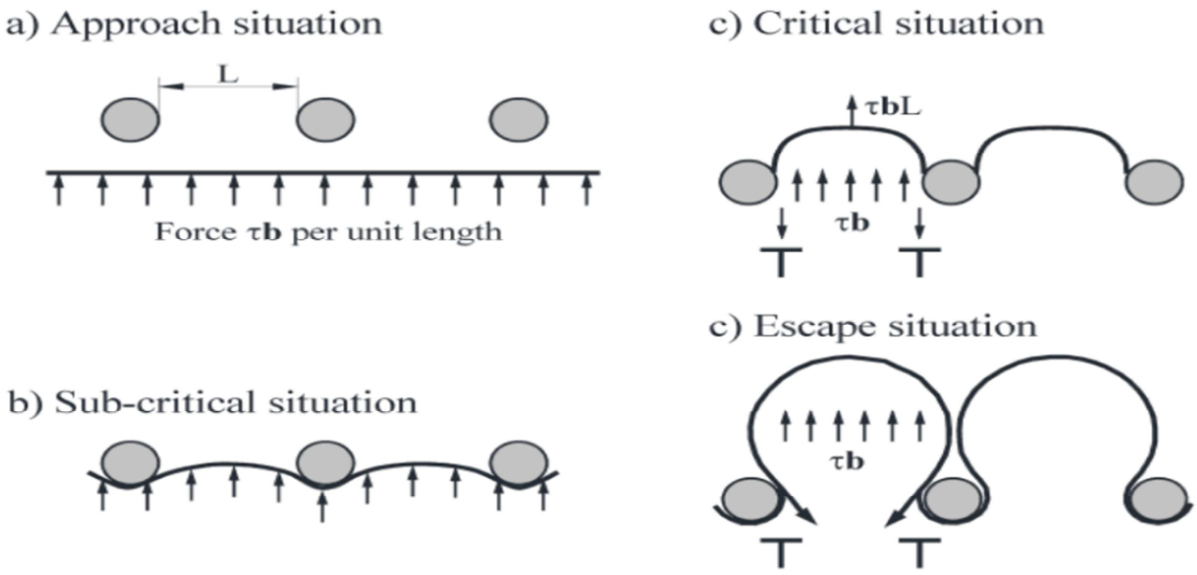

Figure 2-9 Precipitation hardening strengthening mechanism: dislocation release at higher stresses may occur by Orowan looping or by cross-slip [2]

.

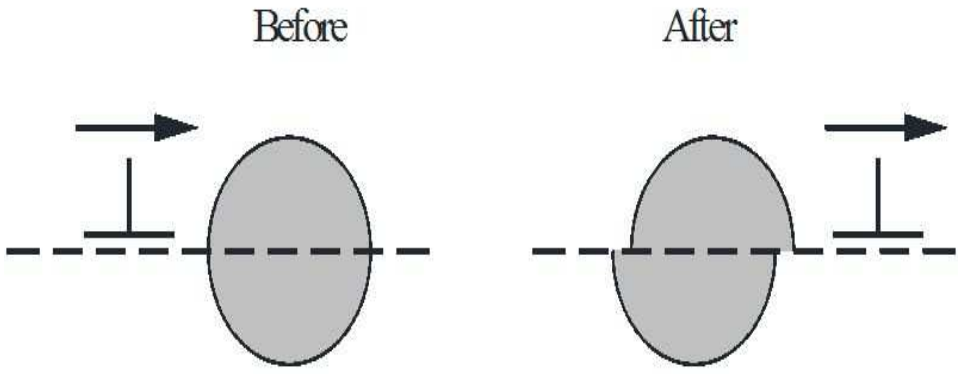

Figure 2-10 Particle shearing mechanism [2]

2.3 Residual stresses

2.3.1 Residual stresses classification

Residual stress is generally referred to as an internal stress, which exists in equilibrium in a component in the absence of any external forces or constraints, temperature gradients, or any other external influences [52]. Residual stresses as shown in Figure 2-11 can be classified into two groups according to their origin: The first one is macroscopic residual stresses which correspond to the residual stresses originating from heat treatment, machining, and mechanical processing, while the second group is microscopic residual stresses which are often originate from lattice defects such as vacancies, dislocation pile-ups and thermal expansion/contraction mismatch between phases and constituents, or from phase transformations [12] [52].

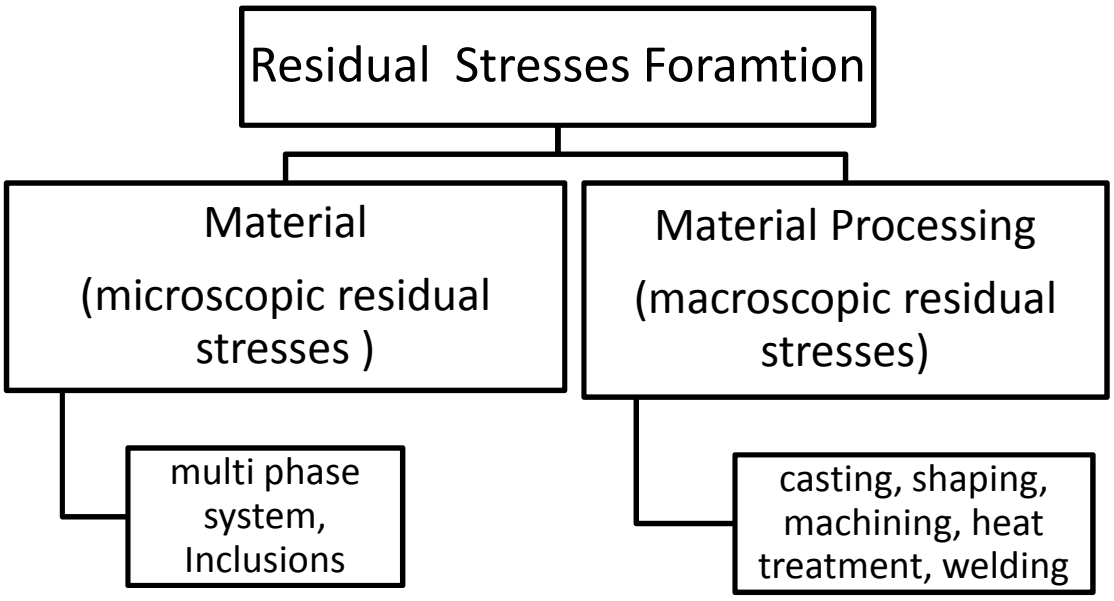

Figure 2-11 Origin of residual stress formation

The most common classification for residual stresses is represented in Figure 2-12. The classification is based on effect range of the residual stresses, where the residual stress

is classified to Type I, Type II, or Type III. Type I corresponds to the macrostresses. This type represents residual stresses that develop in the body of a component on a scale larger than the grain size of the material. Type II represents microstresses which affect only a few grains such as what happens in phase transformations. Type III represents residual stresses that exist within a grain, essentially as a result of the presence of dislocations and other crystalline defects [3].

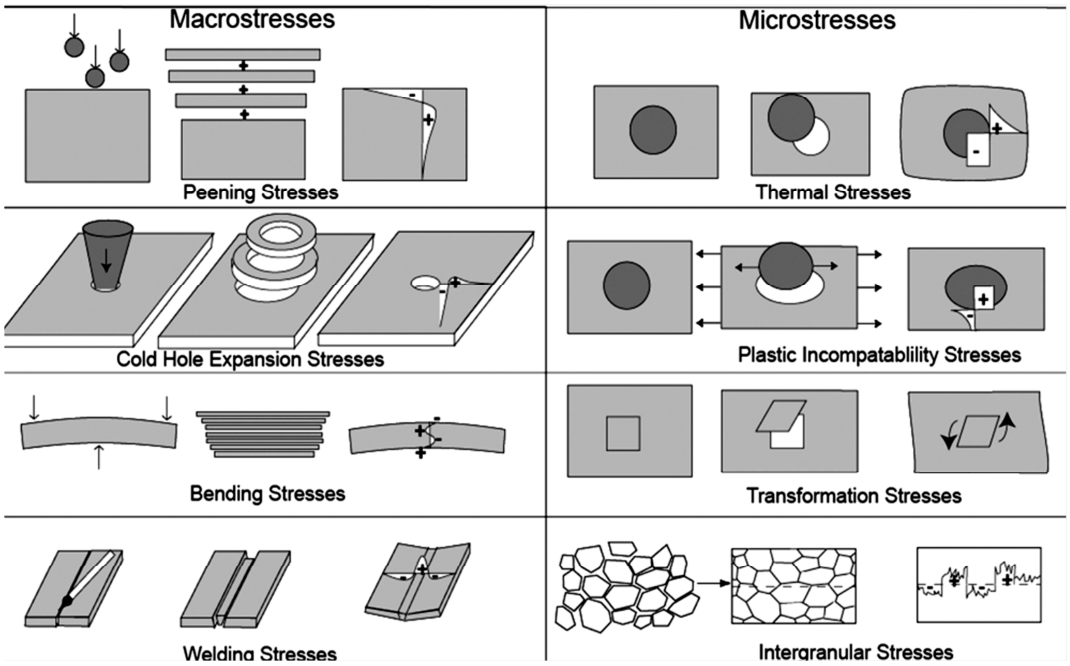

Figure 2-12 Examples of different types of residual macro and micro-residual stress and the resulting stress pattern [1].

2.3.2 Sources of residual stresses

Plastic deformation, thermal stresses, phase transformation, multi-phase materials, and welding are the main sources for residual stresses in any component [1] [3] [53]. Residual stresses are an accidental result or a by-product of processing conditions such as welding, forging, extrusion, casting (particularly after heat treatment). Millions of dollars

have been spent by Boeing Corporation to handle the distortion of aluminum 7050-T7452 encountered during machining due to the presence of residual stresses [52]. Residual stresses can affect the material integrity irrespective of how the part is obtained, whether through casting, or forging, or other means.

The main source of residual stress development is when a component undergoes non-uniform plastic deformation. The first source for such deformation is mechanical. Most shafts or rods are machined by turning, a process that often induces tensile residual stresses near the surface. For example, after unloading, any specimen undergoing bending will experience residual tensile stresses from the surface below and residual compressive stresses on the top surface.

Another major source for residual stresses is due to thermal gradient. Non-uniform heating or cooling such as in quenching can lead to severe thermal gradients and the development of large internal stresses. For non-uniform heating or cooling, the different regions of the material expand or contract by differing amounts, which is dependent on the temperature at each specific region of the component.

A mechanism was introduced by Lados et al. [52] to explain the origin of residual stresses inside a casting during cooling. According to the mechanism, shown in Figure 2-13 the casting specimen will show distortion resulting from compressive stresses at the outer layer and tensile stresses at the core of the casting [52]. During quenching, high significant residual stresses are generated and distortion may occur if these stresses exceed the yield stress [3].

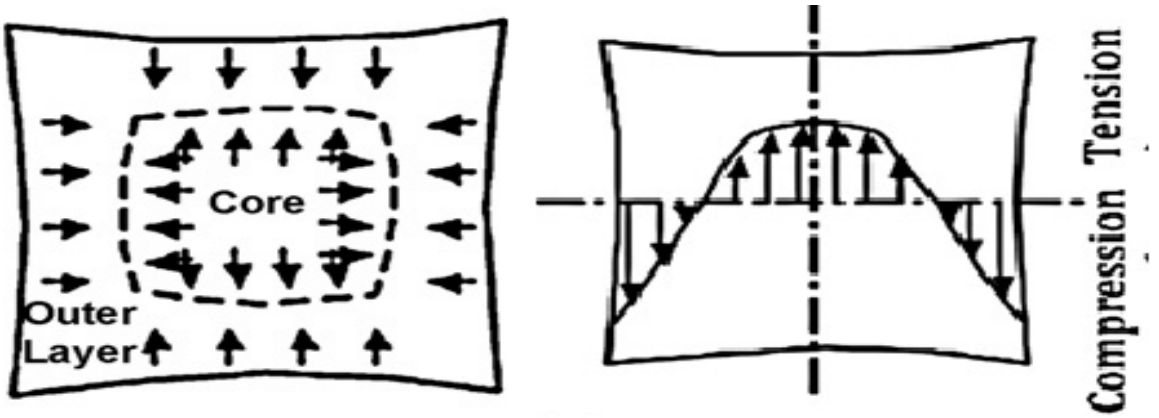

Figure 2-13 Final stage residual stresses [52]

The progress of this mechanism is represented in the Figure 2-14 and takes place through three different stages. The first stage starts with cooling of a large hot ingot. The temperature difference between the edges and center of the ingot results in significant contraction of the cold edges, leading to strain misfit between the cold edges and the hot center and thereby producing residual stresses. During the second stage, the hot center of the ingot has lower yield strength compared to the cold edges, so that plastic deformation will occur in the center to relax some of the compressive stresses induced from Stage one. After cooling of the center, the total contraction at the center will be greater than at the edges, resulting in tensile residual stresses at the center and compression residual stresses at the edges [2].

Due to the strain mismatch related to the difference in contraction between cool and hot parts of the casting during the quenching process, residual stresses arise, leading to large distortions especially in thin sections, necessitating expensive hand finish [2]. During machining, distortions may occur by the development and rearrangement of residual

stresses. Finally, the residual stresses can shorten fatigue life of a component. To summarize, residual stresses in any cast component can result from the following [3]:

- Temperature gradient within the casting
- Hindrance to contraction by the mold; and
- Phase transformation during cooling

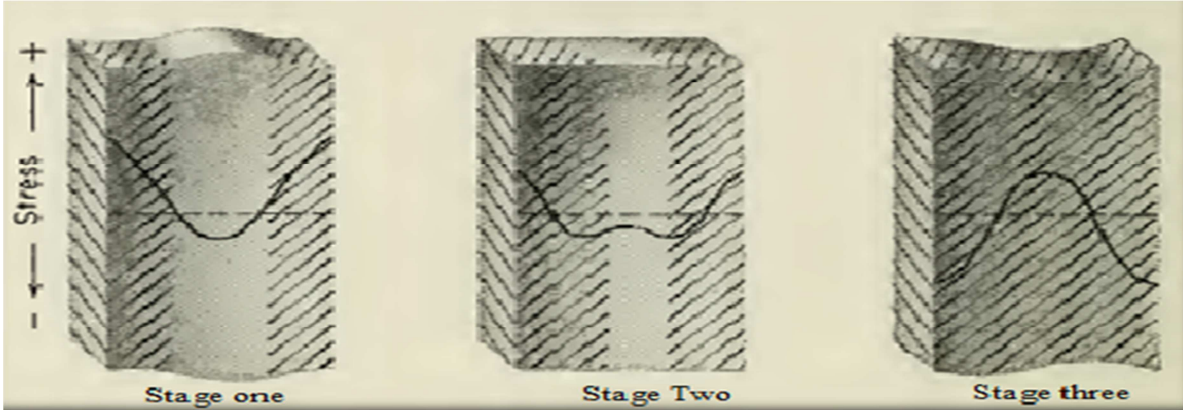

Figure 2-14 Residual stresses inside a casting ingot [2]

The magnitude of residual stress depends on the stress-strain behavior and the degree of the temperature gradient attained during the quenching operation, which produces strain mismatch. It is found that the magnitude of the residual stresses is directly proportional to the yield stress and young's modulus (E). Furthermore, the stress-strain behavior at elevated temperature is an important factor in determining the amount of residual stresses [2]. Certain physical properties also increase the amount of strain mismatch (residual stresses) such as low thermal conductivity (k), high specific heat (c), high coefficient of thermal expansion (α) and high density (ρ) [2].

2.3.3 Methods of stress relief

Residual stresses are often regarded as undesirable and harmful. Prolonging service life of any product can be achieved if such harmful residual stresses are eliminated or reduced. Several methods have been introduced in order to reduce these residual stresses. Annealing is one of these methods which involves exposing the material to very slow rates of cooling and heating with the aim of relieving stresses without altering the microstructure. If the temperature is too high then recrystallization might happen, leading to change in properties such as the yield stress which may not be desirable. The residual stresses relaxation by annealing occurs by one of two main mechanisms. The first is plasticity caused by reduced yield strength at an elevated temperature where instantaneous relief of stress occurs as the temperature is increased. The second mechanism is a creep based mechanism, which allows stress relief to occur over time [1] [54] .

By changing the nature of residual stresses from harmful to useful residual stresses is the second method of stress relieving which involves placing the surface in residual in-plane compression. This technique can be achieved by shot peening, laser peening, burnishing and fretting. The last method is called the pre-stretching or shake down method which involves putting the component under vibrational stresses below the elastic limit or introducing local plastic deformation[1].

Lados et al. [52] suggested an uphill quenching method in order to minimize the residual stresses in Al–Si–Mg cast components. This technique is frequently employed in aluminum parts that have critical tolerances and are subject to heat treatment and/or heavy machine cutting operations [52]. The uphill quenching technique involves a rapid raise in

temperature from a low quenching temperature to a higher one followed by sub-zero quenching (Figure 2-15). The resulting residual stresses are of opposite nature compared to the old residual stresses. This will balance the initial residual stresses originating from the initial quenching, and result in lowering the overall residual stresses produced [52]. The use of this technique results in significant reduction in residual stresses produced during quenching [52]. This concept of an "uphill quench" has been used in aluminum alloys to reduce quenching stresses by as much as 80 % at temperatures low enough to prevent softening [2].

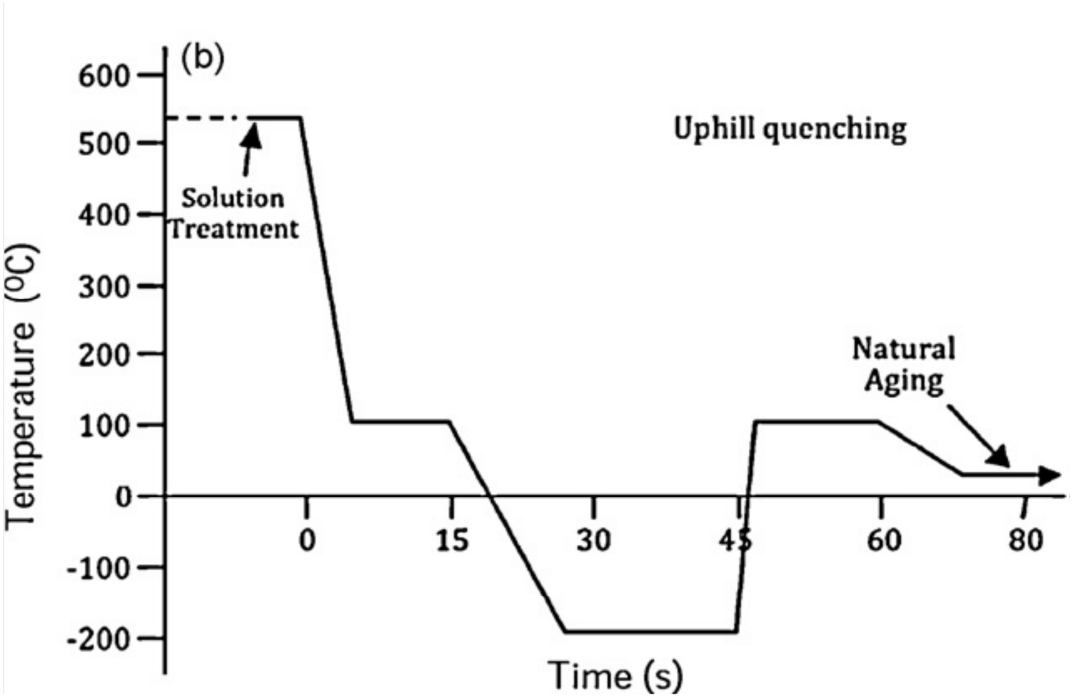

Figure 2-15 Uphill quenching heat treatment processes [52]

Several techniques have been introduced to reduce the amount of residual stresses. One of these techniques is controlling the cooling rate throughout the casting by quenching in boiling water but this method can lead to some loss in mechanical properties. Spray quenching is another technique for maintaining high mechanical properties with less residual stresses but this method requires a complicated control system or the use of uphill quenching. Yet another technique is that of using special quenchants which leads to high mechanical properties with lower residual stresses.

2.3.4 Consequences of residual stresses

Any existing residual stresses are considered as elastic stresses and are kept under static equilibrium. Elastic limit is the maximum value that can be reached by any residual stresses. Any stresses higher than the value of elastic limit with no opposing forces will be relieved by plastic deformation until it reaches the value of the yield stress [2]. It is believed that compressive residual stresses are good for fatigue life, crack propagation and stress corrosion of materials whereas tensile residual stresses reduce their performance capacity because the residual stress is superimposed as a mean stress with dynamic stress [1] [13].

As mentioned before, residual stresses results in warping and distortion during machining. During machining, some of the residual stresses relaxed during removal of the material, causing deviation from the static equilibrium inside the component. This unstable state leads to redistribution of the residual stresses and distortion of the part to construct a new equilibrium condition [2].

Residual stresses are often the most difficult to predict and least expected. It can strongly affect fatigue life, distortion, dimensional stability, corrosion resistance, and brittle fracture. Residual stresses lead to failure through different mechanisms starting from the microstructural scale to the structure integrity itself [1]. Different failure mechanisms are initiated through residual stresses where it can be represented as follows [1]:

- ***Plastic failure***: when the stress exceeds the yield criterion over a subdomain of the component.
- ***Fracture***: where it occurs due to fast crack propagation which initiates from a microscopic defect or flaw.
- ***Fatigue and thermal fatigue***: any fatigue failure involves two mechanisms: the crack nucleation and crack propagation. Also, fatigue can be classified into two groups, that is low cycle fatigue and high cycle fatigue. Residual stresses have no effect on the low cycle fatigue of materials as most of these stresses will be relaxed during first cycles of testing [1]. While residual stresses have a significant effect on shortening the fatigue life of high cycle fatigue material. The total fatigue life depends on the presence of the residuals stresses.
- ***Creep***: it is the inelastic deformation under the effect of a load supported by the material over long periods at an elevated temperature. The growth of cavities at grain boundaries is the dominant creep failure mechanism. Residual stresses can assist the creep failure.

- ***Stress corrosion cracking***: residual stresses can contribute to the stress corrosion cracking mechanism but peening methods which develop controlled compressive stresses on the surface show an increase in stress corrosion cracking resistance.

Despite the fact that occurrence can affect the reliability of structures, the residual stresses are often not considered in practical computations. Most of the time, residual stresses are one of the forgotten areas in the designing of machine parts. Studies have proven that the presence of residual stresses in weldments lead to drastic reduction in fatigue strength. Also, their presence reduces the fatigue life of high cycle fatigue materials. Currently, residual stresses are taken into account during the design and manufacturing of product [55].

2.3.5 Residual stress measurement techniques

Residual stresses can be quantified by many techniques. There are mechanical techniques such as sectioning, hole-drilling, curvature measurements, and crack compliance methods. These techniques correlate the measured residual stresses in components to the distortion. Diffraction techniques cover electron diffraction, X-ray diffraction, and neutron diffraction, which quantify the residual stresses by measuring the elastic strains in components. Other techniques, including magnetic and ultrasonic techniques, and piezo spectroscopy are also used to measure the residual stresses developed [12]. The mechanical techniques are considered destructive tests while the others are non-destructive tests but their accuracy is dependent on the microstructural variation and geometric complexity of the component structure [12].

The development of residual stress induces an elastic deformation of the material, and this deformation is proportional to the stress developed. Residual stress measurements techniques are thus based on a deformation measurement, which is utilized to calculate the residual stress.

2.3.5.1 Mechanical techniques

Residual stresses cannot be quantified directly but can be calculated through the measuring of another property [56]. Measuring the macroscopic strains by removing material from a part loaded with residual stresses is the basis of any mechanical technique used to quantify the residual stress.

The calculation of residual stresses by any mechanical method is through the measurement of the relaxed strains after releasing the locked-in residual strains [2]. The relationship between the residual stresses (σ) in any component and the variation in cooling rate is governed by the following equations [3]:

- $E = \sigma / \varepsilon$,
- $\varepsilon = \Delta L / L = \alpha \Delta T$,
- $\sigma = \alpha E \Delta T$.

where E, σ, ε, α, and ΔT are Young's Modulus, Stress, Strain, Coefficient of thermal expansion and temperature Difference respectively. Different rates of cooling, section thickness, and material strength are the main parameters that can affect the magnitude of residual stress in engineering components such as castings [3] [57].

The sectioning method is a complete destructive test and can be considered the first proposed method in measuring the residual stresses which involves sectioning of the component with a strain gauge attached [1]. In this method, strain gauges are placed on the surface of the component which register the stress relief that results from the removal of material through cutting. The cutting is done to ensure complete relaxation of the specimen. For more precision in measuring the residual stresses, the hole drilling technique was invented which uses a three-strain gauge rosette [1].

The hole drilling technique is one of the most widely used techniques for measuring residual stresses and is considered as a semi-destructive technique. It is relatively simple, inexpensive, quick, accurate and versatile, and can be both laboratory-based and portable. The test method has been standardized in the ASTM Standard Test Methods under the name of E-837.

This semi-destructive technique determines the stresses at the surface of a sample through the incremental introduction of a small shallow hole with a diameter of 2-4mm and depth of the same size, to relax the stresses in that location. Residual stresses are obtained by analytical or numerical analysis by correlating the magnitudes and directions of released strains measured by the strain gauge rosette, dimensions of the hole and material properties. After relaxation, the resultant strains are measured using a strain gauge rosette after each depth increment and the biaxial stress field is then calculated using established equations such as those listed in Equ.1.

This technique involves installing a three-leg or six-element strain gauge rosette on the desired part, then forming a hole using precision milling guide after zero balancing the

strain gauge Figure 2-16. The strain gauges are connected to a computer in order to record the measured relaxed strains corresponding to the residual stresses [58]. Introducing incremental center hole drilling, which involves carrying out the drilling in a series of small steps, enables stress profile maps for further analysis on the variation of residual stress with depth.

$$\sigma_{max},\ \sigma_{min} = -\frac{E}{2}\left(\frac{\varepsilon 3 + \varepsilon 1}{(1+\nu).a} \mp \frac{\sqrt{(\varepsilon 3 + \varepsilon 1)^2 + (\varepsilon 3 + \varepsilon 1 - 2\varepsilon 2)^2}}{\mathrm{b}}\right) \qquad \text{eq.1}$$

Where: ε1,2,3 measured strain relieved from strain gage 1, 2 and 3, respectively, a, b = strain gauge calibration coefficients, in MPa. The introduction of the hole is a very sensitive step as it may introduce additional residual stresses to the surface. Drilling techniques considered suitable for hole drilling include abrasive jet machining, high-speed drilling (up to 400,000 rpm) with an air turbine, and lower speed drilling with modified end mills or carbide drills.

Several considerations should be taken into account when using the hole drilling technique. Firstly, the material should be isotropic and the elastic parameters should be known. Secondly, the analyzed material should be machinable and the hole depth should not exceed half of the hole diameter. Furthermore, local yielding may occur due to the introduction of the hole and to avoid this, the maximal magnitude of the measured residual stress should not exceed 60-70% of the local yield stress [54] [55], to insure no plastic deformation is introduced through the use of an ultra-high speed drilling (up to ~ 400,000 rpm) machine [59]. While some uncertainties may be present due to inaccuracies in drilling

the hole, surface roughness, flatness, and specimen preparation, nevertheless, the hole drilling technique still provides reasonably accurate data regarding the sign and magnitude of the residual stresses.

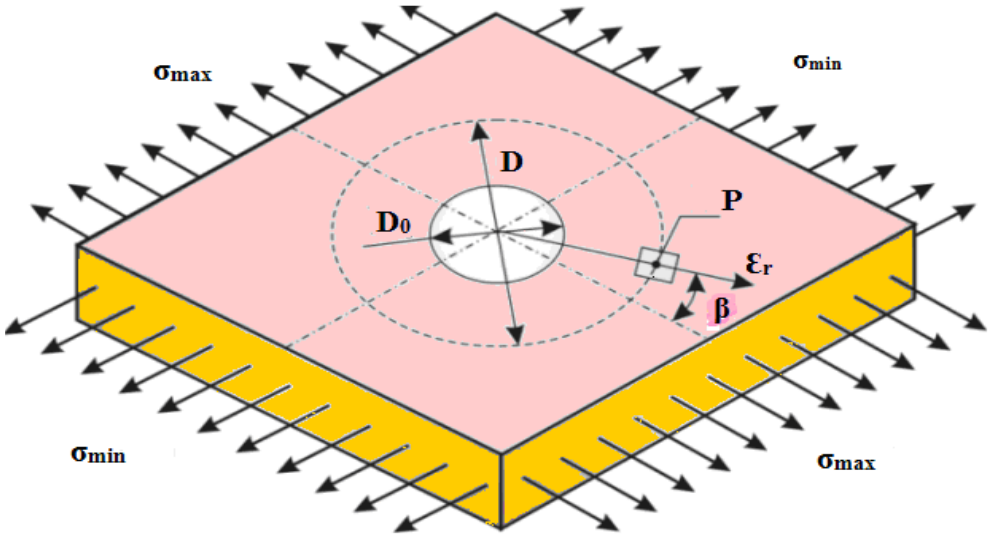

Figure 2-16 Hole drilling principle [60]

The ring core method is a developed technique of hole-drilling method but less common than the hole-drilling method due to complexity of the test and being more destructive. The principal behind ring core method is the same as hole drilling method but instead of drilling a hole through the middle of strain gage rosette, a notch with an internal diameter of 15 to 150 mm is milled around the rosette Figure 2-17 [1] [60] [61]. The ring-core method is a mechanical technique used to quantify the principal residual stresses within a specified depth of material [62]. As in the hole drilling method, a strain gauge is connected to a computer to record the change in strain with the variation of hole depth [62]. This method is less sensitive to errors involved in positioning of the cutting tool relative to

the strain gage and accurate results can be obtained from it due to complete relaxation of the strains at the surface [60] [62].

Lambda Technologies have demonstrated the effectiveness of the ring core method by the agreement of the residual stress results obtained with those derived from X-ray methods in forging and weldments samples [62]. The use of the ring method has several advantages in various aspects of the test like depth, sensitivity, and measurability of the residual stresses. despite its enhanced accuracy compared to hole drilling technique, ring core method is less likely used due to need of determining calibration coefficients which is dependent on type of strain gauge, type of material, geometry and depth of the milled core [60]. Unlike hole-drilling technique, ring core measurement process takes a long time, and the test is not standardized.

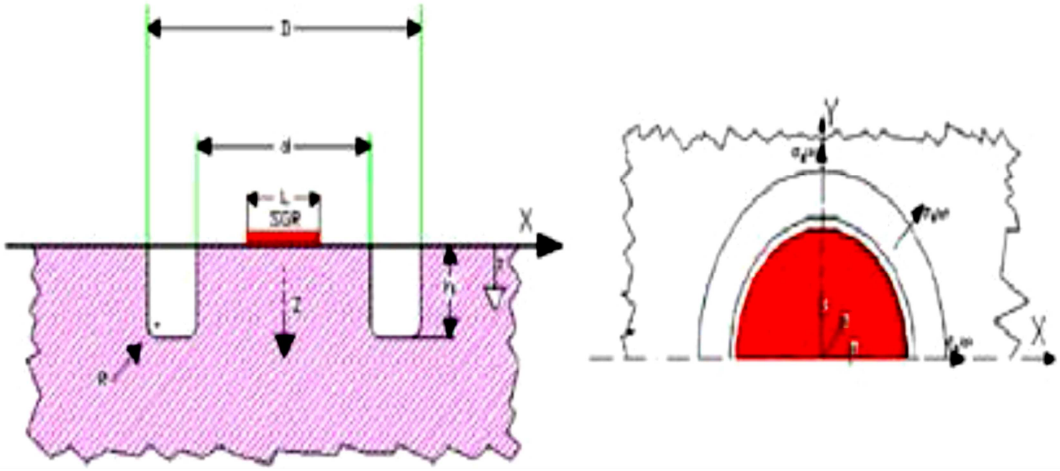

Figure 2-17 Ring core method [60]

Wyatt and Berry investigated the measurement of the residual stresses associated with machining in AA 6061-T6511 aluminum alloy by developing a new low-cost technique [63], which enabled mapping the distribution of residual strains over a wide area by following the change in spacing of a grid of hardness indents placed on the component, after stress relieving. The changes in the spacing of the indents may be negative or positive, depending on the sense of the residual stress (tension or compression) [63].

2.3.5.2 Strain gauges and Wheatstone bridges

Mechanical residual stresses are largely dependent on the strain gauge used as it is the device that measures the deformation caused by residual stresses. Based on the application, several types of strain gauges are used such as uniaxial, biaxial and triaxle strain gauges. Triaxle strain gauge is also called rosette, see Figure 2-18, which is mainly used for the purpose of measuring residual stresses. Strain gauges measure the deformation of the material through the changes encountered in its electrical resistance.

The strain measurements involve quantities in the scale of millistrains which induce very small changes in the resistance of the strain gauge. Therefore, accurate measurement of electrical resistance is required for accurate measure of strains. To fulfill this aim, a Wheatstone bridge is used for magnifying the strain gauge electrical resistance. The Wheatstone bridge is an electrical circuit comprising four resistances and a voltage excitation source (V_{ex}), as shown in Figure 2-19. When all resistances are equal, the voltage output (V_o) will be zero and the bridge is said to be balanced. Any change in resistance in any arm of the bridge will result in a non-zero output voltage, according to the formula: $V_o = V_{ex} (R_1R_3-R_2R_4) / (R_2+R_1)(R_3 +R_4)$ The output voltage (V_o) is characteristic of the

deformation. Each gauge of the rosette needs to be included in a Wheatstone bridge. As mentioned before, the strains expected from the strain gauges are very small and cannot be measured with sufficient accuracy using conventional industrial equipment. A specialized data acquisition system was therefore built where each strain gauge was connected to a Wheatstone bridge circuit with three control gages [64].

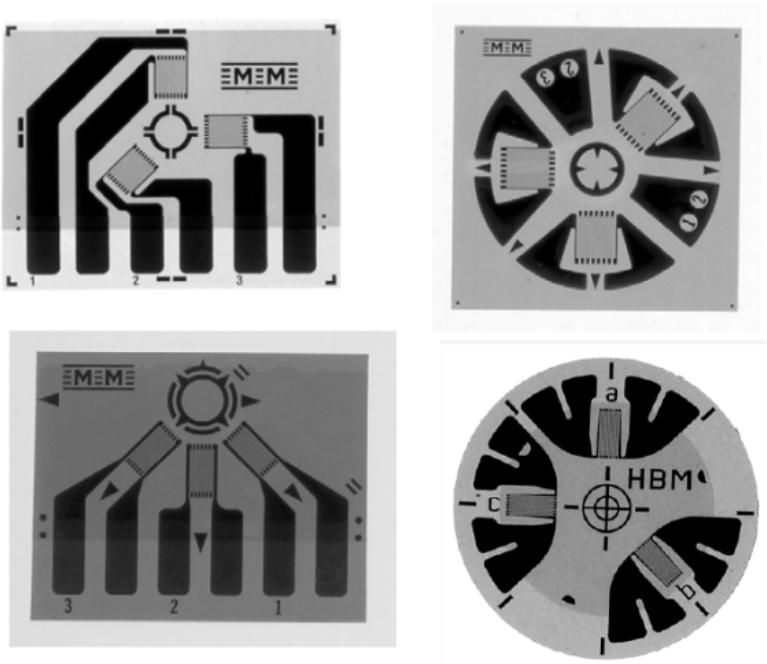

Figure 2-18 Typical strain gauge roseate [59].

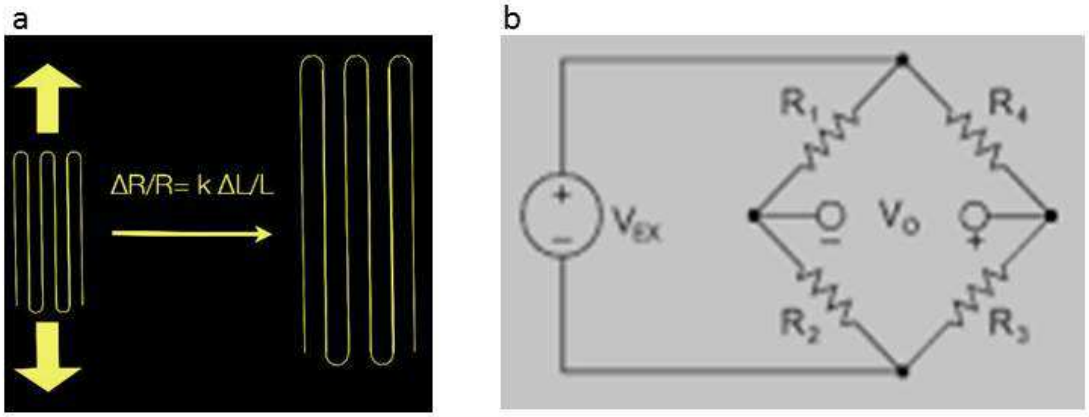

Figure 2-19 (a) Operating principle of strain gauges (b) Quarter Wheatstone bridge [59]

2.3.5.3 Diffraction techniques

X-Ray diffraction is considered a non-destructive testing method for determining the residual stresses in the material, and is based on the linear elasticity produced from the residual stresses calculated from the strain in the crystal lattice. This technique depends on considering interatomic spacing as a gauge length for measuring the strain raised from residual stresses. However, not only surface strains can be measured by XRD but also this technique is limited to characterizing the residual stresses in coarse grain materials such as castings and weldments [2].

In X-ray diffraction and neutron diffraction, the way used to measure residual stresses is by measuring the residual lattice strain distribution [56]. Atoms are arranged regularly through a three-dimensional periodic lattice in a perfect crystalline material. When the X-ray or moving neutron beam incidences at a certain angle that meets the condition expressed in Equation 2, the intensities of scattered waves sum up into a constructive interference and the diffraction pattern can be observed.

$$n\lambda = 2d_{hkl}\sin\theta \qquad \text{equation 2}$$

where d is the spacing between the planes in the atomic lattice, n is an integer, λ is the wavelength of the X-rays or moving neutrons, and θ is the angle between the incident X-ray or moving neutrons and the scattering planes[1].

This technique is based on Bragg's law which correlates the lattice spacing d_{hkl} for the (hkl) plane to the incident wave length (λ) and the diffraction angle (θ). The presence of residual stresses will cause an increase or decrease in the lattice spacing which appears as angle shifts in the diffraction peak positions [1] [2]. Electron, x-ray photon, and neutron beams are the used techniques with suitable wavelengths to measure lattice spacing. The x-ray technique is limited only to surface residual stresses due to fading of the beams at narrow depths.

Neutron diffractions method is very similar to the X-ray diffraction as it relies on elastic deformations within a polycrystalline material that cause changes in the spacing of the lattice planes from their stress-free condition [1]. The advantage of the neutron diffraction method in comparison with the X-ray technique is its lager penetration depth [1].

The constructive beams will be available only when Bragg's law is fulfilled. if the grain size is big, fewer grains will be irradiated and therefore there will be fewer suitably oriented lattice planes fulfilling Bragg‘s Law. In this case, local crystal defect such as dislocations, vacancies, and stacking faults will lead to a local fluctuation of the lattice

spacing, resulting in a peak broadening [1]. This will reduce the accuracy of the X-ray and neutron diffraction methods.

Table 2-8 lists the characteristics of various techniques while Figure 2-20 demonstrates the penetration depth of these different techniques. Although large improvements have been made in the mechanical tests to increase their efficiency, the X-ray diffraction test achieved wider application due to advantages such as easy handling, less time consumption and being non-destructive [56]. Figure 2-20 demonstrates the range of penetration that can be tested for residual stresses measurements using different methods.

Magnetic method and ultrasonic method other non-destructive techniques which have been developed to measure residual stresses recently.as these techniques are under development. The range of application of these methods is narrow and their accuracies are relatively low. For these reasons, these methods are not as popular as the hole-drilling and neutron diffraction method and were not selected for residual stress measurements in the present study.

Table 2-8 Characteristics of techniques used to measure strain to evaluate residual stresses

	Techniques	**required data**	**Surface condition**	**Results**
Mechanical	Sectioning, Hole drilling, Ring core method	Young's Modulus, Poisson's ratio, calibration coefficients functions	Suitable for strain gauge application	Strains caused by releasing of stress.
Diffraction	X-Rays, neutrons method	x-ray elastic constants, lattice constants of non-stressed material (d_0)	Rough surface	Bragg's angle, strains in different directions

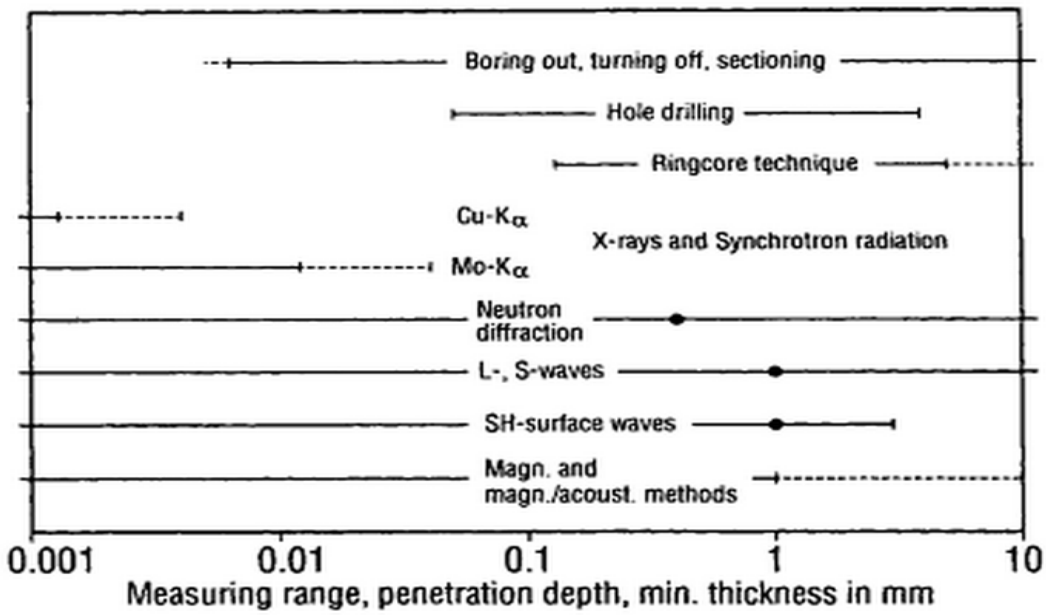

Figure 2-20 Residual stresses measuring range and penetration depth of the different techniques Vs. minimal thickness of the sample to be tested.

2.4 Engine block

Engine block as shown in Figure 2-21 is the largest metal component in the engine and is the most intricate. It holds and supports all other engine components such as cylinders and pistons and contains passages for coolant. The engine block is where combustion converts into mechanical energy that drives transmission propelling the car. Engine block used to be made of iron but today most of them are made of aluminum alloy for fuel efficiency.

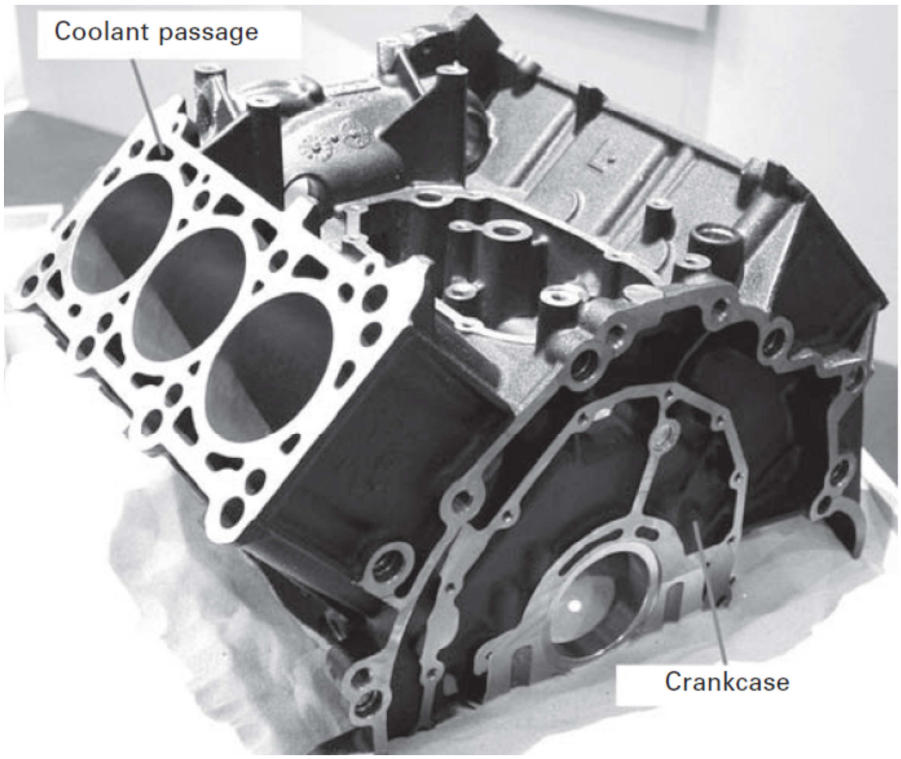

Figure 2-21 Cast iron V-cylinder block (closed deck type) including a crankcase [65]

An engine block is the largest and most complex single component in the car engine to which all other parts are attached. It represents from 3 to 4% of the total weight of the car. The block is typically arranged in a “V,” inline, or I-4 horizontally-opposed (also referred to as flat) configuration and the number of cylinders may range from 3 to as much as 16 [21].

The main objectives that are needed to be achieved for optimum endurance and performance of engine blocks at prolonged service life of the vehicle are housing internal moving parts and fluids, ease of service and maintenance, and the capacity to withstand pressures created by the combustion process [8] [21]. In order for an engine block to meet all of these functional requirements listed above, the engineering material used to

manufacture the block must possess high strength, modulus of elasticity, abrasion resistance, and corrosion resistance. Additional requirements have to be taken into consideration while selecting the material such as good machinability and castability of the metal alloy, low density (for fuel saving purposes), low thermal expansion (to minimize the development of residual stresses during service) , high thermal conductivity (to increase engine performance) and finally good damping absorption characteristics [8].

Cast iron engine blocks were once the most economic material for the production of engine blocks. Recently, aluminum alloys have replaced cast iron for the sake of high power cars and fuel efficiency. By 2003, 60% of the cars in Europe were made of aluminum alloys [65]. Currently, the production of an engine block starts with casting of aluminum followed by proper machining for enhancing the surface quality.

Aluminum is a light and soft material with high thermal conductivity when compared to cast iron. The problem of being soft made it difficult to use as an engine block material but through alloying and heat treatment of aluminum, the availability of obtaining strengths compared to cast iron made it possible for aluminum alloys to replace cast iron. To overcome the lack of wear resistance problems, the implementation of liners were introduced. Until now, due to its higher productivity, cast-in iron liners are the best option for today's passenger car engine blocks [8] [65].

The cylinder bore suffers from local wear during operation due to friction between the wall and pistons, and that is why liners are put inside the cylinders. Several designs of cylinder bores, shown in Figure 2-22, were made in order to enhance the efficiency of the engine block. From Figure 2-22, the monolithic engine is an engine with no liners, also

called liner-less block [65]. This type is made only from one material such as early cast iron blocks. Different casting techniques have been employed for manufacturing engine blocks namely, sand casting, die casting and gravity casting, among which sand casting is the most widespread method. Casting, while liners are in position, is the method commonly used for introducing cast iron liners. This method is also called composite casting [65].

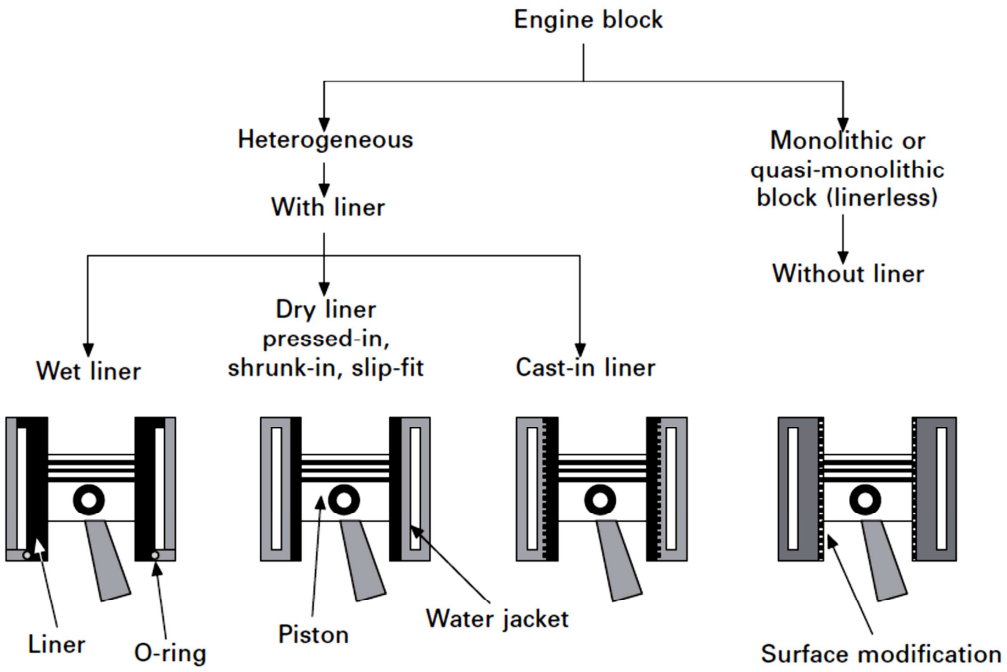

Figure 2-22 Bore designs in engine blocks [65]

After solidification; due to the difference in thermal expansion coefficients between the cast iron liners and the aluminum engine block, compressive stresses are generated in the liners while tensile stresses are generated in the engine block which remains in the block as residual stresses [65]. In order to ensure good bonding between liner and block surface, dimpling the surface of the cast iron liners is carried out. In the casting process, it was found that preheating the liners before pouring was beneficial for maintaining the heat transfer properties of the engine block.

Distortion of the engine block is inevitable with time due to presence of residual stresses. The cylinder liner thickness provides good rigidity of the structure while the metallurgical integrity of the structure provides prolonged interlocking between engine block and liners [65]. Although, increasing the thickness increases the rigidity of the structure, it also deteriorates the heat transfer properties of the structure.

As mentioned before, casting is the main manufacturing method for engine blocks, and includes sand casting, lost foam casting, gravity casting, and high and low pressure die casting. A number of complications are encountered during casting of aluminum engine blocks including shrinkage and oxide entrapment [65]. Several techniques have been introduced in order to produce a sound casting such as the Cosworth process and the Core package system. Table 2-9 summarizes the technologies used for engine block production and their characteristics.

High pressure die-casting is another method used for the manufacturing of engine blocks and is mainly used for large productions. This method requires low mold temperatures (around 200°C) which lead to shorter solidification times and production of the part with good mechanical properties. Surface finish and dimensional accuracy are the added benefits of this method [65].

Gravity die-casting is a technique where molten metal is poured under the force of gravity like in sand casting. In this method, the die temperature should be high enough in order to ensure complete filling of the mold before solidification. This method is preferred when casting hypereutectic Al-Si alloys as it ensures good distribution of the silicon particles [65].

Table 2-9 Technologies used for engine block manufacturing and their characteristics

		Sand casting	lost foam method	high pressure die casting	gravity Die casting
Pressure (MPa)		Gravity	Gravity	100	Gravity
Dimensional accuracy		low	high	high	medium
Quality	**Blow holes**	medium	medium	a lot	few
	T6 heat treatment	possible	possible	impossible	possible
	Shrinkage defects	few	few	a lot	few
Cost		medium	medium	low	medium
Productivity		high	above medium	high	low

2.5 Residual stresses in Aluminum engine blocks

Fuel saving, emission control, and weight reduction are the reasons that made the development of aluminum alloys mandatory for the automobile industry. Cylinder blocks are one of the main applications of aluminum alloys (Al-Si alloys) in the industry not only due to the reasons mentioned above, but also because of their high thermal conductivity and good casting properties. For all these reasons, aluminum alloys have successfully replaced the gray cast iron in cylinder head castings [66]. However, the hypoeutectic aluminum alloys have poor tribological properties; the need for high wear-resistant liners such as gray cast iron was important to preserve vehicle engines from failure [67].

Around 90% of the parts produced for the automotive industry belong to the Aluminum-Silicon-Copper (Al-Si-Cu) or the 3xx.x series of alloys. Strength requirements are met by precipitation hardening, which involves a solution treatment, water quench,

followed by aging treatment at an intermediate temperature. Copper is one of the principal alloying elements for enhancing the alloy strength at room and high temperatures, while magnesium is another alloying element which is also responsible for making the alloy strong, hard, and responsive to heat treatment [68].

The maximum service temperature for Al-Si-Cu alloys is 260°C. At higher temperatures, the alloy suffers from loss of mechanical and fatigue properties [6] [69]. Further development of aluminum alloys to increase and maintain their mechanical performance at higher temperatures is being continually investigated. Alloys developed by NASA, such as Al 354 and Al 388 alloys, have the potential to meet these requirements, reaching optimum service temperatures of 315°C [70].

Engine block manufacturers introduced several aluminum alloys to meet engine blocks requirements, namely 242 (T7 treated), 319 (T6 treated) and 356 (T6 treated) alloys. B319.1 engine blocks have complex structures which, at room temperature, it consists of soft and ductile primary α-aluminum phase and a hard and brittle eutectic silicon phase, secondary intermetallic phases strengthening precipitates following heat treatment, and casting defects such as porosity [36] [71].

In recent years, diesel engines have been developed to increase their efficiency and reduce their weight. For further development, it is important to understand the loading mechanisms and damage accumulation especially at high temperatures which are directly related to microstructural parameters such as the secondary dendrite arm spacing (SDAS), porosity, and the morphology of the eutectic silicon and second phase particles. All these

parameters are very important with respect to the thermal fatigue and high-temperature tensile properties.

In an attempt to enhance the high-temperature mechanical properties, Jeong [72] performed a series of experiments to study the effect of alloying elements such as Si, Cu, Mn and Mg on the high-temperature characteristics on the A356.1 alloy. It was found the addition of these alloying elements produced a finer microstructure, a concomitant increase in the elastic modulus, hardness and tensile strength accompanied by a decrease in the thermal expansion coefficient. The addition of Cu led to stabilizing the final properties up to 250°C while Mg exhibited the same behavior but at lower temperatures (< 170°C) [72].

B319.1 alloy is the best choice for manufacturing of engine blocks. To compensate for lack of wear resistance of the aluminum, cast iron liners are introduced in the engine cylinders as shown in Figure 2-23. Many techniques have been introduced to insert the liners namely shrink in place, press-in and cast-in methods. The latter technique is the one most commonly used for large engine block production [73]. The durability of automotive engine parts can be increased by reinforcing the microstructure with changes in the process and alloying elements, as was confirmed by Jeong who observed significant enhancement in fatigue properties and microstructure with increasing Si, Mn and Cu concentrations in the Al-Si-Mg-Cu cast alloy investigated [72].

Gray cast iron liners are added to Al319 aluminum alloy engine blocks to enhance the erosion resistance. This addition of liners comes with the drawback that excessive residual stresses are developed along the bores of the cylinders, due to the large difference in linear expansion coefficient and a non-uniform cooling rate along the length of the

cylinder between the aluminum alloy and liners resulting in large variations in both mechanical properties and microstructure [74]. These variations may lead to permanent distortion during service. In conclusion, engine blocks suffer from the presence of residual stresses due to differential cooling during processing. These residual stresses cause distortion of critical features during machining leading to difficulty in maintaining the dimensional tolerance [75].

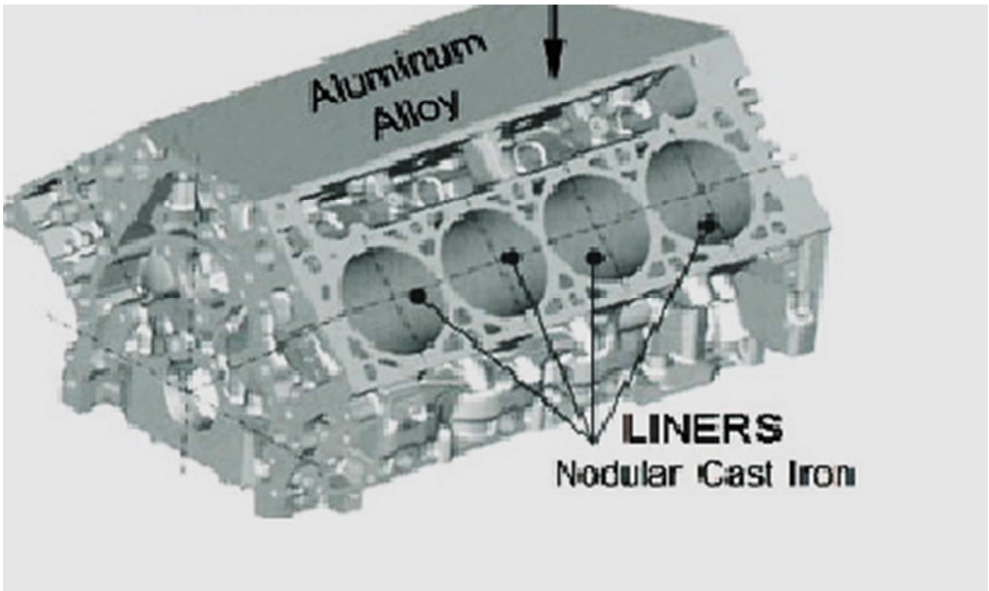

Figure 2-23 Illustrative picture for Al alloy cylinder block with cast-in iron liners

Distortion may either be a product of thermal growth or the product of tensile residual stresses that exceed the yield stress of the material. Thermal growth involves changes in volume during phase transformation through heat treatment of the alloy. In this context, it is found that the T7 treatment offers the best dimensional stability over T4 and T6 as it produces θ (Al_2Cu) which is a stable phase and has a lower specific volume when compared to θ’ (Al_2Cu), neglecting the effect of thermal growth distortion [5]. Distortion

occurs through the introduction of excessive residual stresses, in particular, when these stresses exceed the yield stress of the material [5].

For a standard casting cylinder block of diesel engine, distortion and bending were results of an uneven distribution of residual stresses. Through the manufacturing process of engine block, residual stresses emerge specifically after heat treatment where the residual stresses formed are in an equilibrium state. During machining, this state of equilibrium could be altered, leading to higher amount of deformation. This deformation would cause the casting to be rejected (the machining process causing lower accuracy in dimension and less efficiency in performance) or in some cases used as scrap [76].

Distortion of the cylinder bores results in a loss in compression of the air-fuel mixture due to improper sealing between the cylinder wall and the piston. This loss of seal causes a portion of the compressed air-fuel mixture to leak out of the combustion chamber by a process known as “blow-by” [6] which reduces the engine efficiency. The level of stress relief and distortion is dependent on the residual stress after quenching, the aging temperature and the aging duration [74].

Several factors affect the amount of the residual stresses inside a casting component, namely superheat, mold hardness, mold design and modifiers. All these factors were investigated by Sadrossadat [3]. From the results, it was concluded that as superheat increases, the residual stresses increase due to the non-uniformity of heat distribution. Residual stresses were also found to increase by increasing the mold hardness due to excessive contraction hindrance from the mold. The addition of modifiers such as Sr had a

side effect in increasing the amount of residual stresses despite the enhancement in mechanical properties [3] which contradicts the findings of Haque et al [77].

The presence of protective liners in the combustion chamber with high wear resistance properties such gray cast iron is mandatory [78]. However, despite the importance of these liners, their presence can cause large residual stresses due to the significant difference in thermal expansion coefficient between the Al alloy and the gray cast iron. The residual stresses develop mainly after solution heat treatment of the engine block. This elastic strain results in residual stresses within the material if the contraction is constrained [78] [79]. Also, cast iron liners result in variations in cooling rates during solidification which may lead to non-uniform microstructure and mechanical properties. That can further result in certain sections of the cylinder becoming prone to dimensional distortion when the engine blocks are exposed to service conditions [78].

Residual stress relief was assessed from top to bottom along the V-6 cylinder bridge by Lombardi [74] [78], using ex-situ neutron diffraction. His findings showed that there is an increase in cooling rates as one proceeds deeper along the cylinder bridge. This was attributed to the mold design as the bottom region was near chills which provided higher cooling rates than the top region which was is near to the riser which requires slow solidification [40] [78] [80] [81].

Lombardi et al. [4] also found that residual stresses along hoop, radial, and axial directions were tensile along the cylinder bridge in the TSR condition with average constant magnitudes of 180, 100, and 160 MPa, respectively in the aluminum inter-bore region [78]. These amounts of residual stresses will be higher than YS (195 MPa) of

B319.1 alloy when accompanied with service stresses, which may lead to plastic deformation and distortion of the engine block. It was also found that the variations in microstructure across the length of the engine block led to the conclusion that lower strength sections (large grain structure) are more prone to stress relief and distortion than higher strength part (fine grain structure) [78].

Quenching is considered as the main step in the evolution of residual stresses. Lombardi et al. [5] studied the variation in microstructure, mechanical properties and residual stresses for two different V-6 engine blocks, where the engine blocks went through the same manufacturing parameters except for quenching rate. The quenching rates for the two engine blocks were 1.67 and 0.67 K/s, respectively [5]. It was found that there were no significant changes in microstructure or mechanical properties of the blocks, and all the difference was in the residual stress amounts. One of the engines blocks, which was quenched at a low quenching rate, showed certain amounts of distortion, unlike the other engine block. The distorted block exhibited high levels of tensile residual stresses while the undistorted block showed low levels of compressive residual stresses.

Wiesner et al. studied the residual strains/stresses in a series of heat-treated engine blocks using X-ray and neutron diffraction. They found that the surface hoop stresses show compressive residual stresses decreasing towards zero stress with increasing heat treatment while the radial stresses show a tendency towards increasing tension stresses [75]. Also, it is observed that the residual stresses changed from tensile to slightly tensile or compressive with increasing solution treatment temperatures [75]. This gives reason to believe that precipitation of phases (e.g., Cu, Mg) during heat treatment may also play a role in stress

development and subsequent engine block distortion. This conclusion was confirmed by Lombardi et al. [78] by correlating heat treatment parameters with the microstructure, mechanical properties and residual stresses produced. Annealing, aging, and plastic deformation are the main ways to eliminate the residual stresses inside a casting [82].

Carrera et al. conducted a series of experimental tests to measure the residual stresses using strain gauges attached to different automotive engine blocks. They discovered the development of tensile stresses higher than 150MPa when the engine block contained the cast iron liners, while the engine blocks without cast iron liners exhibited 20MPa compressive stresses in the cylinder bridge [82]. Furthermore, it has been observed that the residual stresses are affected by the dimension of the block and the wall thickness of the cylinder bridge where residual stresses decrease as the thickness increases. it was also found that V-8 engine blocks develop higher residual stresses than I-4 blocks with equivalent walls thickness [82]. These observations match the results for residual stresses obtained from the finite element model made by Su et al. [74].

A study was made by Godlewski et.al [83] to identify the effect of aging on residual stresses in B319.1 casting. Firstly, the study revealed that quenching in boiling water produces lower residual stresses in castings. Secondly, it was found that aging at 190^0C has little effect on relaxation of the residual stresses while aging at 260^0C for one hour reduced the amount of residual stresses by half. The reduction in residual stresses was correlated to the reduction in yield stress at high temperature which leads to relaxation and redistribution of residual stresses in the casting.

The parameter that is considered the main role in developing residual stresses is quenching as thermal gradients can be large enough to produce high levels of residual stresses. Several techniques were introduced to minimize the effect of residual stresses, one being uphill quenching which was described in a previous section; others include the spraying technique, step quenching and using different quenching media. These techniques depend on the fact that reducing the cooling rate results in a significant reduction in residual stresses however it can also be detrimental to the mechanical properties.

Dolan and Robinson [4] studied the effect of step quenching, illustrated in Figure 2-24 on 7175-T73, 6061-T6 and 2017A-T4 alloys on residual stresses. The quenching proceeds in two steps, the first one requires fast cooling to a temperature above the critical temperature region followed by cooling in water. The results illustrate a significant reduction in residual stresses for alloys without loss in mechanical properties.

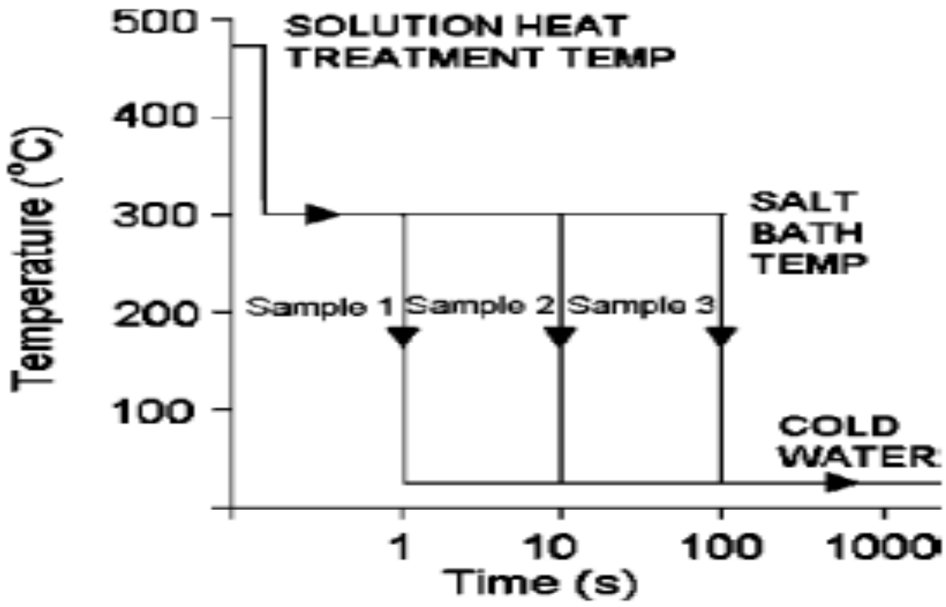

Figure 2-24 Step quenching parameters parameters [4]

During the life time of the cylinder head, it is exposed to high cycle fatigue (HCF) due to millions of combustion cycles and to low cycle fatigue (LCF) resulting from thermal expansion and contraction during engine start-up and engine stop up to ten times a day [66]. Cyclic tensile stresses are subjected to high cycle fatigue (HCF) areas which are located on the water jacket side of the flame deck wall. The key parameters for prolonging high cycle fatigue are microstructure, porosity and surface quality; while the controlling parameters for low cycle fatigue regions, located around the bridge area, subjected to high temperatures and exposed to high cracking tendency, are proper composition and high-temperature strength [66].

Residual stresses in cylinder blocks were found to have a huge impact on shortening the fatigue life of high cycle fatigue areas while its effect on the low cycle fatigue areas was

insignificant. The reason for this is that is that residual stresses in low cycle fatigue areas tend to be relaxed during first cycles or by the application of high plastic strains [1]. Residual stresses measured in cylinder heads made of AlSi10Mg alloy quenched in water, water-polymer and air were 105, 55 and 15 MPa, respectively [66].

Other techniques have been introduced to increase the power efficiency and lower engine weight. Using hypereutectic Al-Si alloys have been used manufacturing engine blocks instead of hypo-eutectic Al-Si alloy as they have higher wear resistance alloy. Newly developed hypereutectic Al-Si alloys such as Alusil and Mercosil are now used by several automobile manufacturers such as Mercedes, Audi, Porsche, BMW, Volvo, VW and Jaguar [8]. However, castability and machinability related problems hinder this material from replacing the hypo-eutectic Al-Si alloys.

Coating the cylinder block with wear-resistant materials such as ceramics is a new innovative technique for the replacing the cast iron liner. Ford was the first company to use thermal spray coating to coat a very hard wear-resistant layer of Fe_2O_3 inside the cylinder bore with the aid of a special plasma gun. This technology has been implemented in two car models: the Ford Mustang Shelby GT500, and the 2009 Nissan GTR [8]. Service testing was carried out to verify the properties of the thermal spray coating, and it was found that engines which used the thermal spray coating had greater wear resistance, accompanied with a decrease in fuel consumption when compared to regular engines [8]. The major drawback of this technique is the integrity of the bond between the bore surface and liner.

The use of metal matrix composites (MMC) is a new alternative that may have the solution for engine problems. Toyota has successfully introduced an engine block that is

made from a metal matrix composite (MMC) consistingof alumina-silica fibers and mullite particles in an aluminum matrix. Honda also changed the cast iron liners with MMC consisting of carbon fiber in an alumina (Al_2O_3) matrix. These materials show better performance over the traditional alloy in regard to weight, power, and wear resistance. This technique is under development as several draw backs face the implementation of MMC as the main engine block. These drawbacks can be summarized as follows [8]:

- The reinforcement must be selected carefully because if it is very hard, the ring will suffer from erosion and loss of engine performance will be observed.
- The reinforcement must be well distributed throughout the soft matrix to eliminate erosion from occurring in softer areas, which could also lead to engine failure.
- The use of MMCs in producing engine blocks involves a complicated and expensive casting process to get an acceptable product.

CHAPTER 3
EXPERIMENTAL PROCEDURES

Chapter 3
Experimental Procedures

3.1 Methodology

For the current study, this investigation will be carried out in two stages. Stage I will comprise investigations carried out on specimens with simple geometry made from B319.1 and A356.1 alloys for determining a correlation between residual stresses and microstructure resulting from the use of different casting parameters. Stage II will concentrate on investigating the evolution of residual stresses in samples with intricate geometries, as for example, in the bridge area of an I4 engine block, subjected to different heat treatments.

3.2 Stage I procedures

3.2.1 Materials and Casting Procedures

The chemical composition of the 356 base alloy coded M and 319 base alloys coded E is shown in Table 3-1. They were cut into smaller pieces, dried and melted in a 120-kg capacity SiC crucible, using an electrical resistance furnace, as shown in Figure 3-1. The melting temperature was maintained at 750 ± 5°C. Both alloys melts were grain refined and modified using Al-%5 Ti- 1% B and Al- 10%Sr master alloys, respectively, to obtain levels of 0.25% Ti and 200 ppm Sr in the melt. Finally, the melts were degassed for ~15-20 min with a rotary graphite impeller rotating at ~130 rpm, using pure dry argon, as shown in Figure 3-2. Following this, the melt was carefully skimmed to remove oxide layers from the surface.

Table 3-1 Chemical composition of B319.1 and A356.1 alloys

Element wt.%	**%Si**	**%Cu**	**%Fe**	**%Mn**	**%Mg**	**%Sr**	**%Ti**	**%Al**
B319.1	7.4	3	0.4	0.2	0.26	0.05	0.26	bal.
A356.1	6.6	<0.1	0.1	0.0	0.36	0.034	0.25	bal.

The melt was poured into different molds for various purposes, namely (a) ASTM B-108 permanent mold, for preparing the tensile test bars; (b) an L-shaped rectangular graphite-coated metallic mold; and (c) a block shaped graphite-coated metallic molds. All molds were preheated to 450°C to drive out moisture and avoid cold shut of the blocks. Regarding ASTM B-108 mold, each casting provides two test bars, with a gauge length of 70 mm and a cross-sectional diameter of 12.7 mm, as shown in Figure 3-3. Three samplings for chemical analysis were also taken simultaneously at the time of the casting; this was done at the beginning, in the middle, and at the end of the casting process to ascertain the exact chemical composition of each alloy.

Figure 3-1 Electrical resistance furnace

Figure 3-2 Graphite degassing impeller

(a)

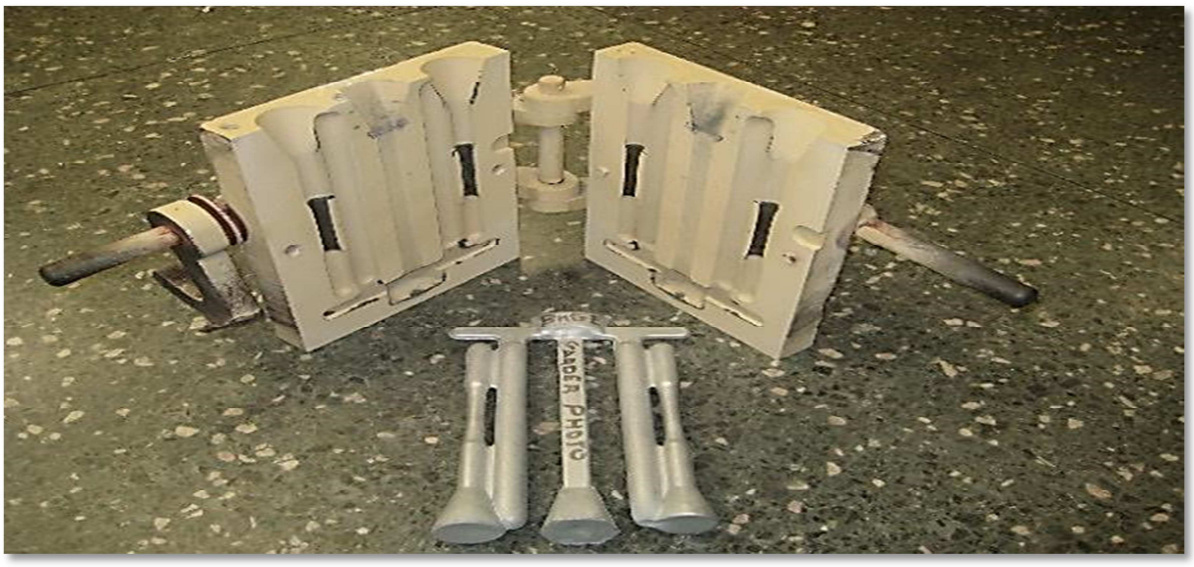

(b)

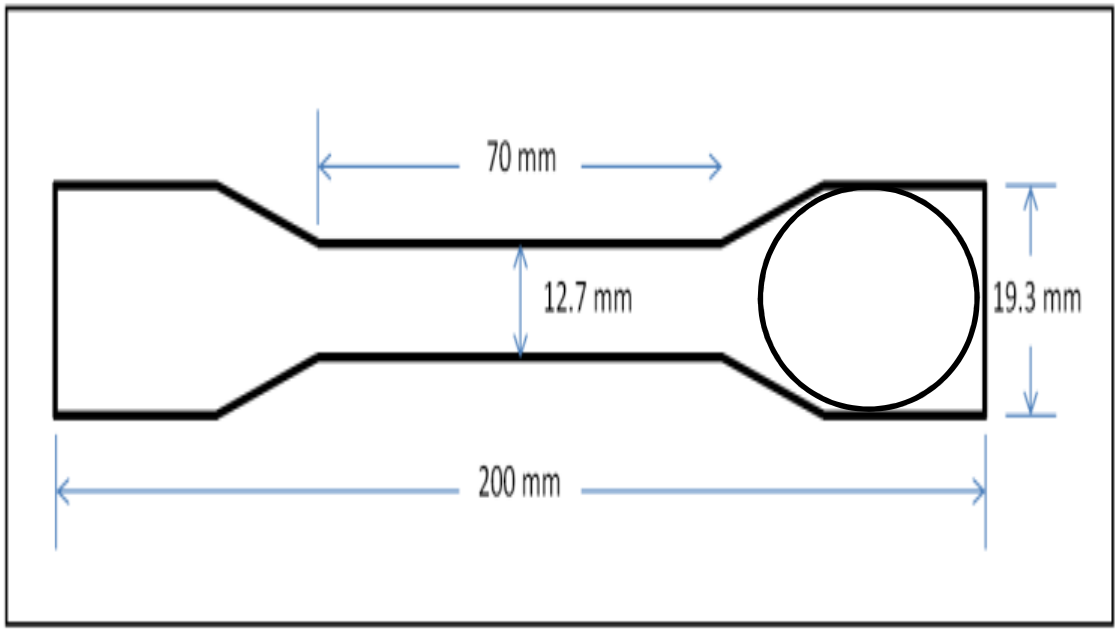

Figure 3-3 Tensile test bars (a) ASTM B-108 permanent mold used for casting tensile test bars (b) Dimensions of the tensile test bar

The L-shaped mold and block castings were mainly used for residual stress measurements and for preparing samples for microstructural examination. The two molds, shown Figure 3-4, were selected to provide two different cooling rates. The molds were preheated to 250°C. Samples were prepared for the measurement of SDAS and grain size in both alloys. Bars as shown in Figure 3-5 were cut from both molds with the dimensions of 200*40*40mm for measuring of residual stresses using the sectioning method.

(a)

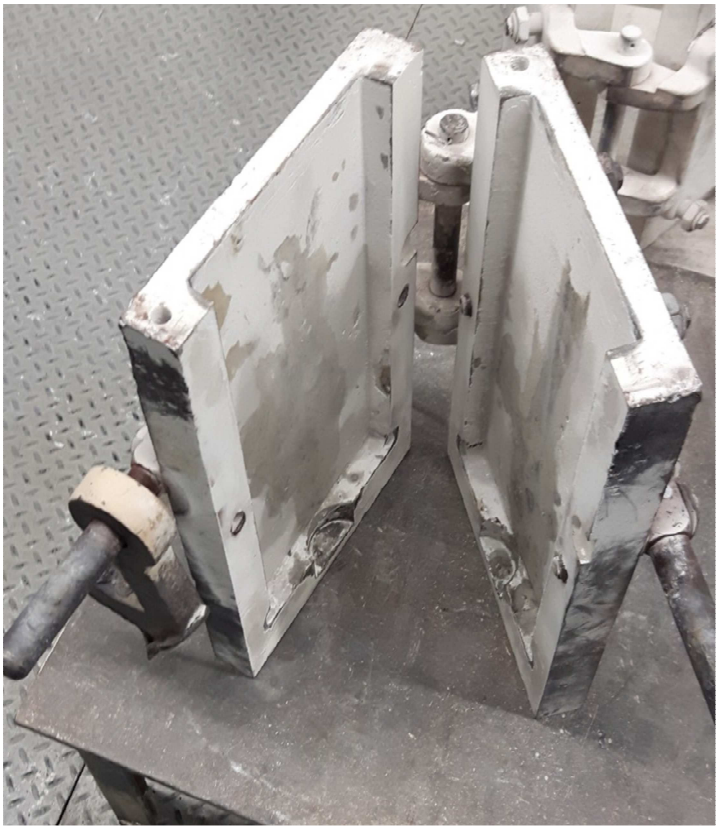

(b)

Figure 3-4 Permanent molds: (a) Block mold (b) L-shaped mold

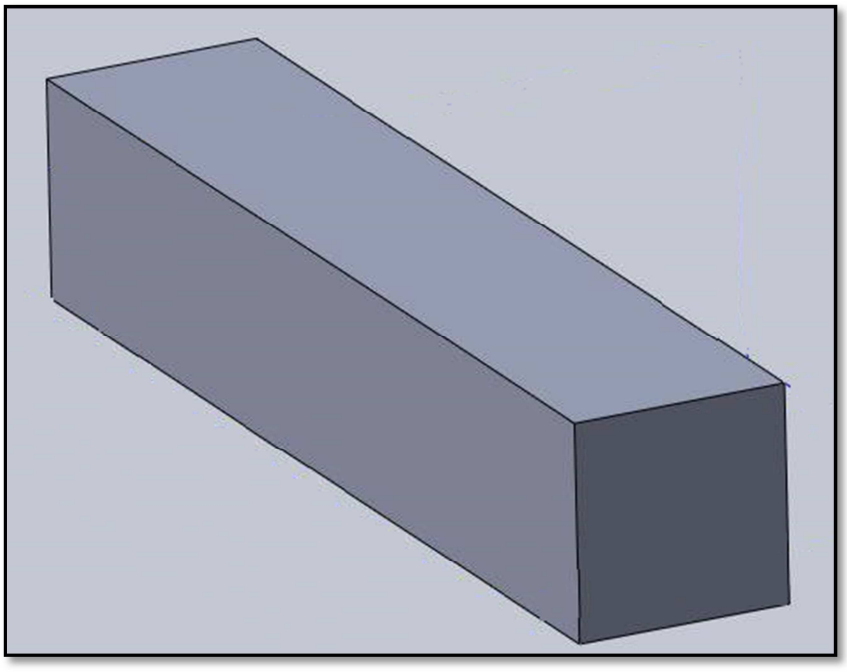

Figure 3-5 Schematic figure of residual stress measurement sample

3.2.2 Heat Treatment

All the samples, tensile test bars and residual stresses bars were heat treated. Both alloys, B319.1 and A356.1 alloys were subjected to the same heat treatment sequence listed in Table 3-2 with the exception that the solution heat treatment (SHT) of B319.1 was carried out at 500°C for 8 hours while that of A356.1 alloy was carried out at 540^0C for the same time period.

Table 3-2 Heat treatment cycles for B319.1 and A356.1 alloys

No.	code	Heat treatment
1	E/M	As cast
2	SH A	SHT + air quench
3	SH W	SHT + warm water quench
4	SH C	SHT + cold water quench
5	T6 A 10	T6 SHT (air) +Aging (170°C/10hrs)
6	T6 W 10	T6 SHT (warm) +Aging (170°C/10hrs)
7	T6 C 10	T6 SHT (cold) +Aging (170°C/10hrs)
8	T6 A 50	T6 SHT (air) +Aging (170°C/50hrs)
9	T6 W 50	T6 SHT (warm) +Aging (170°C/50hrs)
10	T6 C 50	T6 SHT (cold) +Aging (170°C/50hrs)
11	T6 A 100	T6 SHT (air) +Aging (170°C/100hrs)
12	T6 W 100	T6 SHT (warm) +Aging (170°C/100hrs)
13	T6 C 100	T6 SHT (cold) +Aging (170°C/100hrs)
14	T7 A 10	T7 SHT (air) +Aging (250°C/10hrs)
15	T7 W 10	T7 SHT (warm) +Aging (250°C/10hrs)
16	T7 C 10	T7 SHT (cold) +Aging (250°C/10hrs)
17	T7 A 50	T7 SHT (air) +Aging (250°C/50hrs)
18	T7 W 50	T7 SHT (warm) +Aging (250°C/50hrs)
19	T7 C 50	T7 SHT (cold) +Aging (250°C/50hrs)
20	T7 A 100	T7 SHT (air) +Aging (250°C/100hrs)
21	T7 W 100	T7 SHT (warm) +Aging (250°C/100hrs)
22	T7 C 100	T7 SHT (cold) +Aging (250°C/100hrs)

3.2.3 Tensile Testing at Room Temperature

All tensile test samples whether as-cast, solution heat-treated or aged, were tested to the point of fracture using an MTS Servo hydraulic mechanical testing machine, illustrated in Figure 3-6, at a strain rate of 4×10^{-4} s^{-1}. The deformation in the samples was measured using an extensometer. Yield strength (YS) at 0.2% offset strain, ultimate tensile strength (UTS), and percent elongation (%El), were obtained from the data acquisition system of the machine. Five samples were tested from each condition covered in Stage I, were tested, for a total of 21 conditions/110 bars per alloy.

Figure 3-6 Servo hydraulic MTS mechanical testing machine

3.2.4 Measurement of Cooling Rate

In order to evaluate the cooling rate for each mold, the L-shaped casting, Block casting and the residual stress bar are heated to 450°C. Then a high sensitivity Type-K thermocouple, which has to be insulated using a double-holed ceramic tube, is attached to the center of the castings. The temperature-time data is collected using a high speed data acquisition system linked to a computer. From this data, the cooling curves are obtained.

3.2.5 Metallography and Microstructural Characterization

Different techniques were used in order to reach a complete qualitative and quantitative analysis of the microstructural constituents and features, including intermetallic phases, hardening precipitates in the B319.1 and A356.1 alloys.

Samples were sectioned in the as-cast condition, one from the block casting and another one from the L-casting, for metallographic examination. The samples were mounted in bakelite, ground, and polished to a fine finish, using standard polishing procedures. The microstructures were examined using an Olympus PMG3 optical microscope linked to a Clemex Vision P optical microscope and image-analysis system. The set-up is shown in Figure 3-7.

The selected samples were firstly mounted in bakelite was using a Struers LaboPress-3 machine, followed by the grinding and polishing sequence using a TegraForce-5 machine. The grinding stage were performed using a silicon carbide (SiC) abrasive papers starting followed by 120 grit, 240 grit, 320 grit, 400 grit, 800 grit and 1200 grit sizes.

The polishing stage was carried out in three steps, using a sequence of diamond suspension with a particle size of 3 μm, as the first step followed by further polishing using

a suspension containing a smaller diamond particle size of 1 μm. The lubricant used for this polishing stage is a Struers DP-lubricant. The final stage of polishing was carried out using a Mastermet colloidal silica suspension, SiO_2, having a particle size of 0.6 μm. After completing the polishing stage, the samples were ready for optical examination.

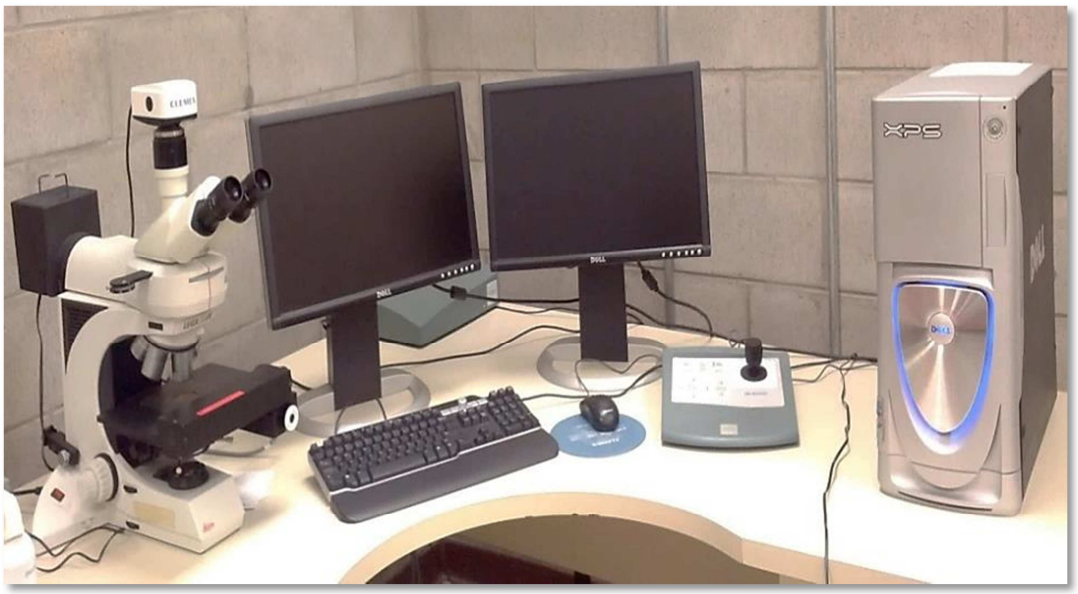

Figure 3-7 Optical microscope-Clemex image analyzer system

The polished as-cast samples were used for secondary dendrite arm spacing (SDAS) and grain size measurements. For grain size measurements, the polished samples were etched for 15 seconds, using a solution containing 2 ml HF (48%) + 3 ml HCl (conc.) + 5 ml HNO3 (conc.) and 190 ml distilled water. The polished surface was swabbed with the etching solution until the contrast in the grains was high enough. To better highlight the grain structure, filtered lights at different incident angles were used; a combination of red, green, blue and yellow light gave an enhanced contrast to the grain structure.

The intermetallics and precipitate formed in the A356.1 and B319.1 alloys were examined using scanning electron microscopy (SEM) and field emission scanning electron

microscopy (FESEM). The aim of using electron microscopy, in this case, was to identify the different intermetallics formed after casting and to examine the density and distribution of the hardening precipitates formed under various treatment parameters/aging conditions.

3.2.6 Measurement of Residual Stresses

The technique proposed for measuring residual stresses in this stage is sectioning technique. The procedure followed for the successful completion of this method was to measure the strains present in the alloys before and after cutting, by using strain gauges. Installing strain gauges requires careful surface preparation to ensure good adhesion between the strain gauge and the specimen surface. The surface is firstly degreased to eliminate any surface contamination followed by grinding the surface of the specimen using sand paper starting with 240 grit and going down to 600 grit size standard papers. The resistance of the gauge at the mentioned point was measured with the aid of a Wheatstone bridge. The specimens were then cut to release the stresses making it possible to measure the residual strain.

Residual stresses in aluminum blocks were evaluated using sectioning technique. Residual stresses were measured at different heat treatment stages for B319.1 and A356.1. Residual stress measurements using the sectioning technique are carried out in four stages:

- **Block surface preparation**: develop a chemically clean and neutral surface with a texture suitable for strain gage bonding. It also creates a lot of fine scratches which enhance the bonding between the surface and the strain gauge.
    - The block surface of the alloy is machined, and then abraded manually using a SiC paper grit size 120, 320 and 600.

- After grinding, the surface is cleaned with a solution of phosphoric acid and neutralized with ammonia using cotton swabs.
- Finally, the place where the strain gauge will be installed is marked.

❖ **Strain gage installation**.

- Removing strain gauges from its cover using tweezers.
- Place strain gauge (bonding side down) on a chemically clean and neutral plastic plate surface.
- Using cellophane tape strain gauges are transported to the center of engine block bridges at the locations marked made in the previous step.
- One end of the tape is lifted and the strain gage is placed bonding side up. The catalyst and glue are added to the strain gauge; then after a few minutes, the tape is removed.
- Wiring the strain gauges using a soldering iron and silver (96%) solder for strain measurement.

❖ . **Strain measurement:** It is important to mention that all strain measurements are performed at the same ambient temperature (23°C) under lab conditions

- After installing strain gauges at each bridge, the initial strain measurement (ε_0) is carried out using a Wheatstone bridge, special software and data acquisition equipment National Instruments with SCXI-1520 universal strain gage input module.
- To protect strain gauges during sectioning, the strain gages are covered with tape.

- Cutting is performed using a band saw machine in vertically and horizontally.
- After sectioning, strain measurement reading obtained (ε_1) after each cut.

❖ **Residual stress calculation:** residual stress is calculated using the Hook's law equation, using the calculated strain values and Young's modulus of 70GPa.

$$\sigma = E\,(\varepsilon_0 - \varepsilon_1)$$

Figure 3-8 shows the test setup for measuring the residual stresses measuring before and after sectioning. Cutting was first done in the vertical cutting plane and the residual stresses were measured. Then another cut was done in the horizontal plane and another measurement of the residual stresses was taken to determine the effect of cutting direction in relieving of the residual stresses. The cutting directions are illustrated in Figure 3-9.

(a) (b)

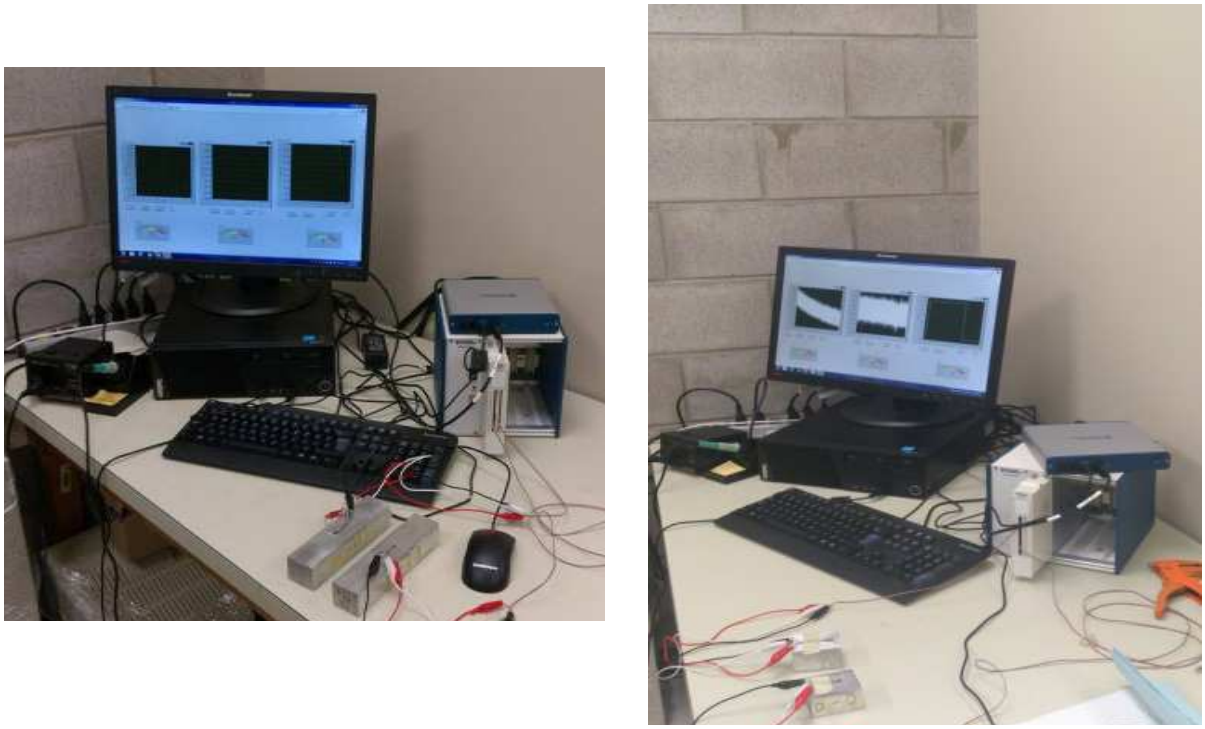

Figure 3-8 Strain gauge setup (a) obtaining initial strain (ε_0) before cutting (b) obtaining final strain (ε_f) after cutting

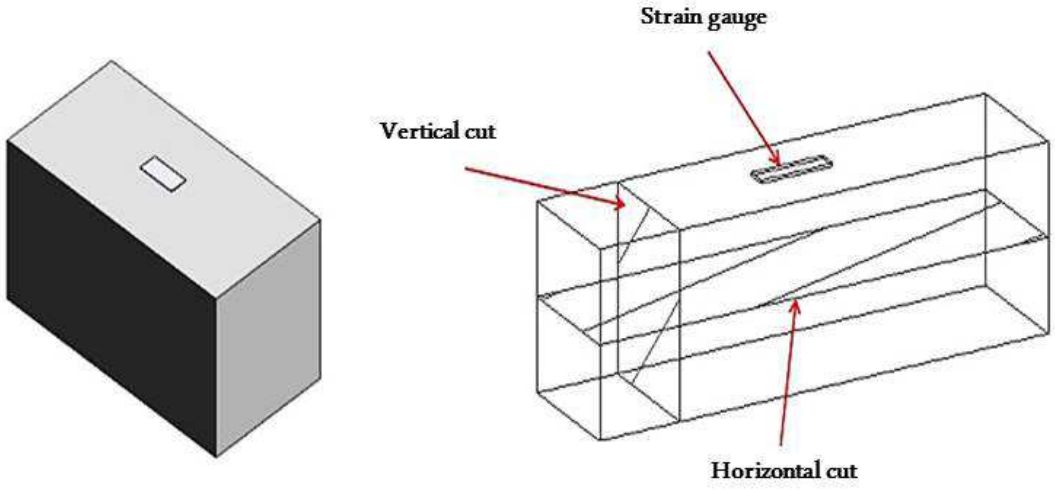

Figure 3-9 Sketch Illustrating cutting directions

3.3 Stage II procedures

The main objective in this stage is to determine the most suitable manufacturing process that provides optimum mechanical performance together with the lowest residual stresses. In this stage, the investigation will focus on the analysis of residual stresses evolved in I-4 and V-6 engine blocks subjected to different of heat treatments. The I-4 and V-6 engine blocks, an example of which is shown in Figure 3-10 and Figure 3-11 , were supplied by the Nemak Centre of Engineering in Windsor, Canada. The cylinder area suffers from high erosion during the operation of the engine. Grey cast iron liners are thus used in order to improve the in-service wear resistance. The liners used in these blocks were preheated to 400°C using induction coils, prior to being inserted into the mold to promote a more uniform microstructure.

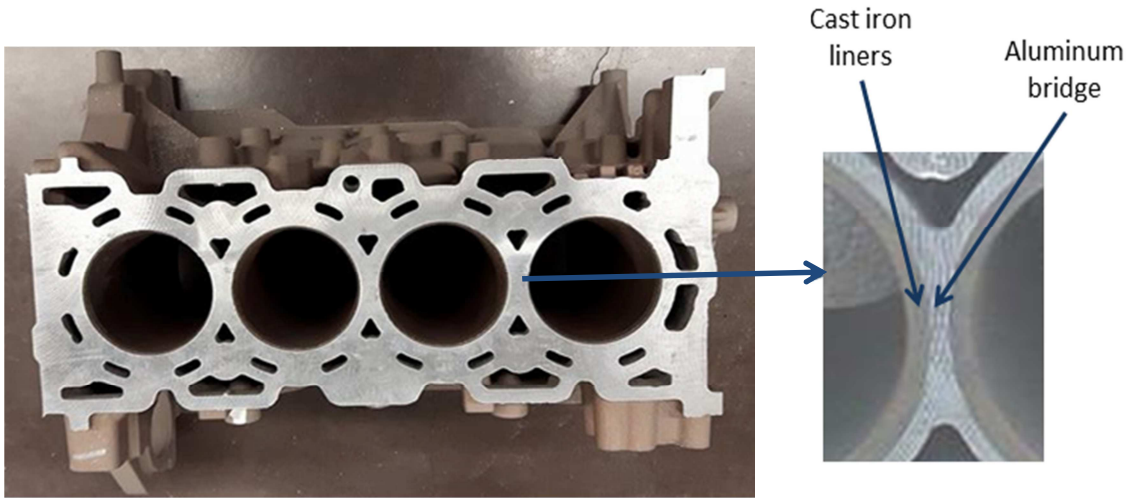

Figure 3-10 I-4 engine block

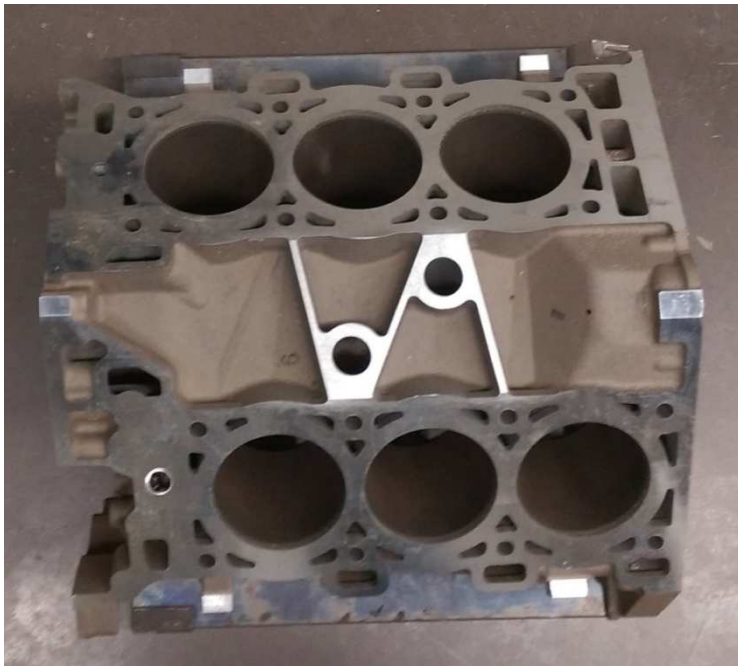

Figure 3-11 V-6 engine block

3.3.1 Materials and Heat Treatment

The aluminum B319.1 alloy used in this research study is the most widely and commercially used in the manufacture of engine block due to the stability of its mechanical properties despite changes in impurity concentrations. The chemical composition for the I-4 engine block is shown in Table 3-3. This alloy is known for its desirable characteristics such as castability, corrosion resistance, and thermal conductivity. Copper at 3-4% is considered relatively high to enable the alloy to retain its strength at elevated temperatures and facilitate machining [21].

The engine blocks used in this study were be made from 319 Al-Si-Cu alloy melts subjected to grain refining and Sr-modification treatments to enhance the microstructure and, hence, the mechanical properties. The blocks will be subjected to different heat treatment conditions starting with solution heat treatment (SHT) at 500°C for 8 hours, then quenching in different media, followed by T6 and T7 aging treatment using various times. Quenching is considered as the main parameter for developing residual stress. Two quenching media, cold water, warm water and air, will be examined to study their effect on residual stresses. With respect to aging, T6 aging is carried out at 170°C for 10, 50 and 100 hrs and at 250° C for T7 treatment, using 10, 50, 100 hours aging times. This treatment will be considered to examine the effect on evolution of residual stresses. The T7 treatment is used industrially in the production of engine blocks.

The treatment used in the industry is called thermal sand reclamation (TSR). This technique involves solution heat treatment (SHT), and then forced air cooling (50-100 °C/minute) and aging to a T7 temper. Table 3-4 shows the actual process for engine block manufacturing.

Table 3-3 Engine block alloy chemical composition

Alloy	**Element (wt %)**							
B319.1	**Si**	**Cu**	**Fe**	**Mn**	**Mg**	**Sr**	**Ti**	**Al**
	8.4	2.7	0.5	0.3	0.37	0.02	0.14	bal.

Table 3-4 Heat treatment cycles used industrially for engine block production

Treatment	**Temperature (°C)**	**Time (hr)**
TSR	495	1
SHT	480	7.5
T7 temper	240	5.5

To facilitate the handling of the engine block in the foundry, the I4 engine blocks were cut in half as shown in Figure 3-12. This procedure was carried out after validating that there would be no change in results between the whole block (four cylinders) and half the block (two cylinders). The proposed plan for this stage is to study all the factors that can affect the evolution of the residual stresses. These factors are quenching rate, freezing, aging temperature, aging time, and cutting. After the application of, and with respect to, each of these factors; residual stresses and hardness measurements, and metallographic analysis will be carried out. In order to show the variation in residual stresses for another type of engine with different shape, V-6 engine blocks will be examined to study the residual stresses development in comparison with I-4 engine blocks.

(a) (b)

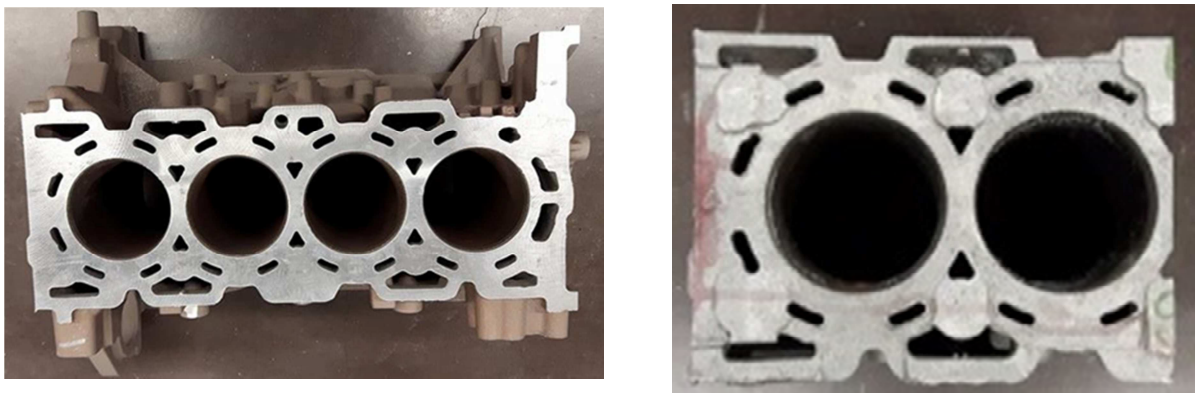

Figure 3-12 Engine blocks (a) Four cylinders (before cutting) (b) Two cylinders (after cutting)

3.3.2 Metallographic Analysis

Selected samples were chosen to analyze the effect of the heat treatment parameters on the development of the microstructure. The same steps and equipment, as described in stage I, were used for carrying out the microstructural analysis. Quantitative measurements of the eutectic Si particle characteristics, namely, area, length, density and aspect ratio, were carried out for as-received, solution heat-treated (two-cylinder) and solution heat-treated (four-cylinder) samples. For each sample, fifty fields were examined over the entire surface of the sample, by traversing it in a regular and systematic manner, and the Si particle characteristics recorded for each field.

3.3.3 Hardness Measurements

In general, hardness refers to resistance to deformation. Hardness has conventionally been defined as the resistance of a material to permanent penetration by another harder material with measurement being made after the applied force has been removed, such that elastic deformation is ignored. Currently, the indentation hardness test is used in practically every metal working plant as a means of checking the quality and

uniformity of metals and metal parts. There are three types of tests used with accuracy by the metals industry; they are the Brinell hardness test, the Rockwell hardness test, and the Vickers hardness test.

The Brinell hardness method is widely used nowadays in determining the hardness of metals. This universally accepted and standardized indentation hardness test was proposed by Brinell in 1900, and consists of indenting a metal surface with a steel ball, 10 mm in diameter, at a load of 3000 kg mass.

For soft metals such as aluminum, the load is reduced to 500 kg to avoid deep impression, while for very hard metals a tungsten carbide ball is used to minimize distortion of the indenter. The load is applied for a standard length of time, usually, 30 seconds, and the diameter of the indentation is measured with a low-power microscope after removal of the load.

The Brinell Hardness Number (BHN) may be obtained by dividing the kilogram load by the surface area of the indentation, in square millimetres, as represented in Figure 3-13 (a) where BHN is the Brinell hardness number, F is the imposed load in Kgf, D is the diameter of the spherical indenter in mm, and d is the diameter of the resulting indenter-impression in mm, as shown in Figure 3-13(a). The load is applied for a standard length of time, usually, 25-30 seconds and the diameter of the indentation is measured using a low-power microscope. The Brinell hardness values for each test block represent the average of at least eight indentation readings obtained along the length of the cylinder, as shown in Figure 3-13 (b).

(a) (b)

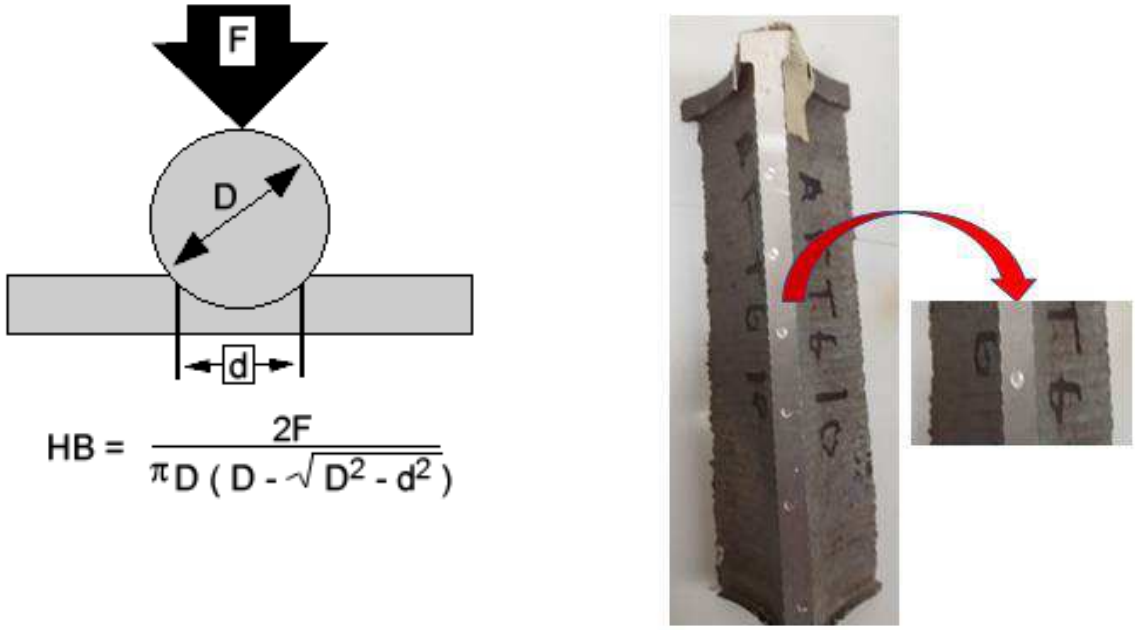

Figure 3-13 (a) Schematic representation of Brinell test; (b) indentation marks

3.3.4 Measurement of Residual stresses

Residual stresses maybe quantified using different techniques, classified into mechanical, diffraction, and other techniques. The mechanical techniques include sectioning, hole-drilling, curvature measurements, and crack compliance methods. These techniques correlate the measured residual stresses in components to the distortion. Diffraction techniques, such as electron, X-ray, and neutron diffraction, quantify the residual stresses by measuring the elastic strains in the examined components. Finally, other techniques, including magnetic, ultrasonic, piezo spectroscopy are used to measure the residual stresses developed [12]. The mechanical techniques are considered destructive tests while the others are non-destructive tests but their accuracy is dependent on the variation in microstructure and the geometric complexity of the component [12].

In the current study, non-destructive techniques such X-ray and neutron diffraction techniques will be excluded due to their inaccessibility since the latter needs a nuclear reactor, the availability of which is limited to facilities in national labs for the most part, while x-ray diffraction provides results for surface residual stresses and requires a degree of crystallinity in the material of the component being examined. For these reasons, the sectioning technique was adopted in the present research as it provides reliable and highly accurate results, and is applicable for most metals and alloys, in addition to being a simple and cost efficient technique.

3.3.4.1 Sectioning Method

The sectioning method is a complete destructive test and can be considered as the first proposed method in measuring the residual stresses. It involves cutting of the component with an electric strain gauge attached [1], and relies on the measurement of local strain (using strain gages)induced due to the release of residual stress upon removal of material from the specimen. The sectioning method consists in making a cut in order to release the residual stresses that were present on the cutting line. For this, the cutting process used should not introduce plasticity or heat, so that the original residual stress can be measured without the influence of plasticity effects on the surface of the cutting planes which can be achieved through wire cutting technique. Figure 3-14 represents the sections that were cut for measuring the residual stresses inside an engine block.

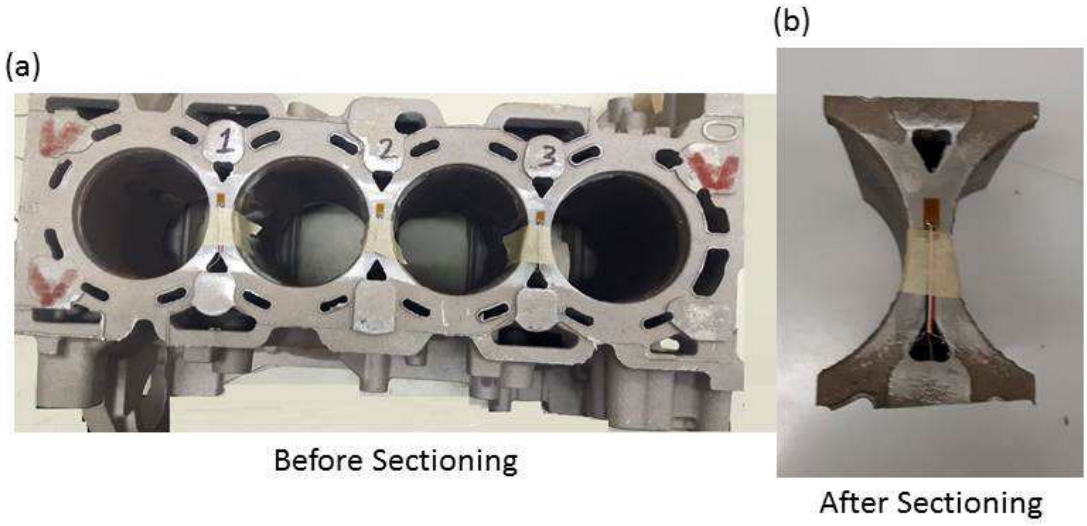

Figure 3-14 Measurement of residual stresses inside engine block using sectioning

Residual stresses in the sectioned aluminum blocks were measured/calculated following different heat treatment stages of the block sections. Figure 3-15 shows the test setup for measuring the residual stresses in a section of a B319.1 engine block. These measurements using the sectioning technique are carried out in four stages:

(i) Block surface preparation: This step involves developing a chemically clean and neutral surface with a texture suitable for strain gauge bonding. It also creates a lot of fine scratches which enhances the bonding between the surface and the strain gauge.

- The block surface of the alloy is machined, then abraded manually using SiC paper of grit size 120, 320, 600 grits in consecutive order.
- After grinding, the surface is cleaned with a solution of phosphoric acid and neutralized with ammonia using cotton swabs.
- Finally, the place where the strain gauge will be installed on the block surface is marked.

(ii) <u>Strain gage installation:</u> The strain gauge is installed as follows

- The strain gauge is removed from its packaging using tweezers.
- It is placed (bonding side down) on a chemically clean and neutral plastic plate surface.
- Using cellophane tape, the strain gauge is transferred to the center of the engine block bridge to the position mark made in the previous step.
- One end of the tape is lifted and the strain gage is placed bonding side up; catalyst and glue are added to the strain gauge; then after a few minutes the tape is removed.
- The strain gauge is wired using a soldering iron and silver (96%) solder for strain measurement.

(iii) <u>Strain measurement</u>: strain gauge is then connected to data acquisition system to take readings before and after cutting. It is important to mention that both strain measurements are performed under the same lab conditions, at the same temperature (23°C).

- After installing strain gages at each bridge, the initial strain measurement (ε_0) is carried out using a Wheatstone bridge, special software and National Instruments data acquisition equipment equipped with a SCXI-1520 universal strain gage input module.
- To protect the strain gauges during sectioning, they are covered with tape.
- Cutting is performed using a band saw machine.
- After sectioning, removing iron liners at the bridge areas are removed, and the final strain measurement (ε_1) is made.

(iv) <u>Residual stress calculation:</u> The residual stress is calculated using the Hooke's Law equation, using the calculated strain values and a Young's modulus of 70 GPa.

$$\sigma = E\,(\varepsilon_0 - \varepsilon_1)$$

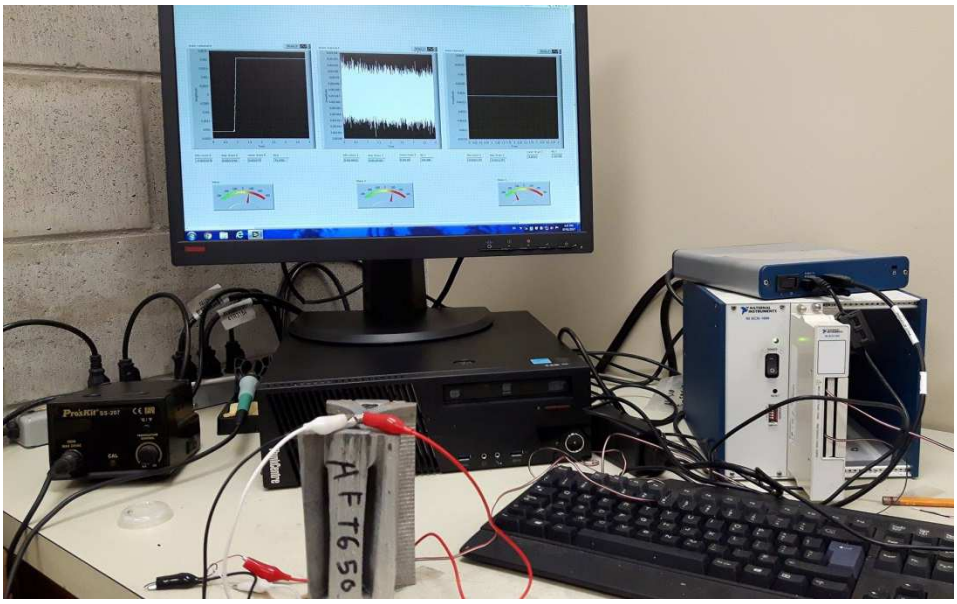

Figure 3-15 Strain gauge measurement set up

CHAPTER 4
RESIDUAL STRESSES DEVELOPMENT IN Al-Si-Cu ALLOYS

Chapter 4
Residual stresses development in Al-Si-Cu alloys

Section I: Effect of Casting Parameters on Development of Tensile Properties and Residual Stresses in Al-Si alloys

4.1 Introduction

This chapter presents the results on the influence of various metallurgical parameters on the tensile properties and the evolution of residual stresses in A356.1 and B319.1 casting alloys. Measurements of mechanical properties and residual stresses were carried out in order to (a) study the interplay between residual stresses and mechanical properties, and (b) examine the microstructural evolution as a function of the different casting parameters employed in the Al-Si-Mg (A356.1) and Al-Si-Mg-Cu (B319.1) alloys investigated, and (c) analyze the relationship between microstructure, mechanical properties and residual stresses as a result of the different variables.

4.2 Microstructural Characterization

This section will discuss the characteristics of the microstructures observed in the B319.1 and A356.1 alloys, including the phases formed, the secondary dendrite arm spacing (SDAS), and the eutectic silicon particle characteristics.

4.2.1 Effect of cooling rate on grain size

The block and L-shaped molds used in this study provided different solidification rates; the schematic of the castings obtained is illustrated in Figure 4-1. Figure 4-2 and Figure 4-3 show the simulation for cooling rates for the two different molds verified by

experimental results. The results indicate that the L-shaped casting reach cooling rates of 15^0C/min while the block casting exhibits a cooling rate of 7°C/min.

(a) (b)

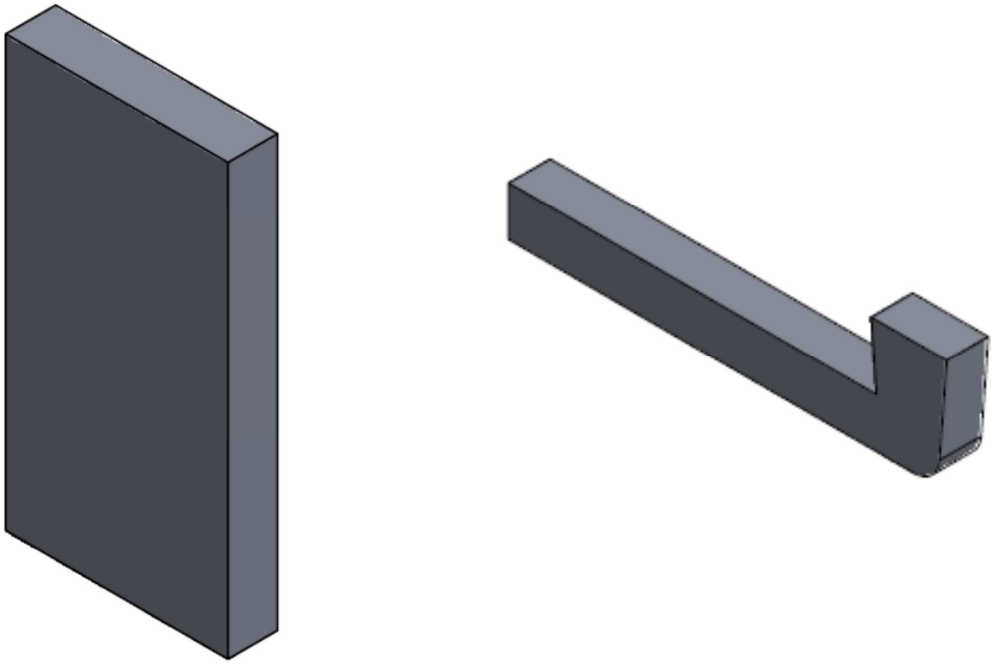

Figure 4-1 Schematic diagram of (a) Block Casting (b) L-shaped casting

Results of secondary dendrite arm spacing (SDAS) measurements are provided in Table 4-1. It was found that the average SDAS for the block casting is 60 µm which is reflected by the large grain size observed in Figure 4-4 (a, b). Due to the high solidification rate obtained with the L-shaped casting, the average SDAS was found to be 25µm, as is also confirmed by the small grain size noted in Figure 4-4 (c, d). The micro- and macro-structures shown in Figure 4-4 indicate the refining achieved during solidification with the L-shaped mold compared to the block mold.

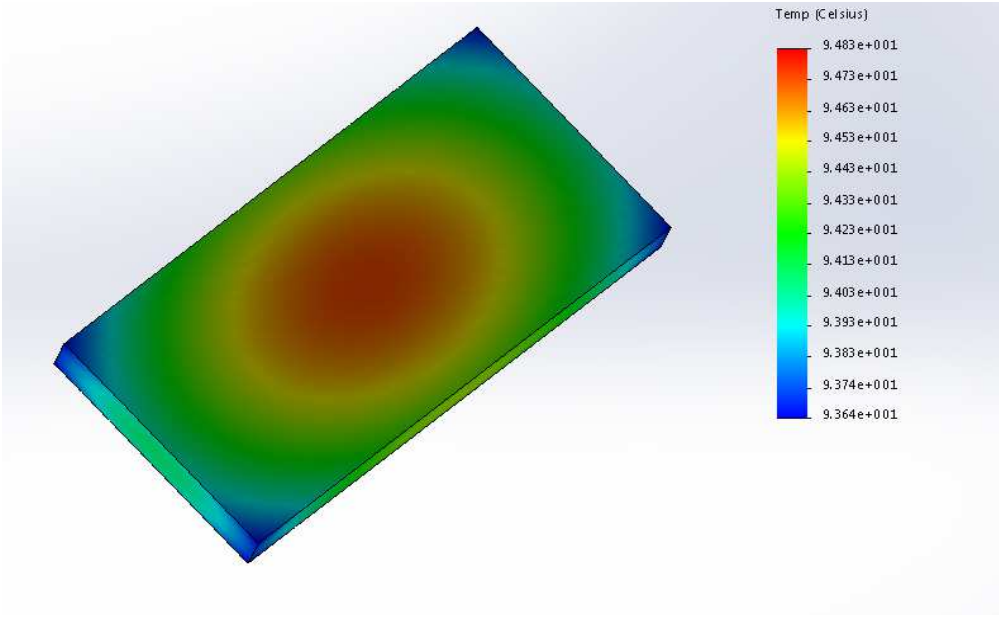

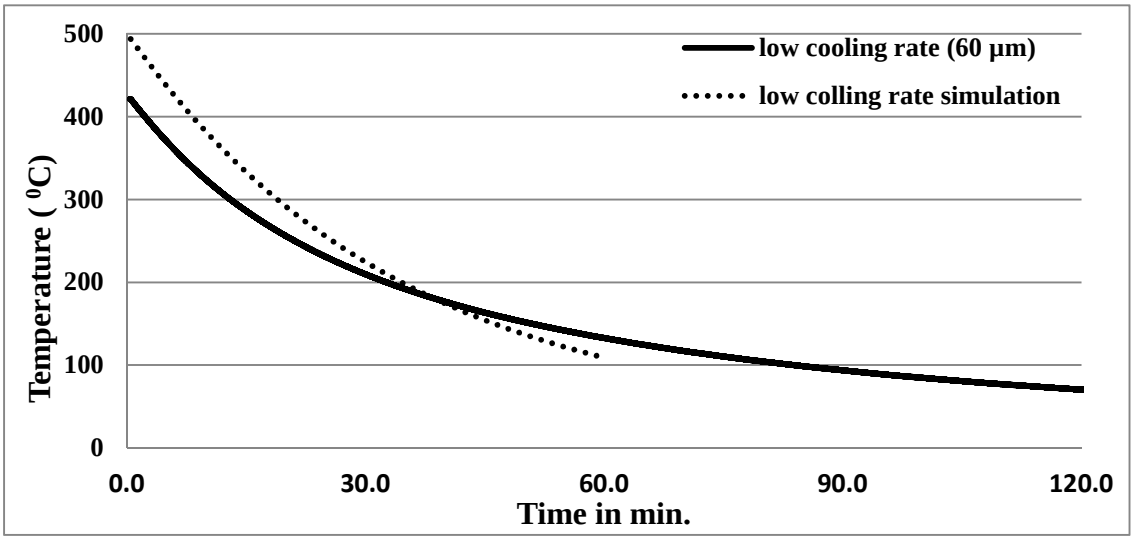

*Actual cooling rate is 7.3°C/min.

** Cooling rate from simulation is 7.9°C/min.

Figure 4-2 Cooling rate simulation vs experimental results for block casting

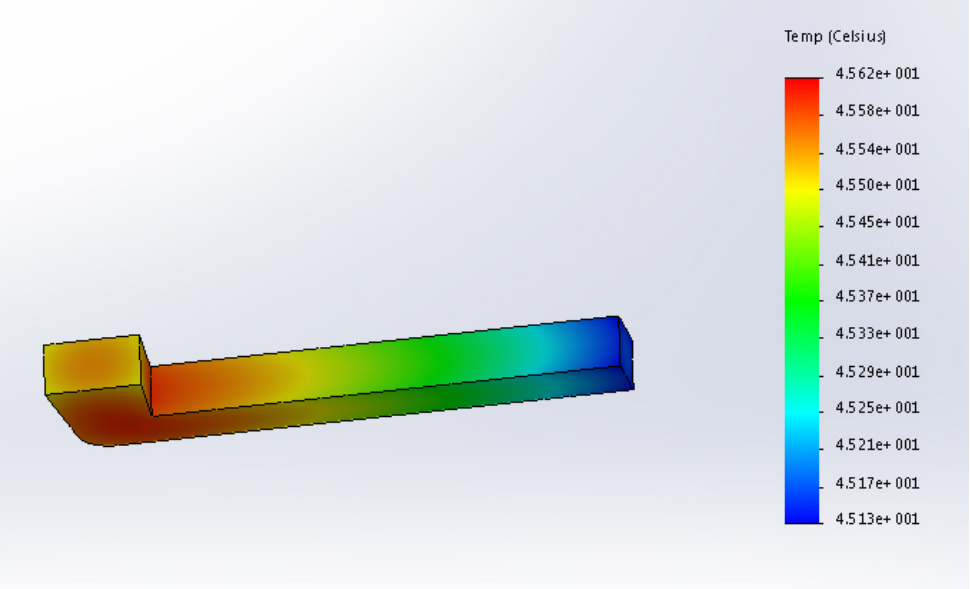

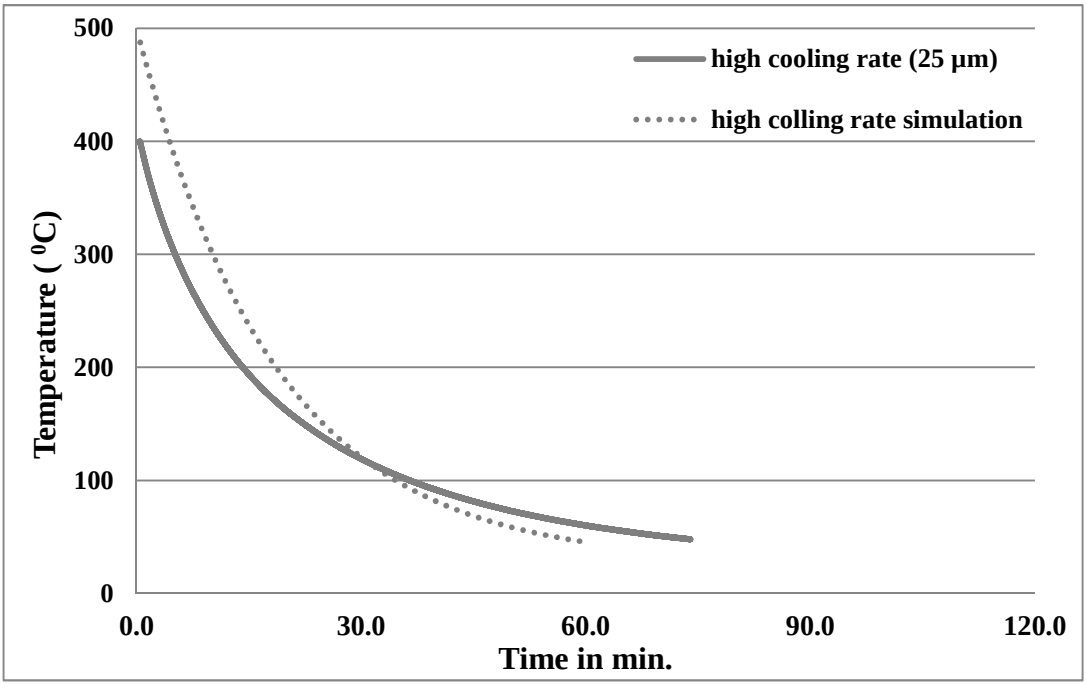

*Actual cooling rate is 14.2°C/min.

** Cooling rate from simulation is 14.8°C/min.

Figure 4-3 Cooling rate simulation vs experimental results for L-shaped casting

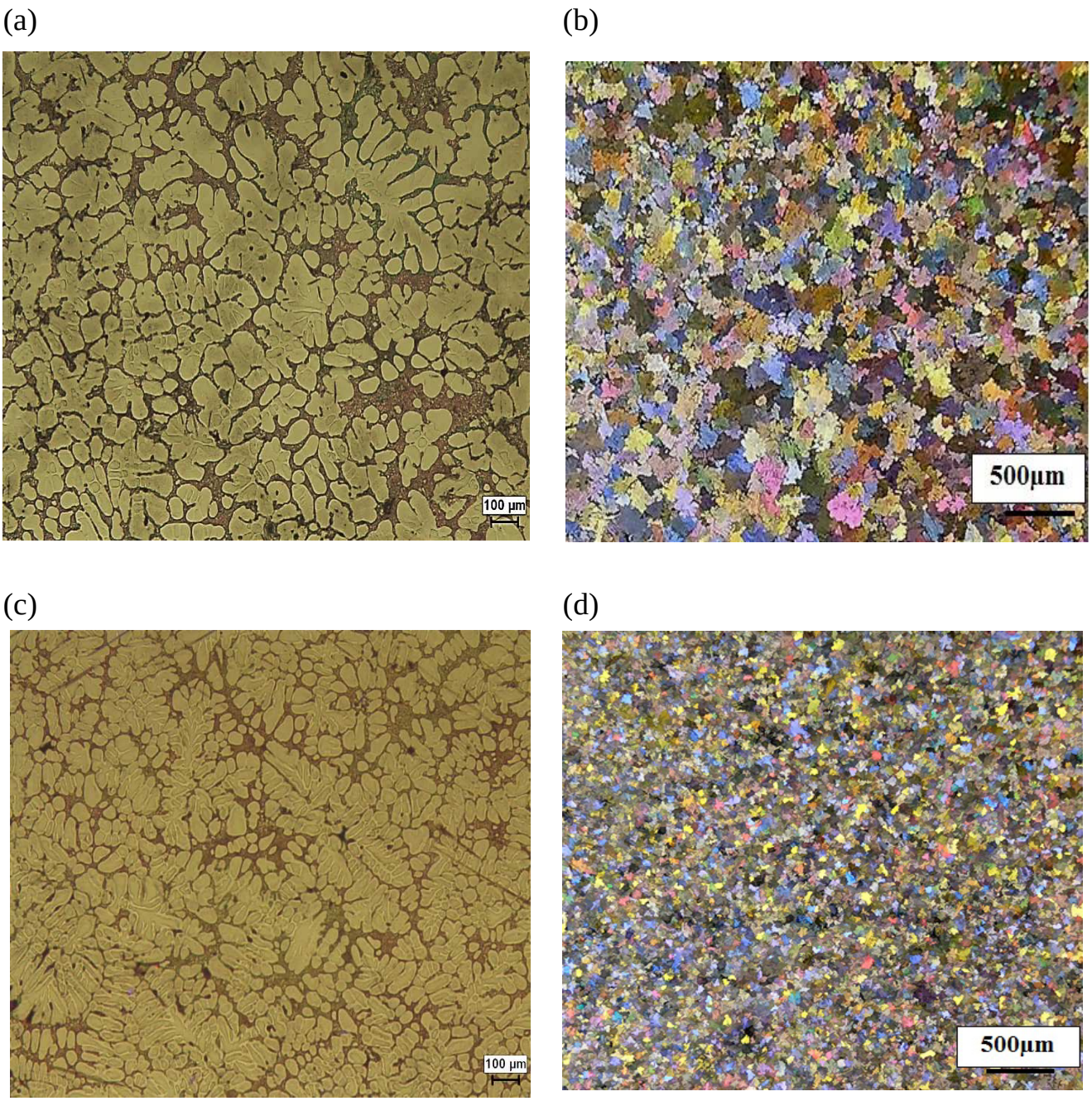

Figure 4-4 *(a, c) Optical micrographs of B319.1 alloy for (a) block casting; (c) L-shaped casting; (b, d) Macrographs showing grain size in (b) block casting; (d) L-shaped casting.*

Table 4-1 Results of dendrite arm spacing measurements

	Block Casting (low cooling rate)		**L-shaped casting(high cooling rate)**	
	SDAS (µm)	**Std.**	**SDAS (µm)**	**Std.**
B319.1	56.5	17.3	30.15	8.08
A356.1	55.9	15.7	27.8	8.2

4.2.2 Analysis of Secondary phases

4.2.2.1 Analysis in the as cast condition

Mechanical properties of castings are notably influenced by the grain size and its morphology, the secondary dendrite arm spacing (SDAS), and the size and distribution of secondary intermetallic phases [84]. For this reason, an in-depth analysis of the secondary intermetallic phases was carried out on the Al-Si-Mg (A356.1) and Al-Si-Cu-Mg (B319.1) alloys. SEM analysis showed that the as-cast microstructure of Al-Si-Mg (A356.1) alloy contains the α-Al dendritic phase, Al-Si eutectic, Mg_2Si intermetallics phases as displayed in Figure 4-5. In Figure 4-6, the Al-Si-Cu-Mg (B319.1) alloy was found to contain Al-Si eutectic, blocky Al_2Cu, platelet β-(Al_5FeSi) and Chinese script α-$Al_{15}(Fe,Mn)_3Si_2$ iron intermetallic phases, and small particles of the Q-$Al_5Mg_8Cu_2Si_6$ intermetallic phases.

Cooling rate has significant impact on the final microstructure of Al-alloys, notably the silicon morphology, and size and distribution of the intermetallic phases [11] [84]. Increasing the cooling rate enhances the distribution of the intermetallics and reduces the size of the blocky Al_2Cu phase, such as that observed in Figure 4-5 and Figure 4-6, which is in good agreement with the findings of Li et al. [27]. By cooling faster from the liquid, the diffusion-controlled formation of strengthening phases is limited, creating a more

saturated solid solution and finer distribution of constituent particles, which are easier to dissolve during heat treatment [85] [86].

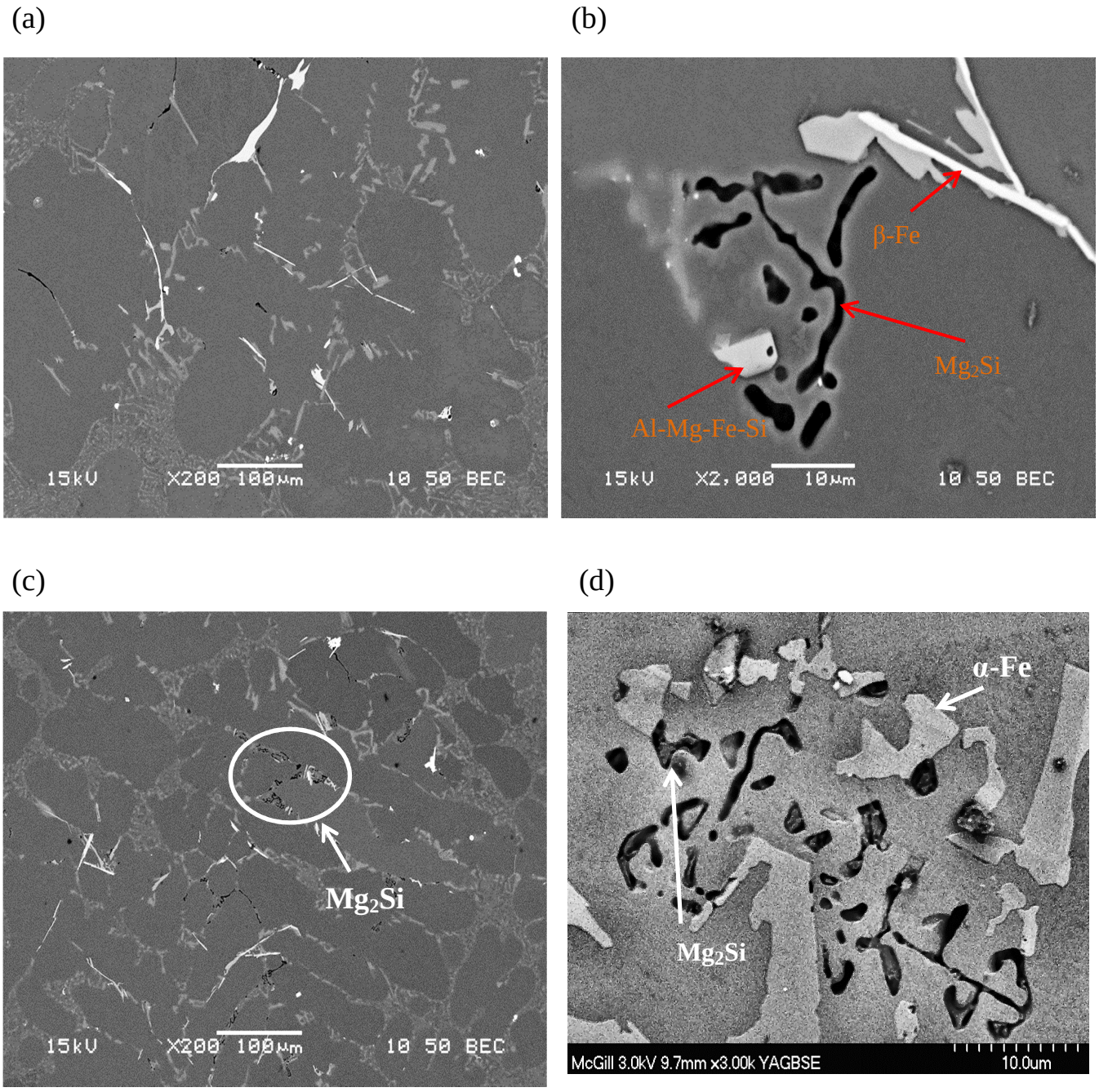

Figure 4-5 Backscattered electron images of as cast A356.1 (a-b) block mold casting. (c-d) L-shaped mold casting

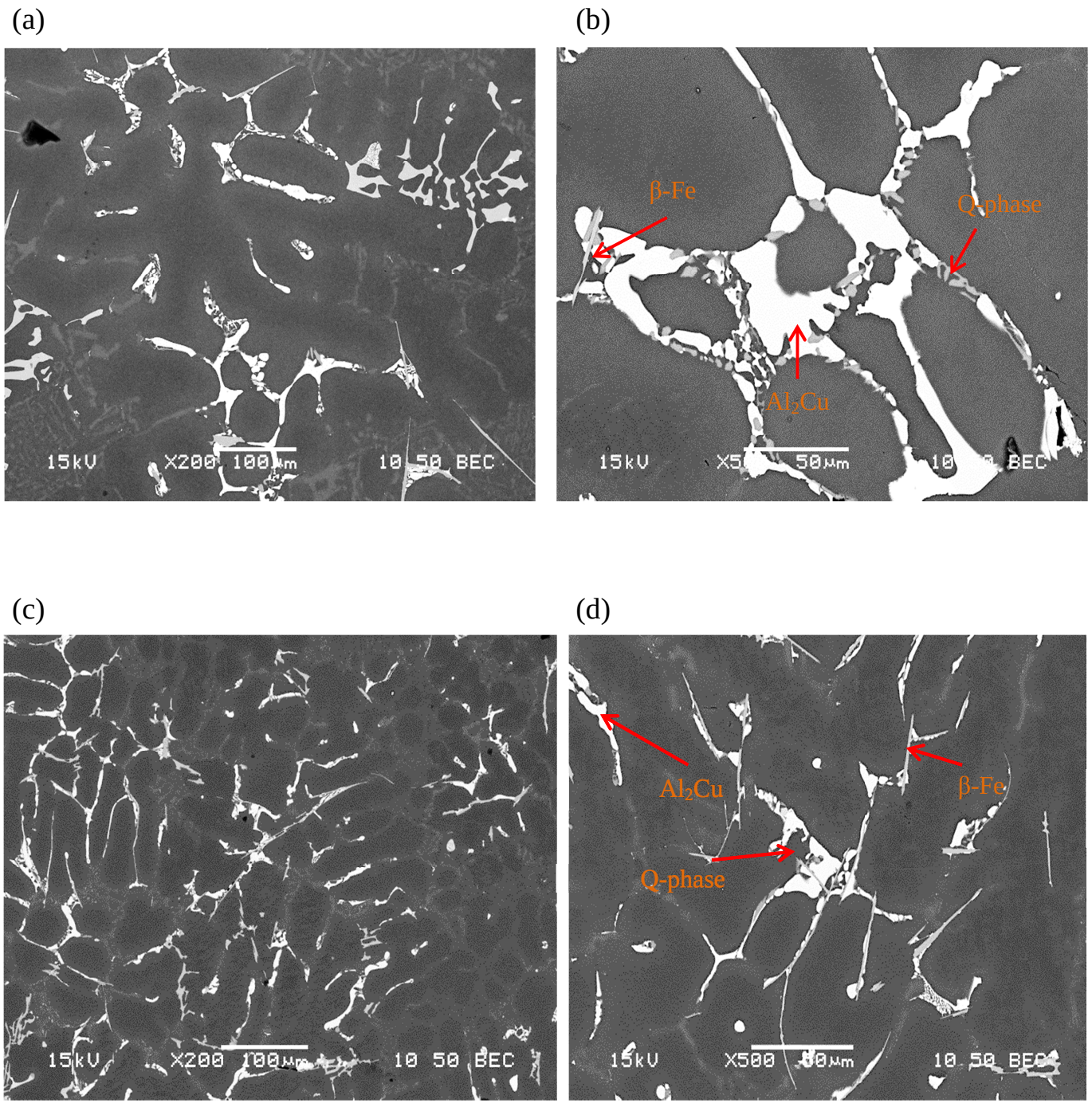

Figure 4-6 Backscattered electron images of as cast B319.1 (a-b) block mold casting. (c-d) L-shaped mold casting.

In Table 4-2, the results indicate that increasing the cooling rate reduced the volume fraction of intermetallics to 5% compared to 8% observed in the low cooling rate sample. It is also worth mentioning that the size of formed intermetallic phases was significantly affected by the cooling rate, where the average particle size was 116 μm^2 for the block casting specimen obtained at low solidification rate was reduced to 40 μm^2 in the L-shaped casting specimen. These consequences influence the outcome of the solution heat treatment process where an increased cooling rate leads to better dissolution of alloying elements compared to low cooling rate samples. The variation in the volume fraction of intermetallics at different cooling rates has been documented by Li et al. [27] who reported that increased cooling rate reduced the volume fraction of the Al_2Cu phase in the interdendritic regions which supports the findings of the current work.

Tensile properties of B319.1.2 alloys at different solidification rates were examined by Samuel and Samuel [87]. Their results showed that as the SDAS increased from 28 to 95 µm, the ultimate tensile strength (UTS) decreased by about 20%, while the elongation decreased by as much as 80%. However, the yield strength (YS) was observed to remain constant regardless of solidification time.

Table 4-2 Volume fraction results for A356.1 and B319.1

	block mold casting		**L-shaped mold casting**	
	B319.1	**A356.1**	**B319.1**	**A356.1**
% intermetallics average vol. fraction	7.5	0.82	4.2	0.85
intermetallic average particle size in μm^2	116.76	30.2	40.5	29.7

4.2.2.2 Analysis in the solution heat-treated condition

Depending on the alloy composition and temperature used for solution heat treatment, phases formed during solidification have its own tendency for dissolution into the matrix during heat treatment. The A356.1 or Al-Si-Mg alloy, can be solution treated at a temperature ranging from 540°C to 550°C. At this temperature, the diffusion rate of Mg into ~~Cu~~ Al is very high hence the dissolution of Mg_2Si phase occurs very fast. Rometsch et al. [88] report that the solution treatment for A356.1 alloy with SDAS 40µm at 540^0C for an hour can completely dissolve and homogenize the alloy thoroughly. Figure 4-7 shows complete dissolution of Mg_2Si phase in samples of both both block and L-shape casting.

(a) (b)

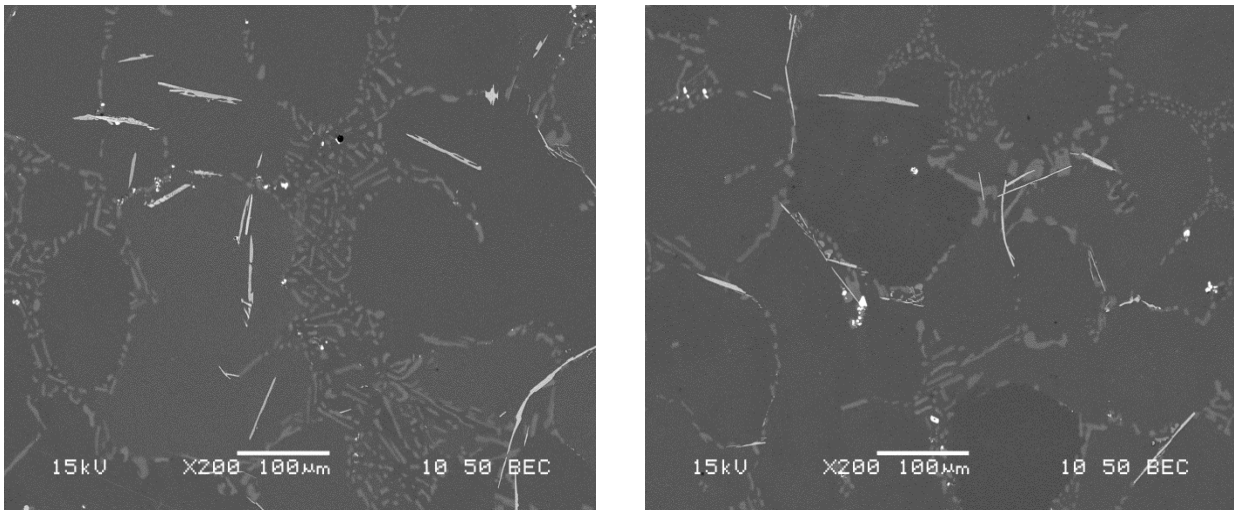

Figure 4-7 Backscattered electron images of A356.1 after solution heat treatment (a) block mold casting. (c) L-shaped mold casting

In contrast, the B319.1 alloy must be solution heat treated at a lower temperature to avoid local melting of Cu-rich phases such as Al_2Cu and the Q-phase. As Cu has low diffusivity in aluminum, it is recommended to prolong the solution heat treatment process to at least 8 hours, to ensure a high and homogenous concentration of alloying elements in solid solution [30] [86]. Figure 4-8 (a) shows incomplete dissolution of Al_2Cu and Q-phase

in the B319.1 sample obtained from the block casting (low cooling rate), whereas the sample shown in Figure 4-8 (b), obtained from the L-shaped casting at high cooling rate, reveals complete dissolution of these phases, as well as fragmentation of the iron bearing phases. These observations concur with the findings of Sjölander et al. [89] who reported that solution temperature and time are largely dependent on the microstructure.

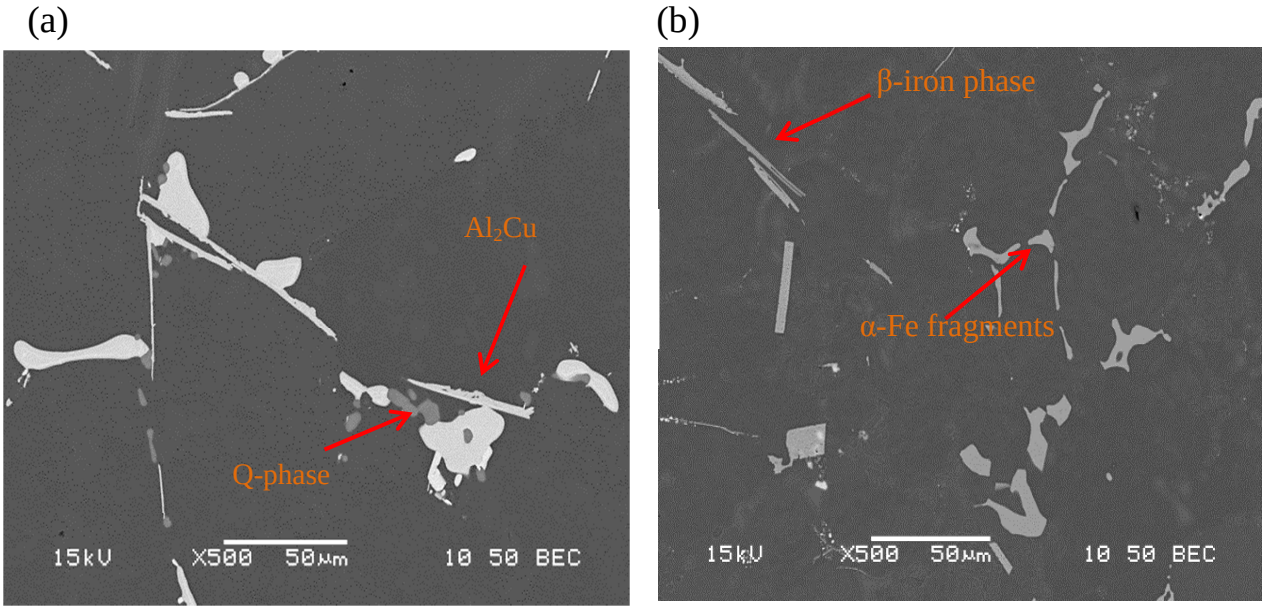

Figure 4-8 Backscattered electron images of B319.1 alloy samples after solution heat treatment: (a) block mold casting. (c) L-shaped mold casting

4.3 Mechanical Properties

Most of the mechanical properties of any casting are initially determined in the solidification (as-cast condition), and may be improved thereafter by subjecting the casting to a suitable heat treatment process. By following the evolution of the microstructure during the process, the heat treatment conditions may be optimized [90].

In 3xx alloys, the main parameters that control the mechanical properties are the iron and copper intermetallics, the eutectic silicon particle characteristics, the porosity size

and distribution, and the supersaturation level of Mg and Cu in the α-Al matrix after solution heat treatment. The addition of Cu and Mg to Al-Si alloys can improve their room temperature strength through the formation of Mg_2Si and Al_2Cu precipitates. The tensile properties of casting alloys are affected mainly by their microstructure, grain size, and casting defects. The fact that the tensile properties depend on several, often interrelated, variables may explain the confusion which exists relating to the properties of cast Al alloys.

All tensile testing was carried out at room temperature, at a strain rate of $4x10^{-4}$ s^{-1}, using an Instron Universal Mechanical Testing machine, where the testing was carried out at room temperature for the as-cast, T6 and T7 heat-treated test bars of the two alloys. Figure 4-9 and Figure 4-10 show the ultimate tensile strength (UTS) and yield strength (YS), as well as the percentage elongation (%El) values obtained at room temperature for the different conditions. The X-axis represents the alloy condition (as-cast, T6-treated for aging times of 10 h, 50 h and 100 h and T7-treated for aging times of 10 h, 50 h and 100 h). The primary Y-axis represents the strength values (UTS and YS), while the secondary Y-axis represents the percentage elongation value obtained for each condition studied.

From Figure 4-9 and Figure 4-10, it will be observed that the strength values for the as-cast alloy samples of A356.1 and B319.1 exhibit UTS values of 229 and 319MPa, respectively. The superior mechanical properties of B319.1 may be attributed to the type of strengthening phases formed during solidification. The B319.1 alloy contains Al, Si and Cu, and Mg and Fe, while the A356.1 alloy is mainly composed of Al, Si and Mg as strengthening element. The primary strengthening phases for the A356.1 alloy is the beta phase, Mg_2Si while the primary strengthening phases for B319.1 is θ phase are the Al_2Cu and eutectic silicon, which are harder than strengthening phases in A356.1. The alloying elements that added to B319.1 enhanced its mechanical properties compared to A356.1.

Figure 4-9 shows the mechanical properties of A356.1 and its response to different aging temperatures, while Figure 4-10 shows those of B319.1. It is observed that yield and tensile strength for B319.1 are generally higher by 60 and 40% respectively, compared to that of A356.1.

The best combination of strength and ductility is achieved from a rapid quenching, such as quenching in cold water. This is the reason why quenching in cold water gives the best mechanical properties. The fast cooling rate results in a higher vacancy concentration enabling higher mobility of the elements in the primary Al phase during ageing. On the other hand, low cooling rates, as in air cooling, for example, have a detrimental effect on the mechanical properties due to several factors, including precipitation during quenching, localized over-ageing, reduction in grain boundaries, an increased tendency for corrosion, and a reduced response to ageing treatment [45]. In other words, the reduction in tensile properties of the sample is due to the reduction in cooling rate, which will affect the microstructures when the sample is quenched in different quenching media.

In both alloys, T6 temper allows for increased strength where it develops more stable mechanical properties with a corresponding loss of ductility. Aging at 170°C for 10 hours hardens the alloy, due to the formation of Guinier-Preston zones and coherent θ’ Al_2Cu particles. Overaging can be done either at high temperatures or prolonged exposure at an intermediate temperature, and results in the simultaneous formation of relatively large, non-coherent θ’ Al_2Cu plates which act as hard non-shearable obstacles to dislocations. Such non-shearable particles lead to lower UTS but with high strain-hardening rate, due to the accumulation of Orowan loops around the strengthening particles. As the strain is increased, the buildup of primary shear loops generates intense stress fields around the strengthening precipitates. In A356.1, overaging starts to be noticeable at 170°C after 10

hours while it takes 50 hours for overaging to be distinguished for B319.1 at the same temperature. In conclusion, aging time and temperature are crucial factors that have a significant effect on the alloy strength.

The elongation values for A356.1 are at least twice the elongation values observed for B319.1 alloy, which is a result of a minimum number of voids/porosity and modification in the developed microstructures by avoiding stress amplification factors through transformation of the Si eutectic from an acicular to a lamellar structure. Another reason for the high ductility of A356.1 is the high volume fraction of the α-Al present, which is tougher, has a lower yield stress than the Si particles, and thus provides a way of confining an advancing crack by application of the classical tip blunting mechanism.

Fractography is considered suitable for highlighting the various features observed on the fracture surface of tensile-tested samples. Samples for fractographic examination were selected from A356.1 and B319.1 alloys in the as-cast, solution heat-treated, and aged conditions (using samples aged at 170°C and 250°C for 100 hours) considered as the main conditions of interest for the analysis. Figure 4-11 shows the fracture surface of the as-cast of B319.1 alloy sample. This figure reveals the presence of two main intermetallic phases, namely α-$Al_{15}(Fe,Mn)_3Si_2$ and θ-Al_2Cu, as confirmed by the corresponding EDX spectra shown in Figure 4-11(b) and Figure 4-11(c), respectively. Solution heat-treatment of this alloy resulted in the dissolution of the Al_2Cu phase as displayed in Figure 4-11(d).

A typical ductile fracture, which involves necking of the tensile test specimen and a large number of medium to large sized fine dimples, can be seen in the B319.1 as-cast sample (Figure 4-12(a)). These dimples are oval-like or cup-like depressions at the fracture surface and are elongated in the direction of the applied load [91]. The shape and size of the dimples are determined by the size and distribution of the microstructural discontinuities

[91]. Same observations were noticed for samples aged at 250°C for 100 hours; as seen from Figure 4-12(c). On the other hand, after aging at 170°C for 100 hours, the fracture surface revealed characteristics of a mixed fracture mechanism, consisting of dimples, cleavage facets and cracks, as shown in Figure 4-12(b). These features are indications of hardening that occurs when aging is carried out at low temperature such as 170°C as a result of reduced ductility due to the formation of fine dense precipitates. Figure 4-13 fracture surface of A356.1 alloy samples examined in the as-cast, after T6 at 170°C, and after T7 at 250°C conditions. The figure shows ductile fracture features where dimples display tendency to increase with ductility.

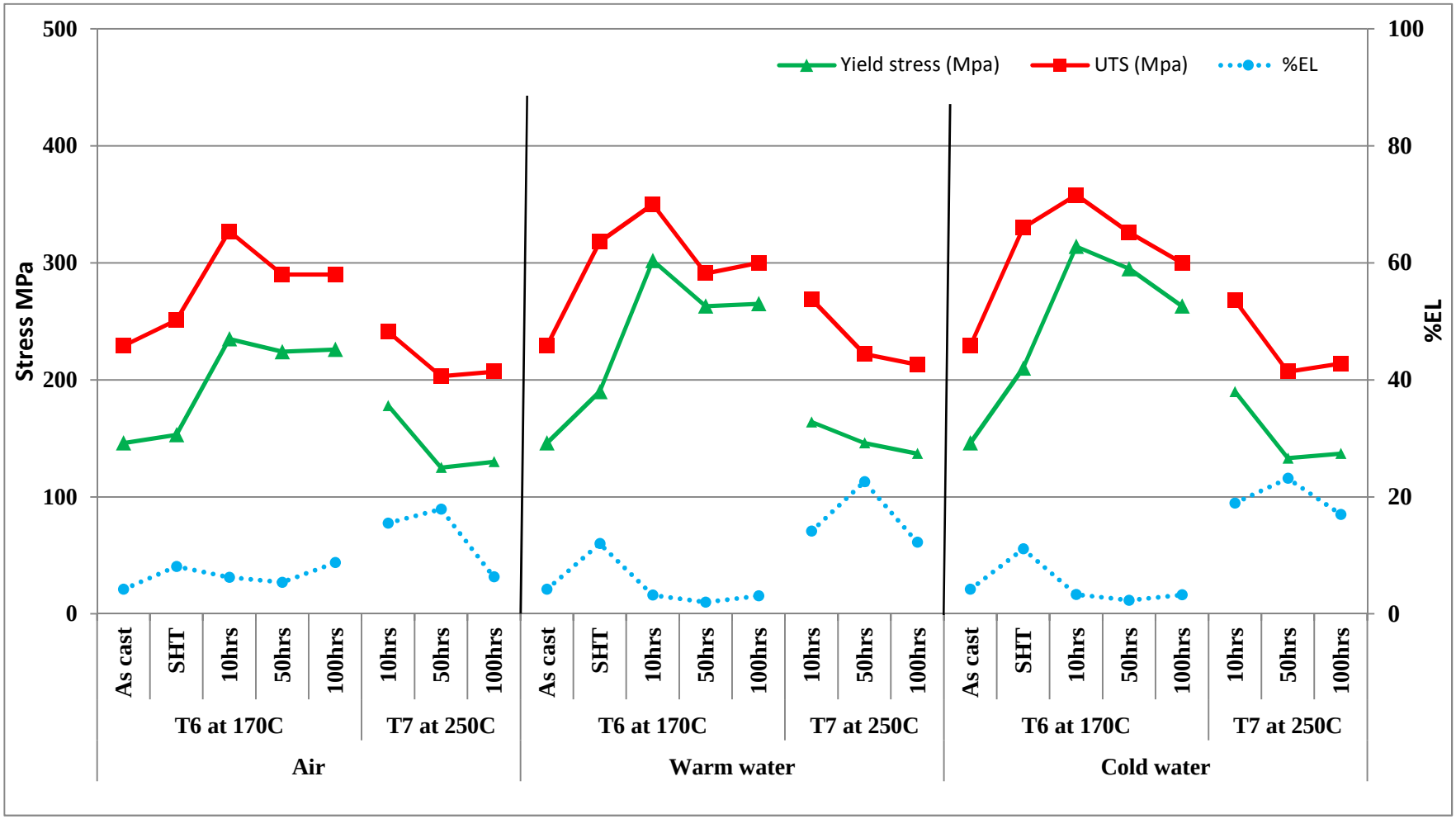

Figure 4-9 Variation in YS, UTS and %El at different quenching rates and different aging parameters for A356.1alloy.

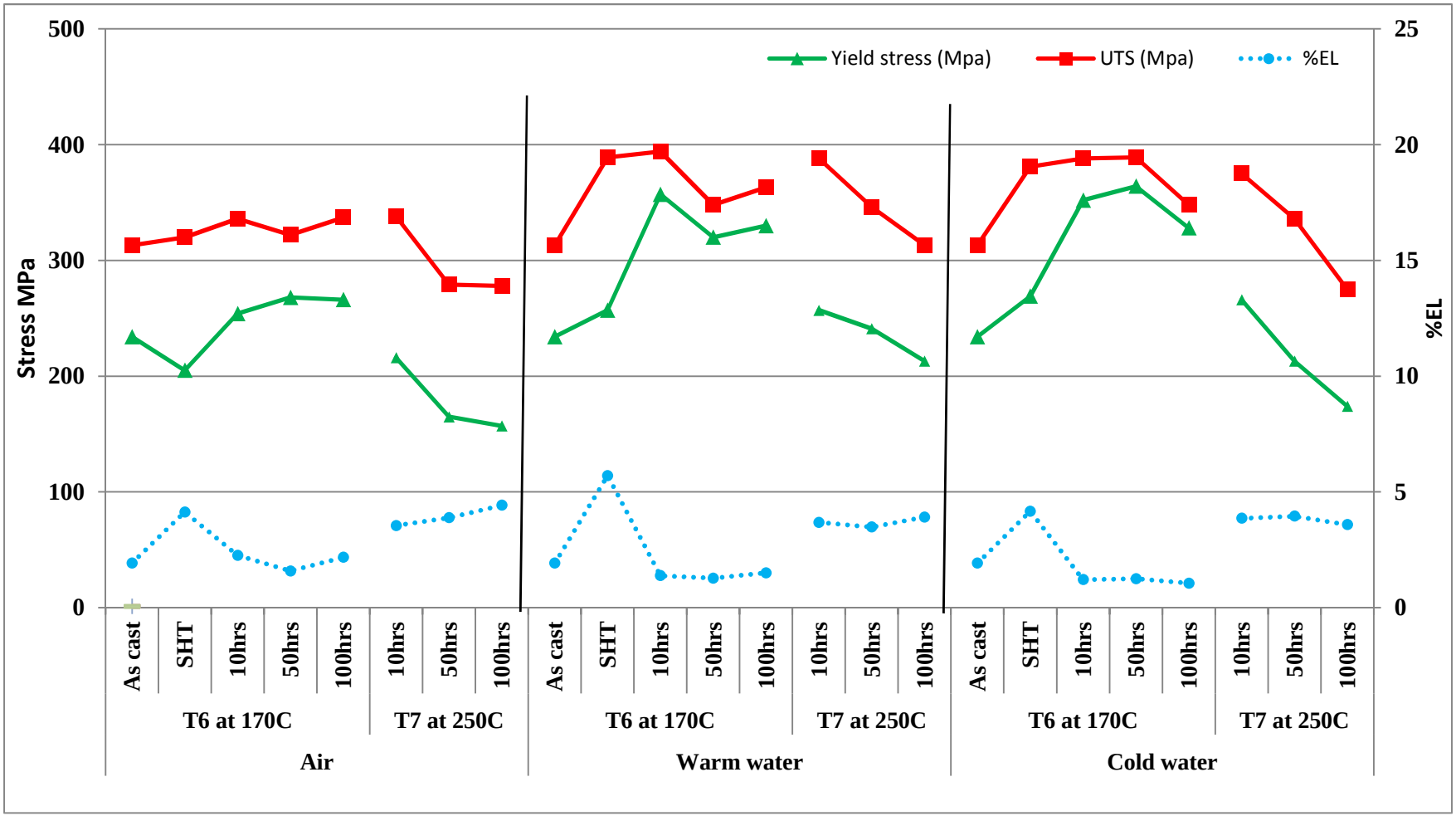

Figure 4-10 Variation in YS, UTS and %El at different quenching rates and different aging parameters for B319.1alloy.

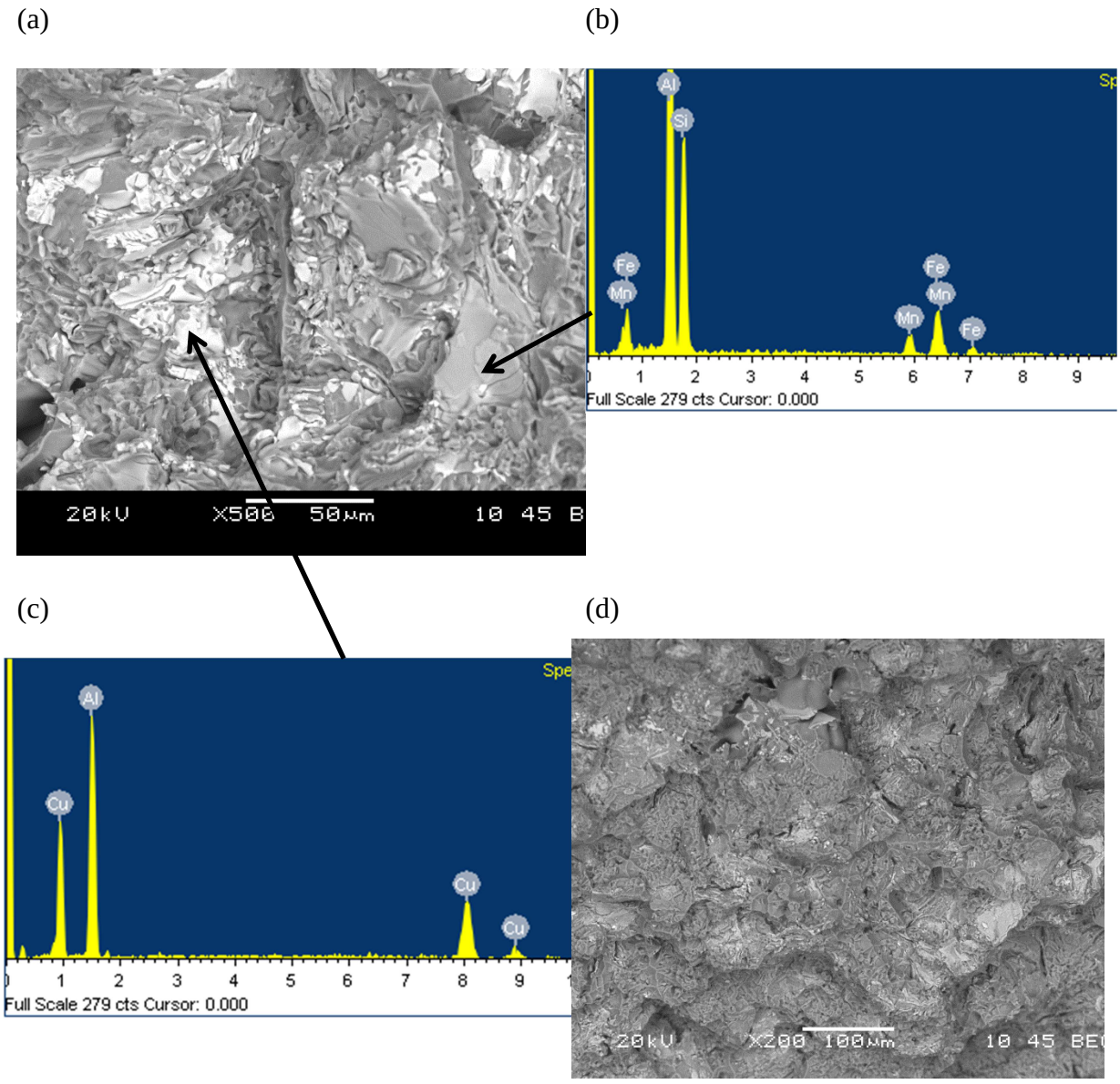

Figure 4-11 (a) Fracture surface of as-cast B319.1 alloy; (b) EDX-ray spectrum corresponding to α-Fe phase in (a); (c) EDX-ray spectrum corresponding to Al_2Cu in (a);and (d) fracture surface of solution heat-treated B319.1 alloy.

(a)

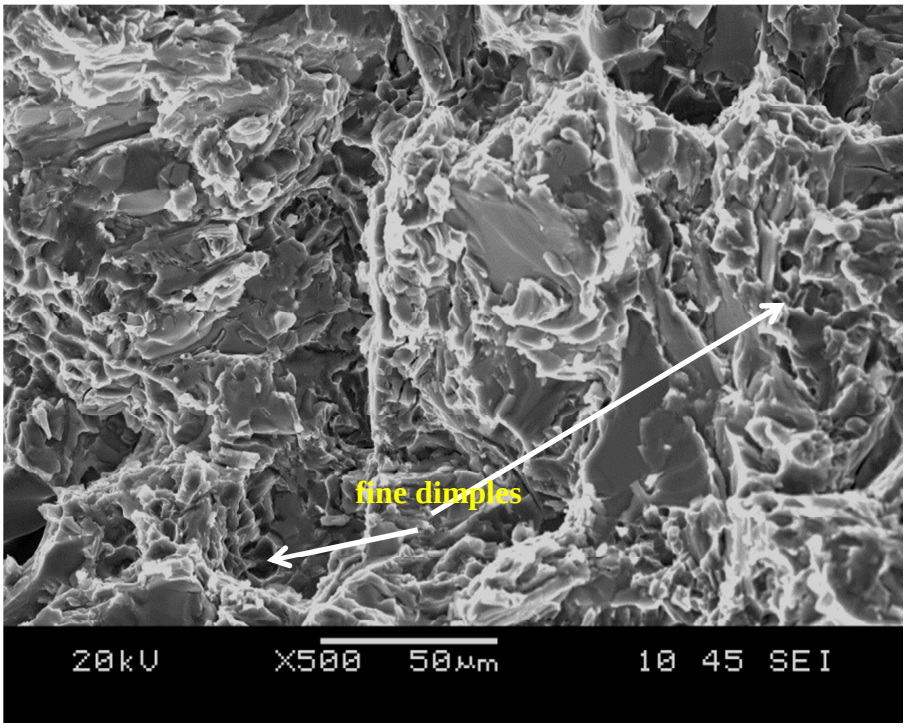
fine dimples
20kV X500 50µm 10 45 SEI

(b)

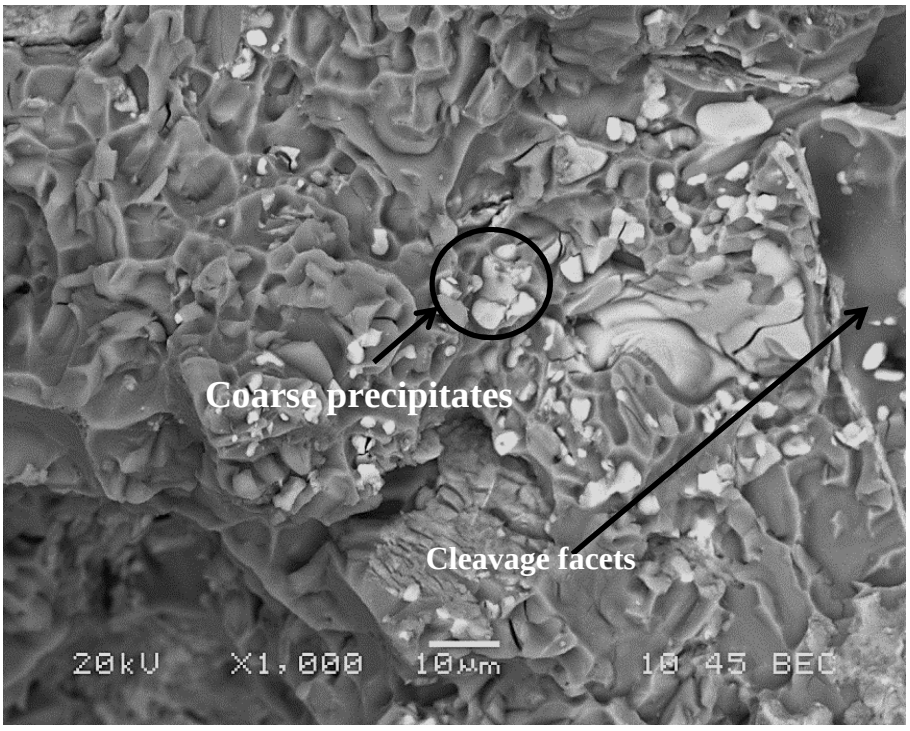
Coarse precipitates
Cleavage facets
20kV X1,000 10µm 10 45 BEC

(c)

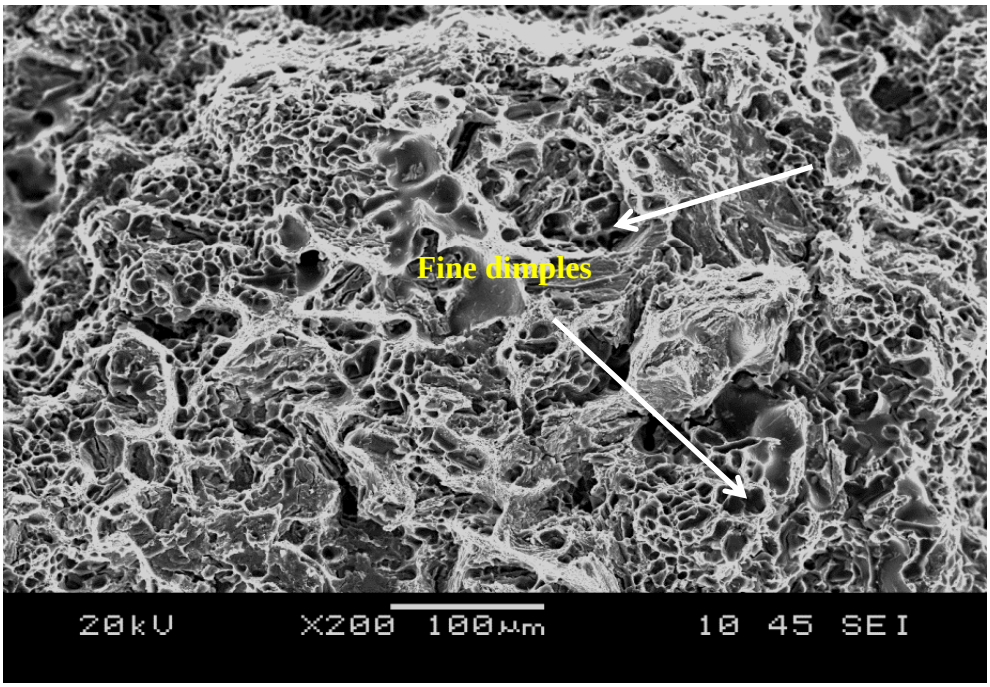

Figure 4-12 SEM images of the fracture surface of the 319 alloy, (a) as-cast, (b) aging at 170°C for 100 hrs, (c) aging at 250°C for 100 hrs.

(a)

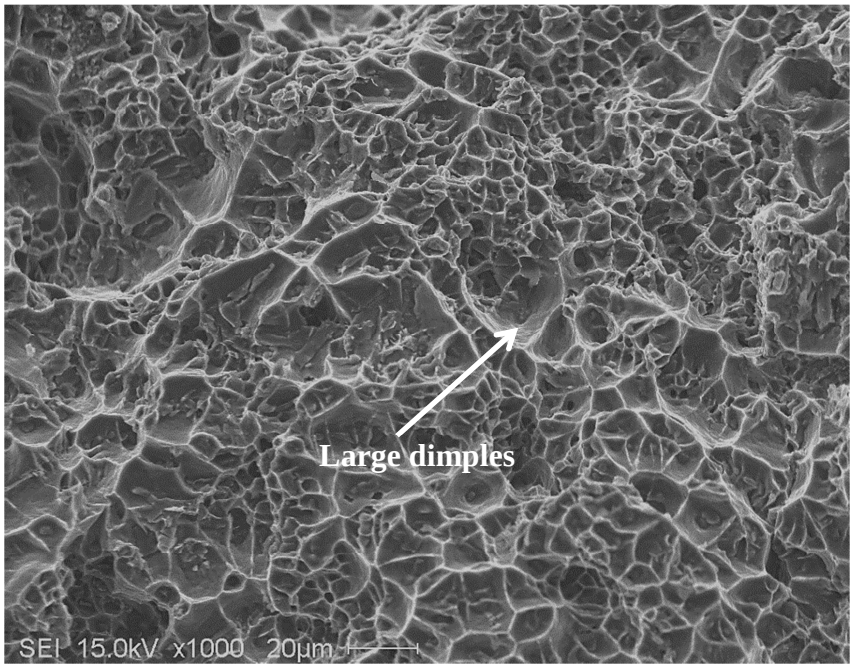

(b)

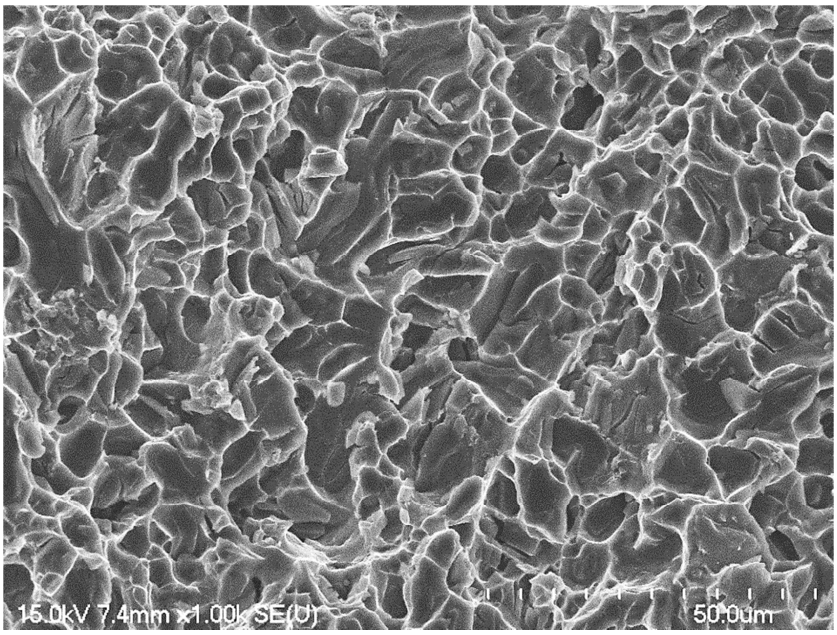

(c)

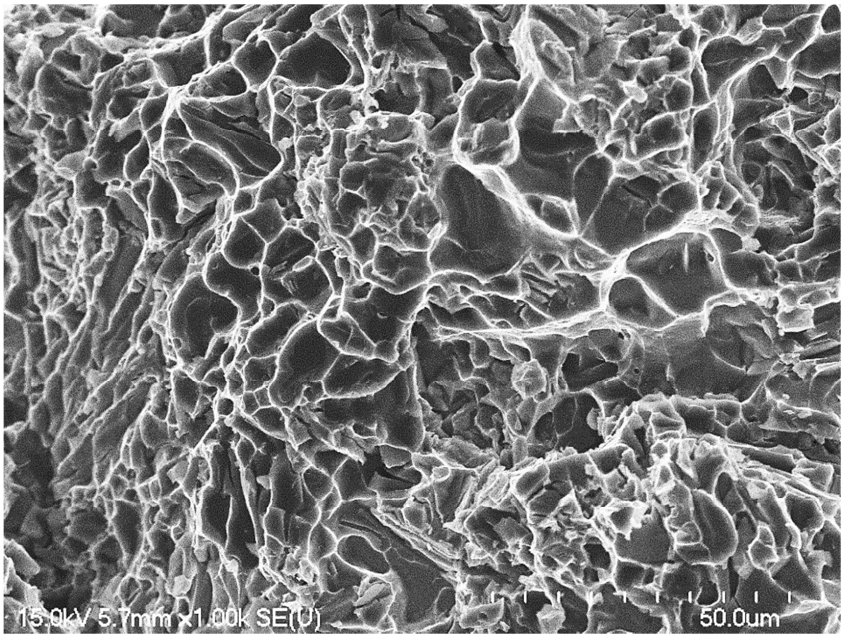

Figure 4-13 SEM images of the fracture surface of the 356 alloy, (a) as-cast, (b) aging at 170°C for 100 hrs, (c) aging at 250°C for 100 hrs.

4.4 Analysis of Precipitates

Aging treatment follows the solution treatment and quenching processes where the castings are subjected to a specified temperature for a certain length of time. Depending on the temperature applied to the casting, the excess solute atoms formed in the supersaturated solid solution (SSS) of α-Al start to diffuse out and eventually form precipitates. The precipitation takes place in high energy regions such as grain and phase boundaries [92]. In the early stages of aging treatment, the solute atoms starts to forms within of SSSS in the form of coherent clusters referred to as Guinier-Preston (GP) zones accompanied by an enhancement in the strength of the alloy. With further increase in the aging time, formation of coherent and semi-coherent transition phases takes place at the GP zone sites which leads to a further increase in the strength of the casting, up to a maximum level at peak-aging. Beyond the peak-strength, any further aging results in over-aging in which equilibrium and coarser phases form and lead to alloy softening and a reduction in the strength [92].

In this section, investigation of the development of precipitate during aging of A356.1 and B319.1 alloys will be discussed. Figure 4-15 and Figure 4-16 are FESEM images, which illustrate the size and distribution of precipitates formed at 170°C and 250°C aging temperatures in A356.1 and B319.1 alloys, respectively. Figure 4-15(a) illustrates the characteristics of the hardening precipitates, which were formed after aging at 170°C for 100 hours in A356.1, while Figure 4-15(b) shows the hardening precipitates formed after aging at 250°C for 100hours; and Figure 4-15(c) shows an EDX spectrum corresponding to the precipitates observed in Figure 4-15. Figure 4-16(a) represents the size and density of precipitates that were formed in B319.1 alloy after aging at 170°C for 100 hours.

Figure 4-16(b) shows the hardening precipitates at 250°C for 100 hours; and Figure 4-16(c) shows an EDX spectrum corresponding to the phases observed.

For A356.1, illustrates that applying aging treatment for 100 hours at 170°C results in the precipitation of fine spherical precipitates in the metal matrix, and that increasing the aging temperature to 250°C leads to coarsening of the precipitates and reduction of their density in the matrix. The shape of the spherical precipitates is in good agreement with the work of Ibrahim et al. [93] while the observed thin plates and/or rod-shaped particles reported by earlier researchers [94] [95] did not form in the present work during aging at 170°C. Aging at 250°C revealed formation of rod shaped precipitates along with spherical shaped ones, as seen in Figure 4-15(b). In the case of the B319.1 alloy, similar observations were noted regarding the coarsening observed due to aging at high temperatures for long periods of time but in this case the precipitates were more plate-shaped in structure, as may be seen in Figure 4-16. This behavior is in accordance with the Ostwald ripening concept [92] [96] [97].

Ostwald ripening concept hypothesizes that in order to reach a more stable system and to reduce the interfacial energy, formation of large precipitates, at the expense of smaller particles, is more thermodynamically favorable, see Figure 4-14. By the application of this behavior, the system tends to lower its energy by making small crystals or solute particles dissolve and redeposit onto larger crystals or solute particles. The coarsening which occurs in the size of the precipitates is the main reason for the reduced strength and subsequently for the diminished quality which was observed when raising the aging temperature applied to the A356.1 and B319.1castings.

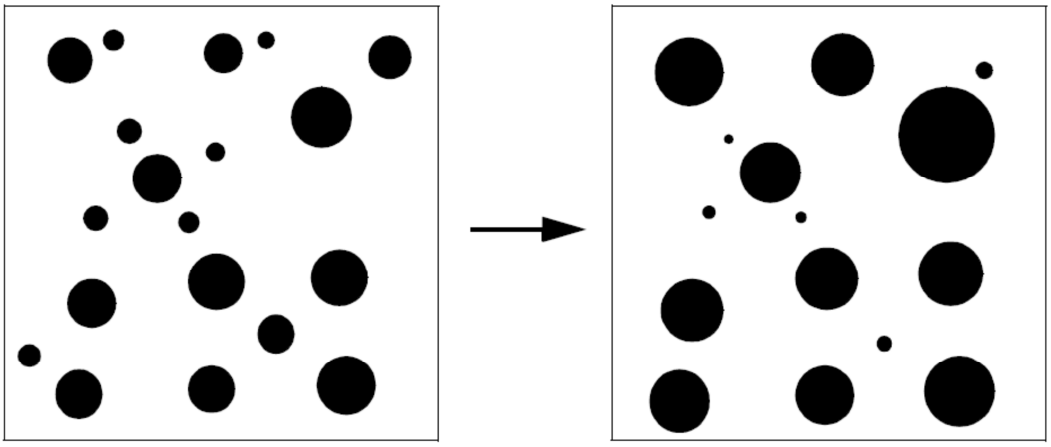

Figure 4-14 *Ostwald ripening mechanism: Larger particles grow at th expense of the smaller particles[98]*

As coarsening occurs, the inter-particle spacing is widened which will have a direct effect on the dislocation motion. According to the Orowan relationship, larger inter-particle spacing results in a decrease in the resistance to dislocation motion thereby facilitating the occurrence of Orowan looping. The increased deformability of the matrix via the easy dislocation motions leads to reduced strength and subsequently diminished quality index values in the castings [2] [99]. Aging at lower temperature results in formation of precipitates; with fine sizs, high density and lower inter-particle spacing; as seen in Figure 4-15(a) and Figure 4-16(a). In this case, the precipitates provide strong resistance to dislocation motion and the occurrence of Orowan looping becomes difficult leading to a hardening of the materials and an increase in the overall strength, as shown in Figure 4-9 and Figure 4-10.

The EDX spectra presented in Figure 4-15 (c) and Figure 4-16 (c) show the composition of the phases precipitated during the aging treatment of the A356.1 and B319.1 alloys, respectively. For A356.1, the EDX spectrum shows peaks for Mg and Si in addition to Al which corresponds to the precipitation of β-Mg_2Si. For the B319.1 alloy, the

EDX spectrum exhibits peaks for Cu, Mg, and Si in addition to Al, indicating that these would most probably correspond to the Q-$Al_5Cu_2Mg_8Si_6$ phase, although other phases such as θ-Al_2Cu, β-Mg_2Si, and *S*-Al_2CuMg may coexist in the matrix. It was not possible, however, for all these precipitates to be identified precisely using the EDX technique because of their small size. It should be noted here that the main objective for using SEM techniques was to provide an overview of the size and density of the precipitates under various aging temperatures and times as applied to the castings.

(a)

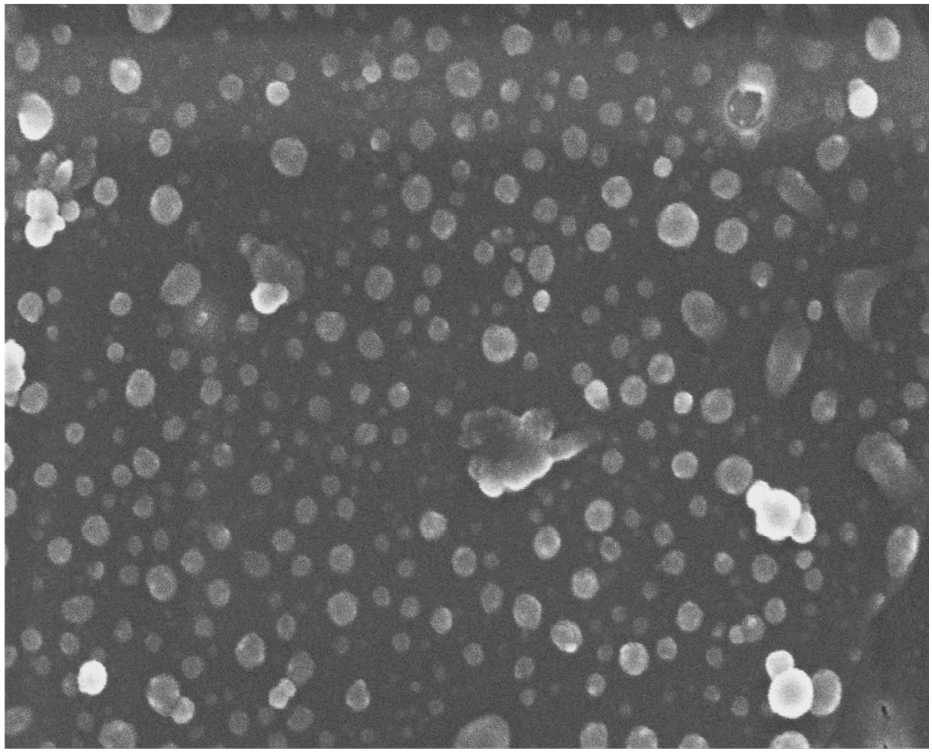

(b)

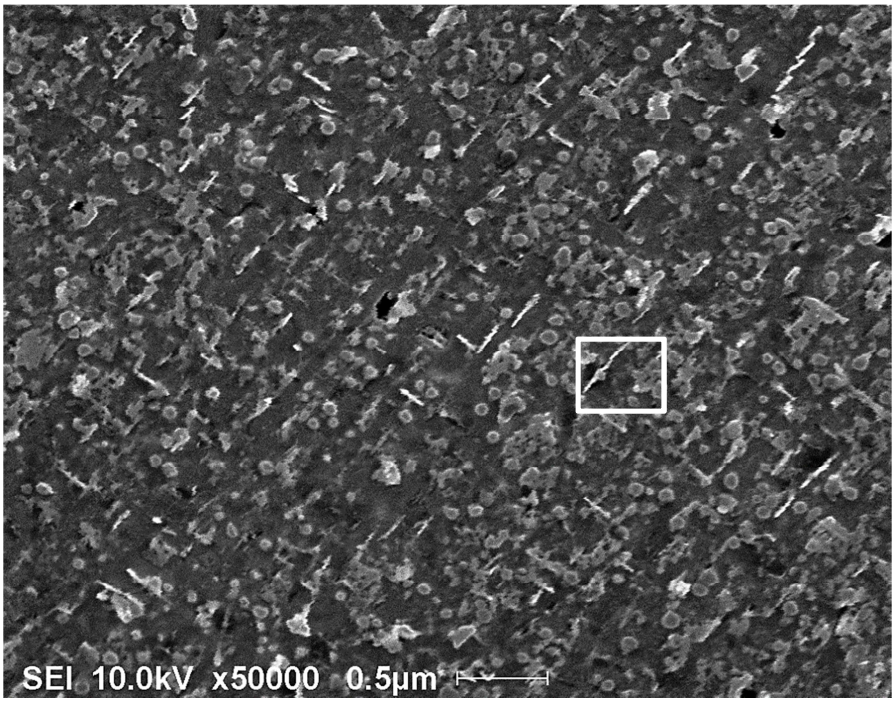

(c)

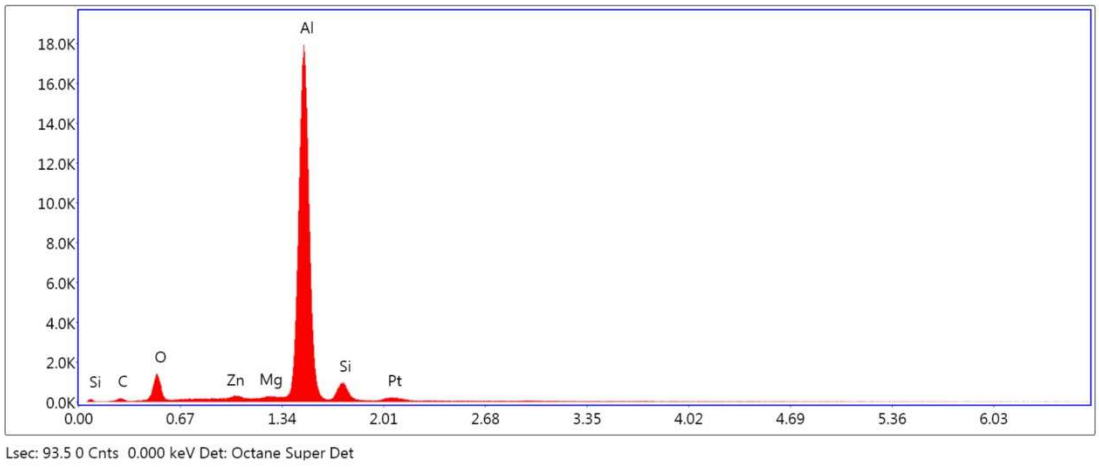

Figure 4-15 Size and density of the precipitates in 356 alloy formed at various aging temperatures (a) SEM image after aging at 170°C for 100 hrs; (b) SEM image after aging at 250°C for 100 hrs; and EDX spectrum corresponding to the precipitates observed in b.

(a)

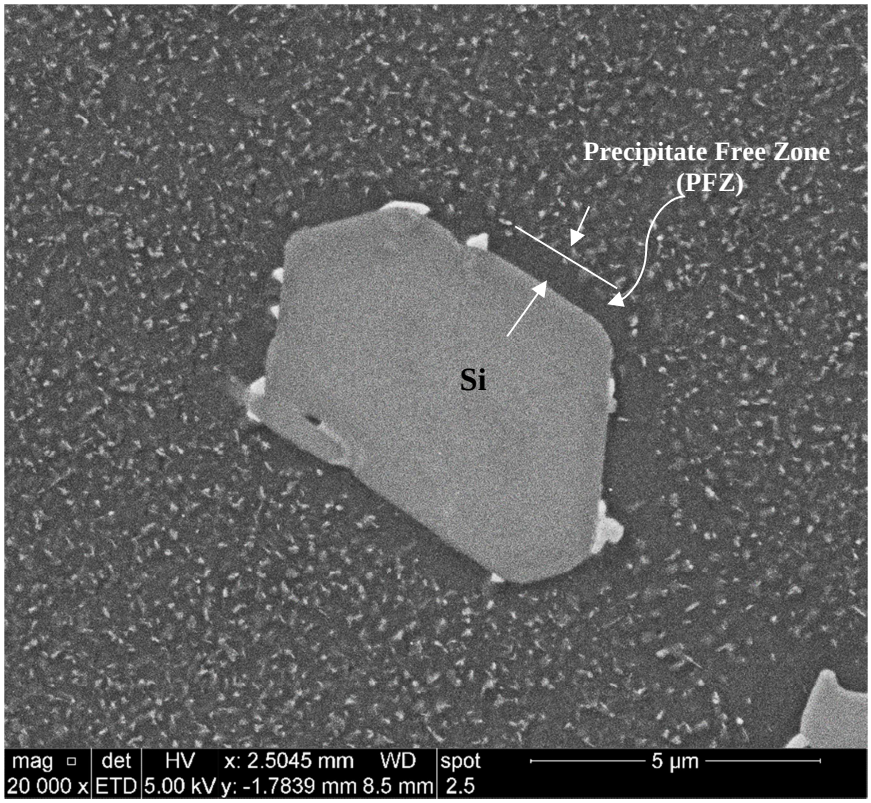
Precipitate Free Zone
(PFZ)
Si
mag det HV x: 2.5045 mm WD spot 5 µm
20 000 x ETD 5.00 kV y: -1.7839 mm 8.5 mm 2.5

(b)

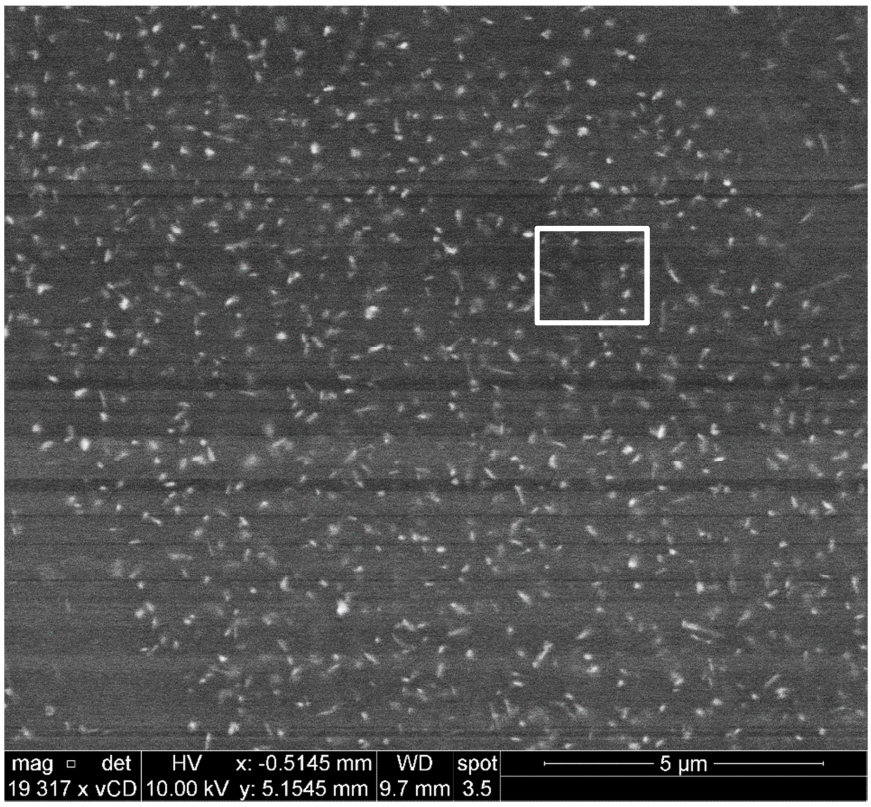
mag det HV x: -0.5145 mm WD spot 5 µm
19 317 x vCD 10.00 kV y: 5.1545 mm 9.7 mm 3.5

(c)

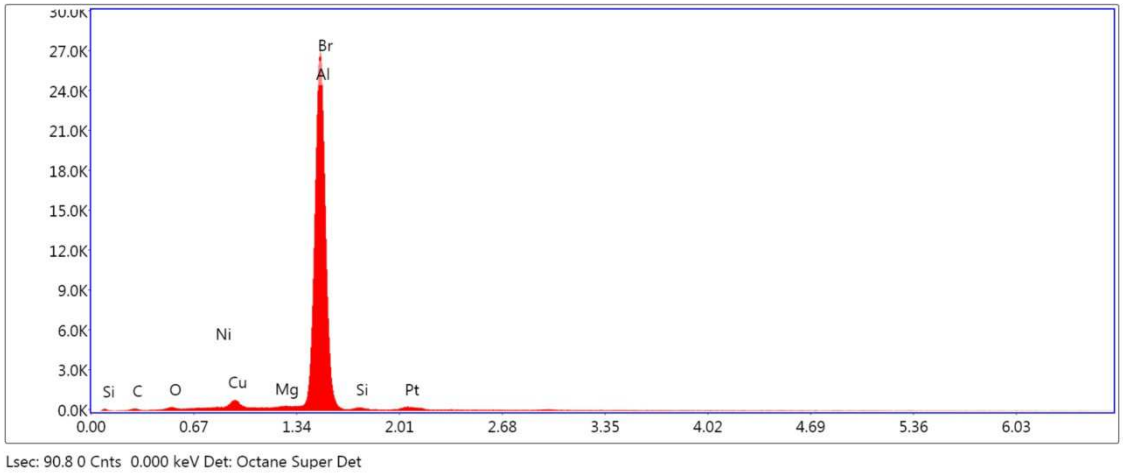

Figure 4-16 Size and density of the precipitates in 319 alloy formed at various aging temperatures (a) SEM image after aging at 170°C for 100 hrs; (b) SEM image after aging at 250°C for 100 hrs; and EDX spectrum corresponding to the precipitates observed.

4.5 Residual stresses

Residual stresses are generated due to different reasons and are generally a counter effect for plastic deformation that is caused by applied mechanical loads, thermal loads or phase changes. Mechanical and thermal processes applied to a component during service may also alter its residual stress state. Plastic deformation during machining is an example related to mechanical loads while difference in solidification of the material during casting is a source for thermal-induced residual stresses. Finally, precipitation or phase transformation resulting in a volume change can also generate residual stresses. In this chapter, residual stresses will be evaluated according to different factors such as casting mold, quenching media, aging time, aging temperature and cutting direction

In many Aluminum alloys, heat treatment is essential to achieve optimum mechanical properties, and involves rapid quenching of the part. After quenching, large thermal gradients are developed especially in big castings, leading to formation of residual

stresses. The reason behind the development of residual stresses inside a part is that the surface; which is the first part to cool down; will have compressive stresses encountered by tensile stresses at the center of the casting [4] [7].

Residual stresses are one of the important factors that can affect the life of a cast component which is not accounted for in the design of the casting. This section is dedicated mainly to study the effect of casting parameters in the development of residual stresses in B319.1 and A356.1 alloys. The sectioning method has been used for decades to measure residual stresses in structural-steel members where it is considered as a reliable, fast and cheap technique. In this technique, the residual stress is calculated using the Hook's law equation, using the measured strain values and a Young's modulus of 70GPa such as mentioned in the previous chapter.

$$\sigma = E\,(\varepsilon_0 - \varepsilon_1)$$

To measure the initial strain (ε_0) and final strain (ε_1), Wheatstone bridge, Labview software, National Instruments data acquisition equipment linked to a a SCXI-1520 universal strain gage input module were employed, as shown in Figure 4-17. Cutting was first done in vertical cutting plane and then the residual strains were measured; following this, another cut was made in the horizontal plane, as illustrated in Figure 4-18, and the residual strains were also measured to determine the effect of the cutting direction in relieving the residual stresses. In this section, residual stresses will be evaluated according to different factors such as the casting mold, quenching media, aging time, aging temperature and cutting direction

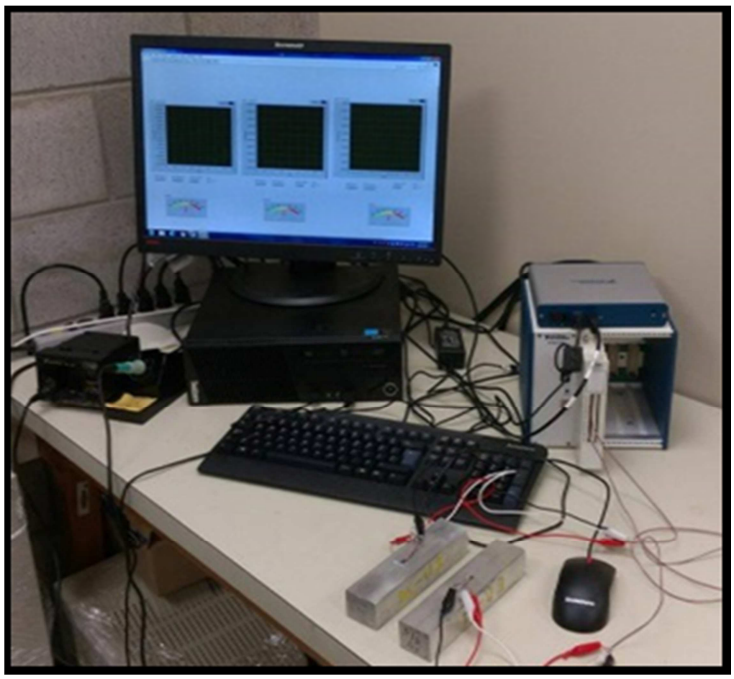

Figure 4-17 SCXI-1520 universal strain gage input module

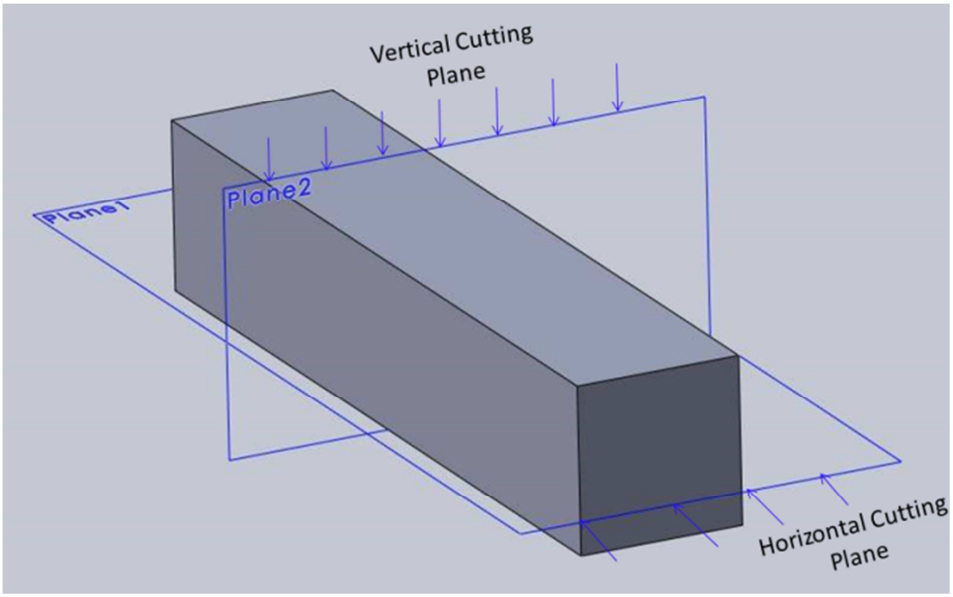

Figure 4-18 Sketch illustrating cutting directions

4.5.1 Residual stresses inside B319.1 and A356.1 alloy

As discussed in Chapter 2, when a solidified casting cools, compression stresses are formed on the surface while the casting interior is subjected to tension stresses. The magnitude of residual stresses is dependent on the quenching rate and casting size. It is found that the residual stresses will increase as thickness of the cast part increases [100].

The results for the evolution of residual stresses in A356.1 and B319.1 alloys in relation to the type of casting mold, quenching media, aging time, aging temperature and cutting direction are illustrated in a series of figures from Figure 4-19 to Figure 4-24. In general, in all figures, it is observed that ~~all~~ the residual stresses measured are compressive in nature, and are generated due to the steep thermal gradient between core and outer layer at the start of quenching/cooling process [52]. It is also clear that the magnitude of residual stresses in B319.1 alloy is about 10% higher than that observed in A356.1 alloy, which may result from the precipitation of complex phases such as α $Al_{15}(Mn,Fe)_3Si_2$, β-$A_{l5}FeSi$ and $CuAl_2$ in the B319.1alloy.

4.5.1.1 Effect of cutting direction

The technique adopted in this study was mainly used for the measurement of residual stresses in the longitudinal direction. Results of cutting in the transverse direction as in cut 1; illustrated in Figure 4-19 and Figure 4-20, proved that cutting in the vertical direction has negligible effect on the measured residual stresses in the longitudinal direction. Residual stresses are balanced through the thickness, which indicates that cutting along the direction of the thickness results in no rearrangement of the locked-in stresses. In conclusion, combining the vertical cut with the horizontal cut causes greater relaxation and

rearrangement of the locked-in residual stresses so that it has a noticeable impact on the strain gauge measurement.

4.5.1.2 Effect of solidification rate and quenching rate on the development of residual stresses

The production of a supersaturated solid solution is the most crucial step in the heat treatment of aluminum alloys. It can only be achieved by suppressing solid state diffusion by quenching from the solution treatment temperature. For best efficacy, cold water is used for quenching. The developed thermal gradient and resultant difference in the timing of the thermal contraction from edges to the center of the bar control the evolution of the residuals stresses.

The effects of solidification rate and quenching rate on the development of residual stresses in A356.1 and B319.1 alloys are shown in Figure 4-19 and Figure 4-20, respectively. The residual stresses were found to gradually decrease with decreasing cooling/quenching rate of the quenching medium. It is observed that quenching in cold water develops the highest, and air cooling develops the lowest, residual stresses. This is due to the large temperature difference between the core and the surface of the casting with the increase in cooling rate. In the figures shown, cooling in air produces the lowest residual stresses compared to other quenching media. The magnitudes of residual stresses in air-cooled samples were found to be in good agreement with those observed for as-cast samples.

For Al-Cu alloys, Dong [101] reported that the maximum compressive stress of samples quenched in 20°C water is103.6 MPa; measured by using the slitting method. When the samples were quenched in warm water at 60°C and 80°C, respectively, the

magnitude of the residual stresses was reduced by 10% and 70%. The residual stresses obtained after quenching for B319.1 and A356.1 alloys in the present study are in good agreement with residual stresses measurement reported by Dong [101]. The major factor that affects the evolution of residual stresses was the quenching in cold water. Several investigation have indicated that residual stresses on the surface of a wrought 7000 series plates can reach values larger than -100Mpa [102] [103]. Examples of residual stresses measurements found in the literature are summarized in Table 4-3.

Goldwiski et al. [83] concluded that aging temperature was found to strongly affect the total amount of relaxation measured in B319.1 alloy. Their results agree with the findings of this study where quenching in cold water produced higher residual stresses, T6 aging had a negligible effect on the relaxation of residual stresses, while aging at T7 resulted in higher amounts of residual stress relaxation.

For both alloys, the maximum residual stress generated in the block casting (low solidification rate) is 30MPa, while the residual stress generated in the L-shaped casting (high solidification rate) is almost 80MPa. In Figure 4-21, the observed variation between material strength and amount of residual stresses evolved confirmed that the two variants are in direct proportionality where the alloy with higher strength exhibits the highest residual stresses. The reason for this behavior is attributed to the fact that as the strength of the material increases, the material resists deformation and so the residual stresses increase [5]. In this context, the higher strength B319.1 alloy will have higher locked-in stresses compared to A356.1 alloy.

The L-shaped castings, which solidified at high cooling rates, and hence exhibit small SDAS values, have better strength properties and also high values of residual stresses compared to the block castings which solidified at low cooling rates. In conclusion,

castings with small SDAS will have higher tensile stresses and generate higher residual stresses which indicates that residual stress is dependent on the structure and properties of the alloy [78] [83].

Table 4-3 Residual stresses in the as-quenched condition as reported in the current study and by other researchers

Author	Alloy	Type	Dimensions (mm)	SHT (°C)	Quenching	measurement Technique	RS (MPa)	Comment
Current study	A356.1	Casting	200*40*40	540	Air	Sectioning Technique	-24.5	average residual on 10mm plate
	A356.1	Casting	200*40*41	540	water/60		-49	
	A356.1	Casting	200*40*42	540	water/20		-71	
	B319.1	Casting	200*40*43	500	Air		8	
	B319.1	Casting	200*40*44	500	water/60		-50	
	B319.1	Casting	200*40*45	500	water/20		-81	
Dong [101]	2014	Plate	100*100*50	500	water/20	Slitting method	-103	near surface stresses
	2014	Plate	100*100*50	500	water/60		-89	
	2014	Plate	100*100*50	500	water/80		-26	
	2014	Plate	100*100*50	500	water/100		-25	
Robinson[104]	7175	Plate	25*25*160	475	water/20	X-ray diffraction	-160	near surface stresses
	6061	Plate	25*20*160	530	water/20		-100	
	2017A	Plate	25*25*160	510	water/20		-170	

(a)

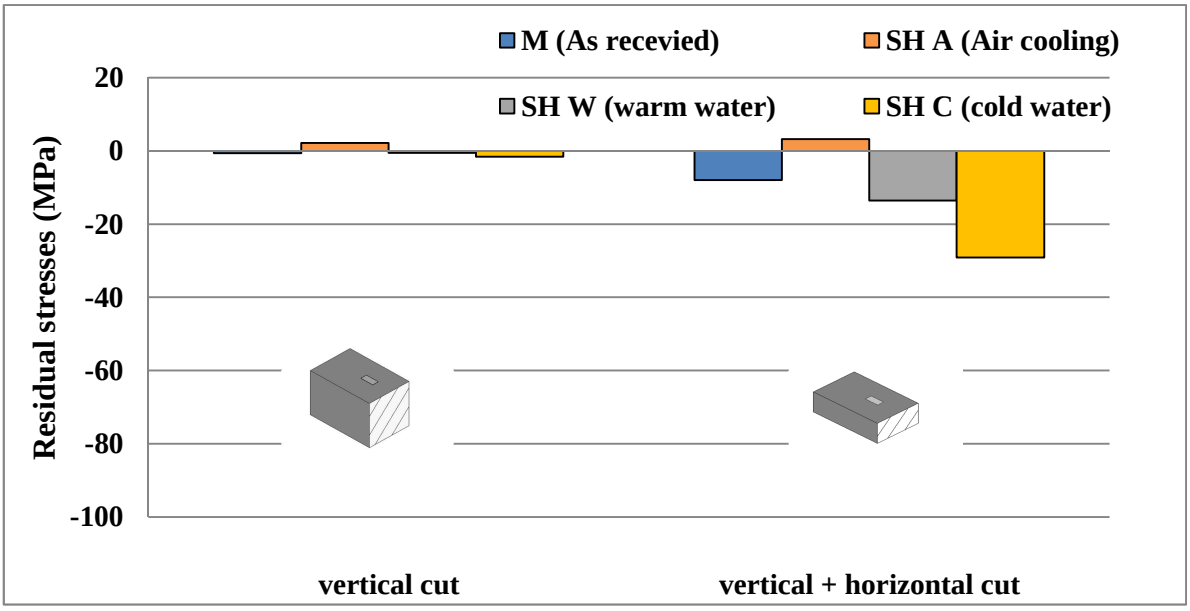

(b)

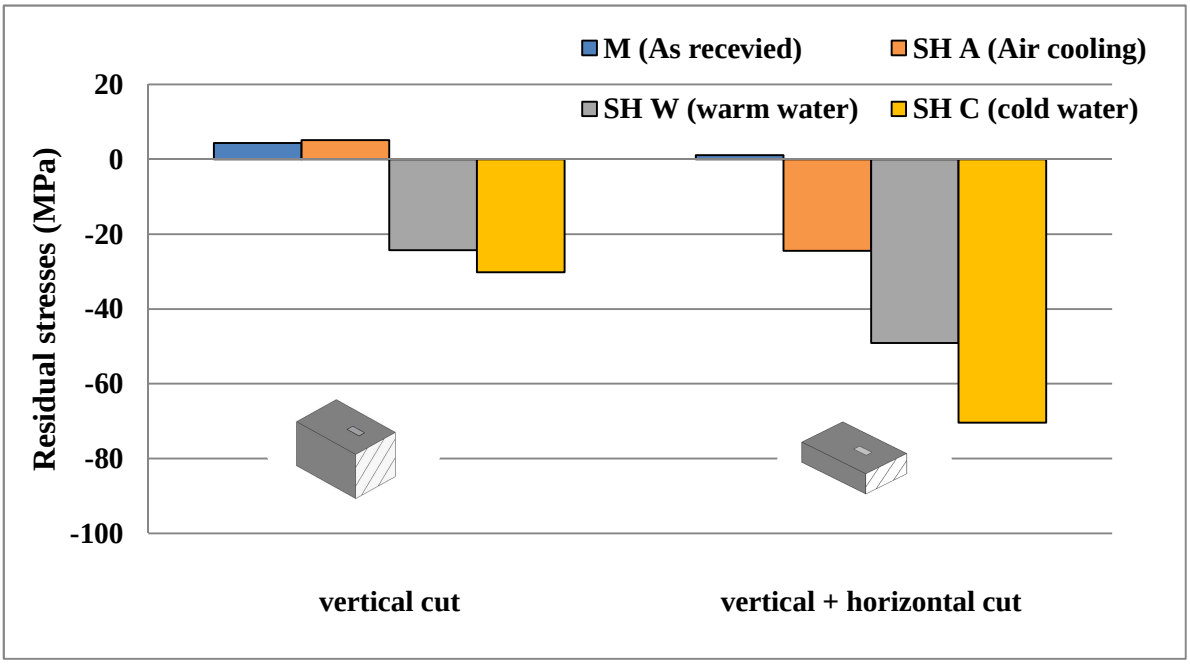

Figure 4-19 Development of residual stresses at different quenching rates in A356.1 alloy (a) block shaped casting (b) L-shaped casting.

(a)

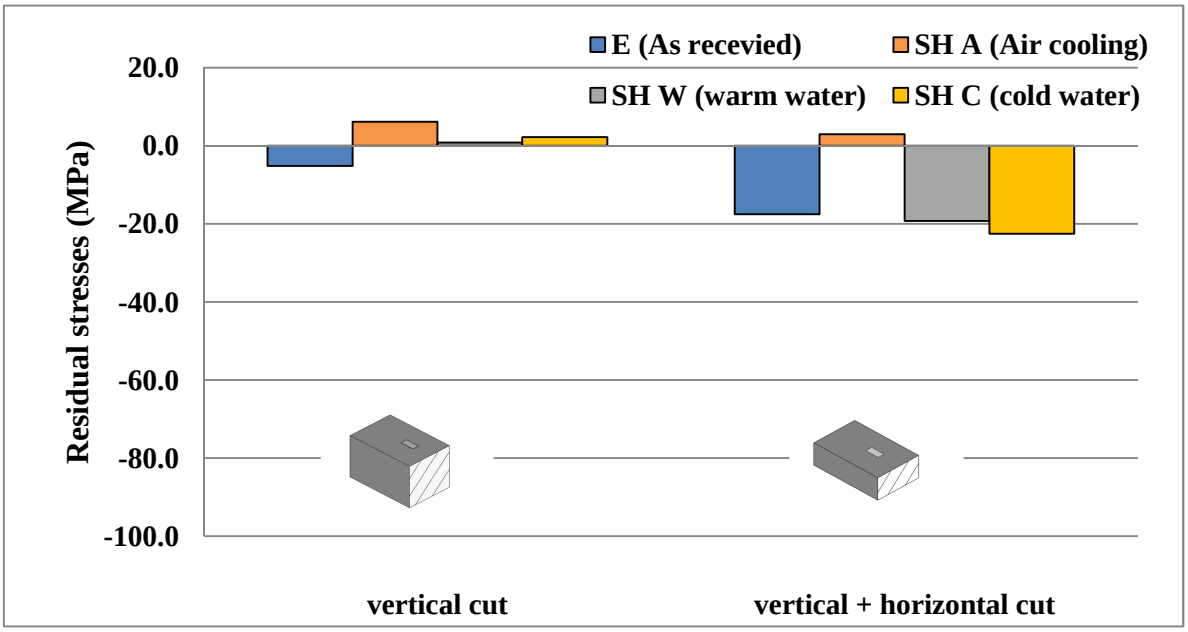

(b)

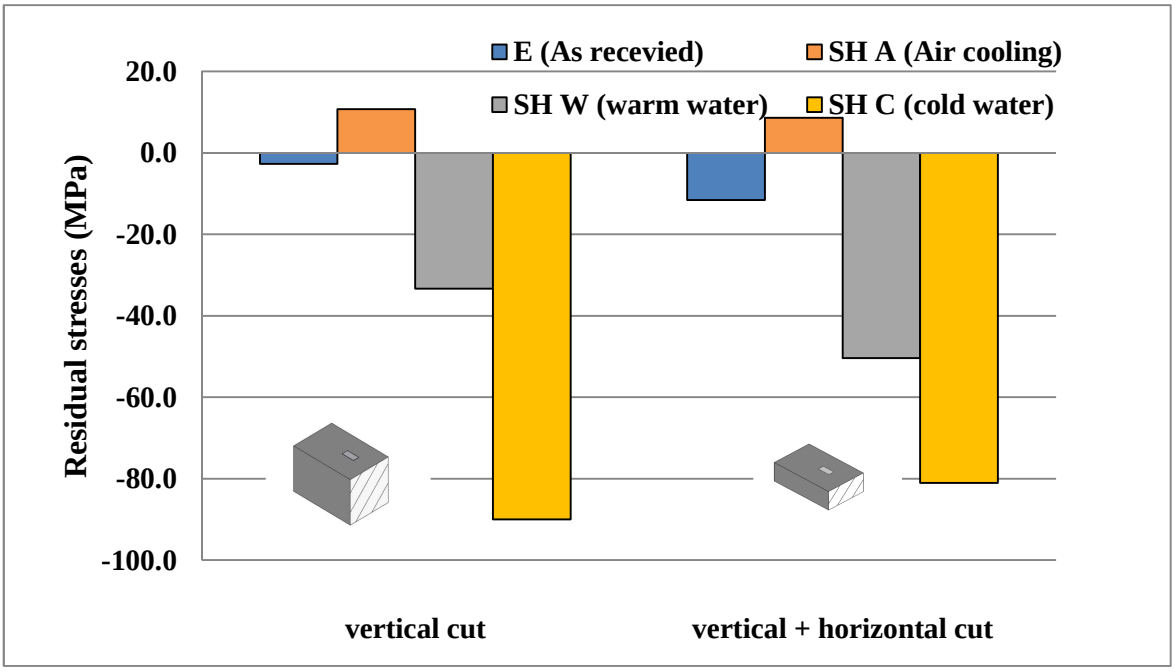

Figure 4-20 Development of residual stresses at different quenching rates in A319.1 alloy (a) block shaped casting (b) L-shaped casting.

.

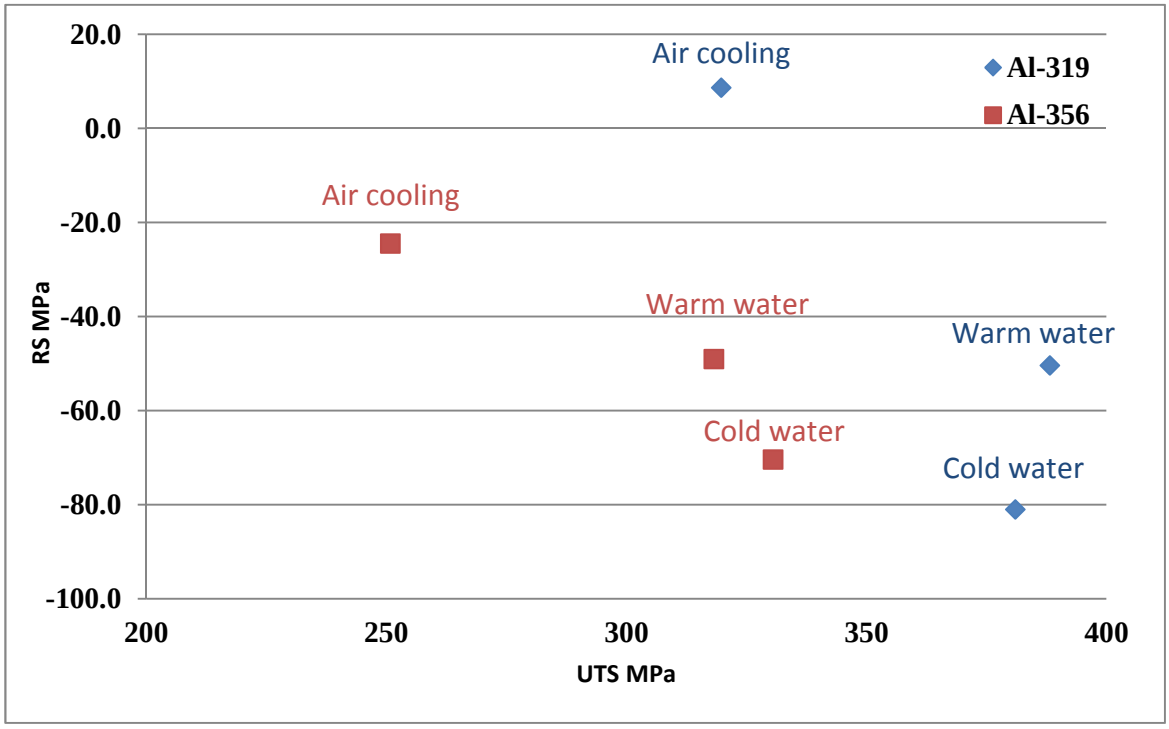

Figure 4-21 Variation in residual stresses as a function of UTS in B319.1 and A356.1 alloys at different quenching rates.

4.5.2 Relaxation of residual stresses

Several methods have been adopted in order to relieve residual stresses which include either plastic deformation or atomic rearrangement such as recrystallization. Thermal and mechanical methods are adopted for the purpose of relieving residual stresses. Thermal methods are based on heating the component to a proper temperature that allows either plastic deformation or phase transformation or recrystallization to occur. Mechanical methods are based on plastically deforming the material at room or at elevated temperature.

Aging causes release of the residual stresses where increasing the temperature or holding time causes further relief of residual stresses [105]. In this section, the relaxation of residual stresses formed in A356.1 and B319.1 will be discussed, in relation to the aging temperature and time.

Generally, stress relief involves uniform heating of a part to a suitable temperature, holding at this temperature for a period of time, followed by slow cooling to prevent the reintroduction of thermal stresses, as stress relieving is highly dependent on the temperature. At high temperatures, such as those used in solution heat treatment, the material yield strength is remarkably reduced, causing plasticity mechanisms to relieve the elastic strain through rapid thermal activation of dislocations. It should be noted that at high temperature, major reduction in residual stresses can be encountered with major decrease in the properties of the material as the precipitates get coarser and lose their hardening capabilities during annealed at high temperatures [104] [106]. In other words, heat-treatable aluminum alloys cannot be stress relieved by annealing as the temperature required to encourage stress relief will coincide with that which promotes the precipitation of the second phase constituents, so that stress relieving must be attained at a lower temperature (i.e. during aging).

Aging encourages the precipitation of coherent or semi-coherent phases, and can be performed naturally or artificially (at elevated temperature). Although precipitation causes micro-strains around the precipitates, it has been shown that it does not affect the resulting residual stresses [105].

In order to maintain the mechanical properties, stress relieving at lower temperatures must be maintained [106]. At lower temperatures, relief of the locked-in residual stresses is brought about through a different mechanism, viz., classical diffusional creep and precipitation of another phase. Creep causes redistribution of tensile and compressive stresses through thermal glide. Micro-plastic strains that occur due to thermal glide or due to dislocation climb to some extent, enable the relaxation of locked-in residual

stresses. The values of residual stresses after T6 and T7 treatments are presented in Figure 4-22 and Figure 4-23.

After aging at 160°C, relaxation of residual stresses is found to be between 5 and 50%, depending on the quenching medium and exposure time. It has been found that in T6 heat-treated Al–Si–Mg alloys, aging for short times does not significantly affect residual stresses [5] [107]. Thus, to release residual stresses, the temperature should be higher. The amount of residual stresses relieved through T6 treatment provides only modest reduction in residual stresses; while aging at 250°C causes at least 75% residual stress relaxation and can annihilate most locked-in residual stresses with increasing time. This behavior could be attributed to the fact that dislocation glide or climb occurs more readily at higher temperatures.

Specimens with large SDAS (60 µm) were also found to be more prone to residual stress relief. In general, the increase in SDAS is found to reduce the amount of residual stresses that originate and facilitate residual stress relaxation which is related to the reduction of mechanical strength at lower solidification rates [6]. Finally, the levels of residual stress are markedly reduced because of stress dissipation through the dislocation glide mechanism.

Residual stresses (RS) are nothing else but elastic accommodation of non-uniform plastic strains generated either thermally or by phase transformation. Generally, the hardness is inversely proportional to the square root of grain size (Hall-Petch equation). Greater the hardness, greater will be the residual stresses. Thus, it could be concluded that grain size has an inverse effect on residual stresses. Hardness also depends on type of microstructure and cooling rate.

Figure 4-24 summarizes the ultimate tensile stress (UTS) and residual stress (RS) values obtained for A356.1 and B319.1 alloys, as a function of different casting parameters and quenching media. The figure demonstrates that material with higher strength, as in the case of B319.1 alloy, produces higher residual stresses compared to material with lower strength, as in the case of A356.1 alloy. It also shows that there is direct proportionality between UTS and RS with quenching rate. The relaxation of residual stresses is significantly dependent on aging temperature and proceeds smoothly with the increase in aging time. A significant increase in the residual stresses is observed in specimens with low SDAS, as in the L-shaped casting, while lower residual stresses are measured in specimens obtained from the block casting, with high SDAS.

(a)

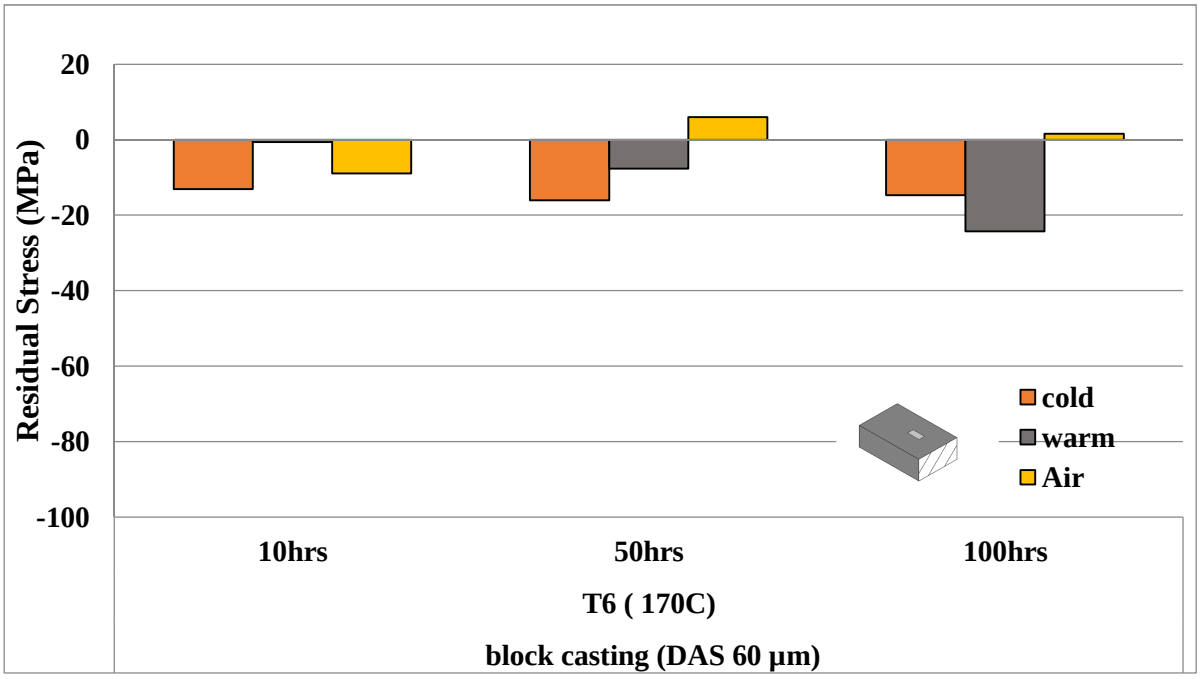
20
0
-20
-40
-60
-80
-100
Residual Stress (MPa)
cold
warm
Air
10hrs
50hrs
100hrs
T6 (170C)
block casting (DAS 60 µm)

(b)

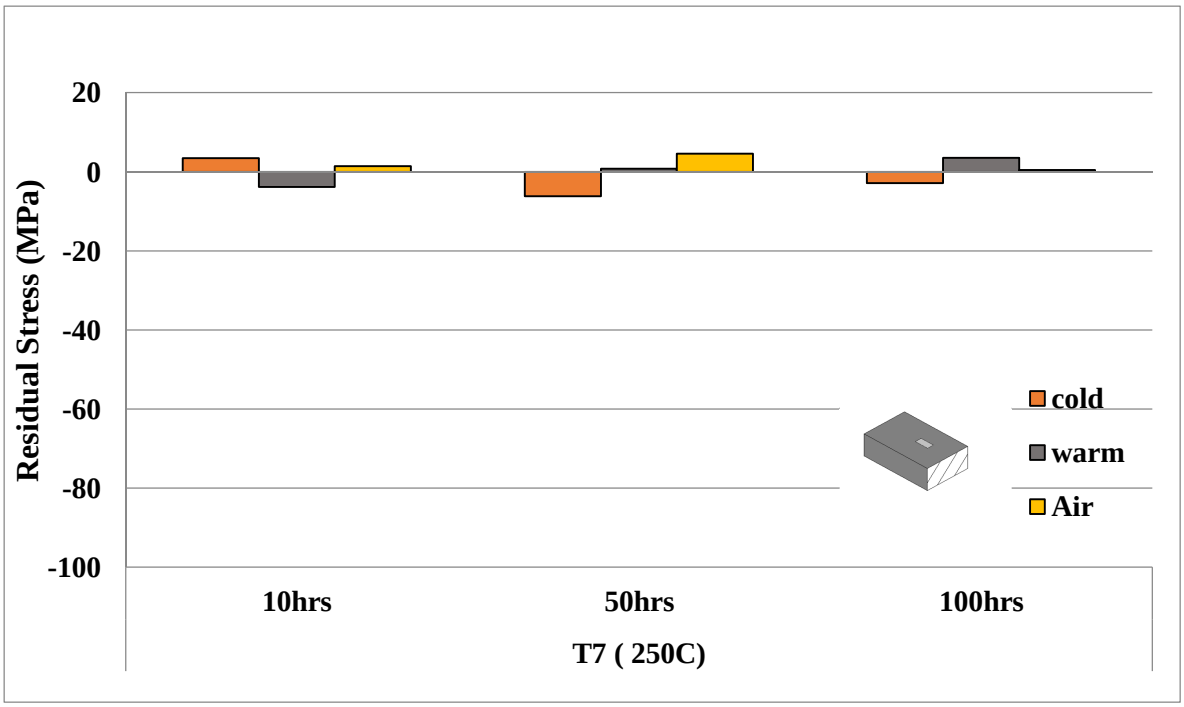
20
0
-20
-40
-60
-80
-100
Residual Stress (MPa)
cold
warm
Air
10hrs
50hrs
100hrs
T7 (250C)

(c)

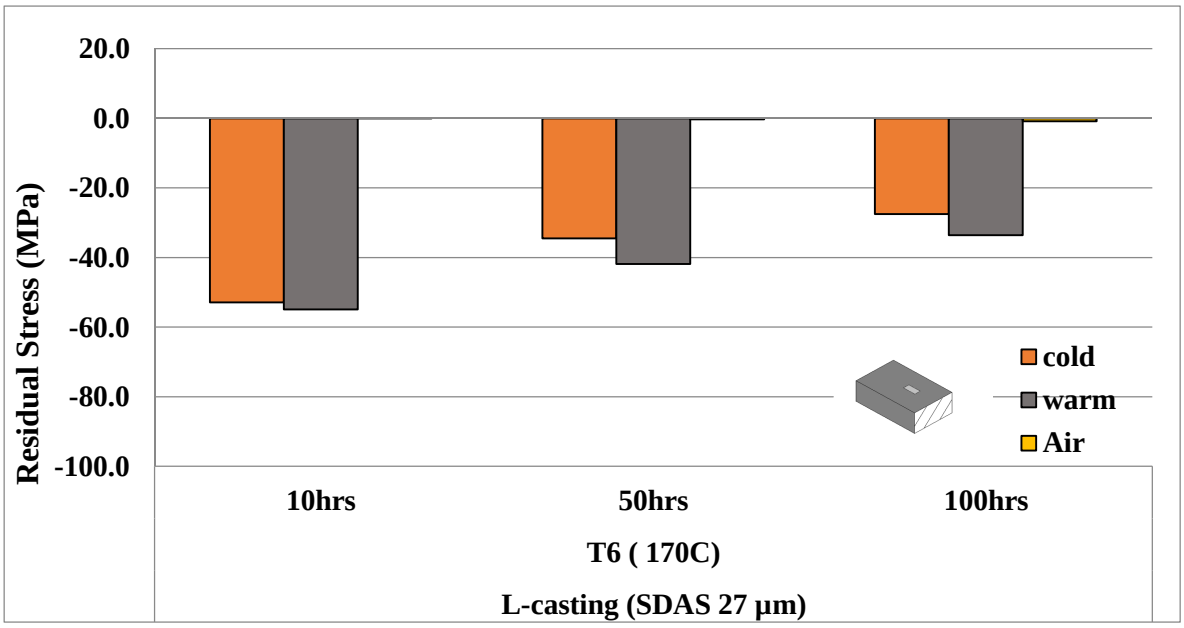

(d)

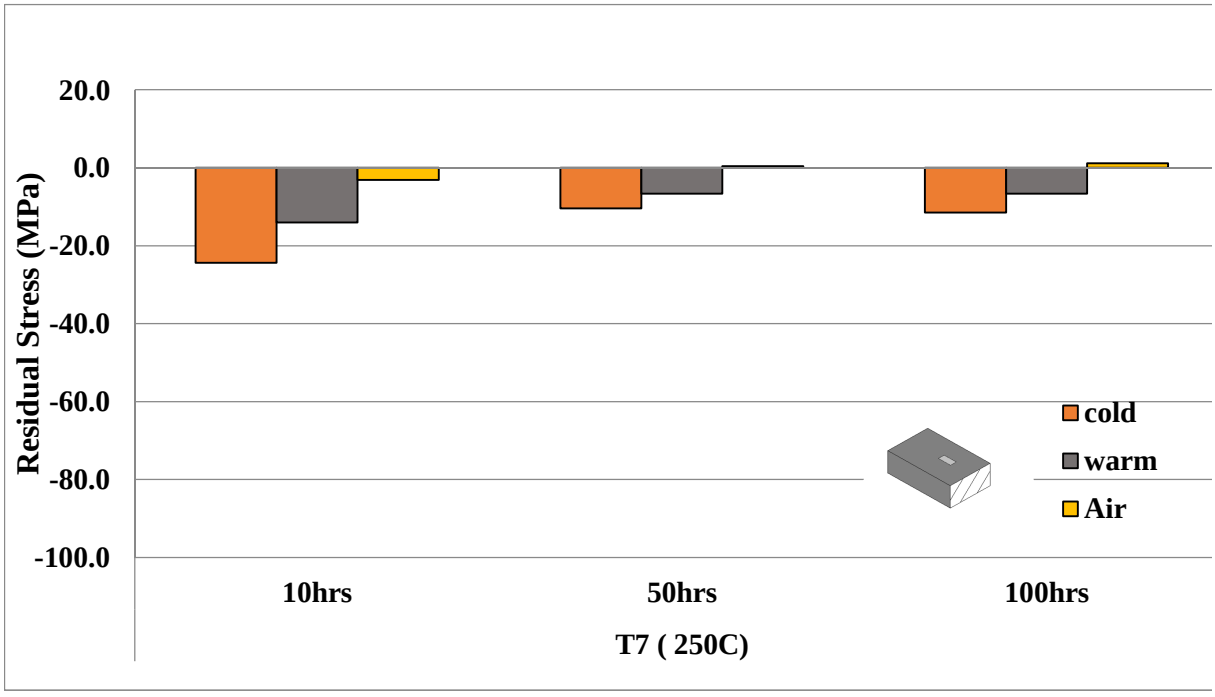

Figure 4-22 Relaxation of residual stresses in A356.1alloy with variation in aging conditions (a) block casting/ T6 (170°C); (b) block casting/ T7 (250°C); (c) L-shaped casting/ T6 (170°C); (d) L-shaped casting/ T7 (250°C).

(a)

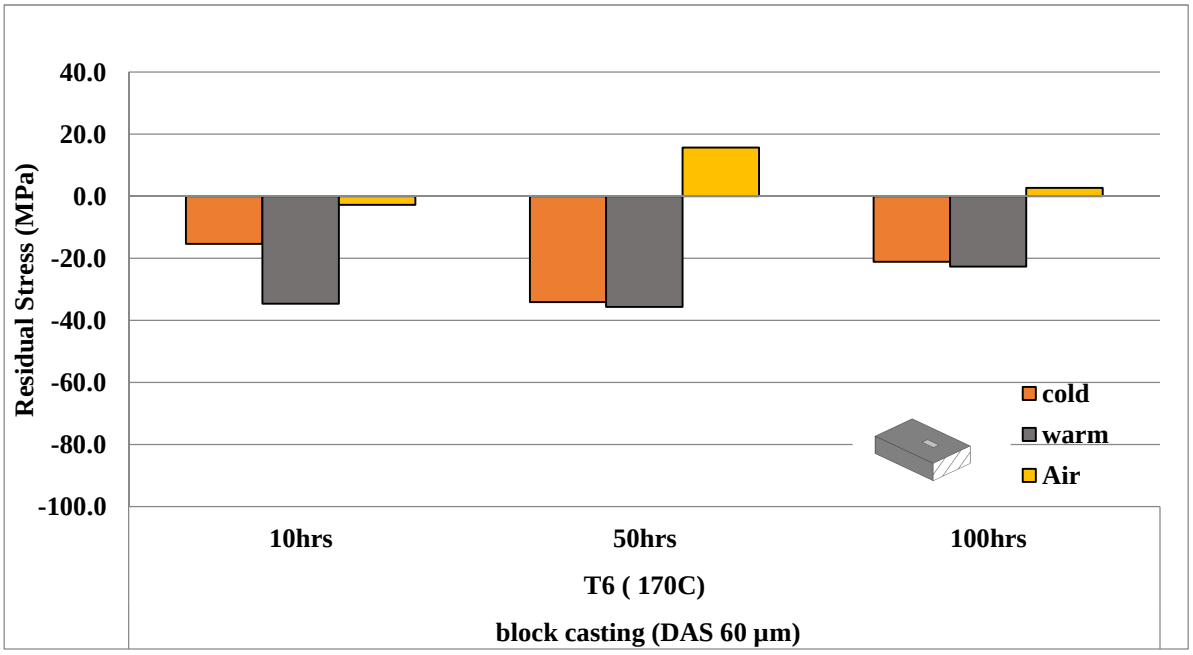
40.0
20.0
0.0
-20.0
-40.0
-60.0
-80.0
-100.0
Residual Stress (MPa)
cold
warm
Air
10hrs
50hrs
100hrs
T6 (170C)
block casting (DAS 60 µm)

(b)

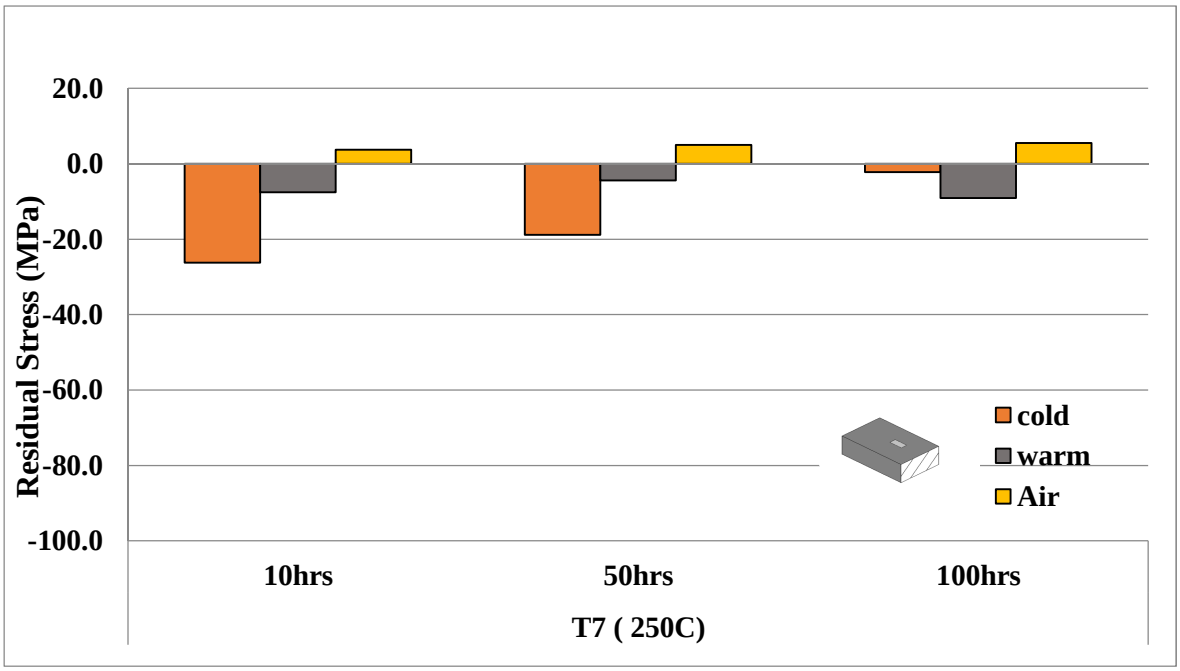
20.0
0.0
-20.0
-40.0
-60.0
-80.0
-100.0
Residual Stress (MPa)
cold
warm
Air
10hrs
50hrs
100hrs
T7 (250C)

(c)

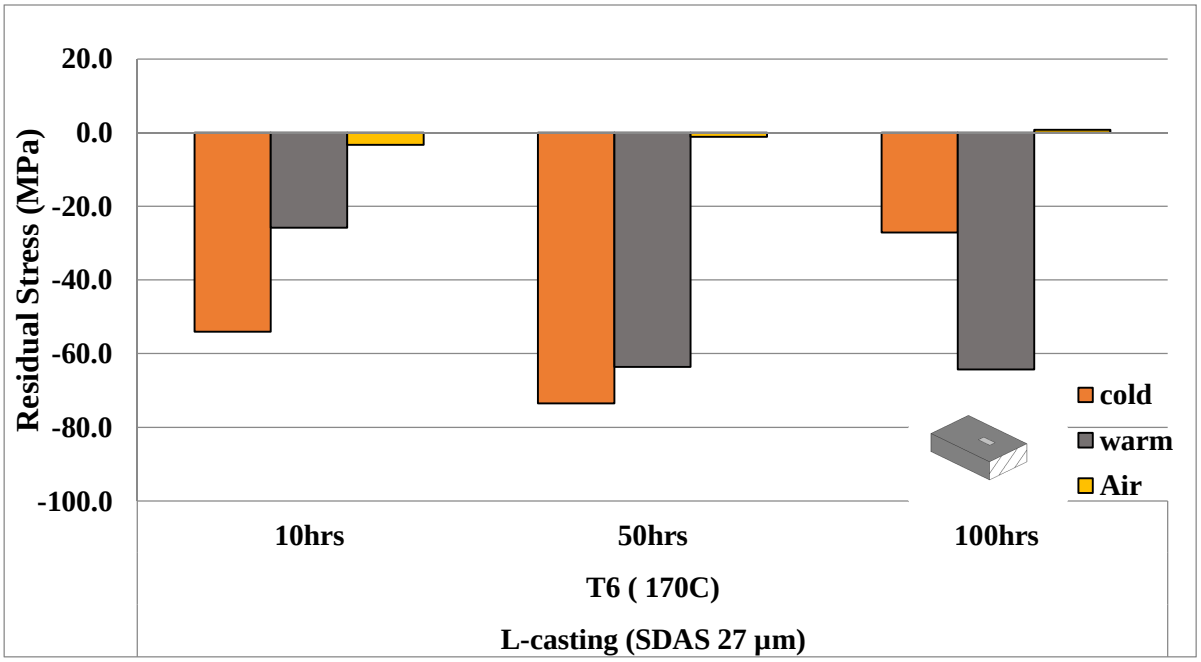

(d)

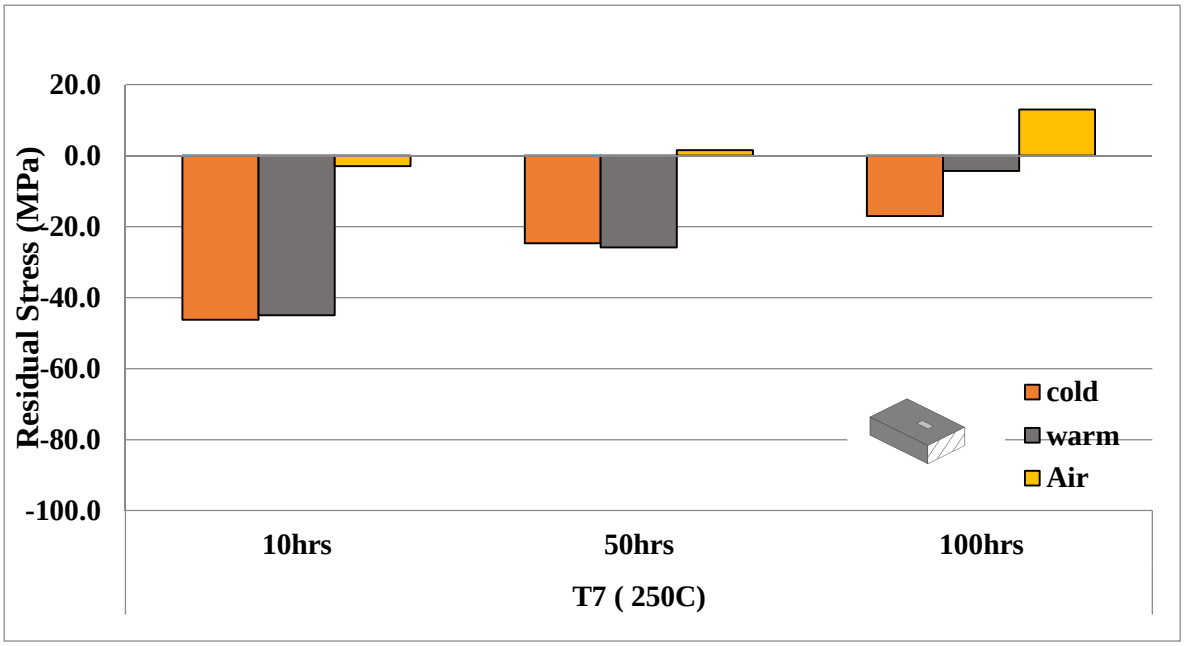

Figure 4-23 Relaxation of residual stresses in B319.1 alloy with variation in aging conditions (a) block casting/ T6 (170°C); (b) block casting/ T7 (250°C); (c) L-shaped casting/ T6 (170°C); (d) L-shaped casting/ T7 (250°C

(a)

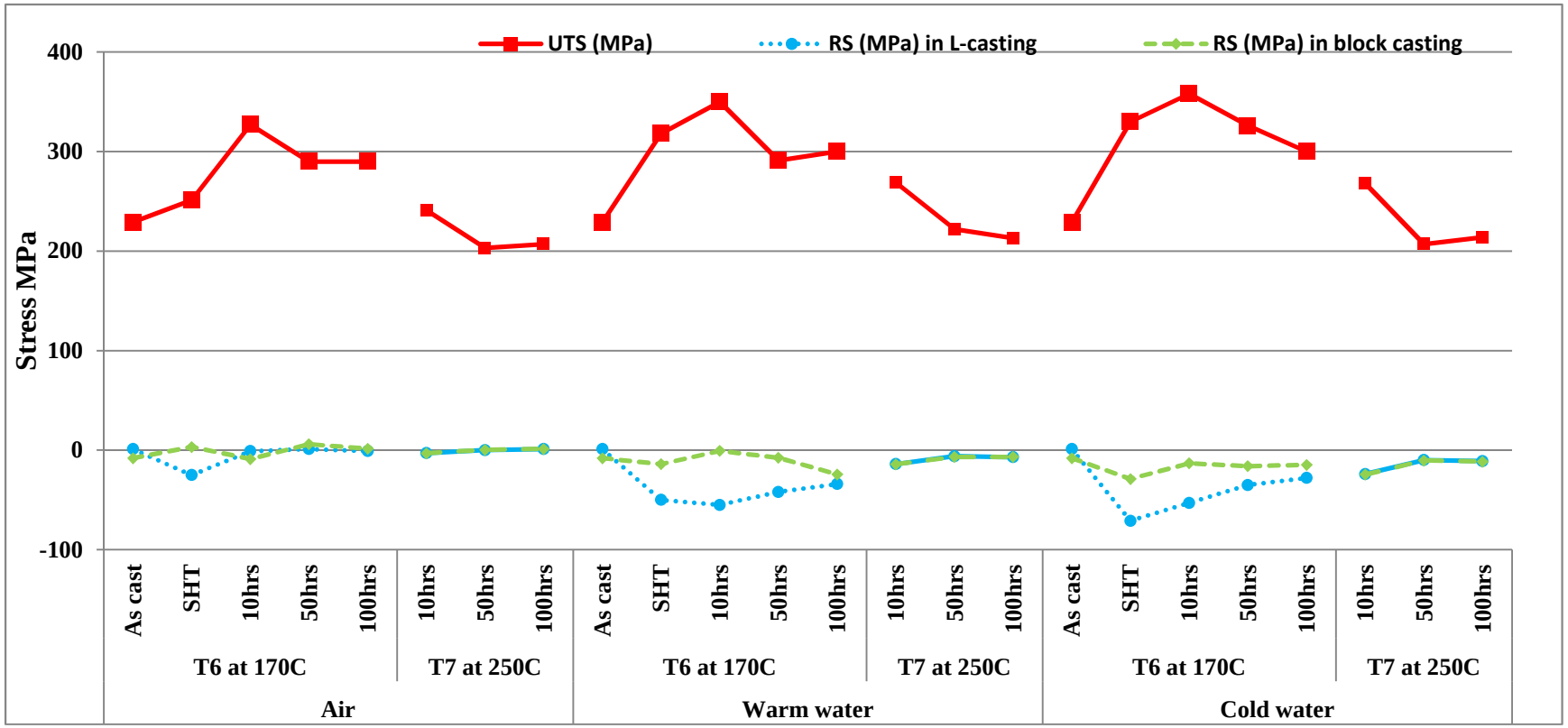
UTS (MPa)
RS (MPa) in L-casting
RS (MPa) in block casting
Stress MPa
400
300
200
100
0
-100
As cast
SHT
10hrs
50hrs
100hrs
T6 at 170C
T7 at 250C
Air
Warm water
Cold water

(b)

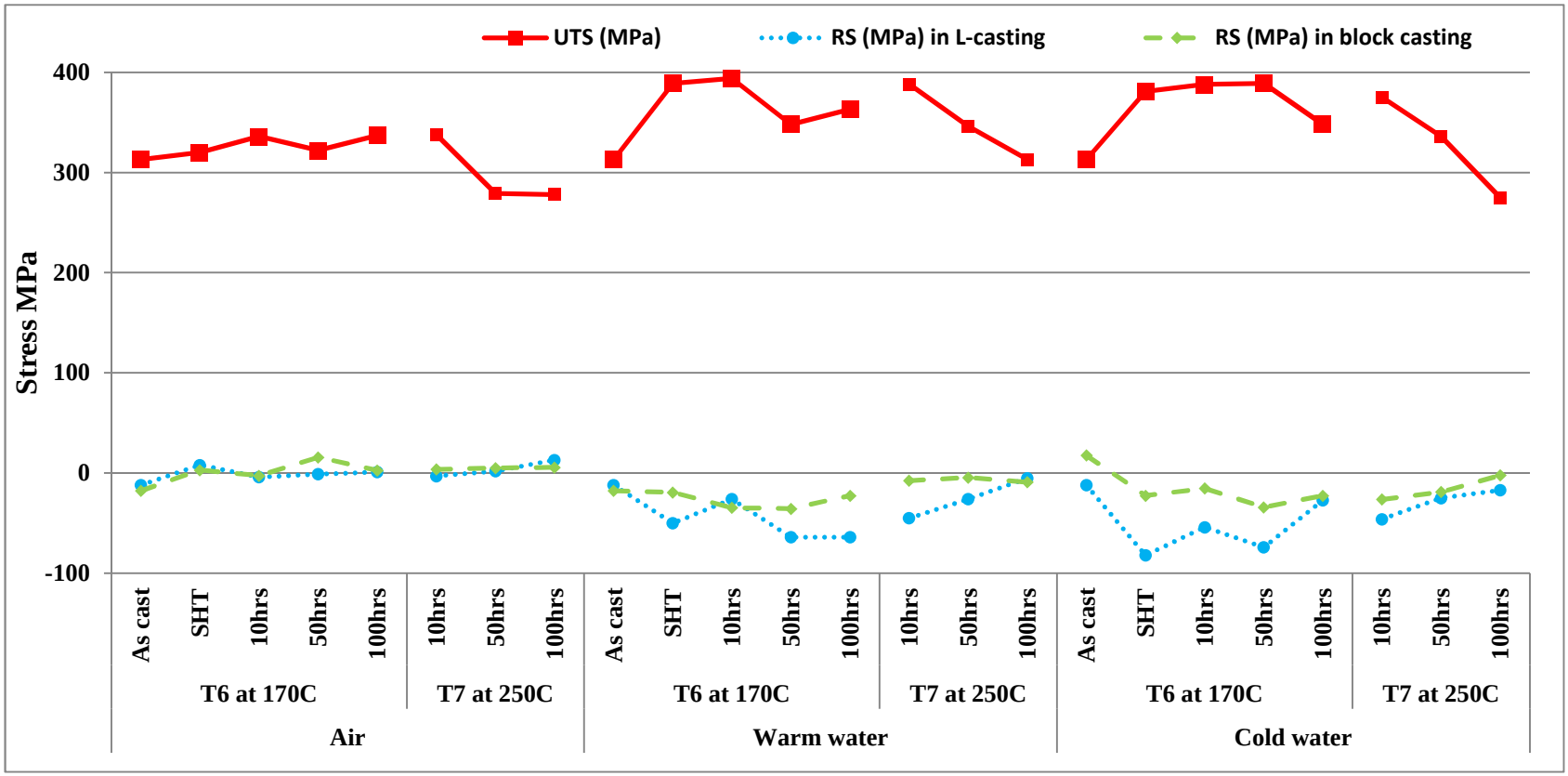

Figure 4-24 Variation of tensile stresses and residual stresses in (a) A356.1 and (b) B319.1, *as a function of different casting parameters.*

Section II: Influence of casting parameters on the development of stresses and hardness of I4 and V-6 engine blocks

B319.1 alloys are brittle at low temperature but can be improved by heat treatment or alloying with elements like strontium. Strontium addition transforms the large brittle flakes of the eutectic silicon present in the unmodified 319 alloy into a fibrous coral type structure resulting in improvement in elongation and tensile strength. Properties of these alloys are generally controlled by addition of modifiers, casting parameters and heat treatment.

With improved casting techniques, the presence of casting defects is reduced, so that other microstructural parameters, namely, dendrite arm spacing, grain size, morphology of Si particles, shape and distribution of intermetallic phases, and precipitation hardening during heat treatment play a dominant role in controlling the properties.

4.6 Dendritic Structure

Microstructural analysis was carried out using optical microscopy to observe the dendrite structure in both I4 and V6 engine blocks at different locations. Optical microscopy revealed a variation in the dendritic structure along the length of the cylinder bridge region of both I-4 and V-6 engine blocks. It was observed that the top of the cylinder bridge contained relatively coarse dendrites, while the bottom of the cylinder contained finer dendrites, see Figure 4-25.

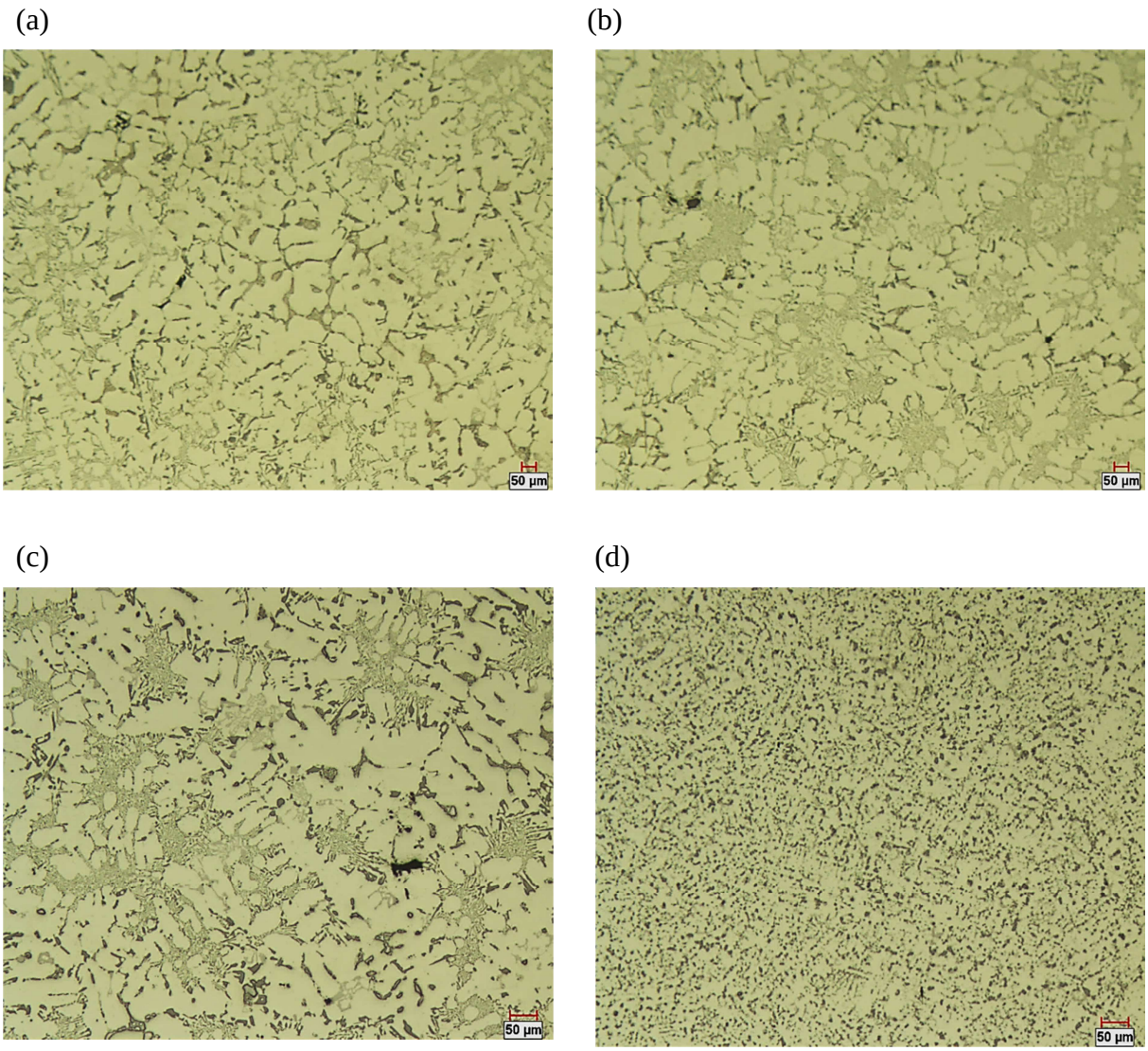

Figure 4-25 Optical micrographs showing the dendrite structure of: (a) top region of I-4 engine, (b) bottom region of I-4 engine, (c) top region of V-6 engine, (d) bottom region V-6 engine block.

The secondary dendrite arm spacing (SDAS) was measured at the top and bottom regions of the cylinder bridges. The results of these measurements are summarized in Table 4-4. The average SDAS was found to decrease from 57µm to 40µm for the I-4 engine block, and from 41µm to 21µm in the case of the V6 engine block. For both types of engine blocks, the SDAS results for the bottom region of the cylinder bridge indicate a shorter solidification time, i.e. a higher cooling rate compared to the top region of the

cylinder bridge [108]. According to lombardi [78], the main reason for SDAS refinement was caused by the sand mould design where a chill plate was inserted very close to the bottom region prior to pouring. In contrast, the top region of the cylinder bridge which was near the risers took a longer time to solidify (since risers are required to solidify last), resulting in the top region exhibiting a large SDAS [78].

Table 4-4 SDAS measurements for I-4 and V-6 engine blocks

	Top region		**Bottom region**	
	SDAS (µm)	**Std.**	**SDAS (µm)**	**Std.**
I-4 engine	57	8.34	41	9.89
V-6 engine	42	8.82	21	3.97

4.7 Effect of Sr-modification on microstructural development

In an Al-Si alloy, the silicon represents the hard phase of the alloy which causes a discontinuity in the soft and ductile matrix of aluminum. Because α-Al is the softer phase and Si is the harder and less ductile one, this can generate large stresses on the softer phase which lead to anisotropic distribution of the plastic deformation. The local plastic constraint in the softer phase leads to a rapid strengthening of the alloy, with dislocations piling up at the αAl/Si particle. This can lead to the formation of cleavage microcracks at these ductile-brittle sites. Under normal cooling conditions, the Si phase is likely to be observed in the form of large acicular plates with sharp sides and ends. This morphology of Si lead is detrimental to the mechanical properties, thus it needs to be altered or ‘modified’.

Three methods are known for the eutectic modification [109] namely (a) chemical modification through the addition of trace levels of alloying elements, (b) quench modification through high cooling rates and rapid solidification, and (c) super heating the melt at 850^{o}C for 15min and fast cooling to the pouring temperature (~680°C prior casting). Chemical modification using Sr addition is the most popular as the resulting eutectic silicon phase is fine and fibrous, nullifying the effect of the acicular morphology.

The addition of Sr leads to formation of fibrous silicon. During heat treatment, the Si particles undergo fragmentation and spheroidization, where the rate of spheroidization is faster in the Sr-modified alloy, compared to unmodified alloys. In this study, the alloys used were modified employing about ~150 ppm strontium. Therefore, it is expected that the microstructure even in the as-cast condition would exhibit a modified eutectic silicon phase. In addition, since the alloy contains Ti, the grains formed will be small. In conclusion, the addition of Ti and Sr enhances the final developed microstructure, thereby leading to a general improvement in the tensile properties compared to the unmodified alloy.

Particle size, shape, and spacing are all factors which characterize the eutectic silicon structure. Table 4-5 summarizes the silicon particle characteristics obtained before and after heat treatment adopted in manufacturing of engine blocks. It is clearly observe that eutectic modification is achieved by the chemical addition of Sr while heat treatment causes partial modification illustrated in the spheroidization of the silicon particles.

The Sr addition causes improvement in the roundness and aspect ratio of the Si-particles. It also reduces the particle size. The modification of the Al-Si eutectic to a partially modified structure in the specimens obtained from the cylinder bridge sections,

and displayed in Figure 4-26 (a) and Figure 4-27 (a), was likely caused by the addition of Sr prior to casting. Figure 4-26 (b) and Figure 4-27 (b) illustrate partial spheroidization of Si eutectic phase after the application of solution heat treatment. However, full modification of the Al-Si eutectic was not observed since the modified B319.1 alloy used in engine block production, contained a larger amount of Si than the standard 319 alloy. To reach full modification of the Al-Si eutectic, larger additions of Sr, longer heat treatment times, and higher cooling rates would be required.

Table 4-5 Silicon particle analysis

Sample/Condition	**SI particle caharsterstics**							
	%Area		**Length (µm)**		**roundness**		**Aspect ratio**	
	Mean	**stdv.**	**Mean**	**stdv.**	**Mean**	**stdv.**	**Mean**	**stdv.**
I-4 engine (As received)	12.54	1.86	8.55	9.64	0.48	0.23	2.15	1.88
I-4 engine (Air cooled)	10.50	2.23	6.06	6.06	0.52	0.21	1.98	2.50
V-6 engine (As received)	10.32	1.72	6.06	7.1	0.58	0.26	2.02	3.02
V-6 engine (Air cooled)	8.28	2.9	6.65	7.94	051	0.22	2.37	2.89

(a)

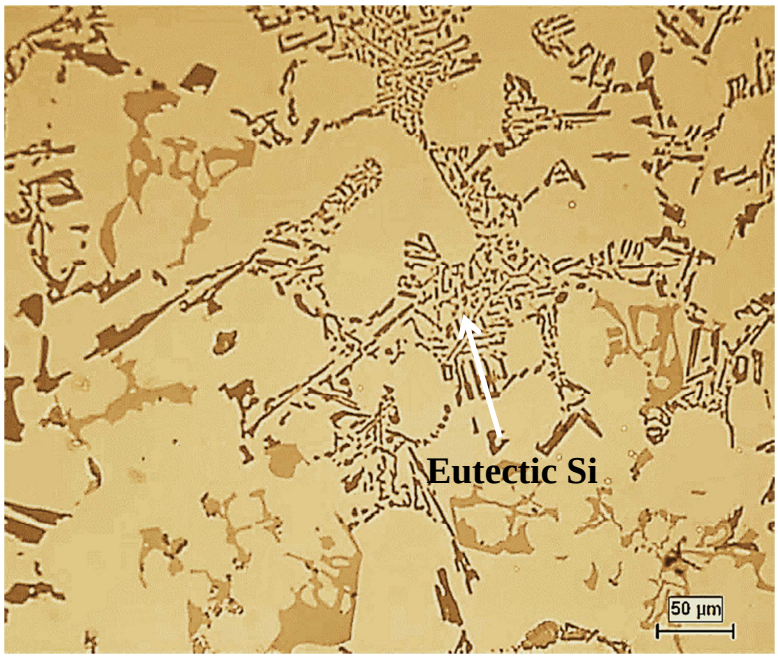

(b)

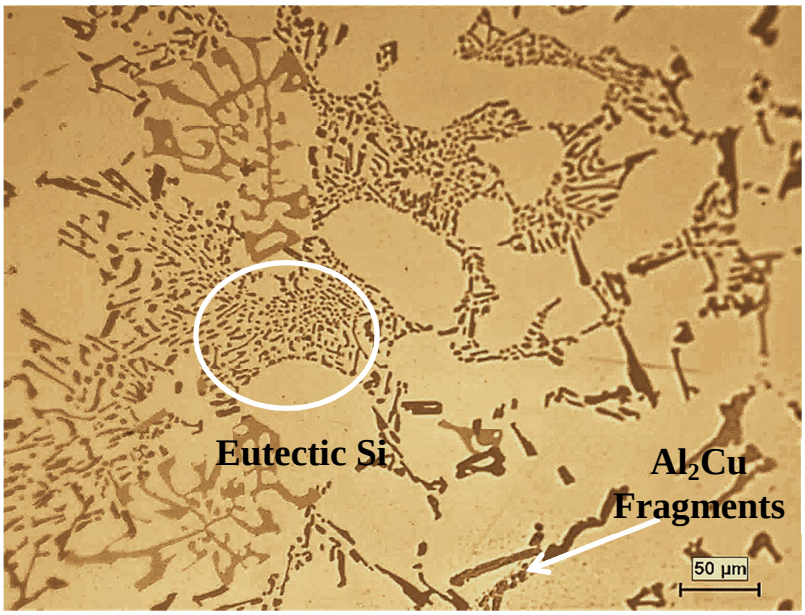

Figure 4-26 Optical micrographs showing the effect of solution heat treatment at 500°C on Si morphology in I4-engine blocks for (a) 0 h and (b) 8 h solution treatment times

(a)

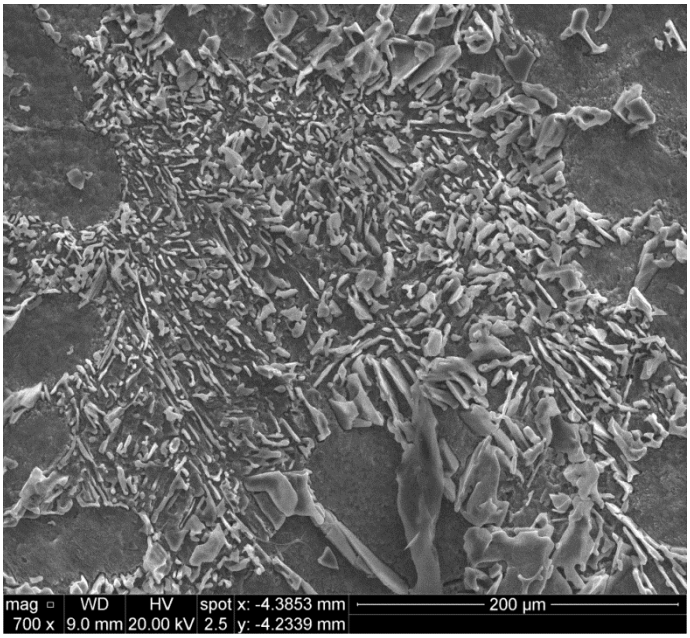

(b)

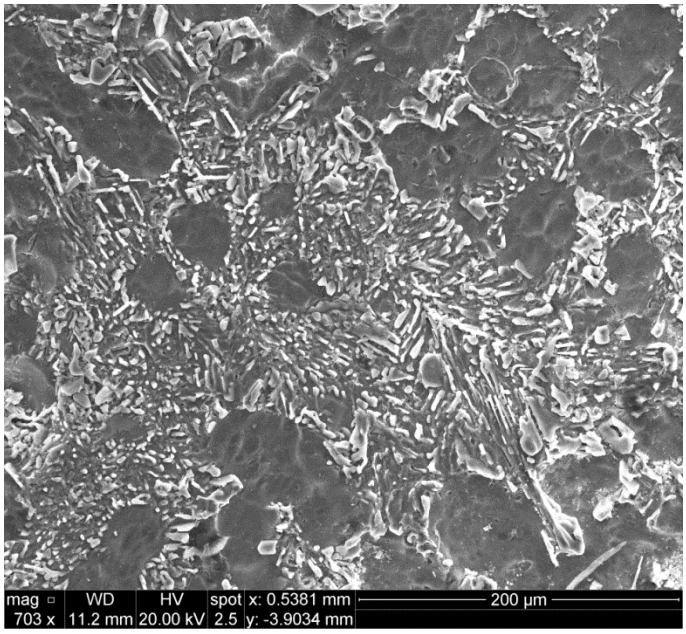

Figure 4-27 Backscattered electron images showing the effect of solution heat treatment at 500°C on Si morphology in I4-engine blocks for (a) 0 h and (b) 8 h solution treatment times

4.8 Alloying elements distribution after aging

The specimens prepared for mapping were deeply etched using hydrofluoric acid (HF- 25% conc.) for 30 seconds and then plated with 4nm thick platinum layer. The back scattered image of the sample obtained from the I-4 engine block casting after aging at 170°C for 100 hours is presented in Figure 4-28 (a), while Figure 4-28 (b) displays the mapping of elements observed in the image. As may be seen, the matrix consists mainly of the α-Al phase (83% Al), and blue areas corresponding to the eutectic Si phase (16% Si/Al), while about 2% corresponds to "unallocated" grey regions interspersed within the matrix. These would probably correspond to trace precipitates of Cu- and Mg-containing intermetallics, namely Al_2Cu and $Al_5Cu_2Mg_8Si_6$ as indicated by the peaks observed in the EDX spectrum obtained from the square region in the backscattered image of Figure 4-28 (a).

Similarly, Figure 4-29 shows the backscattered image, mapping of elements and the EDS spectrum for an I4-engine block sample that was aged at 250°C (T7 treatment) for 100 hours. It is interesting to note that the "unallocated" grey regions in the image have increased to 7% with the T7 treatment. As a result of the etching treatment used for delineating the Si particles, these precipitates could not be viewed clearly. However, the EDX spectrum showed a similar distribution of peaks as that observed in Figure 4-29 (c), indicating them to be the same type of precipitates.

With respect to the unallocated regions in Figure 4-28 (b) and Figure 4-29 (b), the actual size and density of the precipitates appearing in these regions, obtained after T6 and T7 aging treatments, for aging times of 10 and 100 hours are displayed in Figure 4-30 and Figure 4-31, respectively. As may be seen, at the T7 aging temperature of 250°C, the

precipitates are coarser, rod-like in shape, and spread further apart after 100 hours aging time, compared to what is observed at the T6 aging temperature of 170°C.

(a)

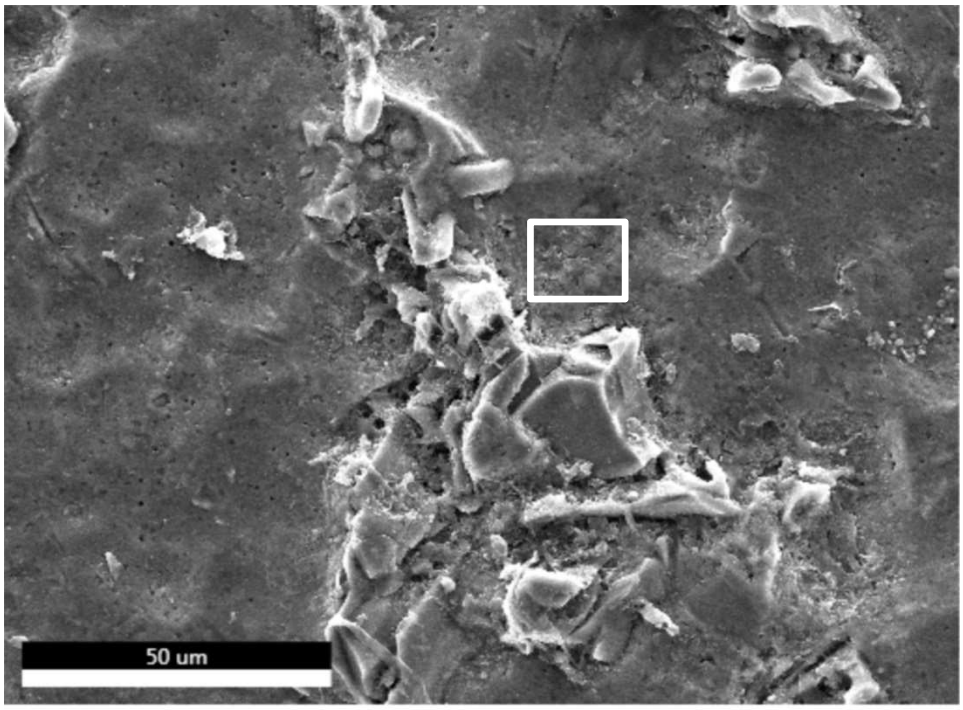

(b)

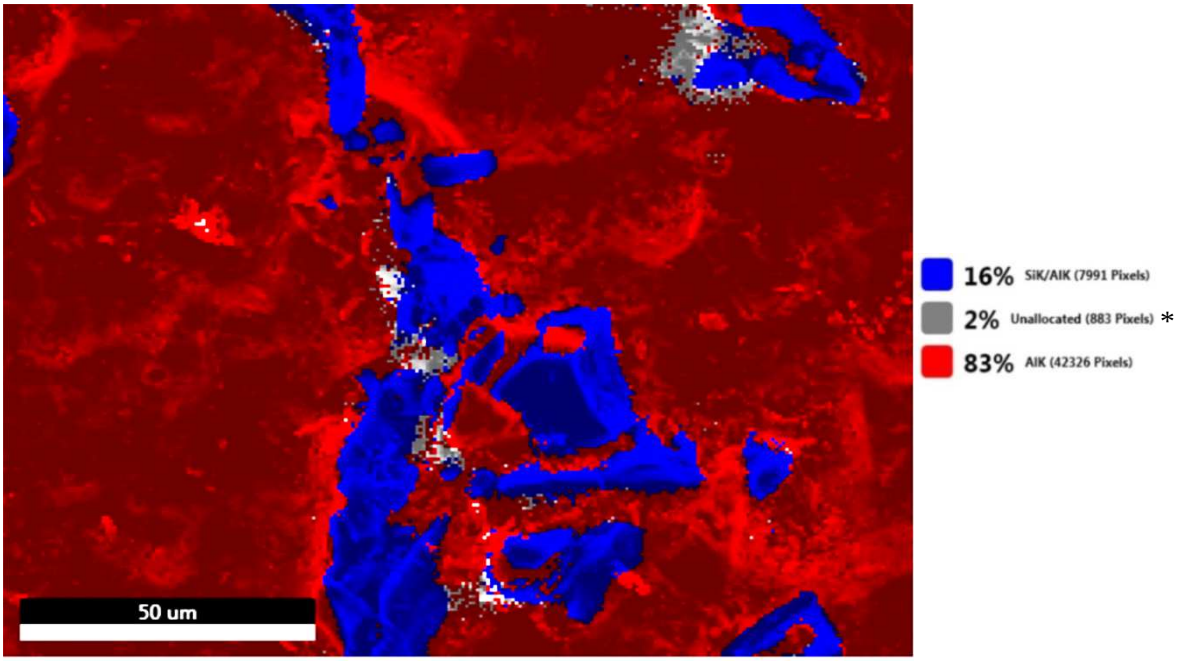

(c)

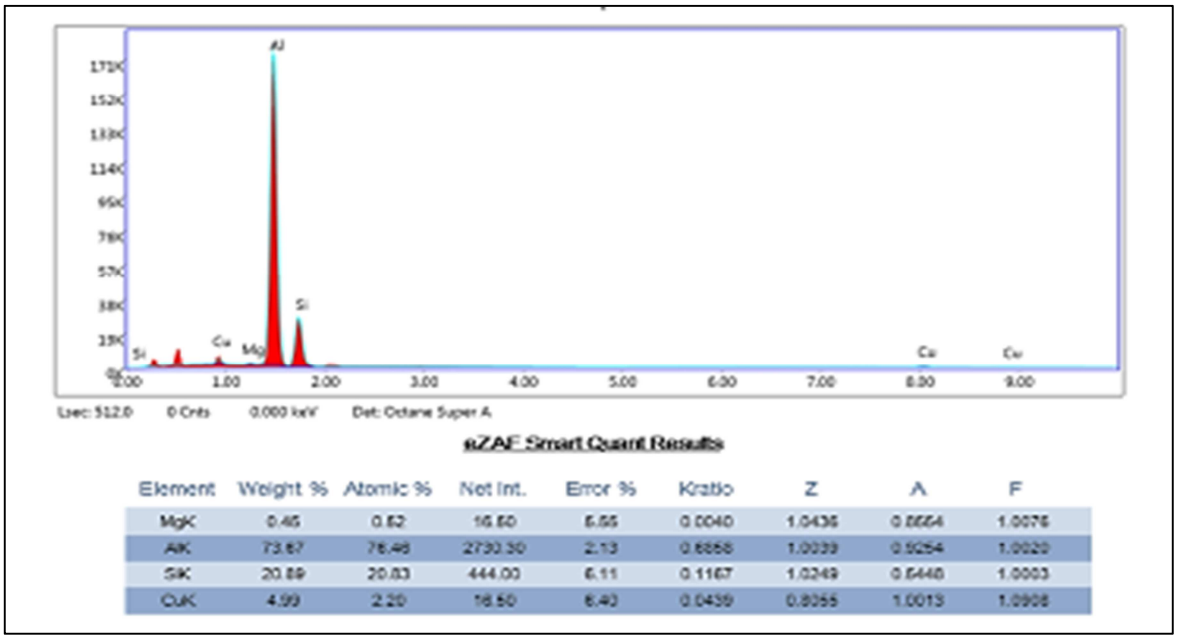

Element	Weight %	Atomic %	Net Int.	Error %	Kratio	Z	A	F
MgK	0.46	0.62	16.60	6.55	0.0040	1.0436	0.8664	1.0076
AlK	73.67	76.46	2730.30	2.13	0.6858	1.0039	0.9054	1.0020
SiK	20.89	20.83	444.00	6.11	0.1167	1.0249	0.8446	1.0003
CuK	4.99	2.20	16.50	8.40	0.0439	0.8055	1.0013	1.0908

*Unallocated region represent the presence of precipitates.

Figure 4-28 Elements distribution I-4- engine blocks after aging at 170°C for 100hrs (a) Backscattered electron image, (b) X-ray maps of element distribution and (c) EDX-ray spectrum corresponding to (a).

(a)

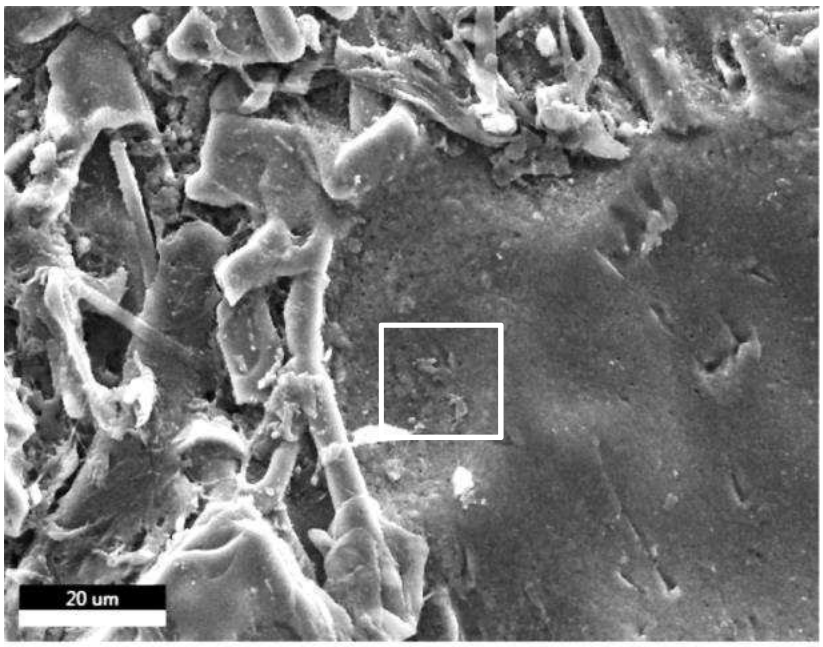
20 um

(b)

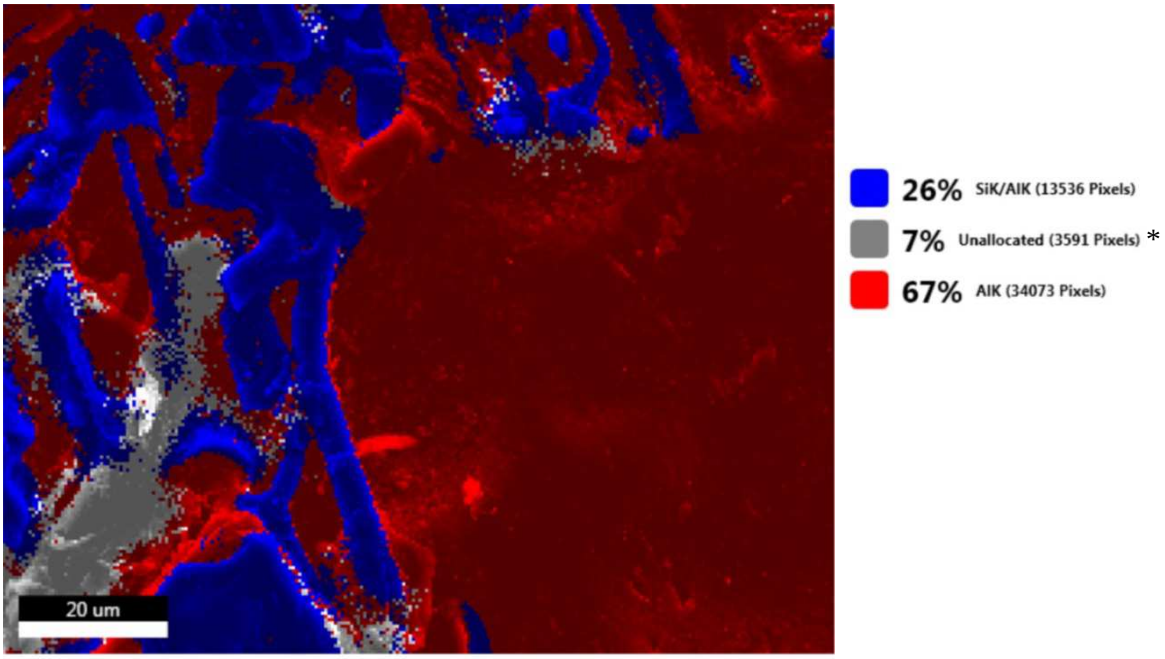
20 um
26% SiK/AlK (13536 Pixels)
7% Unallocated (3591 Pixels) *
67% AlK (34073 Pixels)

(c)

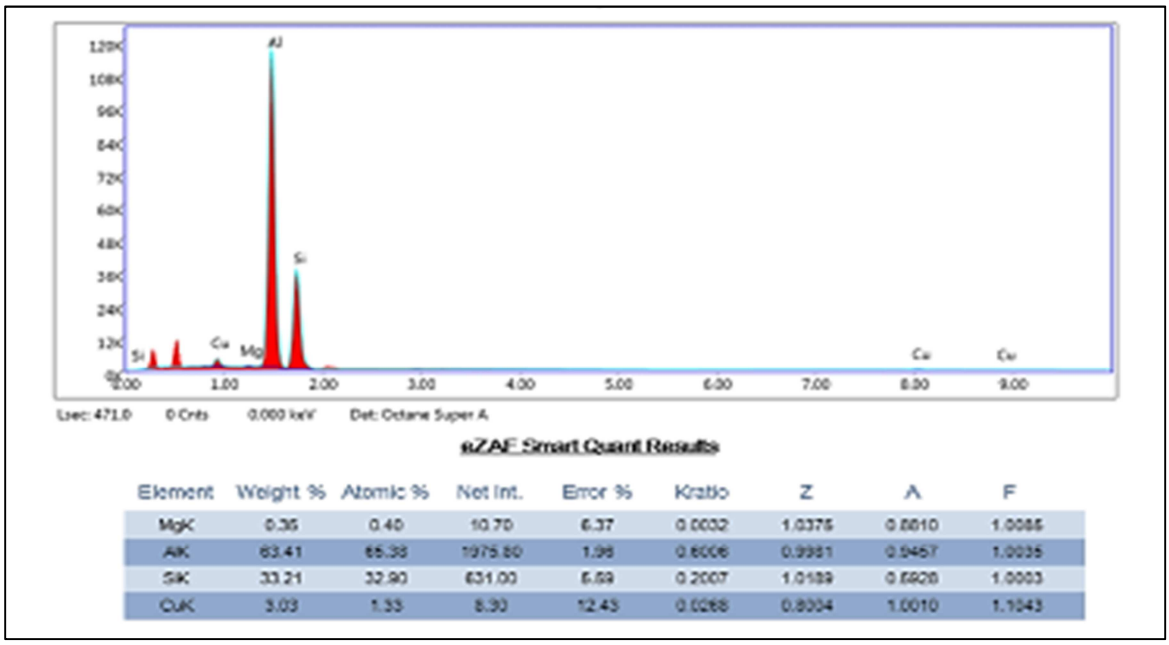

eZAF Smart Quant Results

Element	Weight %	Atomic %	Net Int.	Error %	Kratio	Z	A	F
MgK	0.36	0.40	10.70	6.37	0.0032	1.0375	0.8610	1.0085
AlK	63.41	65.38	1975.80	1.96	0.6006	0.9951	0.9457	1.0035
SiK	33.21	32.90	631.00	5.69	0.2007	1.0189	0.6826	1.0003
CuK	3.03	1.33	8.30	12.43	0.0268	0.8004	1.0010	1.1043

* Unallocated region represent the presence of precipitates.

Figure 4-29 Elements distribution I4- engine blocks after aging at 250°C for 100hrs (a) Backscattered electron image, (b) X-ray maps of element distribution and (c) EDX-ray spectrum corresponding to (a).

(a)

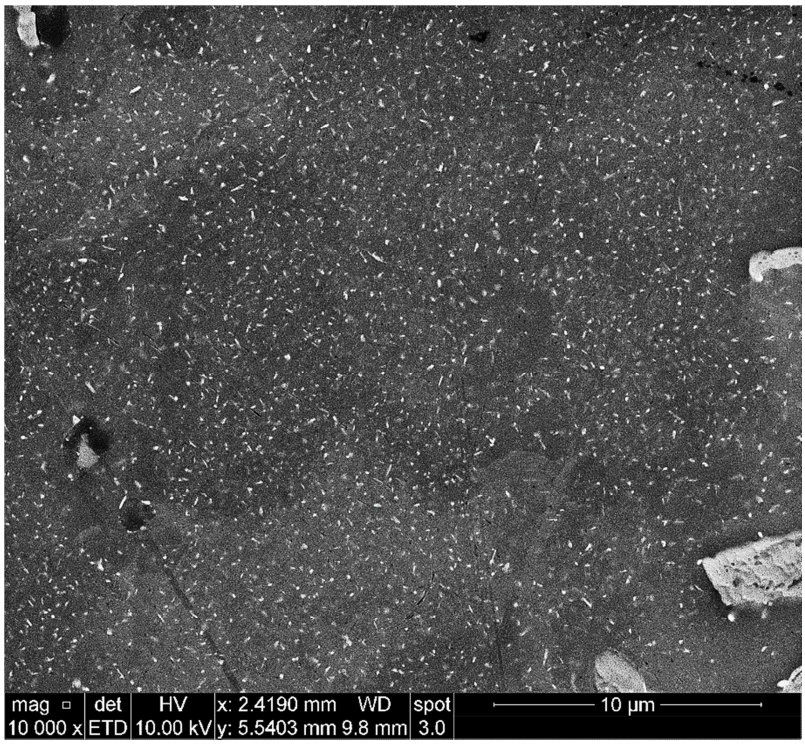

(b)

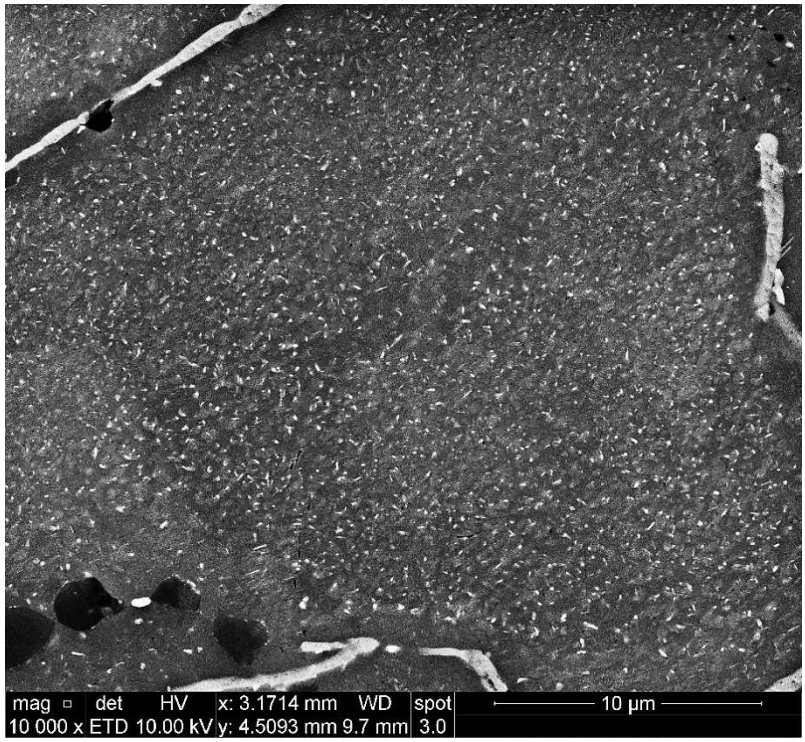

Figure 4-30 Size and density of the precipitates in I-4 engine block (a) SEM image after aging at 170°C for 10 hrs; (b) SEM image after aging at 170°C for 100 hrs.

(a)

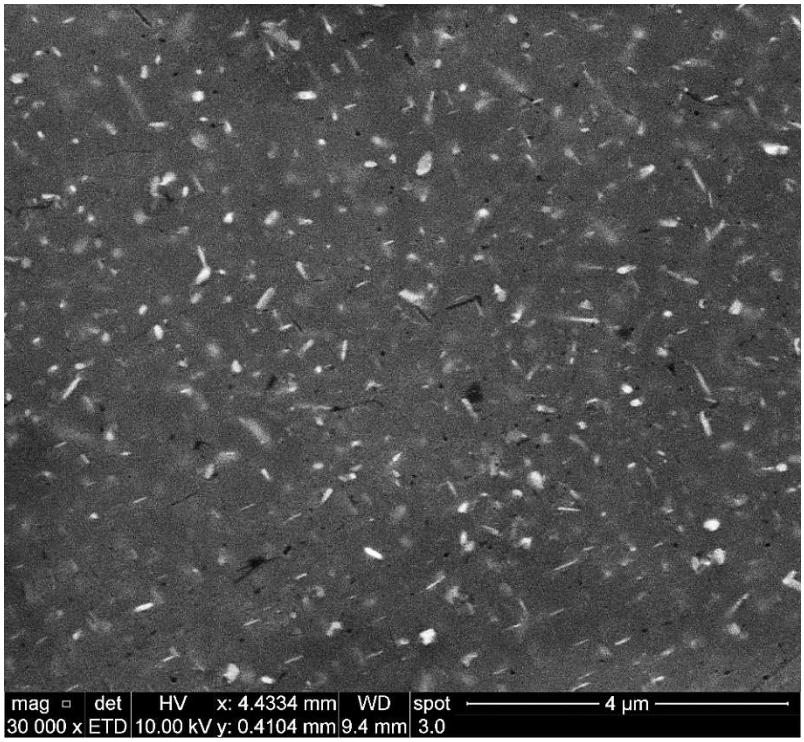

(b)

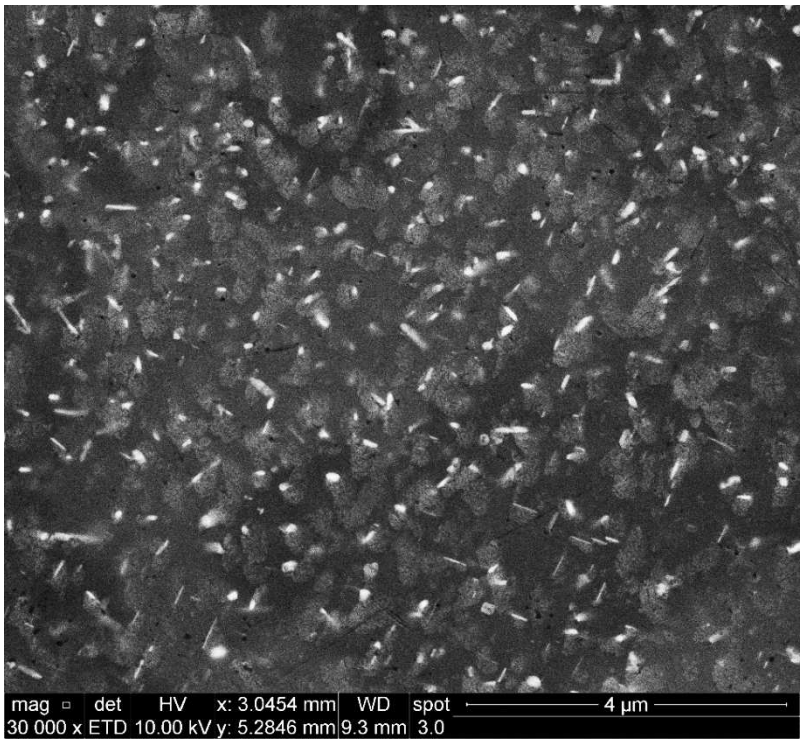

Figure 4-31 Size and density of the precipitates in I-4 engine block (a) SEM image after aging at 250°C for 10 hrs; (b) SEM image after aging at 250°C for 100 hrs.

4.9 Hardness Test Results

The Brinell hardness test is used to relate hardness to tensile strength. The structure and morphology of the precipitates that provide hardness are controlled by the aging time and temperature. The changes in the size, shape and distribution of hardening intermetallics such as the Al_2Cu precipitates that are formed during aging are the main sources for hardening and softening mechanisms of the material. The factors indicated are in a direct correlation with the quenching rate. Several studies [29] [45] have indicated that increasing the quenching rate results in improvement in the material strength. In Figure 4-32, cold water quenching which corresponds to the highest quenching rate results in the highest BHN values. As quenching rate decreases, the hardness tends to decrease as is noted for air-cooled two-cylinder and four-cylinder samples which exhibits hardness values of 81 and 74 BHN, respectively.

Cold water quenching results in high hardness values compared to air cooled samples, giving 100 BHN as the hardness values. With T6 aging, hardness starts to increase reaching its maximum (BHN=115 MPa) after aging for 10hrs. Increasing aging time leads to softening of the material hardness. On the other hand, increasing the aging temperature to 250°C (i.e. T7 treatment), as illustrated in Figure 4-32, also leads to softening as may be noted from the descending trend in hardness. The same trend was also observed for the samples cooled in air.

In general, it can be observed that peak hardness is obtained when aging is performed at 170°C for 10 hours due to the formation of the θ' phase which is a fine, well distributed, and coherent phase. Increasing the aging temperature results in a noticeable decrease in the hardness values compared to those obtained at 170°C, which is mainly

attributed to the coarsening of the Al_2Cu precipitates, loss of coherency, and formation of the equilibrium θ (Al_2Cu) phase.

It should be mentioned here that whereas samples obtained from the I-4 engine blocks were tested for all the aging conditions studied, in the case of the V6 engine blocks, due to the limited number of blocks available, the hardness values were measured only for the solution heat treated condition, and T6 and T7 aged conditions, for aging times of 10 and 100 hours in each case. The Brinell hardness values for the V-6 engine blocks were found to be approximately the same as those of the I-4 engine blocks.

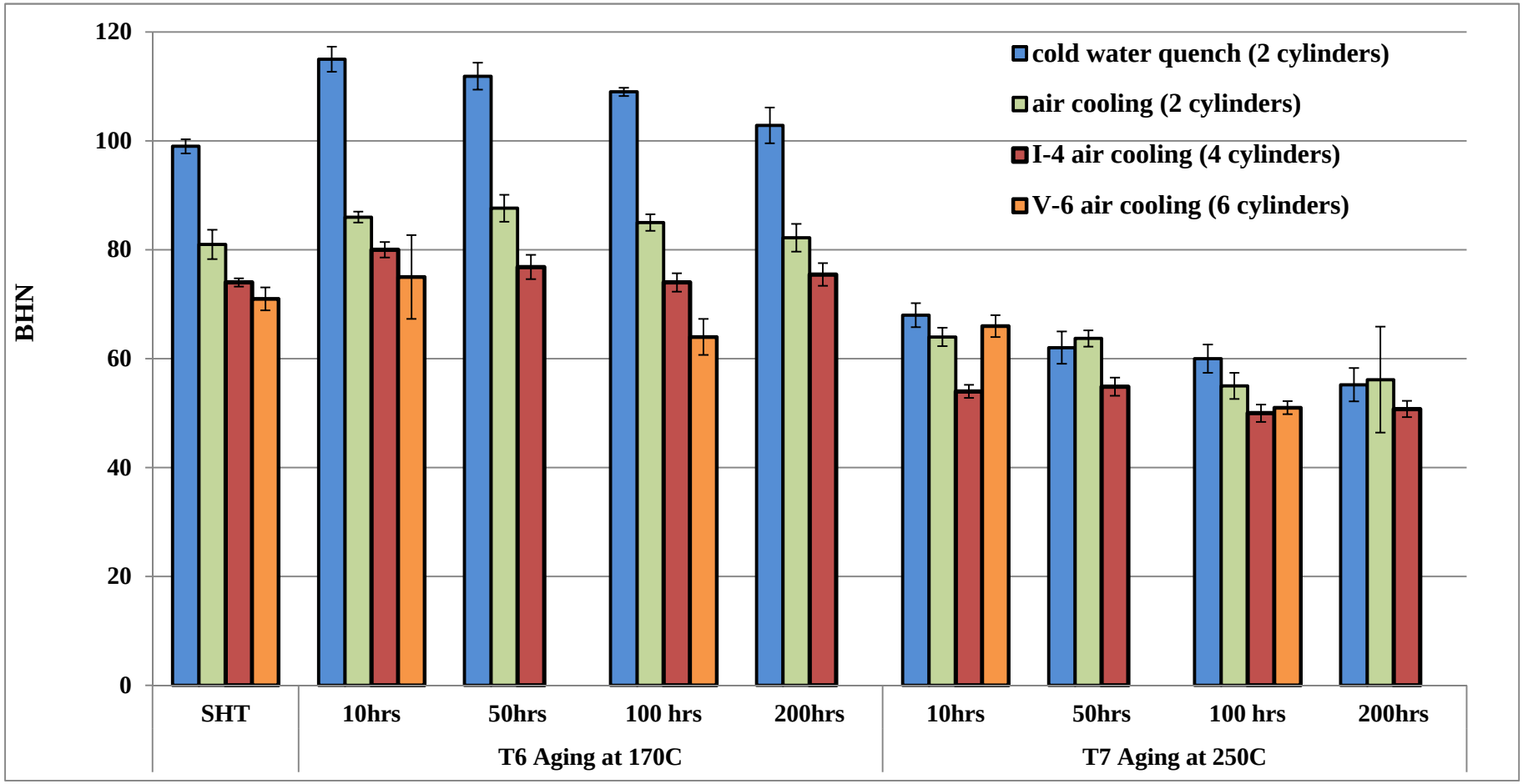

Figure 4-32 Variation of hardness (BHN) in engine block samples as a function of aging temperature and time.

4.10 Residual Stresses

Distortion of an engine block is inevitable with time due to the presence of residual stresses. The distortion may either be a product of thermal growth or the product of tensile residual stresses that exceed the yield stress of the block material or alloy. Thermal growth means changes in volume related to phase transformation during heat treatment of the alloy. In case of thermal growth, it is found that the T7 treatment offers the best dimensional stability over T4 and T6 treatments as it produces the stable θ (Al_2Cu), phase which has a lower specific volume when compared to θ' (Al_2Cu) neglecting the effect of thermal growth distortion [83]. Such distortion may occur through the introduction of excessive residual stresses. When theses residual stresses exceed the yield stress of the material, distortion occurs [74].

In Section I, the development of residual stresses as a function of casting parameters was investigated in B319.1 alloy, using samples with simple geometries. In this section, the development of residual stresses in B319.1 alloy I-4 engine blocks will be studied to examine the effect of the geometry of the structure, as well as the effect of the cylinder region being in contact with a different material, namely, the cast iron liner, on residual stresses, as is the case for engine blocks. Several factors will be examined namely quenching/cooling rate after solution heat treatment, aging temperature, aging time and freezing, with respect to the engine block casting. Freezing will be considered as a way to reduce residual stresses. All I4 engine blocks used in this study were supplied by Nemak Corporation.

4.10.1 Four-cylinders engine Blocks vs two-cylinders engine block

In order to facilitate handling in the laboratory, cutting the engine blocks into two halves was introduced, as represented in Figure 4-33. To verify our measurements, a complete set of experiments were made between whole engine blocks (four cylinders) and sectioned engine blocks (two cylinders) to determine if there would be any difference due to the sectioning/cutting. A comparison between four-cylinder and two-cylinder in different conditions, namely as-received, air quenched and air quenched/freezing, was made and the results are displayed in Figure 4-34.

The residual stresses inside the four-cylinder and two-cylinder engine blocks are found to be the same from which it may be concluded that sectioning has no effect on the development of residual stresses; this, in turn, indicates that there will be no difference between the results obtained from two-cylinder and four-cylinder blocks. It may also be observed that around 35% of the material strength is already locked in as residual stresses in the as-received condition and after solution heat treatment (SHT). This was related to the similar cooling rates for four-cylinder and two-cylinder engine blocks, which were verified by running a simulation using SolidWorks to find the cooling rate values. Figure 4-35 illustrates the cooling rates for both four-cylinder and two-cylinder engine blocks which are found to lie close to 15.5°C/min.

The residual stresses in the I-4 engine blocks in the as-cast, air cooled, and air cooled + freezing conditions were 100, 70, and 50MPa, respectively. These results indicate that the SHT process partially relieved some of the tensile residual stresses which evolved in the Al-cylinder bridge region, with a subsequent reduction when freezing was performed through the operation. The same trend was observed by Lombardi et al. [78] [110] who

measured residual stresses inside V6 engine blocks in the as-cast and air-cooled conditions. The stress relaxation was found to be about 20%.

(a) (b)

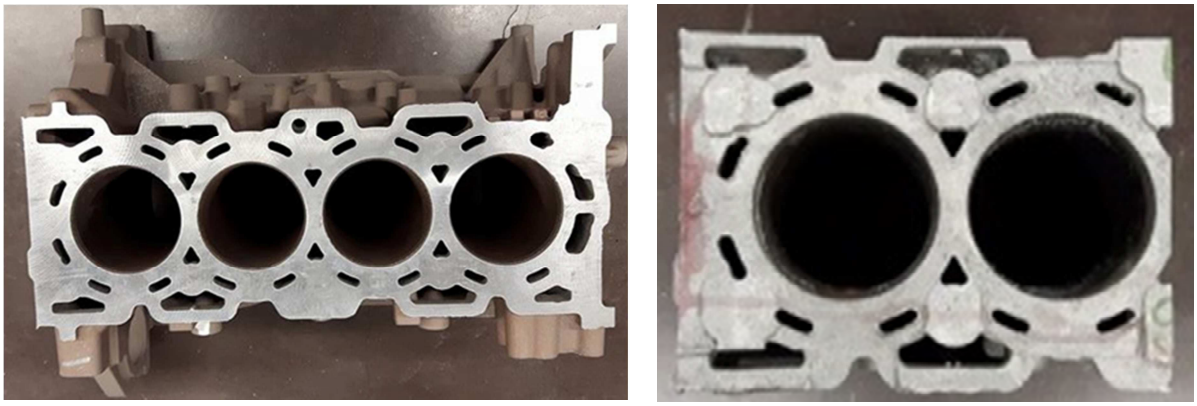

Figure 4-33 I4 Engine blocks (a) Four-cylinder engine block (before cutting) (b) Two-cylinder engine block (after cutting)

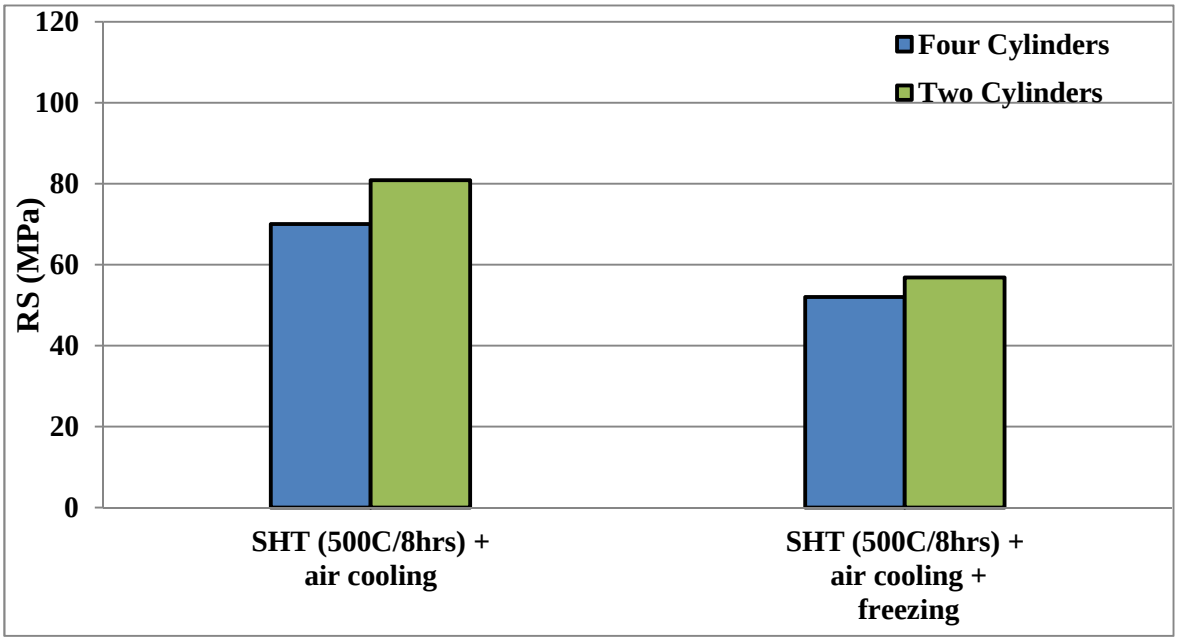

Figure 4-34 Development of residual stresses inside four-cylinders and two-cylinders engine block

(a)

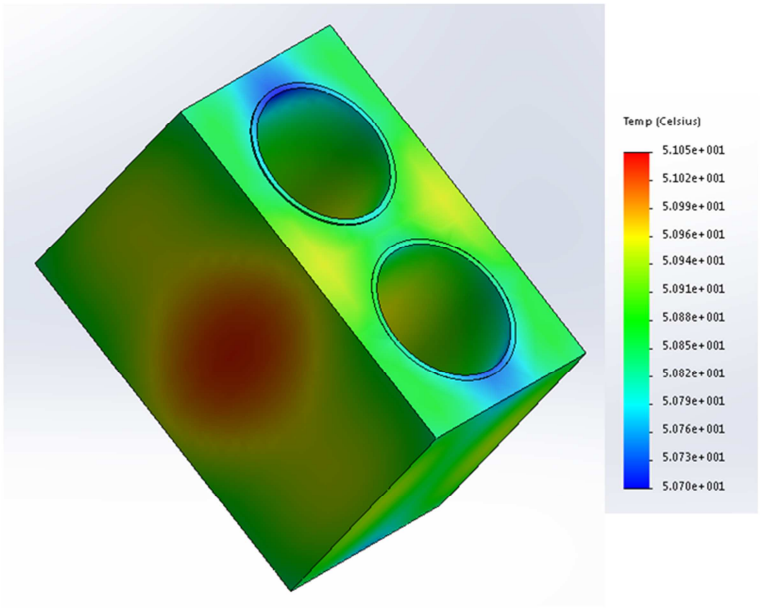
Temp (Celsius)
5.105e+001
5.102e+001
5.099e+001
5.096e+001
5.094e+001
5.091e+001
5.088e+001
5.085e+001
5.082e+001
5.079e+001
5.076e+001
5.073e+001
5.070e+001

(b)

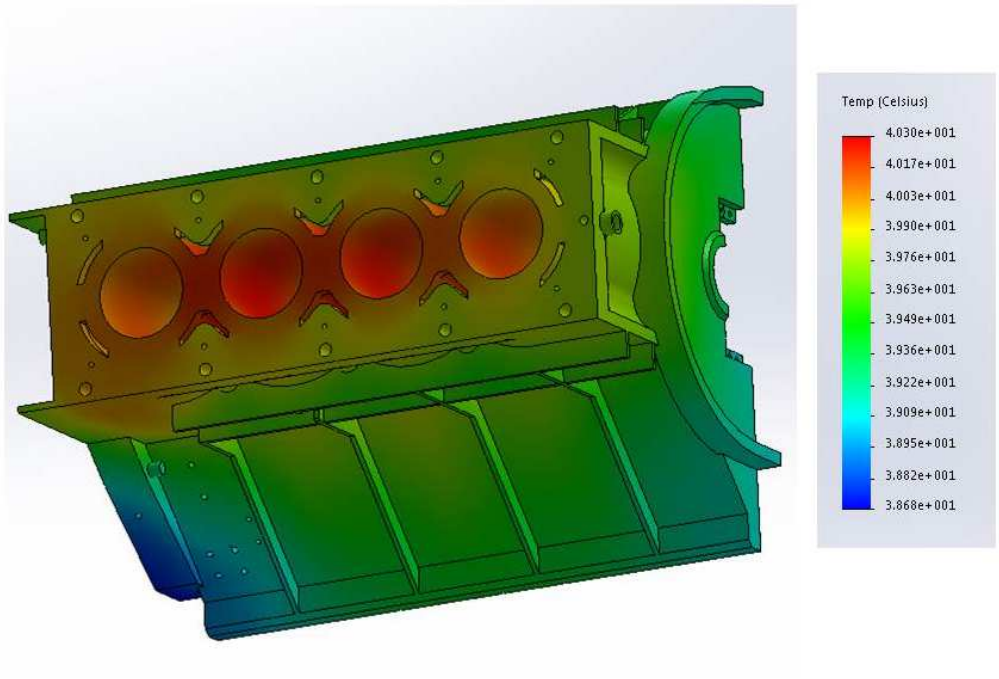
Temp (Celsius)
4.030e+001
4.017e+001
4.003e+001
3.990e+001
3.976e+001
3.963e+001
3.949e+001
3.936e+001
3.922e+001
3.909e+001
3.895e+001
3.882e+001
3.868e+001

(c)

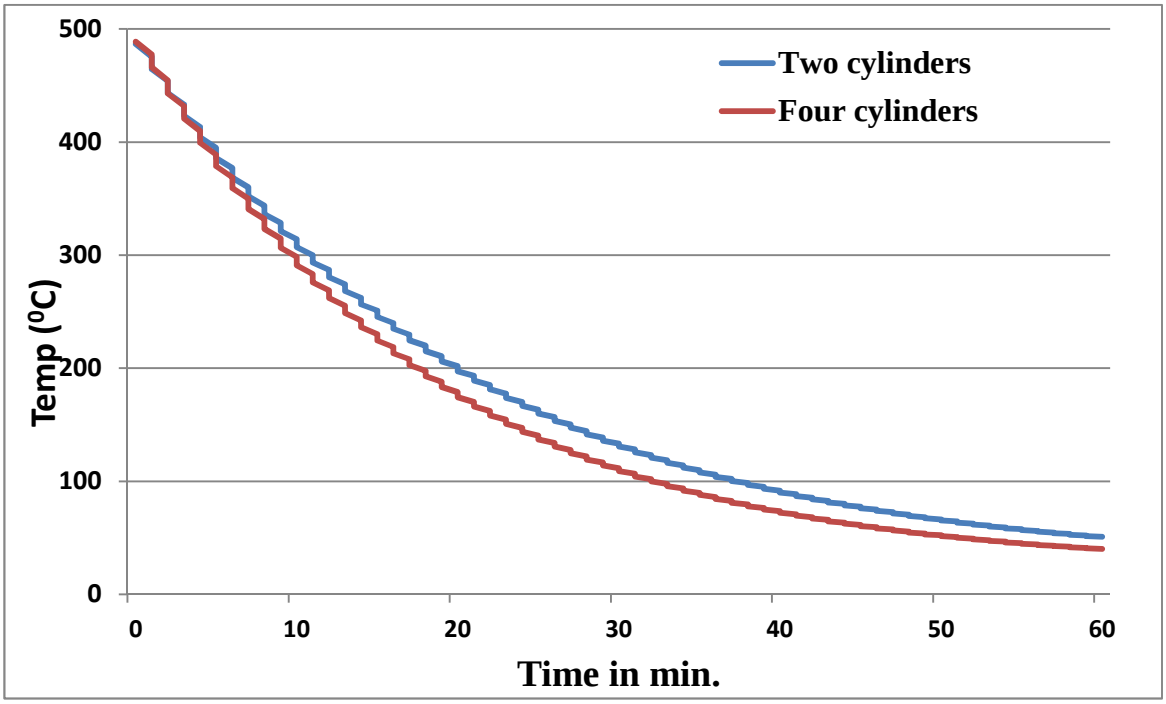

*Cooling rate from simulation is 15.5C /min.

Figure 4-35 Thermal distribution for (a) two cylinders engine block, (b) four cylinders engine block, (c) cooling rates for them, after SHT.

4.10.2 Development of residual stresses inside two-cylinder engine blocks

Figure 4-36 reveals that there is significant relieving of residual stresses ongoing from the as-cast and to the SHT condition where these residual stresses are relieved by 25%, 75 and 65 %, respectively, when subjected to air cooling, warm water quenching and cold-water quenching. This trend indicates that SHT play an important role in the relieving of residual stresses. Previous research studies [1] [52] [83] [111]concluded that residual stresses can be relieved thermally either instantaneously, when locked-in stresses exceed the yield strength or gradually through creep mechanisms.

Relieving of residual stresses through the first mechanism is insignificant compared to the relieving that occurs through creep. Godlewski et al. [83] suggested that relief of

residual stress and strain is brought about by the dislocation creep mechanism. Godlewski et al. [83] also reasoned that the presence of gray iron liners which support the aluminum bridge minimizes the plastic deformation that accompanies residual stress relief. Lombardi et al. [111] found that during solution heat treatment, most of the locked-in stresses were relieved during heating, leaving compressive residual stresses at the end of the solution heat treatment process. Tensile residual stresses were developed during cooling, where their magnitude was dependent on the rate of cooling as was confirmed by the work of Carrera et al. [82].

In the previous section, it was shown that increasing quenching rates resulted in the generation of high residual stresses. Surprisingly, in the case of engine blocks, it was observed that with increasing cooling rate, the residual stresses evolved were found to have decreased. Figure 4-36 shows that air cooling produces the highest residual stress compared to warm water and cold-water quenching. This indicates that the increased cooling rates obtained with quenching lower the amount of residual stresses developed within the engine blocks by ~ 50% compared to air cooling.

The reason for this contradiction is based on two facts related to our experiment. Firstly, the engine blocks contain two different materials with significant differences in their coefficients of thermal expansion ($\alpha_{Al} = 2.4*10^{-5}K^{-1}$, $\alpha_{Fe} = 1.5*10^{-5}K^{-1}$), and secondly, the rate of contraction during quenching will differ given that the cooling rate is the same for both cast iron liners (CI liners) and the surrounding aluminum.

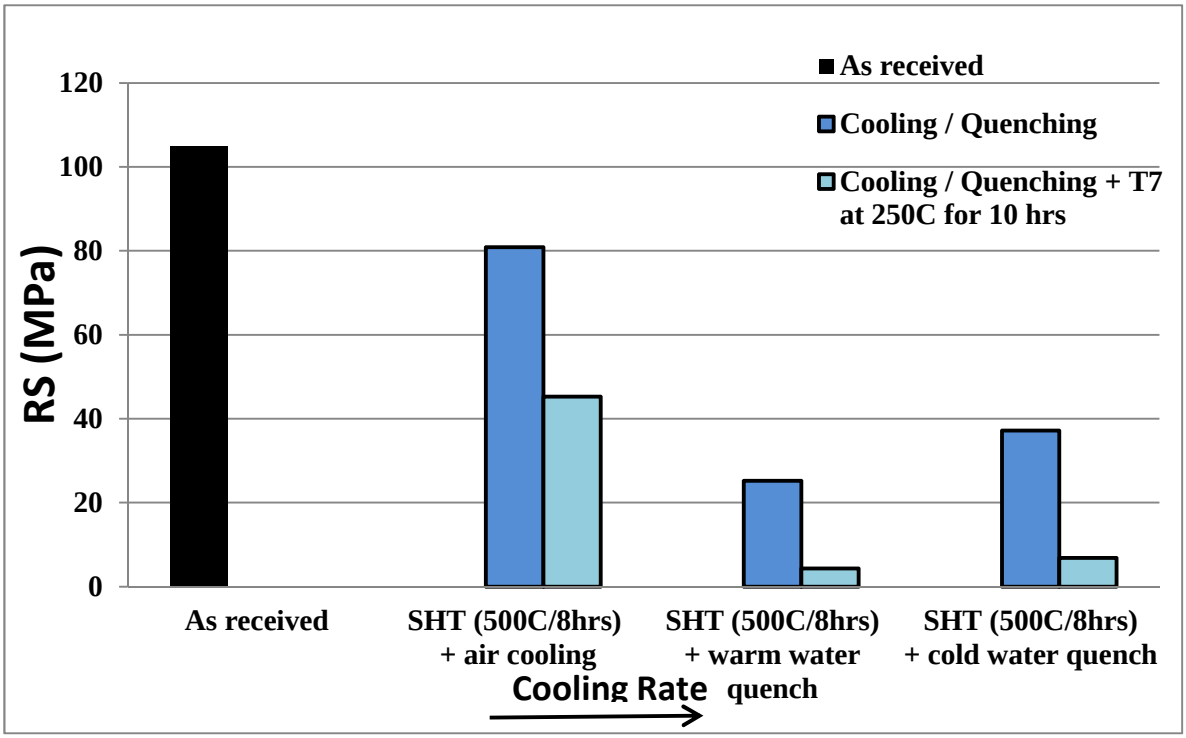

Figure 4-36 Residual stress development with different quenching rates.

At slow cooling rates, there is no significant difference in cooling rates between aluminum and cast iron liners and since the aluminum contracts to a greater extent with decreasing temperature, large residual stresses are developed due to the thermo-mechanical mismatch between the two materials resulting from the hindrance of free contraction of the aluminum. On the other hand, at high cooling rates such as when the blocks are quenched in water, the CI liners, which are in contact with quenching medium, cool at faster rates compared to the surrounding aluminum. This leads to the contraction of both Al and CI liners at similar rates, reducing the thermo-mechanical mismatch between them, resulting in much lower stresses inside the engine blocks.

(a)

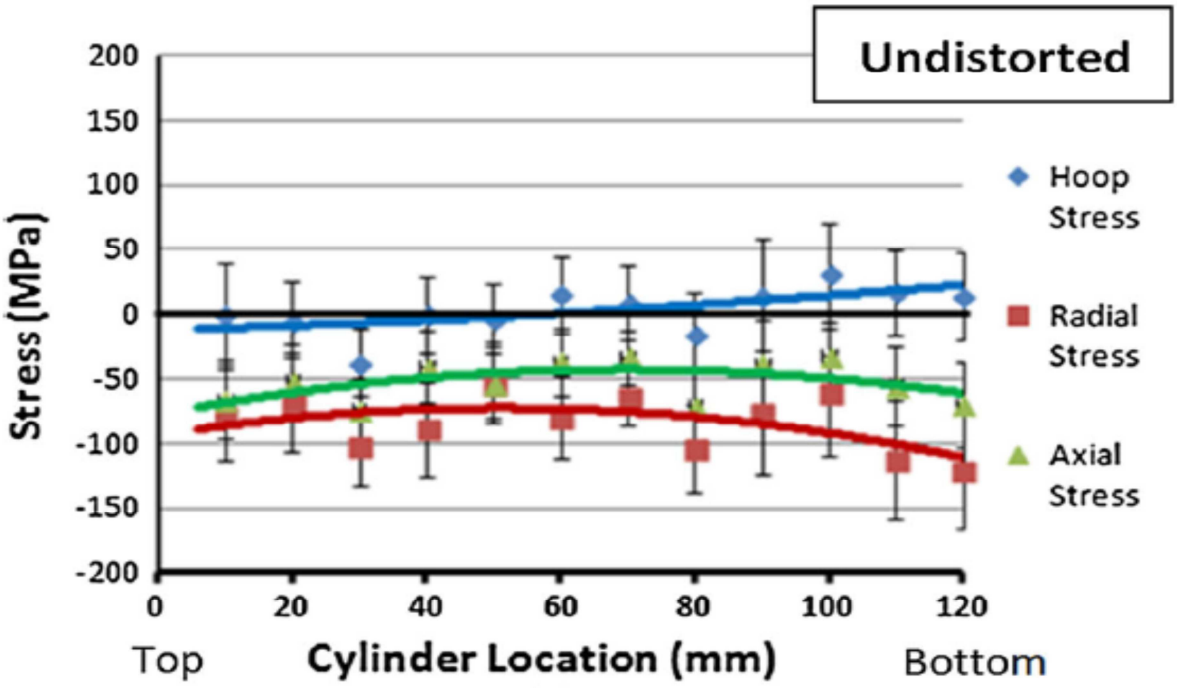

(b)

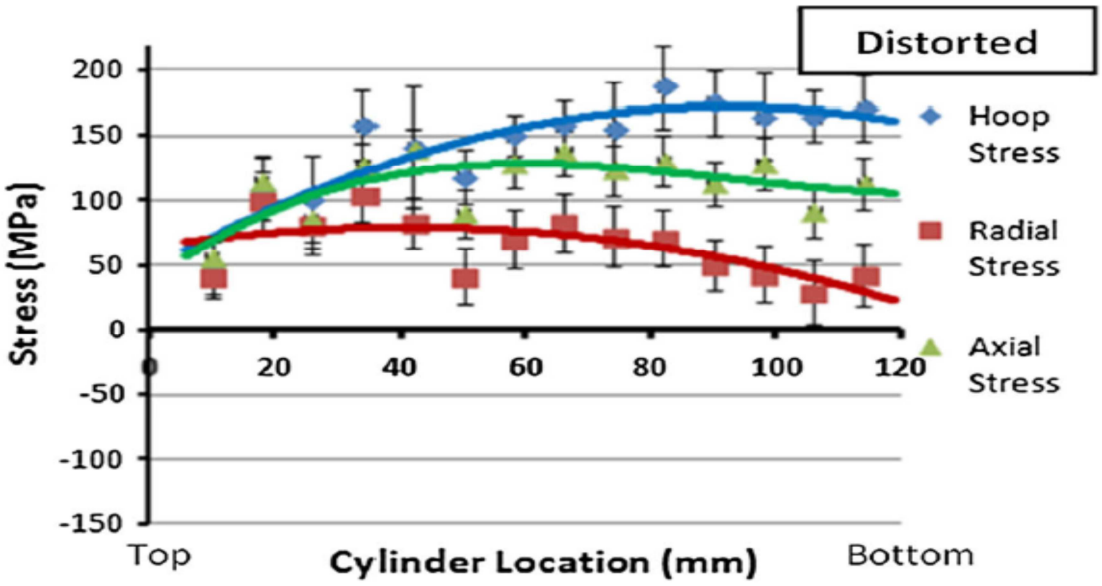

Figure 4-37 Residual stress profiles for the aluminum cylinder bridge of: (a) an engine block cooled at 1.67°K/s, (b)an engine block cooled at 0.67°K/s [5]

Lombardi et.al. [5] investigated the effect of cooling rate on the evolution of residual stresses inside a V6 engine block. After solution heat treatment at 470^{o}C for 7 hours, they used forced air as the quenching/cooling medium at 1.67 and 0.67° K/s, and then performed aging at 240^{o}C for 5 hrs. The results are displayed in Figure 4-37, shows and reveal that quenching at 0.67 K/s promotes distortion and evolution of tensile residual stresses, whereas quenching at 1.67 K/s dampens the distortion and leads to development of compressive stresses [5]. Figure 4-36 also shows that aging can reduce the locked-in residual stresses significantly after aging at 250°C for 10hrs. It is clearly observed that the lowest value of residual stress is generated after cold water quenching, accompanied by aging.

4.10.3 Residual stress relaxation

4.10.3.1 Freezing Treatment

Freezing after quenching is considered one of the techniques which can be used to further reduce the amount of residual stresses by reversing the pattern of thermal gradient imposed during solution heat treatment. Despite the benefits of cryogenic treatment on both mechanical properties and the residual stresses developed in ferrous alloys, there are few reports [52] [104] in the literature related to the freezing treatment of nonferrous materials and the consequent effect on residual stress and mechanical properties.

Alcoa first proposed this technique in the 1960's but due to its complications, it was not exploited. Currently, the cryogenic technique is being reconsidered again, as it has the potential to be applied to complex shapes and castings that cannot be stress relieved by any other method. The idea behind this method is to develop a residual stress that is opposite in nature to that produced from quenching, so that they eliminate each other. To maximize the

outcome of the cryogenic treatment, a thermal gradient as steep as possible is required to be created in the specimen. This can be achieved in two ways: One is to maximize the temperature difference between the sub-zero temperature and quenching medium, and the other is to increase the heat on the specimen surface as fast as possible [52] [104] [112].

The sequence adopted in this study may be termed as a “shallow” cryogenic treatment, as the freezing was extended to -30°C (compared to temperatures of – 100°C used in industrial cryogenic treatments), and is represented schematically in Figure 4-38. It involves exposing the sample to a sub-zero temperature (-30°C) following solution heat treatment and allowing it to stabilize. After stabilization, the surface of the sample is exposed to a sudden increase in temperature by immersing the specimen into water at 60°C, followed by aging.

Figure 4-39 illustrates the effect of freezing on the developments of residual stresses. At least 20% reduction in residual stresses after the implementation of the freezing process is noted, which supports the effectiveness of the freezing treatment. Increasing the freezing time has no significant effect on controlling the residual stresses, as may be seen from Figure 4-40. In Figure 4-40, around 30% reduction in residual stresses is observed after stable freezing despite prolonged exposure to freezing. Reduction in residual stresses reaches 45% after cyclic freezing. However, for most of the current study, stable freezing rather than cyclic freezing was used, where the samples were exposed to -30°C for 24 hrs, for reasons of cost efficiency and easy handling associated with the process.

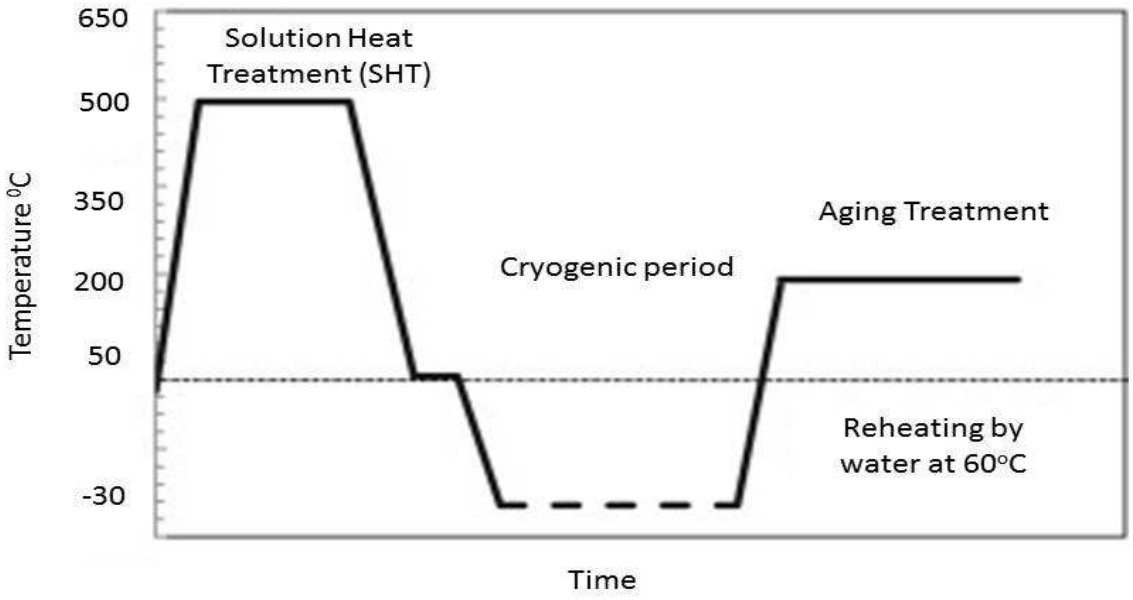

Figure 4-38 Cryogenic treatment sequence

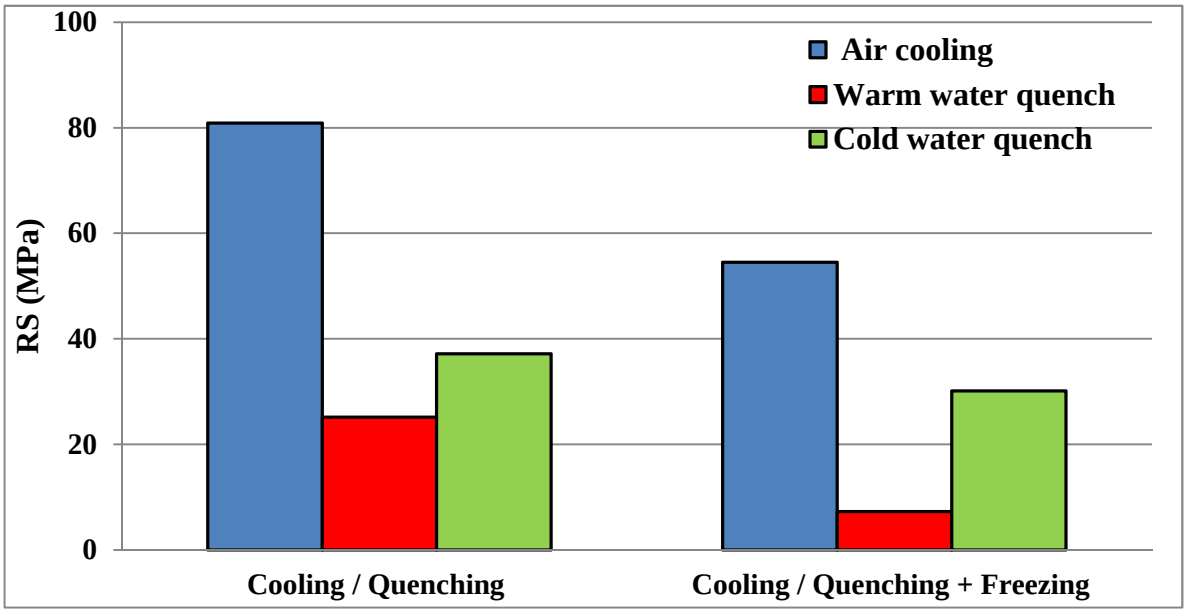

Figure 4-39 Effect of cryogenic treatment on the development of residual stresses in a two-cylinder engine block.

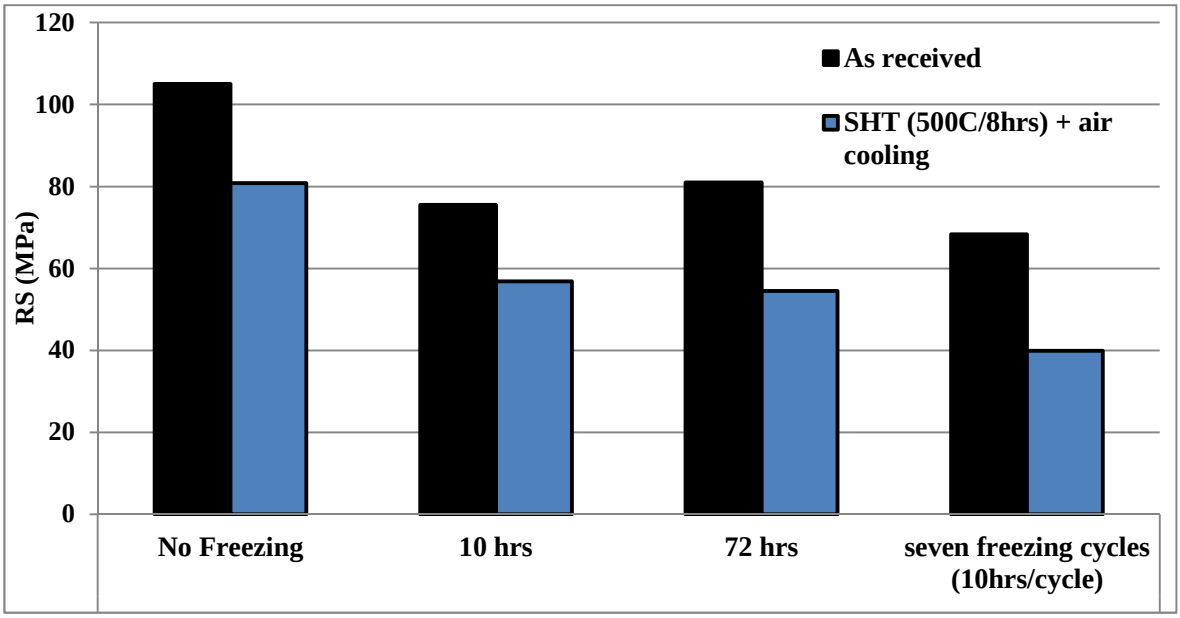

Figure 4-40 Effect of stable vs cyclic freezing on the development of residual stresses.

4.10.3.2 Cryogenic Treatment + Aging

The dual effect of cryogenic treatment and aging on residual stress is illustrated in Figure 4-41 and Figure 4-42. In air-cooled samples, around 40% of the residual stresses are relieved after freezing treatment and with further reduction in following aging at 170°C and 250°C. Prolonging the aging time further reduces the residual stresses, reaching a minimum value of 25 MPa approximately. In cold-water quenched samples, the progression towards residual stress relaxation is slow as the initial values of residual stresses are low, compared to the air-cooled samples. The threshold limit is around 15 MPa for water-quenched samples.

The aging response on residual stresses inside in two-cylinder engine and four-cylinder engine blocks was investigated. The results are presented in Figure 4-42 and reveal that relieving of residual stresses is noticeable in the two-cylinder engine blocks, while

four-cylinder engine blocks show a very low response, which indicates that the size of the component has a direct impact on the amount of stress relief achieved.

The numbers of investigations on the study of residual stresses in engine blocks is very limited. Carrera [82] measured the residual stresses in I-4 engine blocks and found them to be at least 100MPa in the as-cast condition which is in good agreement with our findings. Only 10% reduction in residual stresses was observed when the engine block was aged at 240^{o}C for 6hrs. Lombardi et al. [78] studied the development of residual stresses in V-6 engine blocks, and reported that residual stresses were found to be tensile type along the length of the cylinder, reaching a maximum of 200MPa. They also found that around 70% of residual stresses are relaxed in the top part of the cylinder. Results from other researches are summarized in Table 4-6.

Table 4-6 Results of residual stresses development in engine blocks

Author	Engine Type	Condition	Average RS (MPa)
Carrera [82]	I-4	As Cast	113
	I-4	495°C /4hrs+ quenching at 90°C water +T7 (240°C /4hrs)	94
	V-8		143
Lombardi [74]	V-6	As Cast	150
	V-6	480°C /7.5hrs + forced air cooling +T7 (240°C /5.5hrs)	100

To study the variation in residual stress with change in geometry, a series of experiments were carried out on V-6 engine blocks. The results are summarized in Figure 4-43, and indicate that the variation in geometry or shape does not result in any significant change in the development of residual stresses during heat treatment and aging.

The values of residual stress in the as-received condition were 66 and 98 MPa for V-6 and I-4 engine blocks respectively. The reason for this variation was related to residual stress relaxation induced during machining in the V-6 engine blocks which were received to the final product shape unlike the I-4 engine blocks.

Figure 4-44 shows the change in hardness and residual stresses with different manufacturing parameters. The figure shows that most of the residual stresses are relaxed after the SHT and freezing stage where it drops around 60 and 48% after cold water quenching and air cooling respectively. Through aging, residual stresses in both cold water and air cooled samples are gradually relaxed till they reach the limit at 20 MPa.

Despite the fact that quenching in cold water results in less residual stresses compared to the air-cooled samples, the magnitude of the residual stresses are almost the same after aging. This can be attributed to the fact that material with higher strength tend to relax its locked-in stresses at slower rates. A set of experiment to measure residual stresses and hardness were performed on the I4 and V-6 engine blocks, as presented in Figure 4-45. The HBN results for I-4 engine block show a slight reduction in hardness measurement compared to two-cylinder samples. The V-6 engine block shows the same behavior observed for I-4 engine blocks. Table 4-7 explains the codes used for the different conditions shown in Figure 4-44 and Figure 4-45.

In the case of the I4 engine blocks, the residual stress values indicate some relieving of residual stress is more restricted compared to two-cylinder samples. The average residual stresses achieved after prolonged aging was 45 MPa. This attribute is related to the size of the engine, from which it can be concluded that size plays an important parameter on residual stress relaxation.

Table 4-7 Code breaking used in Figure 4-44 and Figure 4-45

symbol	indication to
A	Air cooling
C	Cold quenching
F	Freezing
T6/ T7	Aging at 170°C/ Aging at 250°C
Numeric digits	Aging time in hours

(a)

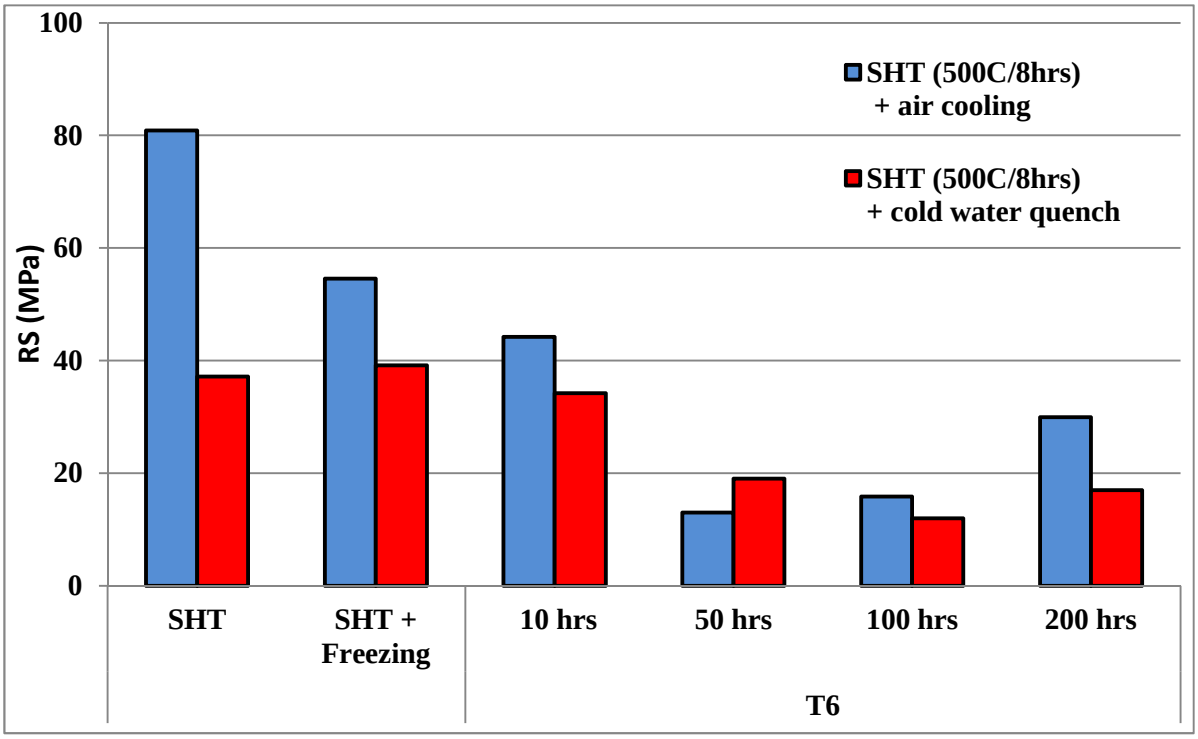

(b)

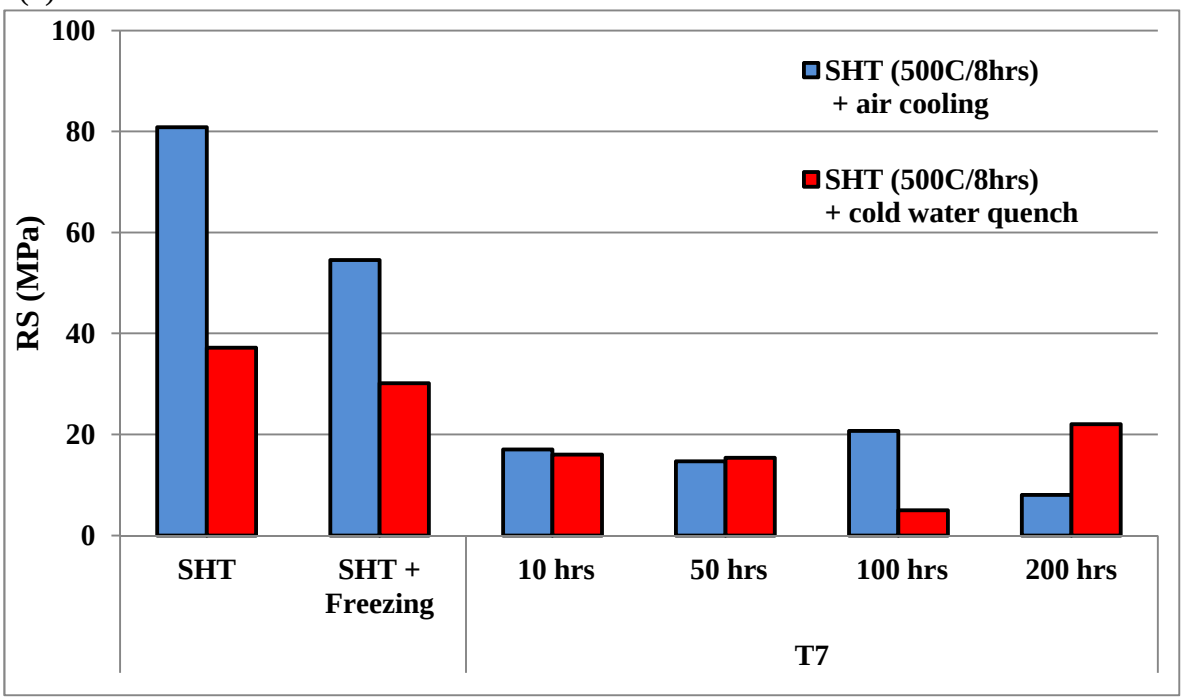

Figure 4-41 Effect of freezing and aging on the development of residual stresses in two-cylinder engine blocks: (a) T6 at 170 °C; (b) T7 at 250

(a)

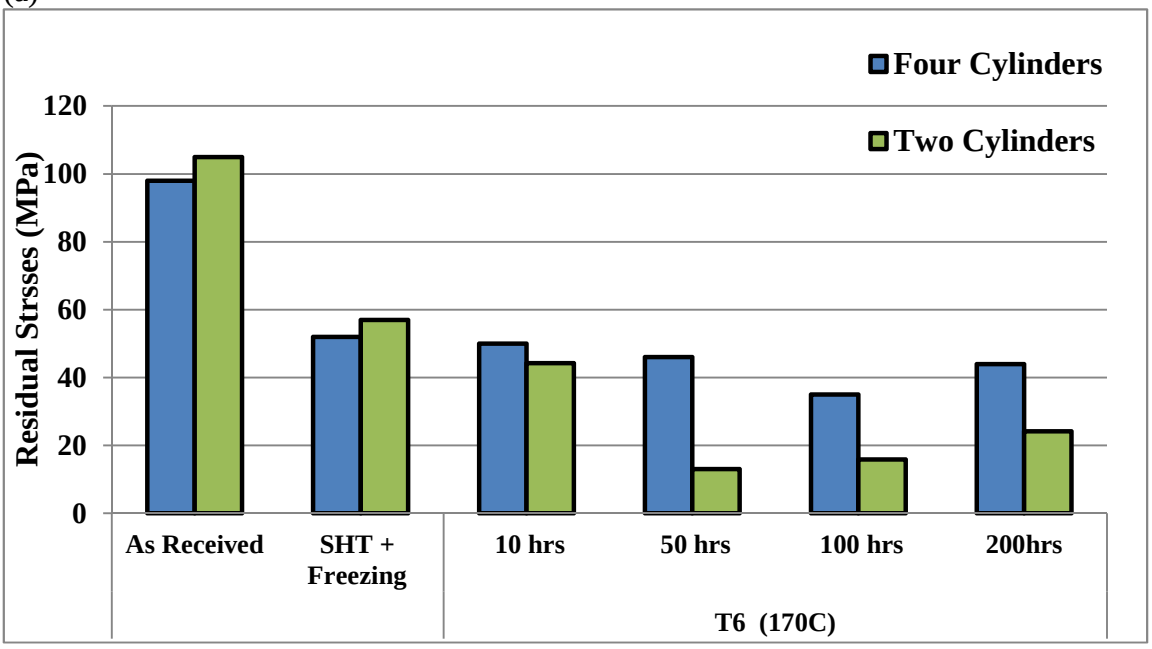

(b)

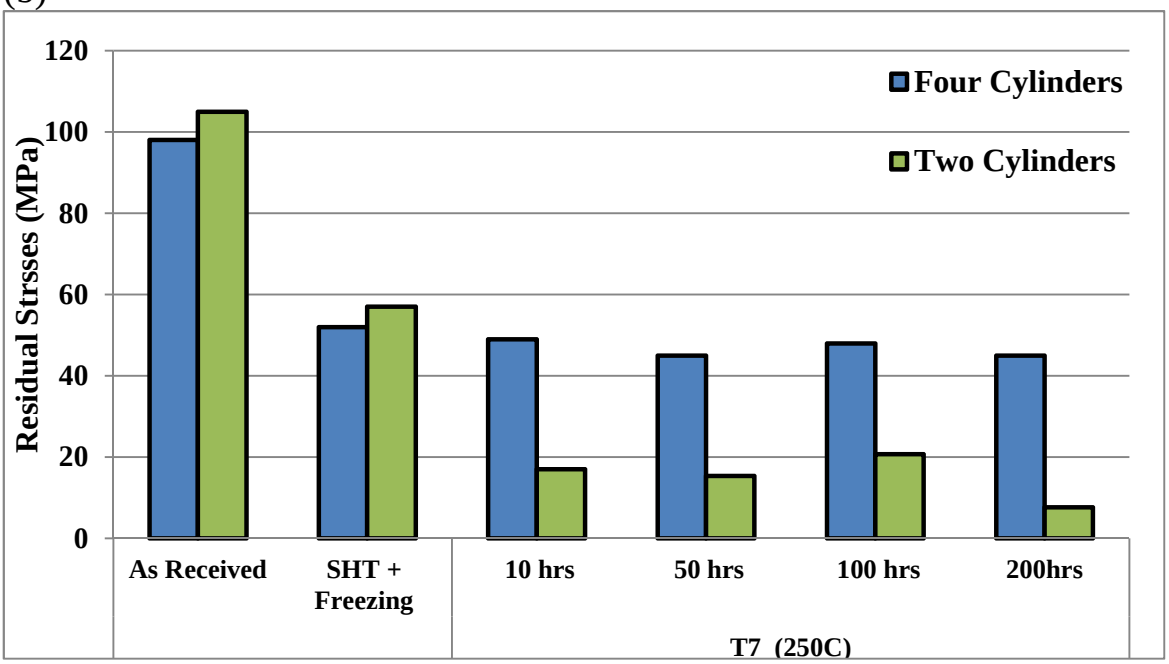

Figure 4-42 Effect of freezing and aging on the development of residual stresses in two- and four-cylinder engine blocks: (a) T6 at 170°C; (b) T7 at 250° C

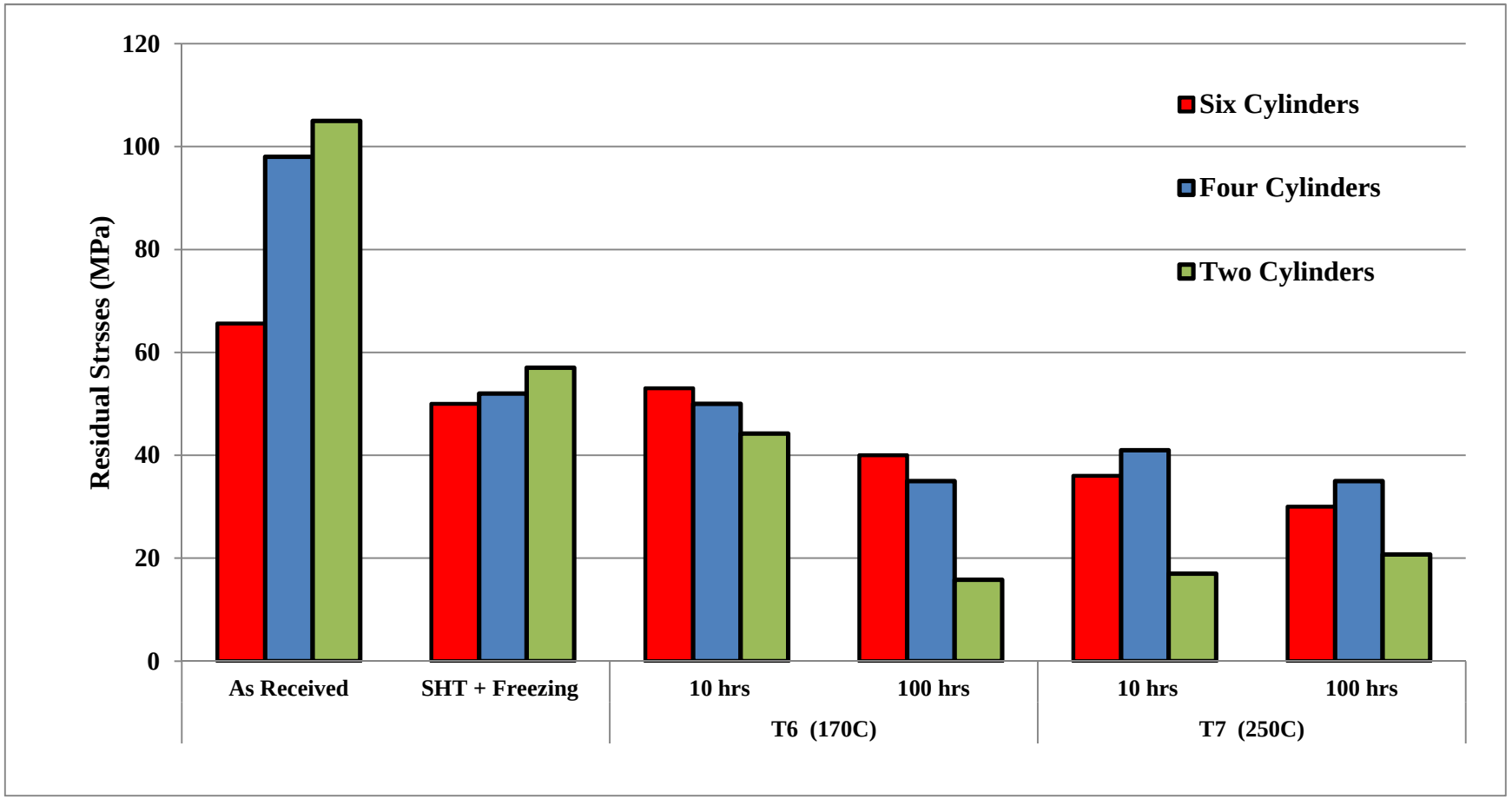

Figure 4-43 Effect of freezing and aging on the development of residual stresses in two-,four-and six-cylinder engine block

(a)

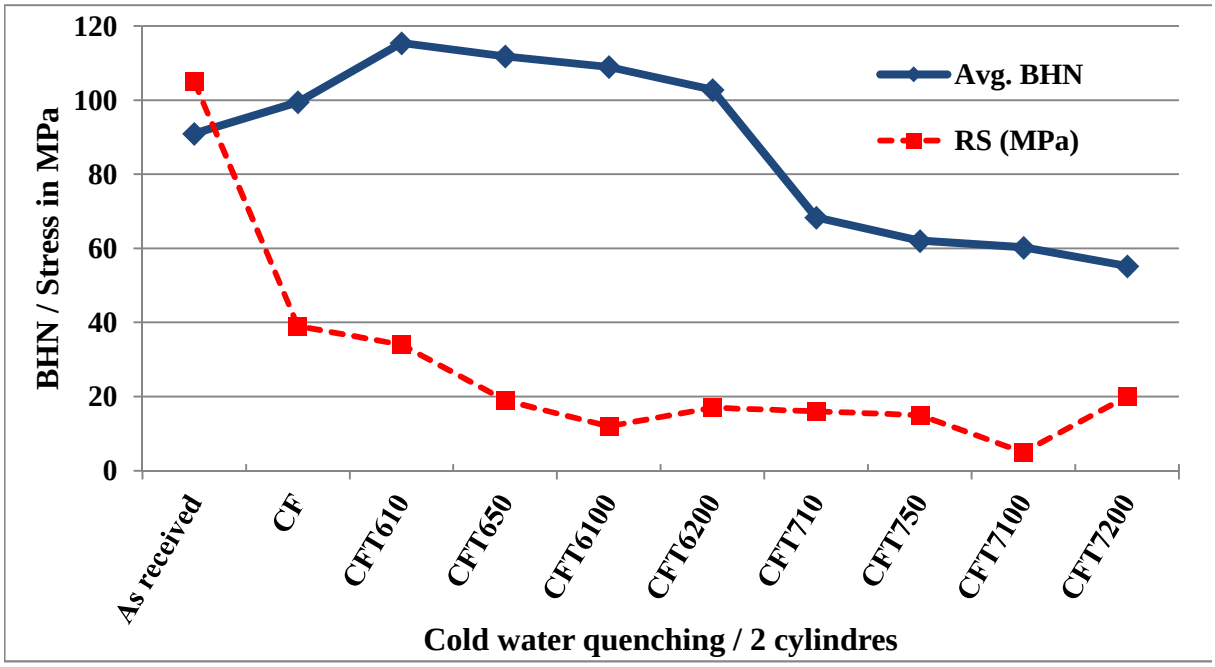

(b)

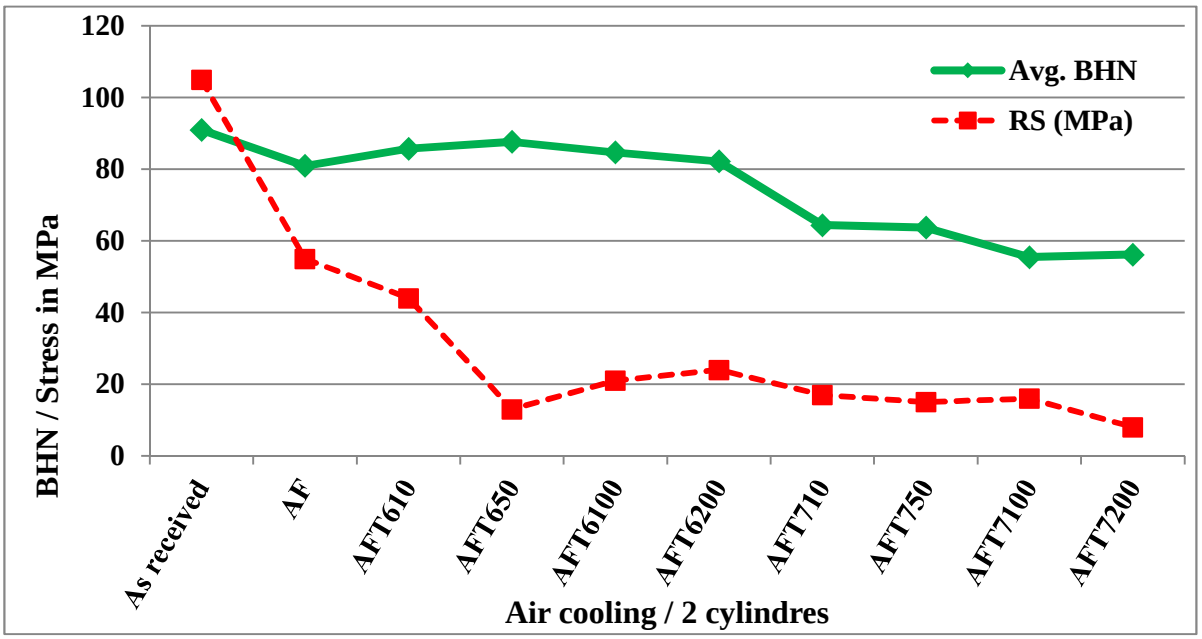

Figure 4-44 Variation of BHN/ Residual stresses at different aging conditions: (a) cold water quenching, (b) air cooling.

(a)

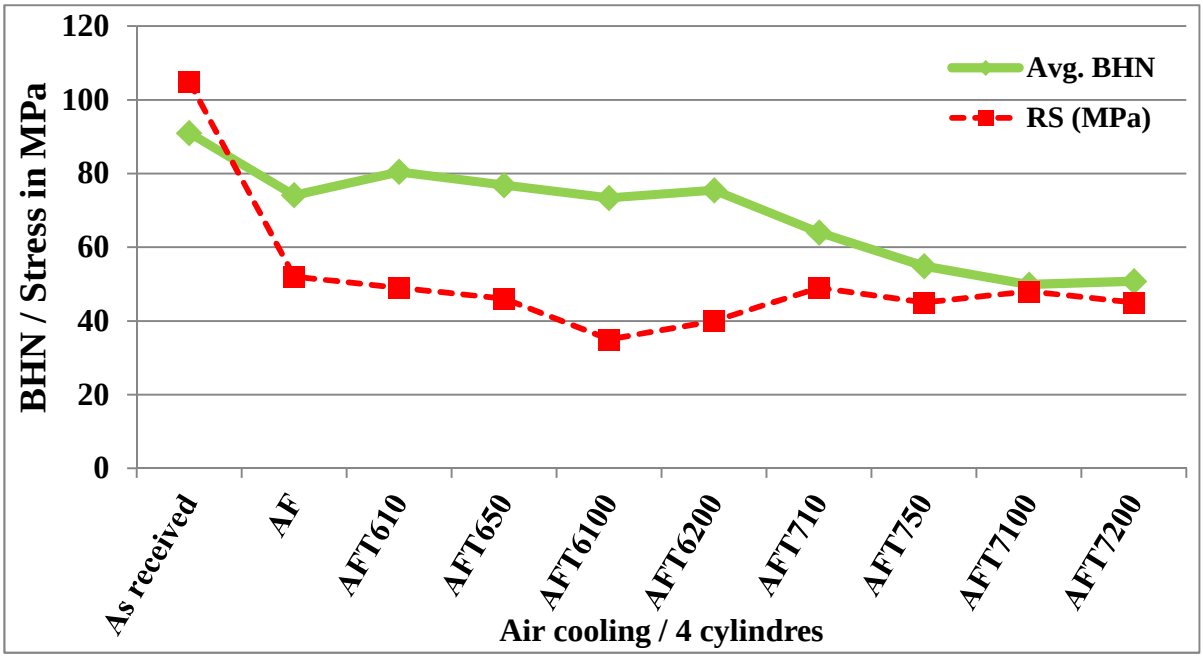

(b)

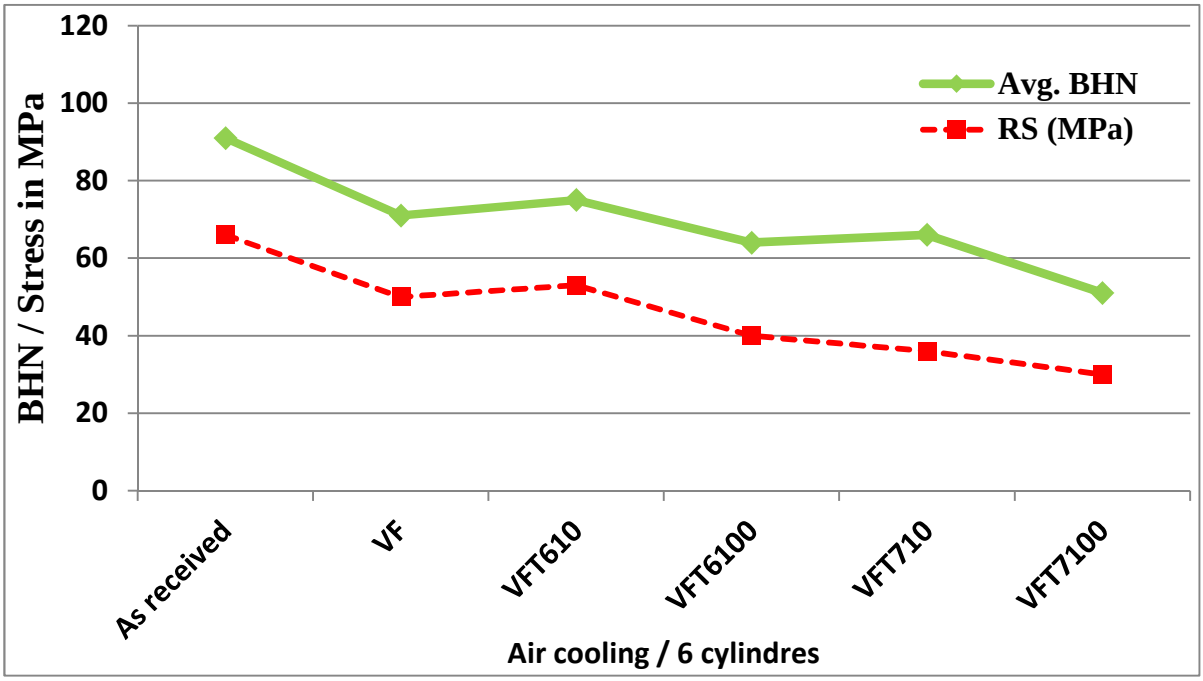

Figure 4-45 Variation of BHN/ Residual stresses at different aging conditions in: (a) I-4 and (b) V-6 engine blocks.

CHAPTER 5
CONCLUSIONS

Chapter 5
Conclusions

The main objective of this thesis has been to investigate the effects of different casting parameters together with heat treatment on the development of the microstructural characteristics, mechanical properties, and residual stresses in Al-Si-Mg (A356.1) and Al-Si-Mg-Cu (B319.1) alloy engine block castings. Microstructural assessment was carried out by using optical microscopy and scanning electron microscopy, while mechanical testing included tensile testing and hardness measurement. Residual stress measurements were carried out using the section technique.

This Chapter presents a summary of the research findings and conclusions obtained from this study, following which, a number of suggestions and recommendations for further research have been provided. The conclusions are divided into two parts, corresponding to the Sections I and II of the results presented in Chapter 4.

Section I

This part represents the findings related to the relation between residual stresses and microstructural evolution in Al-Si alloys based on different casting parameters. From an analysis of the results presented in Section I of Chapter 4, the following conclusions may be drawn.

1- Residual stresses evolved during different heat treatments were compressive in nature.

2- Results obtained for both A356.1 and B319.1 alloys indicate that highest residual stresses are obtained after quenching in cold water whereas in all condition, air quenching produces no significant residual stresses.

3- T6 and T7 treatments show a gradual decrease in residual stresses that is clearly noted in A356.1 alloy.

4- Stress relieving treatments (T6 and T7) lead to the relaxation of residual stresses. Also, the rate of relaxation increases with increasing temperature and time.

5- Cutting direction has considerable effect on the measured residual stresses. It is obvious that the cutting only in the vertical direction does not show any residual stress relaxation in both A356.1 and B319.1.

6- Solidification rate has significant effect on the development of both microstructure and residual stresses. Samples solidified at high rates result in better SHT attributes such as better dissolution of alloying elements and better Si particle spherordization.

7- Significant increase in the residual stresses is observed in specimens with lower SDAS; thus, SDAS has a significant effect on the evolution of residual stresses.

8- Specimens with large SDAS tend to relieve residual stresses more readily compared to specimens with low SDAS.

Section II

The results presented in Section II of Chapter 4 addressed the development of residual stresses and mechanical properties resulting from the use of different quenching

media, cryogenic treatment, and aging conditions (temperature and time). Samples tested were obtained from actual I4, V6 and V8 engine blocks. From an analysis of these results, the following conclusions may be drawn.

9- After quenching, the residual stresses evolved in engine blocks are the same either for the whole block (four cylinders) or for the sectioned half-block (two cylinders).

10- Solution heat treatment and freezing (cryogenic treatment) led to maximum amount of residual stress relaxation where 50% of the residual stresses were reduced after the solution heat treatment step.

11- With freezing, around 30% of residual stress relaxation may be obtained. Increasing the freezing time or the use of cyclic freezing has no significant effect on relieving the residual stress.

12- Air cooling produces the highest residual stresses compared to warm water or cold water quenching. This indicates that in the case of engine blocks, reducing cooling/quenching rates increases the residual stresses developed within the engine blocks.

13- In spite of the effect of quenching rate, residual stresses are gradually relaxed till they reach the limit at 20 MPa.

14- For low aging times, T6 aging has no significant effect on the relaxation of residual stresses, whereas T7 aging diminishes the evolved residual stresses significantly even at low aging times. This shows that aging temperature is the one of controlling parameters in residual stress relaxation.

15- Two-cylinder engine blocks undergo greater residual stress relaxation after aging compared to that observed in four-cylinder engine blocks.

16- The effect of aging is directly related to the size of the casting as large castings (four-cylinder engine blocks) show higher softening rates than smaller castings (two-cylinder engine blocks).

17- The variation in the development of residual stresses was found to be insignificant for I-4 and V-6 engine blocks.

Recommendations for future work

The data obtained in the present research study provided an understanding of the impact of heat treatment on the development of microstructure, hardness and residual stresses in B319.1 alloy castings, more specifically in the case of engine blocks with cast iron liner inserts in the cylinder region, in order to investigate the effect of dissimilar materials in contact with each other on the residual stresses formed.

The following points may be explored for the purposes of providing further knowledge in this field.

1- Studying the development of residual stresses along the length of the cylinder using other measurement techniques such as hole-drilling and neutron diffraction.

2- Examining the variation in residual stress, and the increase in strength following aging, with variation in solution heat treatment temperature from 480°C to 540°C.

3- Examining the relief of residual strain as a function of time during solution heat treatment and artificial aging (T6 and T7 tempers).

4- Measuring the tensile properties at the engine operating temperature (~180°C), to relate the residual stress level to the yield strength of the 319 aluminum alloys under operating conditions.

5- Conducting creep tests at applied stress levels equivalent to the measured residual stress to confirm creep as the mechanism responsible for stress relief.

6- Studying the effect of cryogenic treatment as a mean of residual stress relaxation, in terms of different parameters such as temperature and heat-up rate.

Bibliographie

1. Withers, P.J., *Residual stress and its role in failure.* Reports on Progress in Physics, 2007. **70**(12): p. 2211-2264.
2. Dieter, G.E. and D. Bacon, *Mechanical metallurgy*. Vol. 3. 1986: McGraw-Hill New York.
3. Sadrossadat, M. and S. Johansson, *The effects of casting parameters on residual stresses and microstructure variations of an Al-Si cast alloy.* International Centre for Diffraction Data, 2009. **52**: p. 553-560.
4. Dolan, G. and J. Robinson, *Residual stress reduction in 7175-T73, 6061-T6 and 2017A-T4 aluminium alloys using quench factor analysis.* Journal of materials processing technology, 2004. **153**: p. 346-351.
5. Lombardi, A., et al., *Determining the Mechanism of In-Service Cylinder Distortion in Aluminum Engine Blocks with Cast-In Gray Iron Liners.* Metallurgical and Materials Transactions a-Physical Metallurgy and Materials Science, 2014. **45A**(13): p. 6291-6303.
6. Prasad, P., *Characterization of new, cast, high temperature aluminum alloys for diesel engine applications*. 2006, University of Cincinnati.
7. Heisler, H., *Advanced engine technology*. 1995.
8. Lenny Jr, J., *Replacing the cast iron liners for aluminum engine cylinder blocks: a comparative assessment of potential candidates.* Engineering Thesis Submitted to Graduate Faculty of Rensselaer Polytechnic Institute, Hartford, Connecticut, 2011.
9. Lampman, S.R. and T.B. Zorc, *Properties and Selection of Non-Ferrous Alloys and Special Materials*. 1998, ASM handbook.
10. Dwivedi, D., *Adhesive wear behaviour of cast aluminium–silicon alloys: overview.* Materials & Design, 2010. **31**(5): p. 2517-2531.
11. Tillová, E., M. Chalupová, and L. Hurtalová, *Evolution of phases in a recycled Al-Si cast alloy during solution treatment*, in *Scanning Electron Microscopy*. 2012, InTech.
12. Wang, Q., et al., *Methods of predicting residual stresses and distortion in quenched aluminum castings*. 2012, Google Patents.
13. Wang, Q. *Modeling of residual stresses in aluminum castings*. in *117th Metalcasting Congress*. 2013. Afsinc.
14. James, M. *Residual stress influences in mechanical engineering*. in *Proceedings of the XVIII Congreso Nacional de Ingeniería Mecánica*. 2010.
15. Sticchi, M., et al., *Review of residual stress modification techniques for extending the fatigue life of metallic aircraft components.* Applied Mechanics Reviews, 2015. **67**(1): p. 010801.
16. Davis, J.R., *Aluminum and aluminum alloys*. 1993: ASM international.
17. Cayless, R., *Alloy and temper designation systems for aluminum and aluminum alloys.* 2013.

18. Kaufman, J.G. and E.L. Rooy, *Aluminum Alloy Castings.* Properties, Processes and Applications, ASM International, 2004.
19. Association, A., *Aluminum: properties and physical metallurgy*. 1984: ASM International.
20. Torabian, H., J.P. Pathak, and S.N. Tiwari, *Wear characteristics of Al-Si alloys.* Wear, 1994. **172**(1): p. 49-58.
21. Nguyen, H., *Manufacturing Processes and Engineering Materials Used in Automotive Engine Blocks.* Materials Science and Engineering Section B, EGR250, 2005: p. 1.
22. Samuel, F., A. Samuel, and H. Doty, *Factors Controlling the Type and Morphology of Cu-Containing Phases in 319 Al Alloy (96-30).* Transactions of the American Foundrymen's Society, 1996. **104**: p. 893-902.
23. Boileau, J.M. and J.E. Allison, *The effect of solidification time and heat treatment on the fatigue properties of a cast 319 aluminum alloy.* Metallurgical and materials transactions A, 2003. **34**(9): p. 1807-1820.
24. Gruzleski, J.E. and B.M. Closset, *The treatment of liquid aluminum-silicon alloys*. 1990: Amer Foundry Society.
25. Dahle, A.K., et al., *Eutectic nucleation and growth in hypoeutectic Al-Si alloys at different strontium levels.* Metallurgical and Materials Transactions A, 2001. **32**(4): p. 949-960.
26. Gruzleski, J.E., *Aluminum-silicon eutectic modification—sodium or strontium? A2 - Closset, Bernard*, in *Production and Electrolysis of Light Metals*. 1989, Pergamon: Oxford. p. 131-141.
27. Li, Z., et al., *Effect of alloying elements on the segregation and dissolution of CuAl2 phase in Al-Si-Cu 319 alloys.* Journal of Materials Science, 2003. **38**(6): p. 1203-1218.
28. Tash, M., *Effect of metallurgical parameters on the machining behaviour of 356 and 319 alloys*. 2006, Ph. D. Dissertation. University of Quebec at Chicoutimi.
29. Sjölander, E. and S. Seifeddine, *The heat treatment of Al–Si–Cu–Mg casting alloys.* Journal of Materials Processing Technology, 2010. **210**(10): p. 1249-1259.
30. Samuel, F.H., *Incipient melting of Al5Mg8Si6Cu2 and Al2Cu intermetallics in unmodified and strontium-modified Al–Si–Cu–Mg (319) alloys during solution heat treatment.* Journal of Materials Science, 1998. **33**(9): p. 2283-2297.
31. Samuel, A., et al., *Effect of Mg addition of microstructure of 319 type alloys.* International Journal of Cast Metals Research, 2013. **26**(6): p. 354-363.
32. Samuel, F., et al., *Effect of Mg and Sr additions on the formation of intermetallics in Al-6 wt pct Si-3.5 wt pct Cu-(0.45) to (0.8) wt pct Fe 319-type alloys.* Metallurgical and Materials Transactions A, 1998. **29**(12): p. 2871-2884.
33. Taylor, J.A., *Iron-Containing Intermetallic Phases in Al-Si Based Casting Alloys.* Procedia Materials Science, 2012. **1**(0): p. 19-33.
34. Narayanan, L.A., F.H. Samuel, and J.E. Gruzleski, *Crystallization behavior of iron-containing intermetallic compounds in 319 aluminum alloy.* Metallurgical and Materials Transactions A, 1994. **25**(8): p. 1761-1773.
35. Zhang, L., et al., *Removal of iron from aluminum: a review.* Mineral Processing and Extractive Metallurgy Review, 2012. **33**(2): p. 99-157.

36. Ye, H., *An overview of the development of Al-Si-alloy based material for engine applications.* Journal of Materials Engineering and Performance, 2003. **12**(3): p. 288-297.
37. Tavitas-Medrano, F.J., et al., *Effect of Mg and Sr-modification on the mechanical properties of 319-type aluminum cast alloys subjected to artificial aging.* Materials Science and Engineering: A, 2008. **480**(1–2): p. 356-364.
38. Elsebaie, O., et al., *The role of alloying additives and aging treatment on the impact behavior of 319 cast alloy.* Materials & Design, 2011. **32**(6): p. 3205-3220.
39. Brooks, C.R., *Principles of heat treating of nonferrous alloys.* ASM Handbook, 1991. **4**: p. 823.
40. Lombardi, A., C. Ravindran, and R. MacKay, *Optimization of the solution heat treatment process to improve mechanical Properties of 319 Al alloy engine Blocks using the billet casting method.* Materials Science and Engineering: A, 2015.
41. Samuel, A.M., J. Gauthier, and F.H. Samuel, *Microstructural aspects of the dissolution and melting of Al2Cu phase in Al-Si alloys during solution heat treatment.* Metallurgical and Materials Transactions A, 1996. **27**(7): p. 1785-1798.
42. Lasa, L. and J.M. Rodriguez-Ibabe, *Evolution of the main intermetallic phases in Al-Si-Cu-Mg casting alloys during solution treatment.* Journal of Materials Science, 2004. **39**(4): p. 1343-1355.
43. Han, Y., et al., *Optimizing the tensile properties of Al–Si–Cu–Mg 319-type alloys: Role of solution heat treatment.* Materials & Design, 2014. **58**(0): p. 426-438.
44. Samuel, A., et al., *Defects related to incipient melting in Al–Si–Cu–Mg alloys.* Materials & Design, 2013. **52**: p. 947-956.
45. Mohamed, A.M.A., F.H. Samuel, and S. Al kahtani, *Influence of Mg and solution heat treatment on the occurrence of incipient melting in Al–Si–Cu–Mg cast alloys.* Materials Science and Engineering: A, 2012. **543**(0): p. 22-34.
46. Tavitas-Medrano, F.J., *Artificial aging treatments of 319-type aluminum alloys*. 2008: ProQuest.
47. Reif, W., et al., *Pre-ageing of AlSiCuMg alloys in relation to structure and mechanical properties.* Materials & Design, 1997. **18**(4–6): p. 253-256.
48. Zeren, M., *Effect of copper and silicon content on mechanical properties in Al–Cu–Si–Mg alloys.* Journal of Materials Processing Technology, 2005. **169**(2): p. 292-298.
49. Dobrzański, L., W. Borek, and R. Maniara, *Influence of the crystallization condition on Al-Si-Cu casting alloys structure.* Journal of Achievements in Materials and Manufacturing Engineering, 2006. **18**(1-2): p. 211-214.
50. García-García, G., J. Espinoza-Cuadra, and H. Mancha-Molinar, *Copper content and cooling rate effects over second phase particles behavior in industrial aluminum–silicon alloy 319.* Materials & Design, 2007. **28**(2): p. 428-433.
51. Han, Y., et al., *Study on microstructure and mechanical properties of Al–Mg–Si–Cu alloy with high manganese content.* Materials & Design, 2012. **39**(0): p. 418-424.
52. Lados, D.A., D. Apelian, and L. Wang, *Minimization of residual stress in heat-treated Al–Si–Mg cast alloys using uphill quenching: Mechanisms and effects on static and dynamic properties.* Materials Science and Engineering: A, 2010. **527**(13-14): p. 3159-3165.

53. Withers, P.J. and H. Bhadeshia, *Residual stress. Part 2–Nature and origins.* Materials science and technology, 2001. **17**(4): p. 366-375.
54. Withers, P.J. and H. Bhadeshia, *Residual stress. Part 1–measurement techniques.* Materials science and Technology, 2001. **17**(4): p. 355-365.
55. Rossini, N., et al., *Methods of measuring residual stresses in components.* Materials & Design, 2012. **35**: p. 572-588.
56. Hauk, V., *Structural and residual stress analysis by nondestructive methods: Evaluation-Application-Assessment*. 1997: Elsevier.
57. Sadrossadat, S.M., R.L. Peng, and S. Johansson. *Analysis of residual stress development during thermal processing of Al-Si alloys*. in *Materials Science Forum*. 2011. Trans Tech Publ.
58. TN, T.N., *Measurement of Residual Stresses by the Hole-Drilling* Strain Gage Method.*
59. Grant, P., J. Lord, and P. Whitehead, *The measurement of residual stresses by the incremental hole drilling technique*. 2002: National Physical Laboratory.
60. Šarga, P. and F. Menda, *Comparison of ring-core method and hole-drilling method used for determining residual stresses.* Am. J. Mech. Eng, 2013. **1**(7): p. 335-338.
61. Sharpe, W.N., *Springer handbook of experimental solid mechanics*. 2008: Springer Science & Business Media.
62. Technologies, L., *Measurment of Residual Stresses using Ring-Core Technique* 2005.
63. Wyatt, J.E. and J.T. Berry, *Mapping of Superficial Residual Stresses in Machined Components.* Journal of Industrial Technology, 2009. **25**(4).
64. Mainjot, A.K., et al., *Influence of zirconia framework thickness on residual stress profile in veneering ceramic: Measurement by hole-drilling.* Dental Materials, 2012. **28**(4): p. 378-384.
65. Yamagata, H., *The science and technology of materials in automotive engines*. 2005: Elsevier.
66. Birol, Y. and A.A. Ebrinc, *Critical material issues in cast aluminium cylinder heads.* Foundry Trade Journal, 2008. **181**(3656): p. 196-199.
67. Barbezat, G., *Advanced thermal spray technology and coating for lightweight engine blocks for the automotive industry.* Surface and Coatings Technology, 2005. **200**(5-6): p. 1990-1993.
68. Gowri, S. and F.H. Samuel, *Effect of alloying elements on the solidification characteristics and microstructure of Al- Si- Cu- Mg- Fe 380 alloy.* Metallurgical and Materials Transactions A, 1994. **25**(2): p. 437-448.
69. Lee, J.A. and P.S. Chen, *High strength and wear resistant aluminum alloy for high temperature applications.* 2003.
70. Lee, J.A., *Cast aluminum alloy for high temperature applications.* 2003.
71. Cole, G.S. and A.M. Sherman, *Light weight materials for automotive applications.* Materials Characterization, 1995. **35**(1): p. 3-9.
72. Jeong, C.-Y., *High Temperature Mechanical Properties of Al–Si–Mg–(Cu) Alloys for Automotive Cylinder Heads.* Materials Transactions, 2013. **54**(4): p. 588-594.
73. Helgesen, G.D., R.G. Rentschler, and T.J. Heater, *Method for preparing an engine block casting having cylinder bore liners*. 1994, Google Patents.

74. Lombardi, A., *A Study of Cylinder Bore Distortion in V6 Aluminum Alloy Engine Block,* in *Mechanical Engineering*. 2011, Ryerson University.
75. Wiesner, D., et al., *Residual stress measurements of cast aluminum engine blocks using diffraction.* Int. Centre Diffr. Data, Adv. X-ray Anal, 2005. **48**: p. 136-142.
76. Siyi, T. and L. Lin, *Study and practice of decreasing residual stress with residual heat of casting.* Research & Development, 2008.
77. Haque, M. and M. Maleque, *Effect of process variables on structure and properties of aluminium–silicon piston alloy.* Journal of Materials Processing Technology, 1998. **77**(1-3): p. 122-128.
78. Lombardi, A., et al., *Interplay Between Residual Stresses, Microstructure, Process Variables and Engine Block Casting Integrity.* Metallurgical and Materials Transactions a-Physical Metallurgy and Materials Science, 2012. **43A**(13): p. 5258-5270.
79. Lombardi, A., et al., *Replication of engine block cylinder bridge microstructure and mechanical properties with lab scale 319 Al alloy billet castings.* Materials Characterization, 2014. **87**: p. 125-137.
80. Lombardi, A., C. Ravindran, and R. MacKay, *Improvements in Mechanical Properties of 319 Al Alloy Engine Blocks Through Cost-Effective Solution Heat Treatment.* Journal of Materials Engineering and Performance, 2014. **23**(8): p. 2766-2771.
81. Sediako, D., et al., *Application of Neutron Diffraction in Analysis of Residual Stress Profiles in the Cylinder Web Region of an as-Cast V6 Al Engine Block with Cast-In Fe Liners.* 2011: p. 299-308.
82. Carrera, E., et al., *Measurement of residual stresses in cast aluminium engine blocks.* journal of Materials Processing Technology, 2007. **189**(1): p. 206-210.
83. Godlewski, L.A., et al., *The Effect of Aging on the Relaxation of Residual Stress in Cast Aluminum.* Metallurgical and Materials Transactions A, 2013. **44**(10): p. 4809-4818.
84. Shabestari, S. and H. Moemeni, *Effect of copper and solidification conditions on the microstructure and mechanical properties of Al–Si–Mg alloys.* Journal of Materials Processing Technology, 2004. **153**: p. 193-198.
85. Gil-Figueroa, R.E., *The effect of solidification rate and solutionizing quench rate on the mechanical properties and hardening response of aluminum alloys: A quantitative comparison*. 2016, Michigan Technological University.
86. Seifeddine, S., E. Sjölander, and T. Bogdanoff, *On the role of copper and cooling rates on the microstructure, defect formations and mechanical properties of Al-Si-Mg alloys.* Materials Sciences and Applications, 2013. **4**(03): p. 171.
87. Samuel, A. and F. Samuel, *A metallographic study of porosity and fracture behavior in relation to the tensile properties in 319.2 end chill castings.* Metallurgical and Materials Transactions A, 1995. **26**(9): p. 2359-2372.
88. Rometsch, P., L. Arnberg, and D. Zhang, *Modelling dissolution of Mg2Si and homogenisation in Al-Si-Mg casting alloys.* International Journal of Cast Metals Research, 1999. **12**(1): p. 1-8.
89. Sjölander, E. and S. Seifeddine, *Optimisation of solution treatment of cast Al–Si–Cu alloys.* Materials & Design, 2010. **31,** Supplement 1(0): p. S44-S49.

90. Ammar, H.R., et al., *Influences of alloying elements, solution treatment time and quenching media on quality indices of 413-type Al–Si casting alloys.* Materials Science and Engineering: A, 2008. **489**(1): p. 426-438.
91. Warmuzek, M., *Aluminum-silicon casting alloys: an atlas of microfractographs*. 2004: ASM international.
92. Ammar, H., *Influence of metallurgical parameters on the mechanical properties and quality indices of Al-Si-Cu-Mg and Al-Si-Mg casting alloys*. 2010: Université du Québec à Chicoutimi.
93. Ibrahim, M.F., et al., *Effect of Aging Conditions on Precipitation Hardening in Al–Si–Mg and Al–Si–Cu–Mg Alloys.* International Journal of Metalcasting, 2017. **11**(2): p. 274-286.
94. Matsuda, K., et al., *Crystal structure of the β″ phase in an Al–l.0mass%Mg2Si–0.4mass%Si alloy.* Materials Science and Engineering: A, 1999. **262**(1): p. 232-237.
95. Murayama, M. and K. Hono, *Pre-precipitate clusters and precipitation processes in Al–Mg–Si alloys.* Acta Materialia, 1999. **47**(5): p. 1537-1548.
96. Ratke, L. and P.W. Voorhees, *Growth and coarsening: Ostwald ripening in material processing*. 2013: Springer Science & Business Media.
97. Voorhees, P.W., *The theory of Ostwald ripening.* Journal of Statistical Physics, 1985. **38**(1): p. 231-252.
98. Ogris, E., *Development of Al-Si-Mg alloys for semi-solid processing and silicon spheroidization treatment (SST) for Al-Si-cast alloys*. 2002, ETH Zurich.
99. Gladman, T., *Precipitation hardening in metals.* Materials science and technology, 1999. **15**(1): p. 30-36.
100. Zhang, L., et al., *FEM simulation and experimental study on the quenching residual stress of aluminum alloy 2024.* Proceedings of the Institution of Mechanical Engineers, Part B: Journal of Engineering Manufacture, 2013. **227**(7): p. 954-964.
101. Dong, Y.-B., et al., *Minimization of Residual Stress in an Al-Cu Alloy Forged Plate by Different Heat Treatments.* Journal of Materials Engineering and Performance, 2015. **24**(6): p. 2256-2265.
102. Jeanmart, P. and J. Bouvaist, *Finite element calculation and measurement of thermal stresses in quenched plates of high–strength 7075 aluminium alloy.* Materials science and technology, 1985. **1**(10): p. 765-769.
103. Prime, M.B. and M.R. Hill, *Residual stress, stress relief, and inhomogeneity in aluminum plate.* Scripta Materialia, 2002. **46**(1): p. 77-82.
104. Robinson, J., D. Tanner, and C. Truman, *50th Anniversary Article: The Origin and Management of Residual Stress in Heat‐treatable Aluminium Alloys.* Strain, 2014. **50**(3): p. 185-207.
105. Hunsicker, H.Y., *Dimensional changes in heat treating aluminum alloys.* Metallurgical Transactions A, 1980. **11**(5): p. 759-773.
106. James, M., *Relaxation of residual stresses an overview.* Pergamon Press, Advances in Surface Treatments. Technology--Applications--Effects., 1987. **4**: p. 349-365.
107. Robinson, J. and D.A. Tanner, *Residual stress development and relief in high strength aluminium alloys using standard and retrogression thermal treatments.* Materials science and technology, 2003. **19**(4): p. 512-518.

108. Wang, Q., *Microstructural effects on the tensile and fracture behavior of aluminum casting alloys A356/357.* Metallurgical and materials Transactions A, 2003. **34**(12): p. 2887-2899.
109. Jian, X., T.T. Meek, and Q. Han, *Refinement of eutectic silicon phase of aluminum A356 alloy using high-intensity ultrasonic vibration.* Scripta Materialia, 2006. **54**(5): p. 893-896.
110. Lombardi, A., et al., *Residual stress mapping along the cylinder bores of al alloy engine blocks subjected to production solution heat treatment schedule.* SAE International Journal of Materials and Manufacturing, 2014. **7**(2014-01-0837): p. 415-420.
111. Lombardi, A., et al., *Effect of solution heat treatment on residual stress in Al alloy engine blocks using neutron diffraction.* Materials Science and Engineering: A, 2017. **697**: p. 238-247.
112. Araghchi, M., et al., *A novel cryogenic treatment for reduction of residual stresses in 2024 aluminum alloy.* Materials Science and Engineering: A, 2017. **689**: p. 48-52.